The Coordination Chemistry of Sterically Bulky Guanidinate Ligands with Chromium and the Lanthanide Metals

AU, Chi Wai

A Thesis Submitted in Partial Fulfilment
of the Requirements for the Degree of
Doctor of Philosophy
in
Chemistry

The Chinese University of Hong Kong

May 2014

Abstract

This research work is focused on the coordination chemistry of five closely related guanidinate ligands, namely $[(2,6\text{–}Me_2C_6H_3N)C(NHPr^i)(NPr^i)]^-$ (L^1), $[(2,6\text{–}Me_2C_6H_3N)C(NHCy)(NCy)]^-$ (L^2), $[(2,6\text{–}Me_2C_6H_3N)C\{N(SiMe_3)Cy\}(NCy)]^-$ (L^3), $[(2,6\text{–}Pr^i{}_2C_6H_3N)C\{N(SiMe_3)_2\}(NC_6H_3Pr^i{}_2\text{–}2,6)]^-$ (L^4) and $[(2,6\text{–}Pr^i{}_2C_6H_3N)C(NEt_2)(NC_6H_3Pr^i{}_2\text{–}2,6)]^-$ (L^5), with divalent chromium and lanthanide metal ions. A series of trivalent lanthanide derivatives of the L^1 ligand were also prepared and structurally characterized in this work.

Chapter 1 gives a brief introduction to the chemistry of metal guanidinate complexes.

Chapter 2 reports on the synthesis, structure and reactivity of chromium(II) complexes derived from the bulky L^1 and L^4 ligands. Treatment of $CrCl_2$ with $[KL^1 \cdot 0.5PhMe]$ (**1**) afforded the mononuclear Cr(II) bis(guanidinate) complex $[Cr(L^1)_2]$ (**3**). Reaction of $CrCl_2$ with $[LiL^4(Et_2O)]$ (**2**) resulted in the isolation of ate–complex $[Cr(L^4)(\mu\text{–}Cl)_2Li(THF)(Et_2O)]$ (**4**). Recrystallization of **4** from toluene gave neutral, dimeric $[\{Cr(L^4)(\mu\text{–}Cl)\}_2]$ (**5**). The reaction chemistry of the Cr(II) complex **3** and **4** was studied. Treatment of **3** with I_2, PhEEPh (E = S, Se, Te), $1\text{–}AdN_3$ (1–Ad =

1–adamantyl) gave the corresponding mixed–ligand Cr(III) complexes, namely $[Cr(L^1)_2I]$ (**6**) and $[Cr(L^1)_2(EPh)]$ [E = S (**7**), Se (**8**), Te (**9**)] and Cr(IV) complex $[Cr(L^1)_2\{N(1–Ad)\}]$ (**10**). Besides, the reaction of **4** with NaOMe resulted in the isolation of the Cr(II) methoxide–guanidinate complex $[\{Cr(L^4)(\mu–OMe)\}_2]$ (**11**).

Chapter 3 deals with the synthesis, structure and reactivity of lanthanide(II) complexes supported by the L^1, L^2, L^3 and L^5 ligands. Lanthanide(II) guanidinate complexes were prepared by the reactions of an appropriate lanthanide diiodide with the corresponding potassium guanidinate complexes $[KL^1 \cdot 0.5PhMe]$ (**1**), $[KL^2(THF)_{0.5}]_n$ (**12**), KL^3 (**13**) and $[KL^5(THF)_2]$ (**14**). Reaction of $EuI_2(THF)_2$ with **1** gave the homoleptic complex $[\{Eu(L^1)(\mu–L^1)\}_2]$ (**15**). Metathesis reactions of $LnI_2(THF)_2$ (Ln = Yb, Eu) with **12** and **13** led to the isolation of $[\{Ln(L^2)(\mu–L^2)\}_2 \cdot nC_6H_{14}]$ [Ln = Eu, n = 2 (**16**); Ln = Yb, n = 0 (**17**)], $[Yb(L^2)_2(THF)_2]$ (**18**) and $[Ln(L^3)_2(THF)_2 \cdot 0.25C_6H_{14}]$ [Ln = Eu (**19**), Yb (**20**)]. Direct reaction of $SmI_2(THF)_2$ with **13** yielded the iodide bridged Sm(II) complex $[\{Sm(L^3)(\mu–I)(THF)\}_2]$ (**21**), whilst reaction of $SmI_2(THF)_2$ with **14** gave homoleptic $[Sm(L^5)_2]$ (**22**). The reaction chemistry of **15**, **18**, **20** and **22** as reducing agents was examined. Oxidation of **15** with I_2 afforded the Eu(III) complex $[\{Eu(L^1)_2(\mu–I)\}_2]$ (**23**). Reactions of **18** with PhEEPh (E = S, Se) gave the corresponding Yb(III) chalcogenide complexes

[{Yb(L^2)$_2$(μ–EPh)}$_2$] [E = S (**24**), Se (**25**)], whilst treatment of **18** with CuCl led to the isolation of [{Yb(L^2)$_2$(μ–Cl)}$_2$] (**26**). Besides, addition of complex **18** to PhNNPh yielded binuclear [{Yb(L^2)$_2$}$_2$(μ–η^2:η^2–PhNNPh)] (**27**), whereas treatment of **20** with PhNNPh resulted in the isolation of mononuclear [Yb(L^3)$_2$(η^2–PhNNPh)·PhMe] (**28**). Addition of CS_2 to **22** gave the unsymmetrical coupling product [(L^5)$_2$Sm(μ–η^3:η^2–S_2CSCS)Sm(L^5)$_2$] (**29**).

Chapter 4 describes the preparation and structural characterization of lanthanide(III) complexes derived from L^1. A series of homoleptic lanthanide(III) tris(guanidinate) complexes [Ln(L^1)$_3$] [Ln = Ce (**30**), Pr (**31**), Gd (**32**), Tb (**33**), Ho (**34**), Er (**35**), Tm (**36**)] were prepared by the reactions of an appropriate $LnCl_3$ with three molar equivalents of **1**. Treatment of $CeCl_3$ and $LuCl_3$ with two equivalents of **1** gave the corresponding chloride bridged guanidinate complexes [{Ln(L^1)$_2$(μ–Cl)}$_2$] [Ln = Ce (**37**), Lu (**38**)].

Chapter 5 summarizes the findings of this study. A short description on the future prospect of this work will also be given.

摘要

本項研究工作主要對五個結構類似的胍基配體，即 $[(2,6\text{–}Me_2C_6H_3N)C(NHPr^i)(NPr^i)]^-$ (L^1)，$[(2,6\text{–}Me_2C_6H_3N)C(NHCy)(NCy)]^-$ (L^2)，$[(2,6\text{–}Me_2C_6H_3N)C\{N(SiMe_3)Cy\}(NCy)]^-$ (L^3)，$[(2,6\text{–}Pr^i{}_2C_6H_3N)C\{N(SiMe_3)_2\}(NC_6H_3Pr^i{}_2\text{–}2,6)]^-$ (L^4) 和 $[(2,6\text{–}Pr^i{}_2C_6H_3N)C(NEt_2)(NC_6H_3Pr^i{}_2\text{–}2,6)]^-$ (L^5) 與二價鉻以及二價鑭系金屬 [Sm(II)、Eu(II) 及 Yb(II)] 的配位化學進行研究，同時，一系列由 L^1 配體所衍生的三價鑭系金屬配合物亦成功被合成。

第一章概括介紹了由胍基配體所構築的金屬配合物的研究背景。

第二章敍述了含 L^1 與 L^4 的二價鉻配合物的合成、結構及其化學反應。通過胍基鉀化合物 $[KL^1\cdot 0.5PhMe]$ (**1**) 與二氯化鉻反應可得到單核二價鉻雙胍基配合物 $[Cr(L^1)_2]$ (**3**)。通過胍基鋰化合物 $[LiL^4(Et_2O)]$ (**2**) 與二氯化鉻反應，成功製備了單胍基二價鉻配合物 $[Cr(L^4)(\mu\text{–}Cl)_2Li(THF)(Et_2O)]$ (**4**)。而把二價鉻配合物 **4** 於甲苯溶液中重結晶可得到二聚體的二價鉻配合物 $[\{Cr(L^4)(\mu\text{–}Cl)\}_2]$ (**5**)。另外，我們對二價鉻配合物 **3** 及 **4** 的反應特性也進行了研究。$[Cr(L^1)_2]$ (**3**) 與單質碘、二苯基硫族化合物 PhEEPh (E = S, Se, Te) 以及叠氮金剛烷反應可得相對應的三價鉻混合配體化合物，分別爲 $[Cr(L^1)_2I]$ (**6**)、$[Cr(L^1)_2(EPh)]$ [E =

S (**7**), Se (**8**), Te (**9**)]，及四價鉻配合物 [Cr(L^1)$_2${N(1–Ad)}] (**10**)。 透過單胍基二價鉻配合物 [Cr(L^4)(μ–Cl)$_2$Li(THF)(Et$_2$O)] (**4**) 與 NaOMe 反應可得甲氧基–胍基配合物 [{Cr(L^4)(μ–OMe)}$_2$] (**11**)。

第三章主要報導含 L^1， L^2， L^3 和 L^5 配基的二價鑭系配合物的合成、結構和化學反應特性。 透過 [LnI$_2$(THF)$_2$] (Ln = Sm, Eu, Yb) 與胍基鉀鹽反應，我們成功合成一系列二價鑭系絡合物，包括 [{Eu(L^1)(μ–L^1)}$_2$] (**15**)，[{Ln(L^2)(μ–L^2)}$_2$·nC$_6$H$_{14}$] [Ln = Eu, n = 2 (**16**); Ln = Yb, n = 0 (**17**)，[Yb(L^2)$_2$(THF)$_2$] (**18**)， [Ln(L^3)$_2$(THF)$_2$·0.25C$_6$H$_{14}$] [Ln = Eu (**19**), Yb (**20**)]， [{Sm(L^3)(μ–I)(THF)}$_2$] (**21**) 和 [Sm(L^5)$_2$] (**22**)。本章亦同時探討二價鑭系配合物 **15**， **18**， **20** 和 **22** 作爲還原劑的化學反應特性。 配合物 **15** 與單質碘反應可得三價銪配合物 [{Eu(L^1)$_2$(μ–I)}$_2$] (**23**)。 配合物 **18** 與二苯基硫族化合物 PhEEPh (E = S, Se) 反應，可得相對應的三價鐿配合物 [{Yb(L^2)$_2$(μ–EPh)}$_2$] [E = S (**24**), Se (**25**)]。 **18** 與氯化亞銅反應得到三價鐿配合物 [{Yb(L^2)$_2$(μ–Cl)}$_2$] (**26**)。 除此之外，配合物 **18** 與偶氮苯反應得到雙核配合物 [{Yb(L^2)$_2$}$_2$(μ–η^2:η^2–PhNNPh)] (**27**)， 而 **20** 與偶氮苯的反應可得單核配合物 [Yb(L^3)$_2$(η^2–PhNNPh)·PhMe] (**28**)。 配合物 **22** 與二硫化碳的反應得出不對稱偶合配合物 [(L^5)$_2$Sm(μ–η^3:η^2–S$_2$CSCS)Sm(L^5)$_2$] (**29**)。

第四章敍述由胍基配體 L^1 所衍生的一系列三價鑭系金屬配合物 $[Ln(L^1)_3]$ [Ln = Ce (**30**), Pr (**31**), Gd (**32**), Tb (**33**), Ho (**34**), Er (**35**), Tm (**36**)] 的合成及其結構。 通過相對應的鑭系金屬三氯化物與 **1** 反應可得配合物 **30–36**。 另外，$CeCl_3$ 及 $LuCl_3$ 與 **1** 反應亦可合成 $[\{Ln(L^1)_2(\mu\text{–}Cl)\}_2]$ [Ln = Ce (**37**), Lu (**38**)]。

第五章總結了本項研究工作，並對本工作的未來發展作出建議。

Acknowledgement

I would like to give my sincere thanks to my supervisor, Prof. Hung Kay Lee, for his patient guidance and valuable advice during my four–years research study.

I am also grateful to Prof. Thomas C. W. Mak, Ms. Bella H. -S. Chan, Mr. C. W. Lin and Dr. C. K. Hau for crystallographic assistance. I would also like to thank Ms. Sarah H. Y. Ng for carrying out the variable temperature ^{1}H NMR studies.

Thanks are also given to my group members, especially Dr. George F. Wong and Mr. Lei Yun for their encouragement and helpful suggestions.

Finally, I would like to thank my family for their love and support which gives me strength to overcome any problems.

Chi Wai Au

December 2013

Table of Contents

Abbreviations

General

Me	methyl	Et	ethyl
Pr^i	isopropyl	Bu^n	*n*–butyl
Bu^t	*t*–butyl	Ph	phenyl
Cp	cyclopentadienyl	Cy	cyclohexyl
Ar	aryl	Mes	2,4,6–trimethylphenyl
Ad	adamantyl	THF	tetrahydrofuran
Et_2O	diethyl ether	TMEDA	*N*,*N*,*N*′,*N*′–tetramethylethylenediamine
DME	1,2–dimethoxyethane	r.t.	room temperature
h	hour(s)	d	day(s)
M.p.	melting point	dec.	decomposed
Anal.	analysis	Calc.	calculated

NMR Spectroscopy

s	singlet	d	doublet
dd	double of doublet	t	triplet
q	quartet	m	multiplet
br	broad signal	*m*	meta

p	para	δ	chemical shift
J	coupling constant	ppm	parts per million
Hz	hertz		

UV–Vis Spectroscopy

ε	molar extinction coefficient	λ_{max}	wavelength of maximum absorption
M	molarity		

IR Spectroscopy

w	weak	m	medium
s	strong	br	broad

List of Compounds

Complex **13**	KL^3	$C_{24}H_{40}KN_3Si$	p. 109
Complex **14**	$[KL^5(THF)_2]$	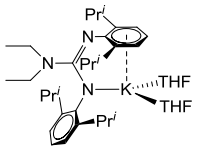	p. 109
Complex **15**	$[\{Eu(L^1)(\mu\text{–}L^1)\}_2]$	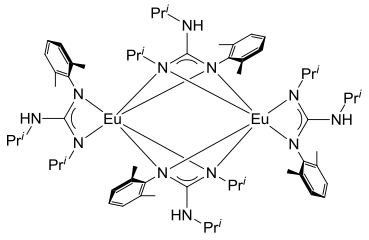	p. 117
Complex **16**	$[\{Eu(L^2)(\mu\text{–}L^2)\}_2 \cdot 2C_6H_{14}]$	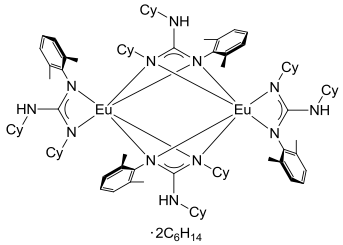	p. 118
Complex **17**	$[\{Yb(L^2)(\mu\text{–}L^2)\}_2]$	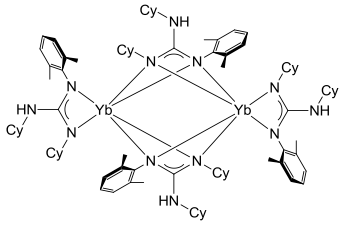	p. 118
Complex **18**	$[Yb(L^2)_2(THF)_2]$	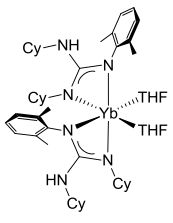	p. 118

Complex **25** $[\{Yb(L^2)_2(\mu\text{–}SePh)\}_2]$ 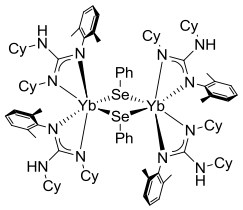 p.146

Complex **26** $[\{Yb(L^2)_2(\mu\text{–}Cl)\}_2]$ 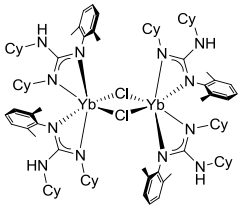 p.146

Complex **27** $[\{Yb(L^2)_2\}_2(\mu\text{–}\eta^2\text{:}\eta^2\text{–}PhNNPh)]$ 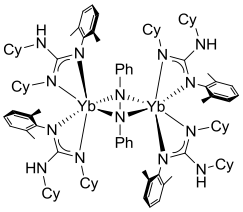 p.147

Complex **28** $[Yb(L^3)_2(\eta^2\text{–}PhNNPh)\cdot PhMe]$ 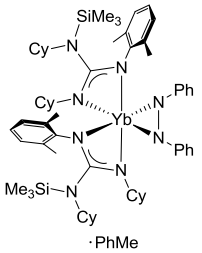 p.147

Complex **29** $[(L^5)_2Sm(\mu\text{–}\eta^3\text{:}\eta^2\text{–}S_2CSCS)Sm(L^5)_2]$ 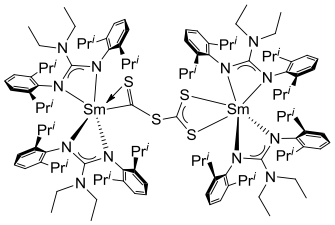 p.148

Complex **30** $[Ce(L^1)_3]$ 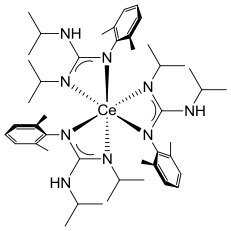 p. 197

Chapter 1

An Overview on Metal Complexes Supported by Guanidinate Ligands

1.1 General Characteristics

Guanidinates, with the general formula of $[(RN)C(NR'_2)(NR)]^-$ (R, R' = H, alkyl, aryl, trimethylsilyl), are close analogues of amidinates $[(RN)C(R')(NR'')]^-$ (Chart 1–1). In both ligand systems the anionic charge can delocalize over the NCN moiety. Guanidinate anions are flexible ligands due to their tunable steric and electronic properties by introduction of various substituents at the nitrogen atoms.

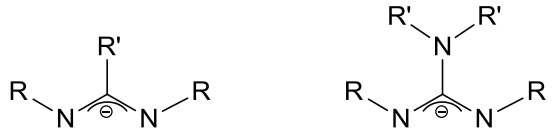

R, R' = H, alkyl, aryl, silyl

Amidinates Guanidinates

Chart 1—1

Compared to amidinates, guanidinate ligands have an extra amino group (NR'_2). The lone–pair electrons on this amino group can delocalize on to the NCN moiety (Chart 1–2). The potential for the formation of imido/diamide type resonance form (B) means that guanidinates are more basic than amidinates. It has been proposed that more basic ligands can provide extra electron density to the metal, reducing its oxidation potential, and hence, capable of stabilizing metal complexes in higher oxidation states.[1] By using cyclic voltammetric method, Bailey and co–workers have proved that the Mo(II) guanidinate complex $[Mo_2\{\mu–\eta^2–(NPh)_2CNHPh\}_4]\cdot 2.2Et_2O$ with oxidation waves at –0.05 and +0.85 V (versus Ag/AgCl) has a lower oxidation potential than its amidinate counterpart

$[Mo_2(form)_4]$ (form = $[(p\text{–tol})NCHN(p\text{–tol})]^-$), which has a higher oxidation potential at +0.21 and +1.3V (versus Ag/AgCl).[1]

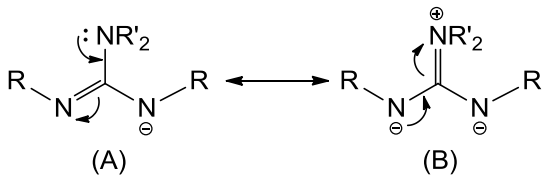

Chart 1—2

Carboxylates, carbamates and trimethylenemethane (TMM) (Chart 1–3) are close analogues of guanidinates. All of them have a Y–shaped geometry, in which the central carbon atom is surrounded by three atoms (C, N or O). Due to the electronegative behavior of O atoms, the negative charge on carobxylates and carbamates can delocalize over the O–C–O ligand backbone. On the other hand, the number of valence electrons in O (two valence electrons) are less than that in N (three valence electrons), this lead to a less variation in ligand substituents in carobxylates and carbamates. TMM is a dianionic ligand, which can bind to the metals in either η^2– or η^3– coordination mode (Chart 1–4). In addition, the TMM ligand can also adopt an η^3– coordination mode. In the latter coordination mode, the TMM ligand undergoes an 'umbrella' distortion in which the three methylene carbon atoms are "leaning" towards the metal atom, whilst the methylene hydrogens are directed away from the metal.[22a] This distortion may be considered as a partial rehybridisation of the methylene carbon atoms from sp^2 to sp^3 such that the lone-pair electrons reside on

these carbon atoms and are directed towards the metal ion.[22a]

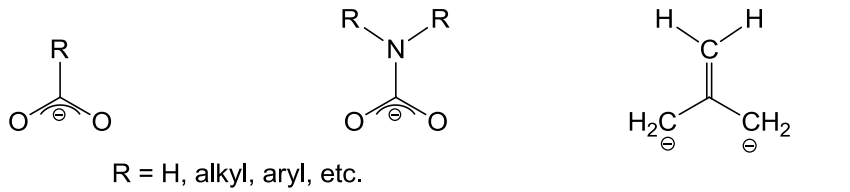

Chart 1—3

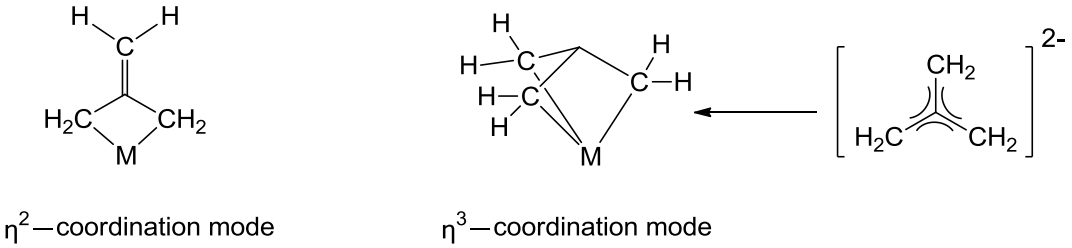

Chart 1—4

1.1.1 Coordination Modes of Guanidinate Ligands

The general coordination modes of guanidinate ligands are shown below (Chart 1–5).

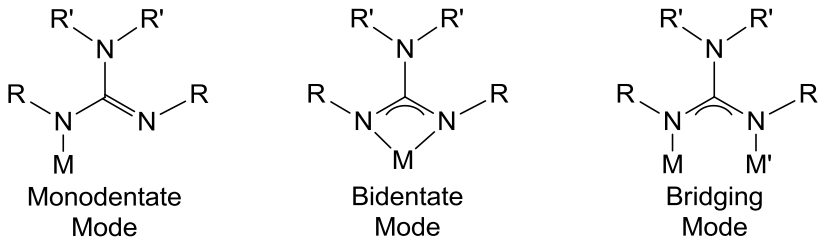

Chart 1—5

The monodentate coordination mode involves the formation of a bond between one of the guanidinate nitrogen atoms and the metal ion. Although several examples of the closely related metal amidinate complexes have been reported to have this type of coordination mode (Chart 1–6),[2a-d] examples of metal guanidinate complexes

which adopt the monodentate coordination mode are rare (Chart 1–7).[2e] This type of coordination mode has been observed when a small metal ion is bonded to a sterically demanding guanidinate ligand.

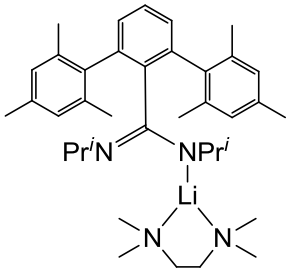

Arnold *et al*.[2a]

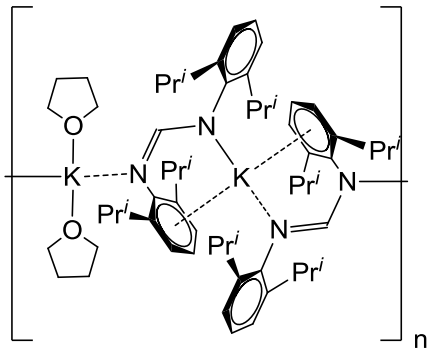

Junk *et al*.[2b]

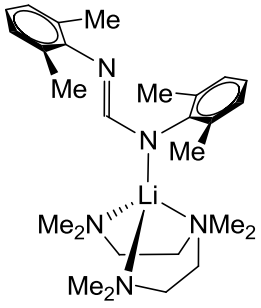

Junk *et al*.[2c]

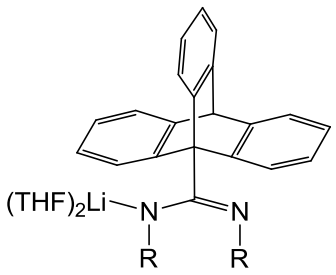

R = Pr^i, Cy

Jones *et al*.[2d]

Chart 1—6

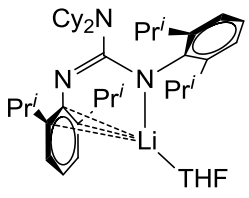

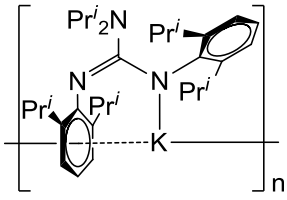

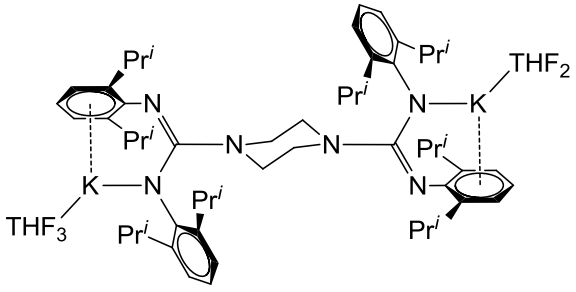

Junk *et al*.[2e]

Chart 1—7

The bidentate coordination mode is the most common coordination mode. It involves a σ,σ' bond formation between the two guanidinate nitrogen atoms and a metal, which results in a highly strained four–member $\overline{\text{MNCN}}$ ring. The N–M–N bite angle is generally acute (varies from 50° to 70°). Several examples of metal guanidinate complex bearing a bidentate coordination mode are shown in Chart 1–8.[3,16b]

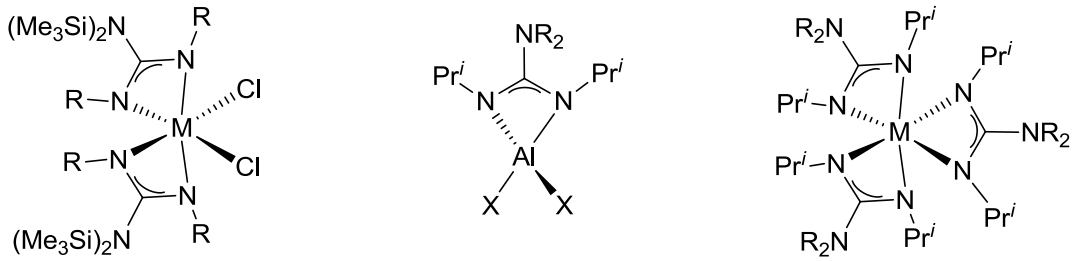

Chart 1—8

For the bridging coordination mode, the guanidinate ligand is shared by two metal ions. Each nitrogen atom forms a σ bond with one of the metal centers. This type of coordination mode is generally observed with most of the d–block metals.[4] Guanidinate ligands exhibiting this type of coordination mode always have less bulky substituents around the nitrogen atoms. The ligand substituents become less repelled and the nitrogen lone pairs adopt a close to parallel alignment (Chart 1–9). In contrast, guanidinate ligands with more bulky substituents have the nitrogen lone pairs converge to the same metal, resulting in a bidentate coordination mode.

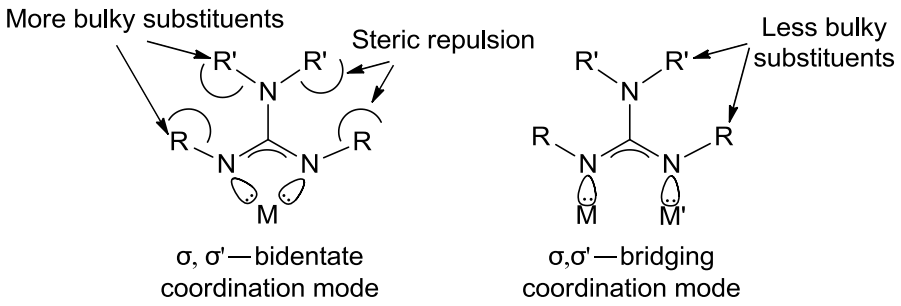

Chart 1—9

1.1.2 Preparation Methods

General synthetic methods for guanidinate ligands are shown below:

1) Insertion of carbodiimide into a metal–nitrogen bond:

This synthetic method can be applied to the preparations of transition metal and lanthanide guanidinate complexes, or the preparation of Group 1 guanidinate complexes as ligand–transfer reagents (Scheme 1–1).[5]

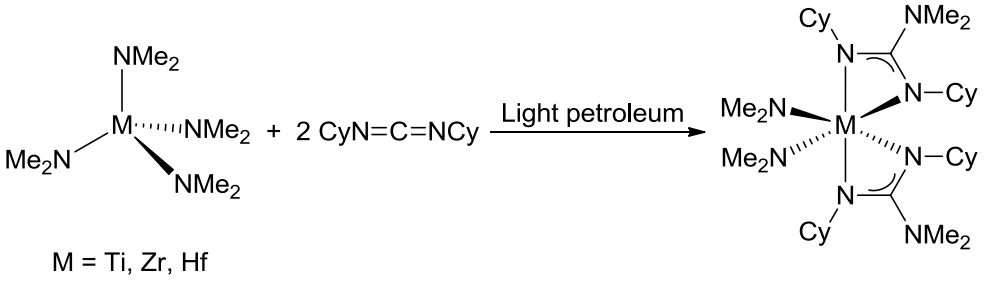

Scheme 1—1[5]

2) Deprotonation of a free guanidine with metal alkyl reagents:

The reaction of a free guanidine with a metal alkyl reagent, undergoes a ligand substitution process, gives the corresponding metal guanidinate complex and a volatile alkane (Scheme 1–2).[6] This synthetic route is not applicable to

the preparations of lanthanide metal guanidinates due to the limited access to lanthanide alkyls.

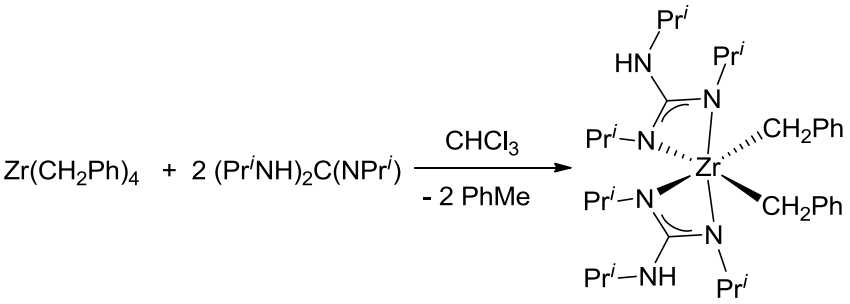

Scheme 1—2[6]

3) Salt metathesis reactions between a metal halide and a metal guanidinate

A metal halide reacts with a metal guanidinate through a metal–metal exchange process to form the targeted metal guanidinate complex. This is the most common method for the preparations of transition metal or lanthanide guanidinate complexes due to the availability of metal halides (Scheme 1–3).[7] Group 1 metal guanidinates are often used as ligand–transfer reagents, which can be prepared by Method 1 or Method 2 as described above.

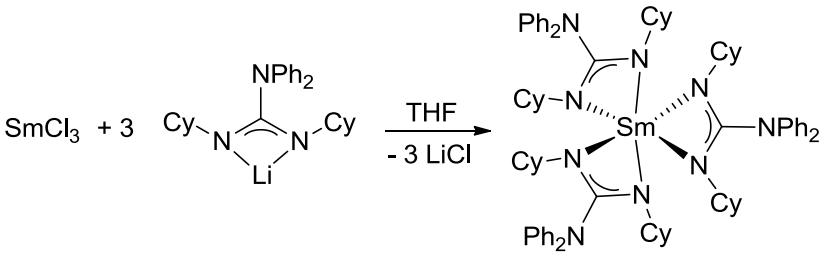

Scheme 1—3[7]

1.2 The Coordination Chemistry of Guanidinate Ligands with Different Groups of Metals

After Wade and coworkers reported the first metal guanidinate complex in 1968,[8] a number of metal guanidinate complexes were successfully synthesized in the following decades. Nowadays, the coordination chemistry of guanidinates covered nearly all metal groups, including the main–group metals, transition metals and the rare earth metals.

1.2.1 Main–Group Metal Guanidinates

Group 1 Metal Guanidinates

Group 1 metal guanidinate complexes are generally used as ligand transfer reagents. The first example of alkali–metal guanidinate, $[(Me_2N)_2CNLi]_2$, was reported in 1968.[8] Unfortunately, the solid state structure of this complex was not determined. It was not until 1983 that the first structurally characterized alkali–metal guanidinate complex was reported (Scheme 1–4).[9]

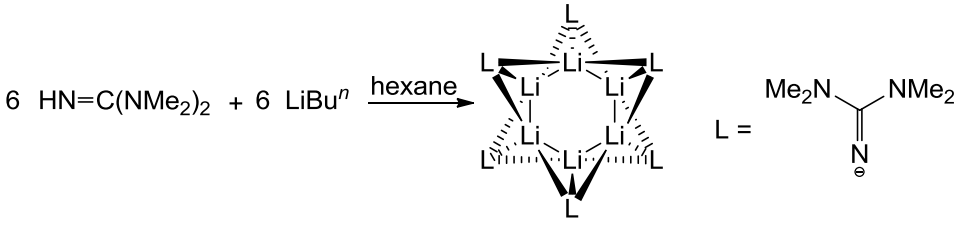

Wade *et al*.[9]

Scheme 1—4

Because Group 1 guanidinate compounds were often generated in situ for use as ligand–transfer reagents in transmetallation reactions, not many examples of these complexes were structurally characterized. Recently, a few examples of Group 1 metal guanidinate complexes with monomeric, dimeric and polymeric structures have been reported (Chart 1–10).[2e, 10.]

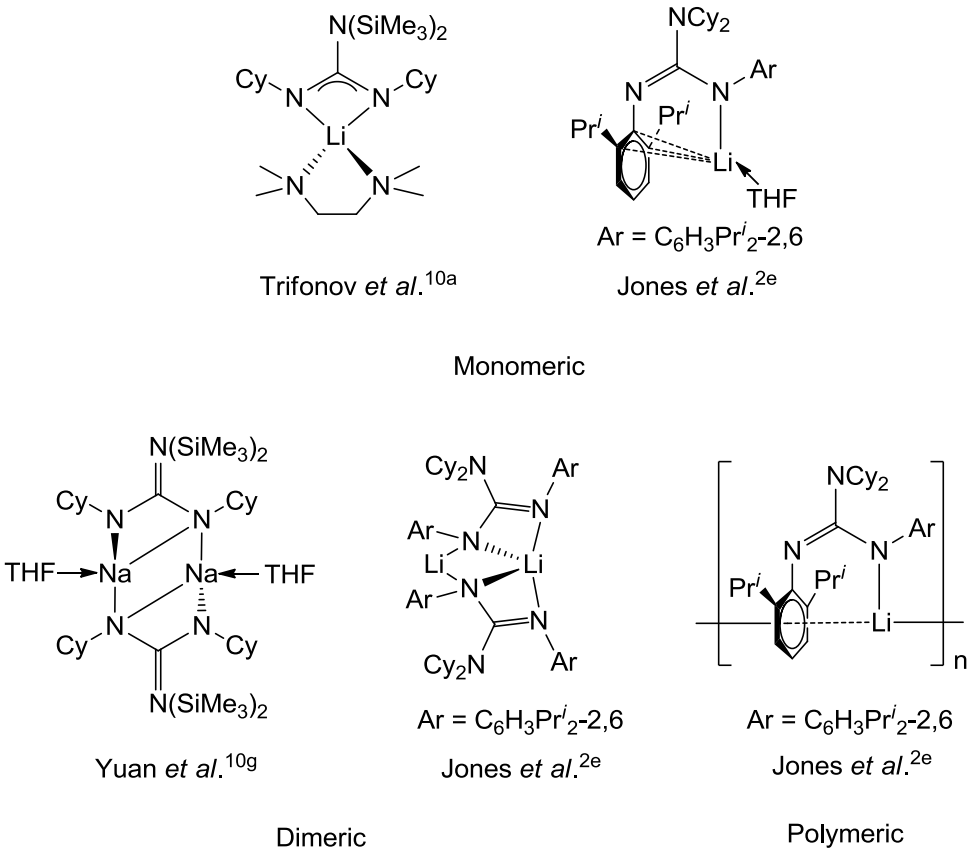

Chart 1—10

Group 2 Metal Guanidinates

It is noted that cations of a high charge–to–ionic–radius ratio exert a greater effect in polarizing anions. Therefore, the character of a metal–ligand bond changes from one with a higher covalent bond character to one with more ionic bond character

when going down the group. For the heavier Group 2 metals, Ca^{2+} and Sr^{2+}, they are sometimes used to compare with the rare earth elements, Sm^{2+}, Eu^{2+} and Yb^{2+}.[11] This is not only because of a similarity in their ionic radii (Ca^{2+} : 1.00 Å, Yb^{2+} : 1.02 Å; Sr^{2+} : 1.18 Å, Sm^{2+} : 1.22 Å, Eu^{2+} : 1.17 Å),[12] but also their bonding characters (due to poor shielding of the 4f orbitals, metal–ligand bonds are predominantly ionic in lanthanide complexes).

Recently, a series of Mg(II), Ca(II), Sr(II) and Ba(II) guanidinate complexes have been reported (Chart 1–11).[13] A few examples of Group 2 metal guanidinate complexes were reported to be catalysts for hydroamination reactions or styrene polymerization reactions.[13b,d]

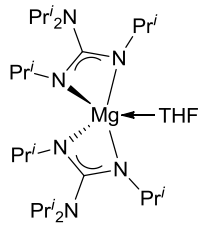

Chang *et al*.[13a]

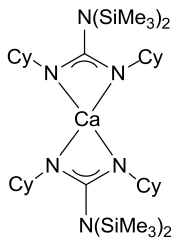

Harder *et al*.[13b]

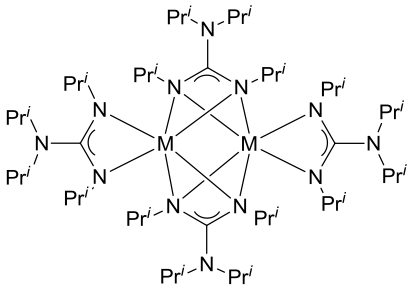

M = Sr, Ba

Cameron *et al*.[13c]

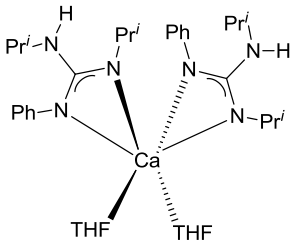

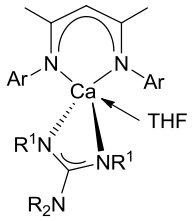

R$_2$N = ArNH, R^1 = Pr^i,Cy
R$_2$N = Ph$_2$N, R^1 = Cy
Ar = C$_6$H$_3$Pr$^i_2$-2,6

Barrett *et al*.[13d,e]

Chart 1—11

By increasing the steric bulkiness of the ligand, Group 2 metal guanidinates can form heteroleptic complexes of the form LMX (L = guanidinate ligand, M = Group 2 metal, X = halide). The latter type of metal complexes are potential precursors for the synthesis of dimeric metal(I) complexes, LMML, which could be obtained by the reduction of LMX with potassium metal or potassium graphite (KC_8). In 2007, Jones and co–workers have reported on the first example of a Mg(I) complex supported by the bulky guanidinate ligand $[ArNC(NPr^i_2)NAr]^-$ ($Priso^-$). The precursor complex $[(Priso)Mg(\mu–I)_2Mg(OEt_2)(Priso)]$ was first prepared by the reaction of the free guanidine PrisoH with equal molar amount of Grignard reagent MeMgI (Scheme 1–5).[14] Treatment of $[(Priso)Mg(\mu–I)_2Mg(OEt_2)(Priso)]$ with excess potassium metal led to the formation of di–Mg(I) complex, $[(Mg(Priso)]_2$. The Mg–Mg bond in this Mg(I) complex measured 2.851(1) Å.

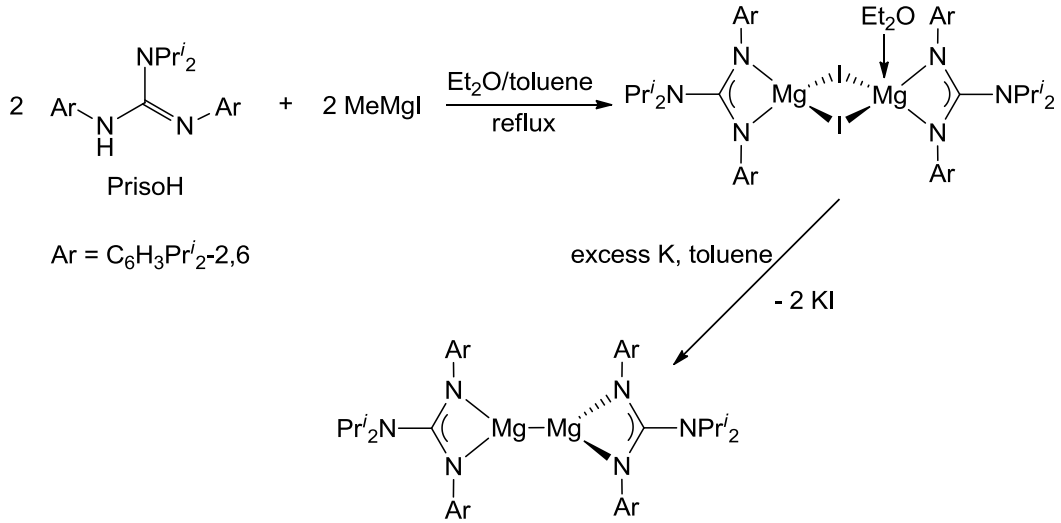

Jones *et al.*[14]

Scheme 1—5

Group 13 Metal Guanidinates

Group 13 guanidinates are active catalysts and potential precursors to important materials in industries.[15,16b,] Early development in the chemistry of Group 13 guanidinates was focused on Al(III) complexes. In 1998, Chang and coworkers have studied the reaction of AlR_3 (R = Me, Et) and AlX_2Y (X = Cl, R; Y = Cl, NR'_2) with 1,3–diisopropyl– and 1,3–di–tert–butylcarbodiimides in various stoichiometric ratios.[16a] Jordan and co–workers have also reported on the synthesis and characterization of a series of Al(III) alkyl complexes containing guanidinate ligands $[R_2NC(NPr^i)_2]^-$ [R = Me, Et, Pr^i] and 1,3,4,6,7,8–hexahydropyrimido[1,2–a]pyrimidinate (hpp^-).[16b] Using the $[Me_2NC(NPr^i)_2]^-$ ligand, Barry and co–workers have successfully prepared a series of Al(III) guanidinate complexes $[\{Me_2NC(NPr^i)_2\}_nAl(NMe_2)_{3-n}]$ [n = 1, 2, 3].[16c]

Low valent guanidinate complexes of the heavier elements Ga, In and Tl were first reported in 2006.[17] By using a sterically demanding ligand, $[(Ar)NC(NCy_2)N(Ar)]^-$ ($Giso^-$), Jones and co–workers have successfully isolated monovalent Ga(I), In(I) and Tl(I) guanidinate complexes [M(Giso)] (M = Ga, In and Tl) (Scheme 1–6). Interestingly, the guanidinate ligand exhibits different coordination modes in these complexes. It binds to Ga(I) and In(I) in a *N*,*N'*–chelating mode, but is bonded in a *N*,arene–chelating mode in the Tl(I)

derivative. Conceivably, this difference in the coordination behaviour of the Giso$^-$ ligand may be attributed to a difference in the ionic size of Ga(I)→Tl(I).

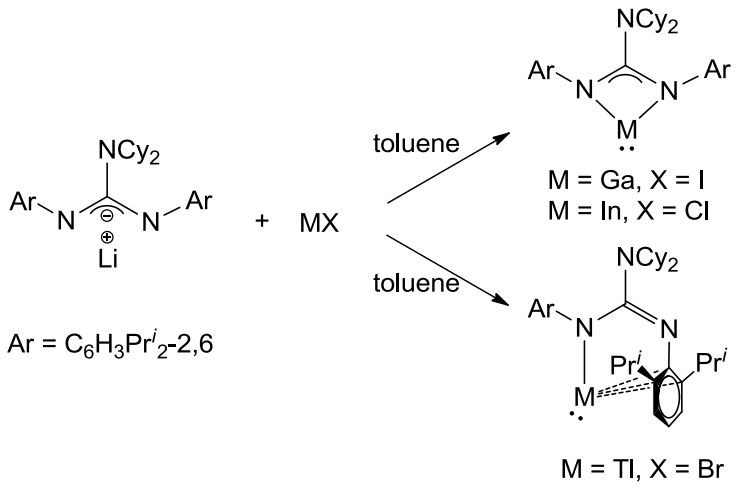

Jones *et al*.[17]

Scheme 1—6

Group 14 Metal Complexes

In 2002, Richeson and co–workers have successfully isolated the first Sn(II) and Sn(IV) guanidinate complexes using *N*,*N*′,*N*″–trialkylguanidinate ligands $[(RN)_2C(NRH)]^-$ (R = cyclohexyl and isopropyl), and the 1,3,4,6,7,8–hexahydropyrimido[1,2–a]pyrimidinate (hpp^-) ligand (Scheme 1–7 to Scheme 1–9).[18]

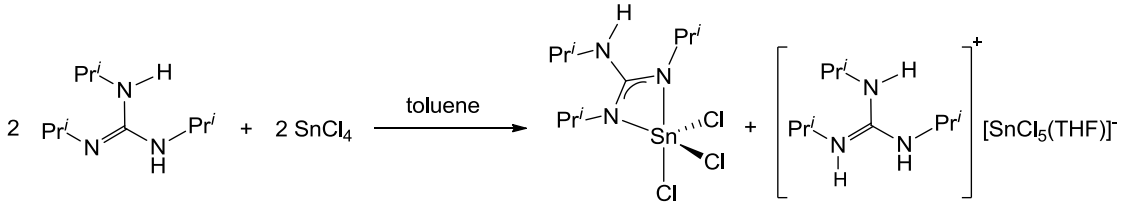

Richeson *et al*.[18]

Scheme 1—7

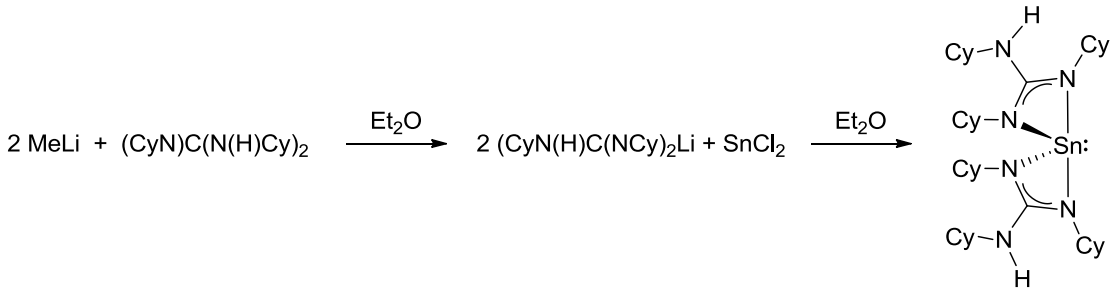

Richeson *et al*.[18]

Scheme 1—8

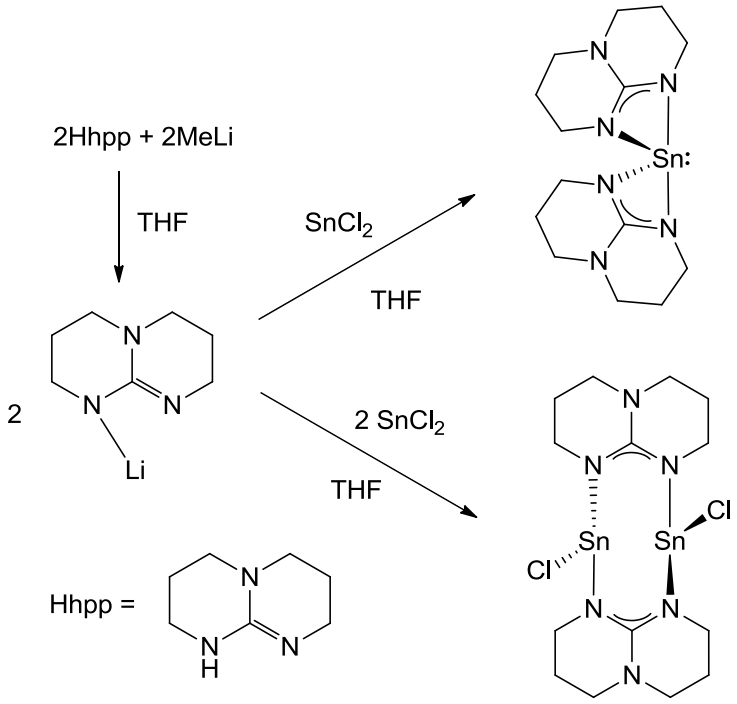

Richeson *et al*.[18]

Scheme 1—9

In 2006, Jones and co–workers reported on the first Ge(I) guanidinate complex, $[Ge(Giso)]_2$ (Giso = $[(Ar)NC(NCy_2)N(Ar)]^-$; Ar = 2,6–$Pr^i_2C_6H_3$). The precursor complex [Ge(Giso)Cl] was prepared by a two–step procedure: GisoH was first deprotonated by $LiBu^n$, followed by the reaction with one equivalent of $GeCl_2$·dioxane (Scheme 1–10).[19] Treatment of [Ge(Giso)Cl] with excess potassium metal in toluene gave the Ge(I) dimer, $[Ge(Giso)]_2$. The solid–state structure of the

latter complex was determined by X–ray crystallography, which revealed a Ge(I)–Ge(I) bond distance of 2.672(1) Å.[19]

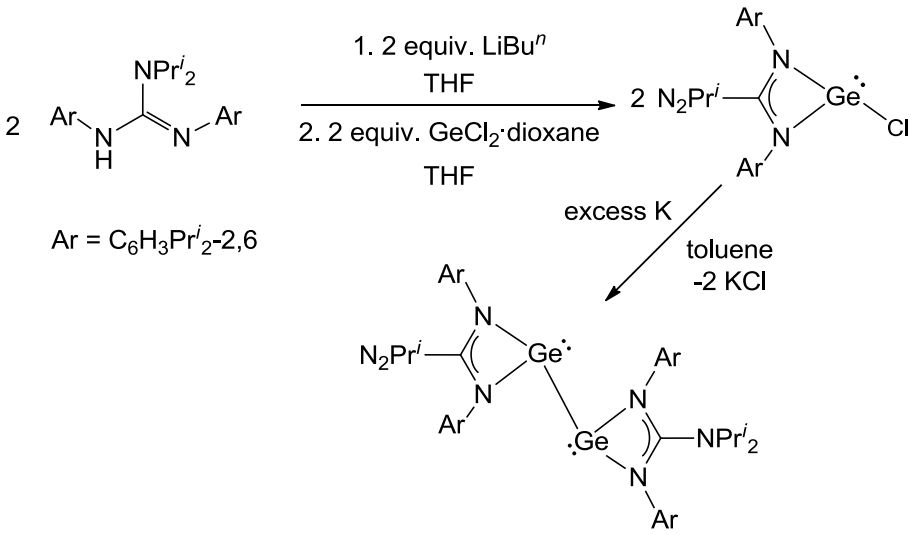

Jones *et al*.[19]

Scheme 1—10

Group 15 Guanidinate Complexes

Group 15 guanidinate complexes are rare as compared to their Group 13 and Group 14 counterparts. Bailey and co–workers have prepared a Sb(III) complex, [Sb{(Pr^{i}N)$_2$CNHPr^i}{(Pr^{i}N)$_2$CNPr^i}] by the reaction of 1,2,3–triisopropylguanidine [(Pr^{i}NH)$_2$C=NPr^i] with antimony tris(dimethylamide) [Sb(NMe$_2$)$_3$] (Scheme 1–11).[20]

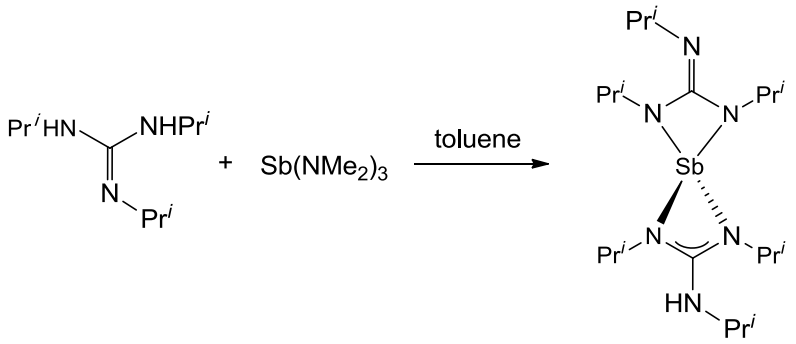

Bailey *et al*.[20]

Scheme 1—11

Recently, Jones and co–workers have performed a synthetic study on As(III) and Sb(III) guanidinate complexes (Scheme 1–12).[21] Reduction of [As(Priso)Cl_2] (Priso = [(Ar)NC(NPr$^i_2$)N(Ar)]$^-$; Ar = 2,6–Pr^{i}C$_6$H$_3$) or [As(Giso)Cl_2] (Giso = [(Ar)NC(NCy$_2$)N(Ar)]$^-$; Ar = 2,6–Pr$^i_2$C$_6$H$_3$) with excess KC_8 yielded the corresponding As(I) complexes, [As(Priso)]$_2$ and [As(Giso)]$_2$.

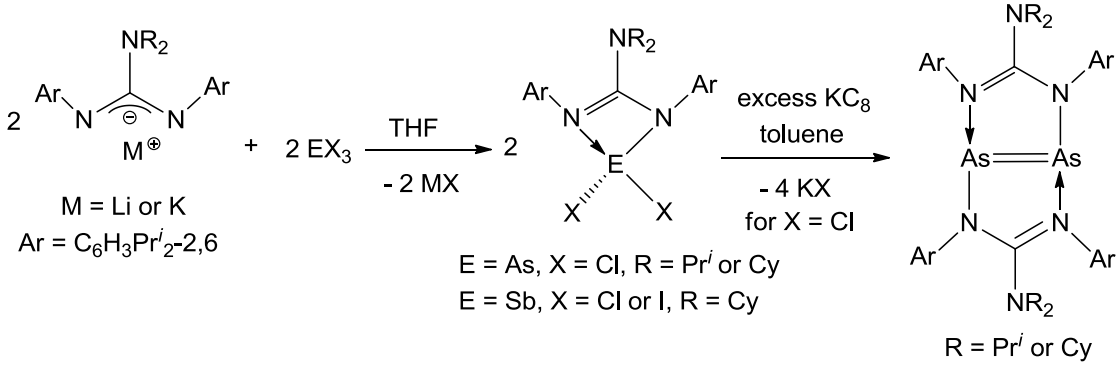

Jones *et al*.[21]

Scheme 1—12

1.2.2 Transition Metal Guanidinates

The coordination chemistry of guanidinate ligands with transition metals has been extensively studied in the past decades.[4,22] The first transition metal guanidinate complexes, [(Me$_2$N)$_2$M{(CyN)$_2$CNMe$_2$}$_2$] (M = Ti, Zr, Hf), were reported by Lappert and co–workers in 1970 (Scheme 1–13).[5]

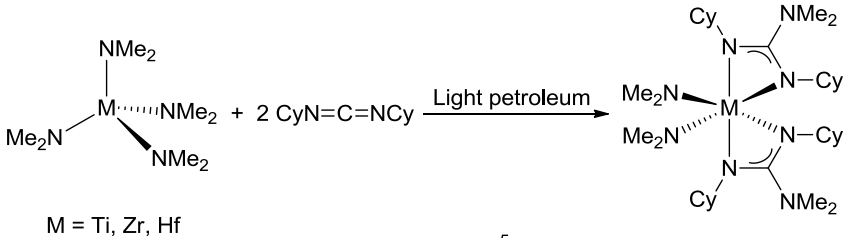

Lappert *et al*.[5]

Scheme 1—13

In the following decades, considerable research efforts have been devoted to the study of the reaction chemistry of transition metal guanidinate complexes. These included small molecule activation and the applications of transition metal guanidinate complexes in industrial chemistry, such as olefin polymerization (Scheme 1–14)[23] and hydroamination of alkynes (Scheme 1–15).[24]

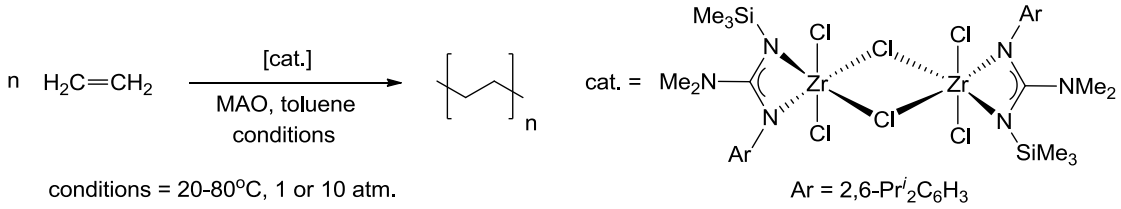

Zhou *et al*.[23]

Scheme 1—14

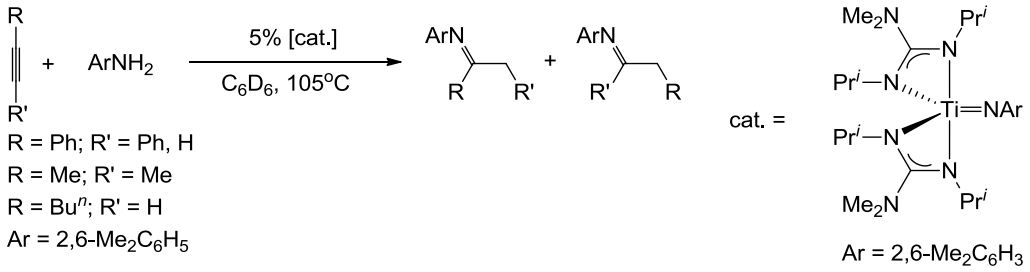

Richeson *et al*.[24]

Scheme 1—15

In general, the guanidinate ligands in these complexes exhibit two common coordination modes, namely the *N*,*N*′–chelating mode and the *N*,*N*′–bridging mode. Cotton and co–workers have reported on a number of dimeric transition metal guanidinates, which contain a $M_2(\mu\text{–guanidinate})_n$ (n = 3, 4) core.[4,25] These complexes generally exhibit a "paddlewheel" or "lantern" structure, with metal–metal multiple bonds. One representative example of these "paddlewheel" complexes is $[Ru_2(hpp)_4Cl_2]$ (hpp^- = 1,3,4,6,7,8–hexahydropyrimido[1,2–a]pyrimidinate), which

was reported in 1996 (Scheme 1–16).[26] Afterwards, Cotton and co–workers have reported on a series of middle and late transition metal complexes of the hpp⁻ ligand. All of these complexes contain metal–metal multiple bonds (Chart 1–12).[25]

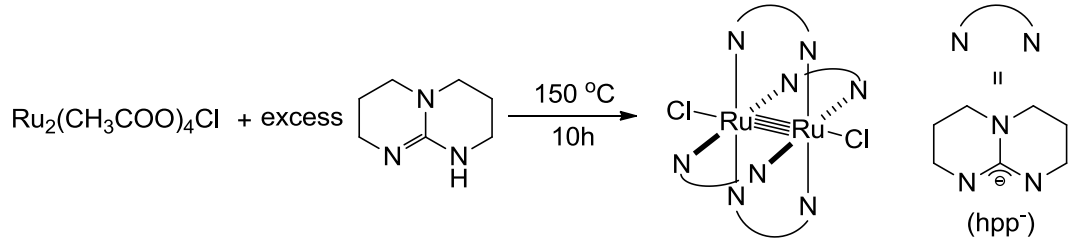

Bear *et al*.[26]

Scheme 1—16

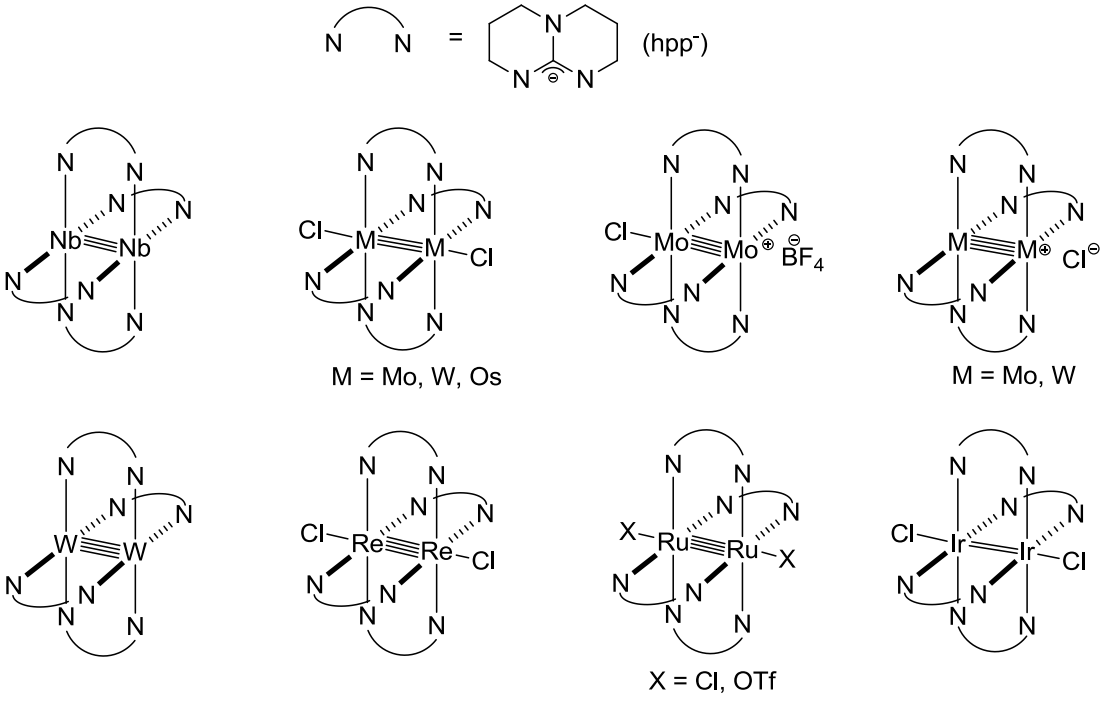

Cotton *et al*.[25]

Chart 1—12

Recently, Jones and co–workers have successfully synthesized the first cobalt(I) guanidinate complexes (Scheme 1–17).[27] By using the $[(Ar)NC(NCy_2)N(Ar)]^-$ ($Giso^-$) and $[(Ar)NC(NPr^i_2)N(Ar)]^-$ ($Priso^-$) ligands, monomeric cobalt(I) guanidinate

complexes [(Giso)Co(η^6–toluene)], [(Priso)Co(η^6–toluene)] and dimeric [{Co(μ–Giso)}$_2$] were prepared. The dimeric Co(I) complex, [{Co(μ–Giso)}$_2$], was found to have a Co–Co metal bond of 2.1345(7) Å, which is shorter than a normal Co–Co single bond, and, hence, it is considered to have a double bond character.

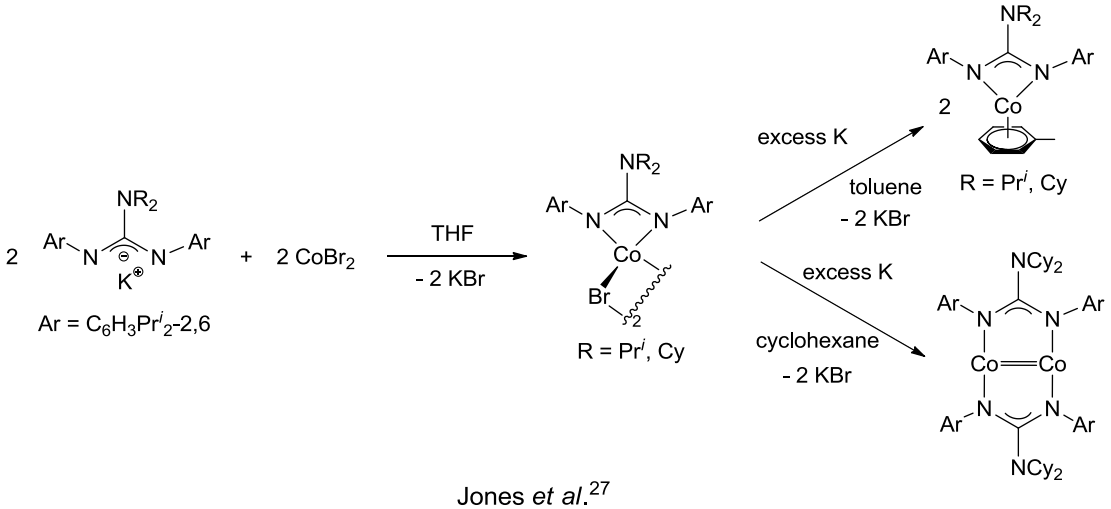

Jones *et al*.[27]

Scheme 1—17

Very recently, Jones and co–workers have isolated the first iron(I) guanidinate complex by employing the sterically more bulky [(ArN)$_2$C(*cis*–2,6–Me$_2$NC$_5$H$_8$)]$^-$ (Pipiso$^-$) ligand (Scheme 1–18).[28] Instead of using the readily accessible magnesium and potassium metal as reducing agents, a milder reducing agent, [{(^{Mes}Nacnac)Mg}$_2$] (^{Mes}Nacnac$^-$ = {[2,6–(2,4,6–Me$_3$–C$_6$H$_2$)N(Me)C)]$_2$CH}$^-$) was employed in their study. The iron(I) complex crystallized in a dimeric form with an Fe–Fe bond length of 2.1270(7) Å, which is considered to have a double bond character.

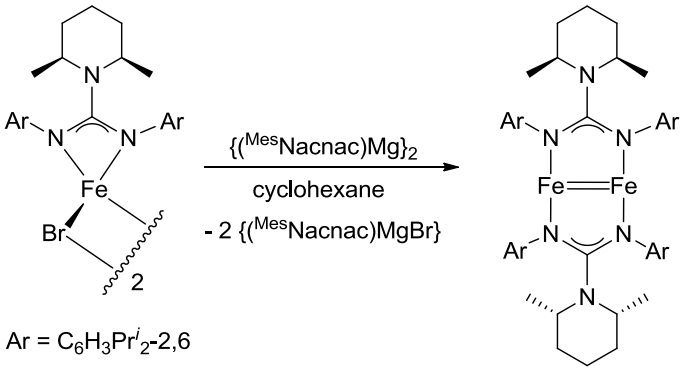

Jones *et al*.[28]

Scheme 1—18

Among first row transition metals, chromium has the potential to form the shortest metal–metal multiple bond due to the possible formation of a quintuple bond between two chromium atoms. The first di–chromium(I) complex [Ar'CrCrAr'] (Ar' = C_6H_3–2,6(C_6H_3–2,6–Pr^i_2)$_2$),[29a] was reported by Power and co–workers. Later, several dimeric chromium(I) complexes with metal–metal bond were reported by Theopold,[29b] Kempe[29c] and Tsai[29d,e] (Refer to Chapter 2 for detailed description). In 2009, Kempe and co–workers have isolated the first chromium(I) guanidinate complex [Cr{$Me_2NC(NAr)_2$}]$_2$ by treating the dimeric chromium(II) complex [Cr{$Me_2NC(NAr)_2$}Cl]$_2$, with excess KC_8 in a THF solution (Scheme 1–19).[30] This chromium(I) complex has a short Cr–Cr distance of 1.729(1) Å.

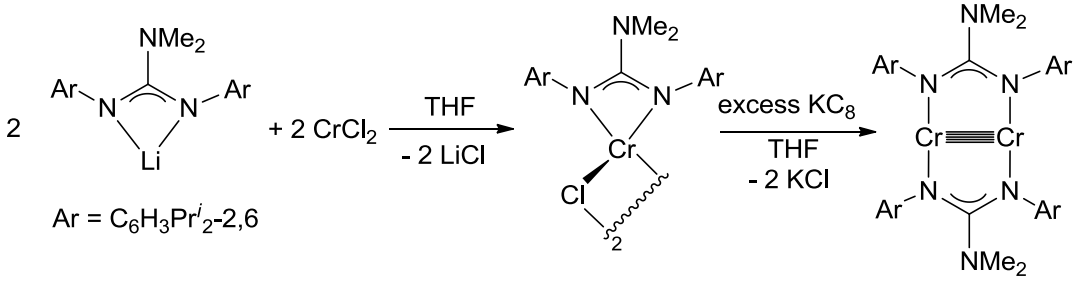

Kempe *et al*.[30]

Scheme 1—19

1.2.3 Rare Earth Metal Guanidinates

The lanthanide metals together with scandium and yttrium are known as rare earth metals. The most common oxidation state for rare earth metals is the +3 oxidation state. The simplest rare earth metal guanidinate complexes have the formulation of $[Ln(L)_3]$ (Ln = rare earth metals, L = guanidinate ligands). Shen and co–workers have prepared a few lanthanide(III) tris(guanidinate) complexes by (i) addition of a carbodiimide to a lanthanide(III) amide (Scheme 1–20),[7] and (ii) the direct reaction of an alkali metal guanidinate with a lanthanide(III) trichloride (Scheme 1–21).[7]

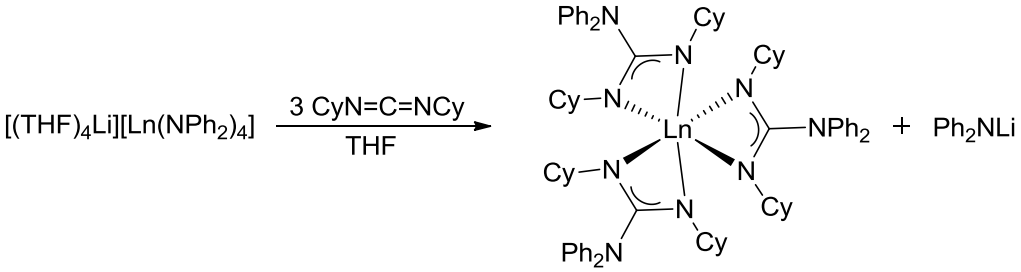

Shen *et al*.[7]

Scheme 1—20

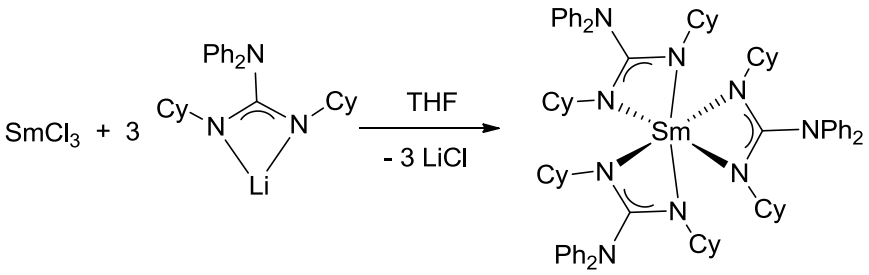

Shen *et al*.[7]

Scheme 1—21

Lanthanide(II) guanidinate complexes are rare as compared to their

lanthanide(III) counterparts. The first lanthanide(II) guanidinate complex, $[CyNC(NSiMe_3)_2NCy]_2Yb(TMEDA)$, was reported by Richeson and co–workers (Chart 1–13).[31] Later, Jones and co–workers have used the bulky $[(Ar)NC(NCy_2)N(Ar)]^-$ ($Giso^-$) and $[(Ar)NC(NPr^i_2)N(Ar)]^-$ ($Priso^-$) ligands to support a series of Sm(II), Eu(II) and Yb(II) complexes.[32a,b] Please refer to Chapter 3 for a detailed description on the chemistry of lanthanide(II) guanidinates.

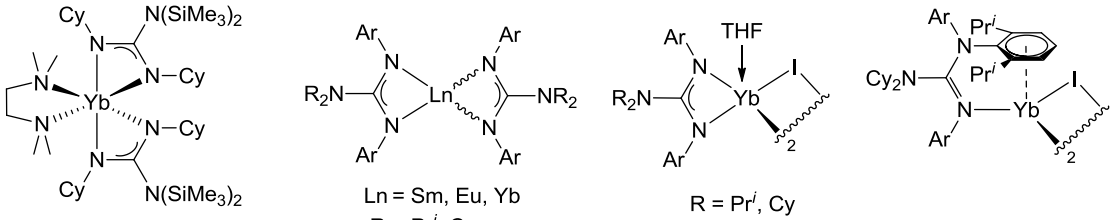

Richeson *et al*.[31] Jones *et al*.[32a,b]

Chart 1—13

Lanthanide guanidinate complexes were found to have promising catalytic properties towards polymerization reactions.[22b,33] Two important polymerization reactions are summarized as follows.

Olefin Polymerizations

In 2004, Trifonov and co–workers have carried out a preliminary study on the polymerization of ethylene, propylene and styrene using the lutetium(III) hydride complex $[Lu\{(Me_3Si)_2NC(NPr^i)_2\}_2(\mu\text{–}H)]_2$ as an initiator (Scheme 1–22).[34] The

lutetium(III) complex was found to be active towards polymerization of ethylene, and maintained its catalytic property after three days. Unexpectedly, the lutetium(III) complex can also catalyze the polymerization of propylene without loss of catalytic property within one hour. This catalytic property is not commonly observed for other lanthanide complexes.

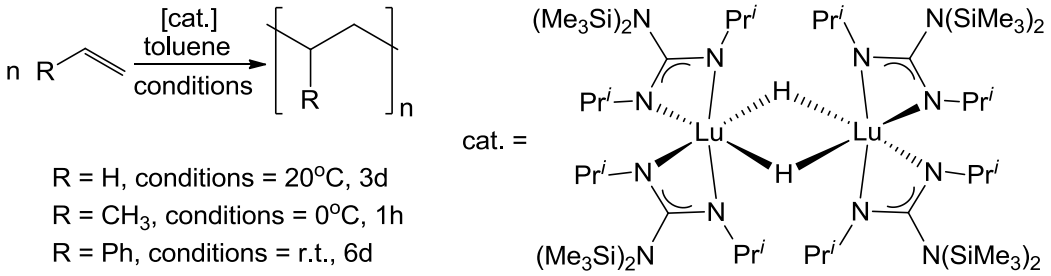

Trifonov *et al*.[34]

Scheme 1—22

Cyclic Ester Polymerizations

Lanthanide(III) complexes are oxophilic and, thus, they are good initiators for polymerization of lactone monomers. Cyclic esters (Chart 1–14), can be readily polymerized by releasing their ring strain in the presence of a catalyst (Scheme 1–23).

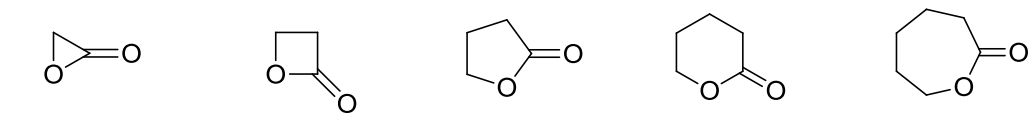

Chart 1—14

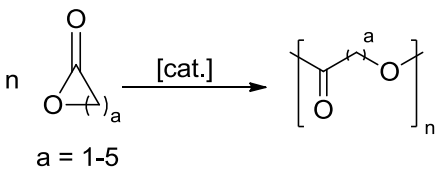

Scheme 1—23

Lanthanide catalyzed ring–opening polymerization of cyclic esters provides an efficient access to polyesters with controlled and narrow molecular weight distributions. Recently, Shen and co–workers have prepared a few lanthanide(III) bis(guanidinate) complexes [{$(SiMe_3)_2NC(NPr^i)_2$}$_2$Ln(μ–Me)$_2$Li(TMEDA)] (Ln = Yb, Nd)[35a] and tris(guanidinate) complexes [{R'NC(NR")$_2$}$_3$Ln·$(Et_2O)_n$] (Ln = Yb, n = 1, R' = Pr^i_2, R" = Cy; Ln = Nd, n = 0, R' = Pr^i_2, R" = Pr^i, Cy; Ln = Nd, n = 0, R' = $(CH_2)_5$, R" = Pr^i).[35b] These complexes could catalyze the ring–opening polymerization of ε–caprolactone. In their studies, [Nd{$(Pr^i_2N)C(NPr^i)_2$}$_3$][35b] was found to be an active initiator, even when the monomer–to–initiator ratio was raised up to 2000:1. The conversion approached to 100% within 5 minutes.

1.3 Objectives of This Work

As it has been mentioned in the previous sections, guanidinate ligands belong to a class of versatile ligands which form stable complexes with interesting structures and oxidation states. Recently, a series of first row late transition metal complexes supported by unsymmetrical guanidinate ligands $[(2,6\text{–}Me_2C_6H_3N)C(NRR')NR']^-$ (R = H, R' = Pr^i, Cy; R = $SiMe_3$, R' = Cy) have been prepared by our research group.[36] Continuing our study on the coordination behaviour of these guanidinate ligands with transition metals, we extended our work to the chemistry of divalent chromium guanidinates (Chapter 2).

Divalent lanthanide guanidinates are rare. There are only few reports on their chemistry.[31,32] Accordingly, we carried out a detailed synthetic and reactivity studies on lanthanide(II) (Sm(II), Eu(II), Yb(II)) complexes derived from $[(2,6\text{–}Me_2C_6H_3N)C(NRR')NR']^-$ (R = H, R' = Pr^i, Cy; R = $SiMe_3$, R' = Cy) and $[(2,6\text{–}Pr^i{}_2C_6H_3N)C(NEt_2)(NC_6H_3Pr^i{}_2\text{–}2,6)]^-$ ligands (Chapter 3). Our study is the first systematic investigation on the coordination properties of guanidinate ligands with divalent lanthanide ions. Besides, a series of lanthanide(III) derivatives of the $[(2,6\text{–}Me_2C_6H_3N)C(NHPr^i)NPr^i]^-$ ligand were also prepared in this work. The coordination chemistry of this ligand towards $LnCl_3$ (Ln = Ce, Pr, Gd, Tb, Ho, Er, Tm, Lu) in different stoichiometric ratios was studied (Chapter 4).

1.4 References for Chapter 1

1. (a) Bailey, P. J.; Bone, S. F.; Mitchell, L. A.; Parsons, S.; Taylor, K. J.; Yellowless, L. J. *Inorg*. *Chem*. **1997**, 867–871.

   (b) Cotton, F. A.; Feng, X.; Matusz, M. *Inorg*. *Chem*. **1989**, 594–601.

2. (a) Schmidt, J. A. R.; Arnold, J. *Chem*. *Commun*. **1999**, 2149–2150.

   (b) Cole, M. L.; Junk, P. C. *J*. *Organomet*. *Chem*. **2003**, *666*, 55–62.

   (c) Cole, M. L.; Davies, A. J.; Jones, C.; Junk, P. C. *New J*. *Chem*. **2005**, *29*, 1404–1408.

   (d) Baker, R. J.; Jones, C. *J*. *Organomet*. *Chem*. **2006**, *691*, 65–71.

   (e) Jin, G.; Jones, C.; Junk, P. C.; Lippert, K. -A.; Rose, R. P.; Stasch, A. *New J*. *Chem*. **2009**, *33*, 64–75.

3. (a) Wood, D.; Yap, G. P. A.; Richeson, D. S. *Inorg*. *Chem*. **1999**, *38*, 5788–5794.

   (b) Devi, A.; Milanov, A. P.; Fischer, R. A. *Inorg*. *Chem*. **2008**, *47*, 11405–11416.

4. Cotton, F. A.; Murillo, C. A.; Walton, R. A. *Multiple Bonds Between Metal Atoms*, 3rd ed., Springer, New York, **2005**.

5. Chandra, G.; Jenkins, M. F.; Lappert, M. F.; Srivastava, R. C. *J*. *Chem*. *Soc*. **1970**, 2550–2558.

6. Bazinet, P.; Wood, D.; Yap, G. P. A.; Richeson, D. S. *Inorg. Chem.* **2003**, *42*, 6225–6229.

7. Zhou, L.; Yao, Y.; Zhang, Y.; Xue, M.; Chen, J.; Shen, Q. *Eur. J. Inorg. Chem.* **2004**, 2167–2172.

8. Pattison, I.; Wade, K.; Wyatt, B. K. *J. Chem. Soc. A* **1968**, 837–842.

9. Clegg, W.; Snaith, R.; Shearer, H. M. M.; Wade, K.; Whitehead, G. *J. Chem. Soc. Dalton Trans*. **1983**, 1309–1317.

10. (a) Trifonov, A. A.; Lyubov, D. M.; Fedorova, E. A.; Fukin, G. K.; Schumann, H.; Mühle, S.; Hummert, M.; Bochkarev, M. N. *Eur. J. Inorg. Chem.* **2006**, 747–756.

(b) Giesbrecht, G. R.; Shafir, A.; Arnold, J. *J. Chem Soc., Dalton Trans.* **1999**, 3601–3604.

(c) Coles, M. P.; Hitchcock, P. B. *Chem. Commun.* **2005**, 3165–3167.

(d) Pang, X.; Yao, Y.; Wang, J.; Sheng, H.; Zhang, Y.; Shen, Q. *Chin. J. Chem.* **2005**, *23*, 1193–1197.

(e) Luo, Y.; Yao, Y.; Zhang, Y.; Shen, Q. *Chin. J. Chem.* **2007**, *25*, 562–565.

(f) Zhou, M.; Tong, H.; Wei, X.; Liu, D. *J. Organomet. Chem.* **2007**, *692*, 5195–5202.

(g) Yuan, F.; Zhu, Y.; Xiong, L. *J. Organomet. Chem.* **2006**, *691*, 3377–3382.

(h) Ong, T.; O'Brien, J. S.; Korobkov, I.; Richeson, D. S. *Organometallics* **2006**, *25*, 4728–4730.

11. (a) Hu, H.; Cui, C. *Organometallics* **2012**, *31*, 1208–1211.

(b) Glock, C.; Loh, C.; Görls, H.; Krieck, S.; Westerhausen, M. *Eur. J. Inorg. Chem.* **2013**, 3261–3269.

12. Shannon, R. D. *Acta Cryst.* **1976**, *A32*, 751–767.

13. (a) Srinivas, B.; Chang, C. -C.; Chen, C.; Chiang, M. Y.; Chen, I.; Wang, Yu.; Lee, G. *J. Chem. Soc., Dalton Trans.* **1997**, 957–963.

(b) Fell, F.; Harder, S. *Eur. J. Inorg. Chem.* **2005**, 4438–4443.

(c) Cameron, T. M.; Xu, C.; Dipasquale, A. G.; Rheingold, A. L. *Organometallics* **2008**, *27*, 1596–1604.

(d) Lachs, J. R.; Barrett, A. G. M.; Crimmin, M. R.; Koclok-Köhn, G.; Hill, M. S.; Mahon, M. F.; Procopiou, P. A. *Eur. J. Inorg. Chem.* **2008**, 4173–4179.

(e) Barrett, A. G. M.; Crimmin, M. R.; Hill, M. S.; Hitchcock, P. B.; Procopiou, P. A. *Dalton Trans.* **2008**, 4474–4481.

14. Green, S. P.; Jones, C.; Stasch, A. *Science* **2007**, *318*, 1754–1757.

15. (a) Dagorne, S.; Guzei, I. A.; Coles, M. P.; Jordan, R. F. *J. Am. Chem. Soc.* **2000**, *122*, 274–289.

(b) Meier, R. J.; Koglin, E. *J. Phys. Chem. A* **2001**, *105*, 3867–3874.

16. (a) Chang, C. -C.; Hsiung, C. -S.; Su, H. -L.; Srinivas, B.; Chiang, M. Y.; Lee, G. -H.; Wang, Y. *Organometallics* **1998**, *17*, 1595–1601.

(b) Aeilts, S. L.; Coles, M. P.; Swenson, D. C.; Jordan, R. F.; Young, V. G., Jr. *Organometallics* **1998**, *17*, 3265–3270.

(c) Kenny, A. P.; Yap, G. P. A.; Richeson, D. S.; Barry, S. T. *Inorg. Chem.* **2005**, *44*, 2926–2933.

17. Jones, C.; Junk, P. C.; Platts, J. A.; Stasch, A. *J. Am. Chem. Soc.* **2006**, *128*, 2206–2207.

18. Foley, S. R.; Yap, G. P. A.; Richeson, D. S. *Polyhedron* **2002**, *21*, 619–627.

19. Green, S. P.; Jones, C.; Lippert, K. -A.; Stasch, A. *Chem. Commun.* **2006**, 3978–3980.

20. Bailey, P. J.; Gould, R. O.; Harmer, C. N.; Pace, S.; Steiner, A.; Wright, D. S. *Chem. Commun.* **1997**, 1161–1162.

21. Green, S. P.; Jones, C.; Jin, G.; Stasch, A. *Inorg. Chem.* **2007**, *46*, 8–10.

22. (a) Bailey, P. J.; Pace, S. *Coord. Chem. Rev.* **2001**, *214*, 91–141.

(b) Edelmann, F. T. *Adv. Organomet. Chem.* **2008**, *57*, 183–352.

(c) Jones, C. *Coord. Chem. Rev.* **2010**, *254*, 1273–1289.

23. Zhou, M.; Zhang, S.; Tong, H.; Sun, W. -H.; Liu, D. *Inorg. Chem. Commun.* **2007**, *10*, 1262–1264.

24. Ong, T. -G.; Yap, G. P. A.; Richeson, D. S. *Organometallics* **2002**, *21*, 2839–2841.

25. Representative examples of transition metal guanidinate complexes containing metal–metal multiple bonds:

(a) Cotton, F. A.; Matonic, J. H.; Murillo, C. A. *J. Am. Chem. Soc.* **1997**, *119*, 7889–7890.

(b) Cotton, F. A.; Gu, J.; Murillo, C. A.; Timmons, D. J. *J. Chem. Soc.*, *Dalton Trans*. **1999**, 3741–3745.

(c) Clérac, R.; Cotton, F. A.; Daniels, L. M.; Donahue, J. P.; Murillo, C. A.; Timmons, D. J. *Inorg. Chem*. **2000**, *39*, 2581–2584.

(d) Cotton, F. A.; Daniels, L. M.; Murillo, C. A.; Timmons, D. J.; Wilkinson, C. C. *J. Am. Chem. Soc*. **2002**, *124*, 9249–9256.

(e) Cotton, F. A.; Huang, P.; Murillo, C. A.; Timmons, D. J. *Inorg. Chem. Commun*. **2002**, *5*, 501–504.

(f) Cotton, F. A.; Murillo, C. A.; Wang, X.; Wilkinson, C. C. *Inorg. Chim. Acta*. **2003**, *351*, 191–200.

(g) Cotton, F. A.; Huang, P.; Murillo, C. A.; Wang, X. *Inorg. Chem. Commun*. **2003**, *6*, 121–126.

(h) Cotton, F. A.; Murrilo, C. A.; Reibenspies, J. H.; Villagrán, D.; Wang, X.; Wilkinson, C. C. *Inorg. Chem*. **2004**, *43*, 8373–8378.

26. Bear, J. L.; Li, Y.; Han, B.; Kadish, K. M. *Inorg*. *Chem*. **1996**, *35*, 1395–1398.

27. Jones, C.; Schulten, C.; Rose, R. P.; Stasch, A.; Aldridge, S.; Woodul, W. D.; Murray, K. S.; Moubaraki, B.; Brynda, M.; Macchia, G. L.; Gagliardi, L. *Angew*. *Chem*. *Int*. *Ed*. **2009**, *48*, 7406–7410.

28. Fohlmeister, L.; Liu, S.; Schulten, C.; Moubaraki, B.; Stasch, A.; Cashion, J., D.; Murray, K., S.; Gagliardi, L.; Jones, C. *Angew*. *Chem*. *Int*. *Ed*. **2012**, *51*, 8294–8298.

29. a) Nguyen, T.; Sutton, A., D.; Brynda, M.; Fettinger, J., C.; Long, G., J.; Power, P., P. *Science*, **2005**, *310*, 844–847.

b) Kreisel, K. A.; Yap, G. P. A.; Dmitrenko, O.; Landis, C. R.; Theopold, H. *J*. *Am*. *Chem*. *Soc*. **2007**, *129*, 14162–14163.

c) Noor, A.; Wagner, F. R.; Kempe, R. *Angew*. *Chem*. *Int*. *Ed*. **2008**, *47*, 7246–7249.

d) Tsai, Y.–C.; Hsu, C.–W.; Yu, J.–S. K.; Lee, G.–H.; Wang, Y.; Kuo, T.–S. *Angew*. *Chem*. *Int*. *Ed*. **2008**, *47*, 7250–7253.

e) Hsu, C.–W.; Yu, J.–S. K.; Yen, C.–H.; Lee, G.–H.; Wang, Y.; Tsai, Y.–C. *Angew*. *Chem*. *Int*. *Ed*. **2008**, *47*, 9933–9936.

30. Noor, A.; Glatz, G.; Müller, R.; Kaupp, M.; Demeshko, S.; Kempe, R. *Z*. *Anorg*. *Allg*. *Chem*. **2009**, *635*, 1149–1152.

31. Zhou, Y.; Yap, G. P. A.; Richeson, D. S. *Organometallics*, **1998**, *17*, 4387–4391.

32. a) Heitmann, D.; Jones, C.; Junk, P. C.; Lippert, K. -A.; Stasch, A. *Dalton Trans*. **2007**, 187–189.

    b) Heitmann, D.; Jones, C.; Mills, D. P.; Stasch, A. *Dalton Trans*. **2010**, *39*, 1877–1882.

33. (a) Edelmann, F. T. *Chem. Soc. Rev.* **2009**, *38*, 2253–2268.

    (b) Trifonov, A. A. *Coord*. *Chem*. *Rev*. **2010**, *254*, 1327–1347.

    (c) Edelmann, F. T. *Struct*. *Bonding* **2010**, *137*, 109–164.

    (d) Edelmann, F. T. *Chem. Soc. Rev.* **2012**, *41*, 7657–7672.

34. Trifonov, A. A.; Fedorova, E. A.; Fukin, G. K.; Bochkarev, M. N. *Eur*. *J*. *Inorg*. *Chem*. **2004**, 4396–4401.

35. (a) Luo, Y.; Yao, Y.; Shen Q.; Y, K.; Weng, L. *Eur*. *J*. *Inorg*. *Chem*. **2003**, 318–323.

    (b) Chen, J. -L.; Yao, Y. -M.; Luo, Y. -J.; Zhou, L. -Y.; Zhang, Y.; Shen, Q. *J*. *Organomet*. *Chem*. **2004**, *689*, 1019–1024.

36. Yeung, L. F. *M*. *Phil*. *Thesis*, The Chinese University of Hong Kong, 2010.

Chapter 2

The Coordination Chemistry of Chromium Complexes Supported by Guanidinate Ligands

2.1 The Development of Divalent Chromium Complexes Derived from N–donor Ligands

Chromium, with the electronic configuration of $[Ar]3d^5 4s^1$, is classified as an early transition metal in the first row. According to Pearson's hard and soft, acid and base concept,[1] low valent chromium metal is relatively hard, comparing to its late transition metal counterparts. Over the past decades, great efforts have been devoted to the coordination chemistry of divalent chromium metal by hard N–donor ligands.[2,3]

Early work in this field involved the use of the bulky $[N(SiMe_3)_2]^-$ ligand. Bradley and co–workers reported the preparation of Cr(II) amide, $Cr[N(SiMe)_3]_2(THF)_2$ in 1972.[4] This complex is monomeric in the solid state with the two $[N(SiMe)_3]^-$ ligands located in a trans square planar geometry (Chart 2–1).

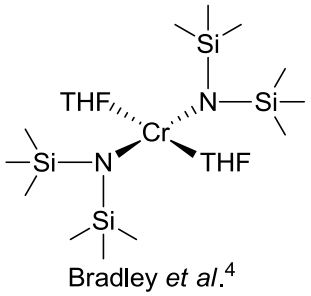

Bradley *et al*.[4]

Chart 2—1

Apart from the silylamido ligand mentioned above, Cr(II) complexes derived form alkylamido[5a,b] and arylamido[5b,c,6] ligands have also been reported. Gambarotta and co–workers have reported on a series of homoleptic Cr(II) alkylamido complexes, $[\{Cr(NR_2)(\mu\text{–}NR_2)\}_2]$ (R = Pr^i, Cy),[5a,b] and arylamido complexes such as,

[{Cr(NPh$_2$)(μ–NPh$_2$)(THF)}$_2$],[5b] [Cr(NPh$_2$)$_2$(py)$_2$][5b] and [(Cr{N(1–Ad)(C$_6$H$_3$Me$_2$–3,5)}{μ–N(1–Ad)(C$_6$H$_3$Me$_2$–3,5)}$_2$] (Chart 2–2).[5c] Interestingly, these complexes exist in either a dimeric or monomeric form, in which the Lewis base (THF, py) coordinates to the metal. Apparently, the formation of these two coordination modes is related to the steric property of the ligand.

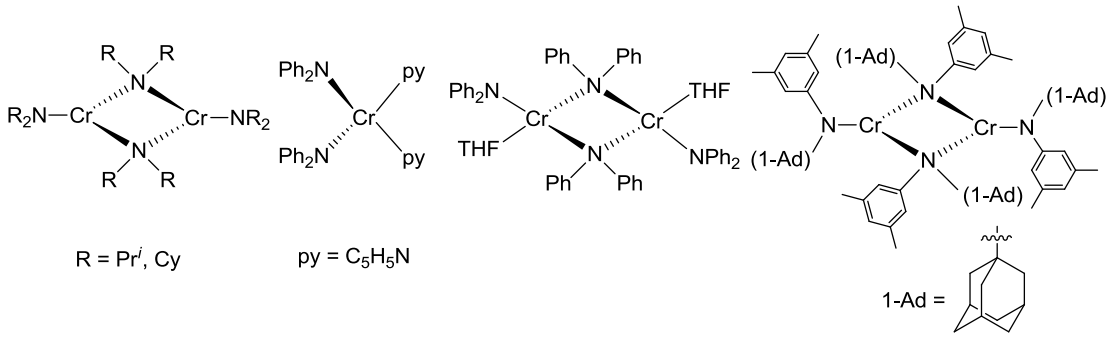

Gambarotta *et al*.[5]

Chart 2—2

By increasing the steric bulkiness of the ligand, the tendency to form bridging, or Lewis base containing complexes can be reduced. Power and co–workers have studied the chemistry of the more bulky [N(Mes)(BMes$_2$)]$^-$ and [N(Ph)(BMes$_2$)]$^-$ ligands, where Mes = 2,4,6–Me$_3$C$_6$H$_2$.[6a,b] A few monomeric, two–coordinate Cr(II) arylamide complexes, including [Cr{N(Ph)(BMes$_2$)}$_2$], [Cr{N(Mes)(BMes$_2$)}$_2$] and [Cr{NH(C$_6$H$_3$Ar$_2$–2,6)}$_2$] (Ar = C$_6$H$_5$) were successfully isolated and structurally characterized (Chart 2–3).[6a,b] Short Cr···C$_{ipso}$ distances were observed in [Cr{N(Ph)(BMes$_2$)}$_2$] (2.328(2) and 2.406(2) Å)and [Cr{N(Mes)(BMes$_2$)}$_2$] (2.383(2) and 2.391(2) Å). More recently, the same research group has modified the aryl substituents and reported on several new two–coordinate Cr(II) arylamide complexes,

namely [Cr{N(H)Ar$^{Pr^i_6}$}$_2$] (Ar$^{Pr^i_6}$ = C_6H_3–2,6–(C_6H_2–2,4,6–Pr^i_3)$_2$), [Cr{N(H)Ar$^{Pr^i_4}$}$_2$] (Ar$^{Pr^i_4}$ = C_6H_3–2,6–(C_6H_3–2,6–Pr^i_2)$_2$) and [Cr{N(H)Ar^{Me_6}}$_2$] (Ar^{Me_6} = C_6H_3–2,6–(C_6H_2–2,4,6–Me_3)$_2$).[6c] The former two complexes have a linear geometry around the metal center; the N–Cr–N bond angles in both complexes measured 180°.

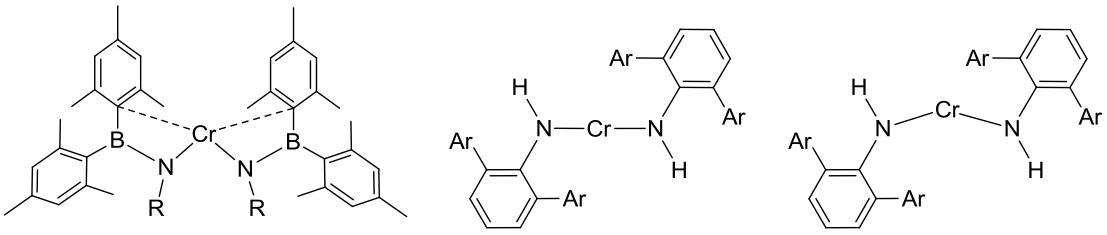

R = Mes, Ph

Ar = C_6H_2-2,4,6-Pr^i_3, C_6H_3-2,4-Pr^i_2

Ar = C_6H_2-2,4,6-Me_3

Power *et al*.[6]

Chart 2—3

Apart from the monodentate silyl–, alkyl– and arylamido ligands, bidentate N–donor ligands such as β–diketiminates, 2–pyridylamides, amidinates and guanidinates have also been employed in Cr(II) coordination chemistry. Theopold and co–workers have reported on the homoleptic [Cr{(Ph)$_2$nacnac}$_2$] [(Ph)$_2$nacnac = *N*,*N*′–diphenyl–2,4–pentanediimine anion], which was synthesized by the reaction of [Cr{(Ph)$_2$nacnac}Cl$_2$(THF)$_2$] with LiR (R = Me_3SiCH_2, Me) (Scheme 2–1).[7a] The heteroleptic [Cr{(Ar)$_2$nacnac}I(Sol)] [(Ar)$_2$nacnac = bis(2,6–diisopropylphenyl)pentane–2,4–ketiminate, Sol = tetrahydrofuran, acetonitrile, or α–picoline] with different donor solvents were also reported.[7b] They were prepared by salt elimination method from CrI_2 and lithium salt Li[(Ar)$_2$nacnac] in the appropriate donor solvent. On the other hand, the heteroleptic dinuclear Cr(II)

[{Cr{(Ar)$_2$nacnac}Cl(THF)}$_2$] and [{Cr{(Ar)$_2$nacnac}Cl}$_2$] can be prepared by the reaction of [{Cr{(Ar)$_2$nacnac}Cl$_2$}$_2$] with BzMgCl (Bz = $PhCH_2^-$), in which the coupling product Bz–Bz was also isolated (Scheme 2–2).[8] Several homoleptic and heteroleptic Cr(II) β–diketiminate complexes were also isolated in which the diketiminate ligands contained substituents of different bulkiness. Some of them are depicted in Chart 2–4.[9]

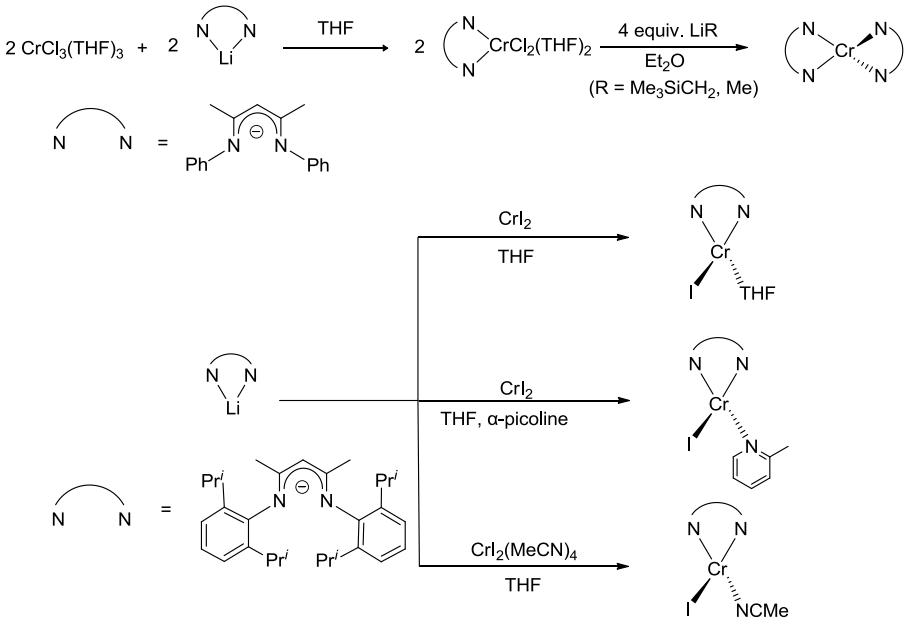

Theopold *et al*.[7]

Scheme 2—1

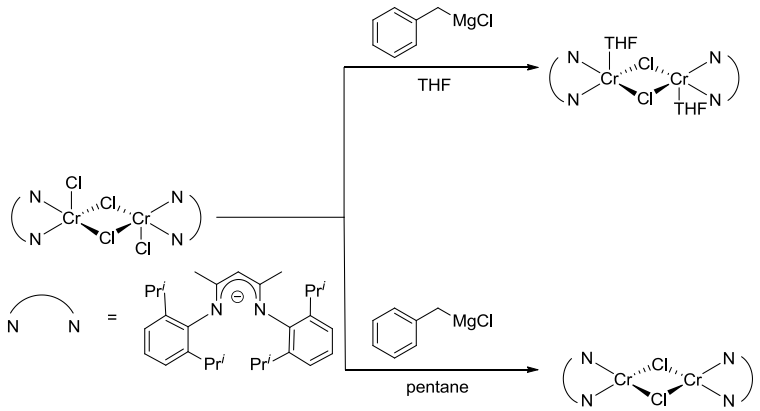

Gibson *et al*.[8]

Scheme 2—2

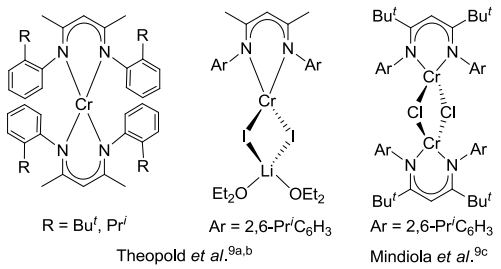

Theopold *et al*.[9a,b] Mindiola *et al*.[9c]

Chart 2—4

The heteroleptic Cr(II) complex [{(nacnac)Cr(μ–Cl)}$_2$] (nacnac = [ArNC(Bu^t)]$_2$CH$^-$, Ar = C$_6$H$_3$Pr$^i_2$–2,6) has been shown to be a good starting material for the preparation of other Cr(II) silyl, amide, aryloxide and hydrocarbyl complexes (Scheme 2–3).[9c]

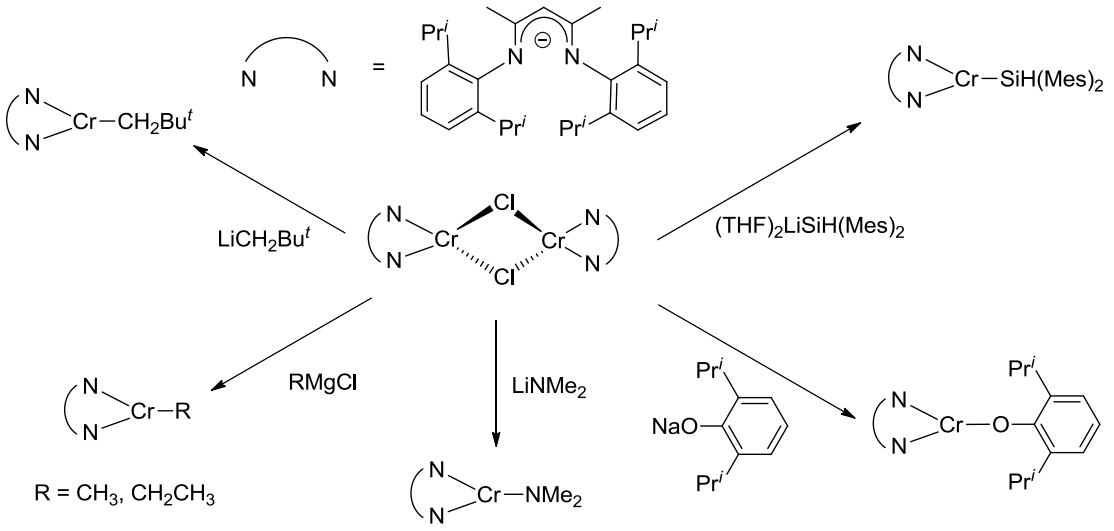

Mindola *et al*.[9c]

Scheme 2—3

A few examples of divalent chromium complexes supported by bulky 2–pyridylamido ligands have been reported by Kempe and co–workers (Chart 2–5).[10] Heteroleptic Cr(II) [{(L)Cr(μ–Cl)(THF)}] [L = {6–(2,4,6–triisopropylphenyl)pyridin–2–yl}(2,4,6–trimethylphenyl)amide or {6–(2,6–dimethylphenyl)pyridin–2–yl}(2,6–diisopropylphenyl)amide] were

synthesized by reactions of $CrCl_2$ with LiL. Reductions of [{(L)Cr(μ–Cl)(THF)}] with KC_8 led to the dichromium(I) complex [{Cr(μ–L)}$_2$] in which the chromium(I)–chromium(I) bond has a five–fold bond order [Cr–Cr = 1.749(2) and 1.750(1) Å, respectively] (Scheme 2–4).[10]

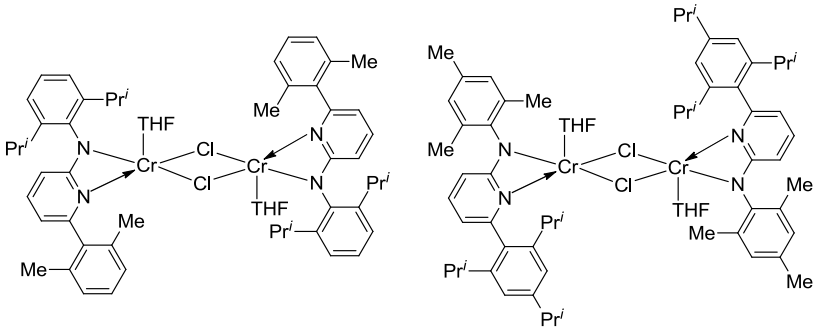

Kempe *et al*.[10]

Chart 2—5

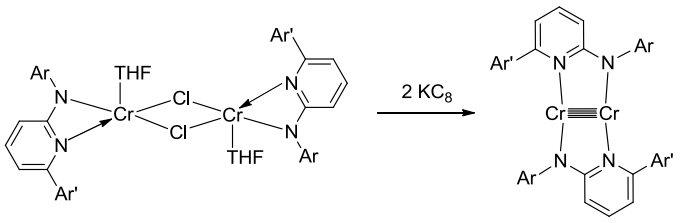

Ar = 2,6-$Pr^i_2C_6H_3$, Ar' = 2,6-$Me_2C_6H_3$
Ar = 2,4,6-$Me_3C_6H_2$, Ar' = 2,4,6-$Pr^i_3C_6H_2$

Kempe *et al*.[10]

Scheme 2—4

The chemistry of amidinate ligands has attracted much research interest over the past decade due to a flexible bonding mode of these ligands. Edelmann and co–workers reported the first homoleptic Cr(II) [Cr{(Ph)C(NSiMe$_3$)$_2$}$_2$] in 1991.[11] Subsequently, a number of Cr(II) amidinate complexes were reported in the

literature.[12–15] A few examples are listed in Chart 2–6. Some of these complexes contained a metal–metal multiple bond. Notably, the structures of these compounds depend on the steric properties of the amidinate ligands.

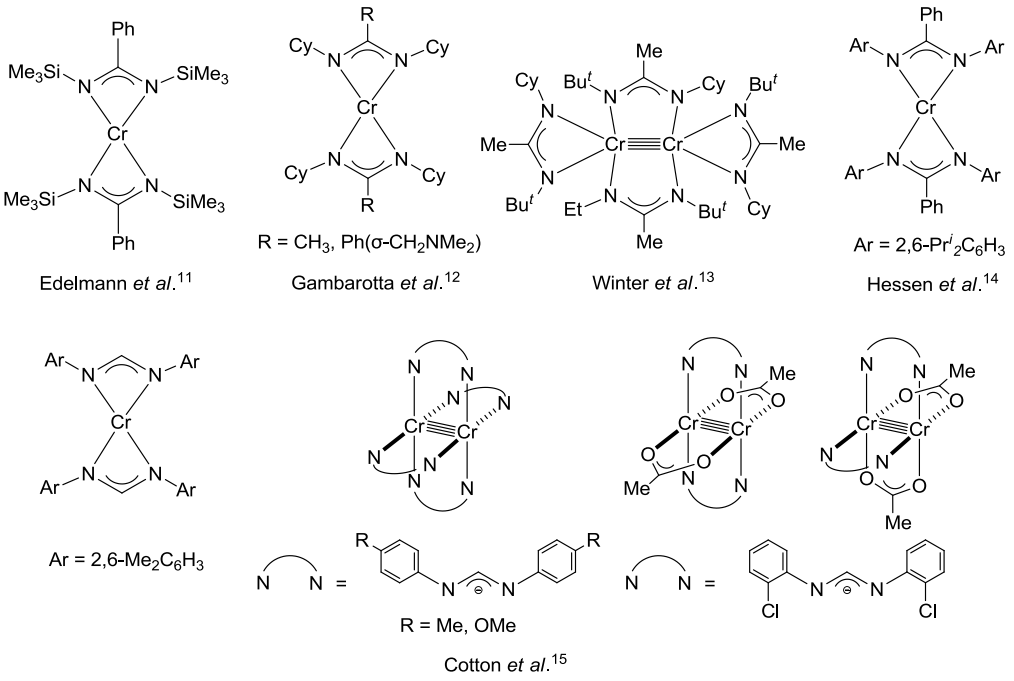

Chart 2—6

Figure 2–1 shows an energy level diagram of the molecular orbitals formed by overlapping of the atomic metal *d* orbitals. The $d_{x^2-y^2}$ orbitals, which are directing towards the ligands, are involving in the formation of metal–ligand bonds. Hence, the latter orbitals are occupied by electrons contributed by the ligands. A di-chromium(II) complex of the type X_4CrCrX_4 has a total of eight *d* electrons (each Cr(II) ion contributes four *d* electrons), which fill the bonding orbitals to give a $\sigma^2\pi^4\delta^2$

electronic configuration. In other words, the metal–metal bond has a bond order of four.

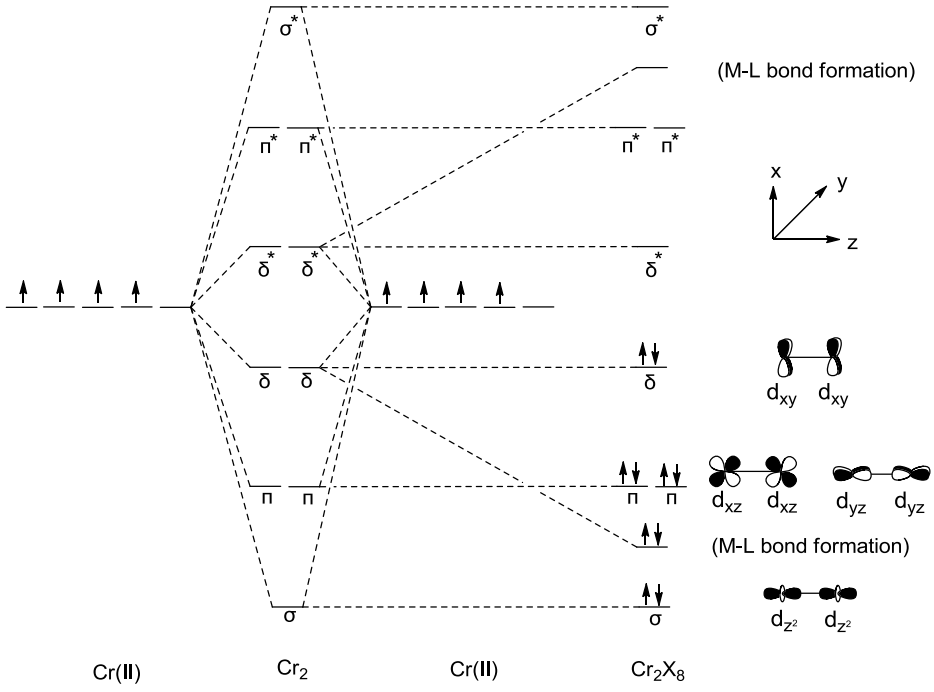

Figure 2—1

The [Cr{(Ph)C(NSiMe$_3$)$_2$}$_2$] complex has proved to be a good starting material for the preparation of Cr(III) bis(amidinate) complexes via single electron oxidation. Smith and co–workers have reported on a series of Cr(III) bis(amidinate) complexes. The reactivity of [Cr{(Ph)C(NSiMe$_3$)$_2$}$_2$] with AgO$_2$CPh and I$_2$ was examined (Scheme 2–5).[16] The same research group has also prepared a Cr(III) allyl complex, [Cr{(Ph)C(NSiMe$_3$)$_2$}$_2$(η^3–C$_3$H$_5$)], by the reactions of [Cr{(Ph)C(NSiMe$_3$)$_2$}$_2$(I)(THF)] or [Cr{(Ph)C(NSiMe$_3$)$_2$}$_2$(O$_2$CPh)] with C$_3$H$_5$MgCl.

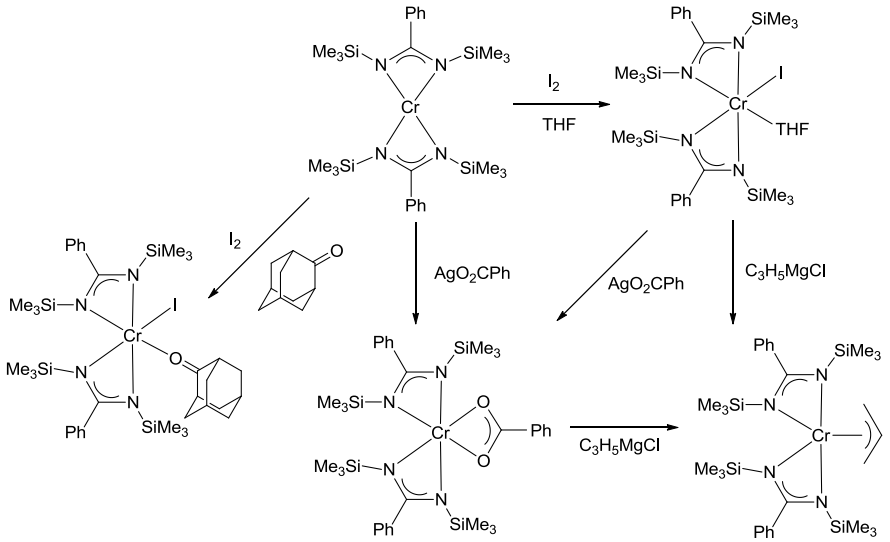

Scheme 2—5

Guanidinate ligands are close analogues of amidinate ligands. An early work on chromium(II) complexes supported by guanidinate ligands was reported by Cotton and co–workers.[17] The chromium(II) complexes $[Cr_2(hpp)_4]$[17a] (hpp = 1,3,4,6,7,8–hexahydropyrimido[1,2–a]pyrimidinate) and $[Cr_2(DPPC)_4]$[17b] (DPPC = $[(PhN)_2CN(CH_2)_4]^-$) were synthesized by the reaction of an appropriate guanidine (hppH or DPPCH) with $LiBu^n$ followed by a salt metathesis reaction with anhydrous $CrCl_2$ (Scheme 2–6). The metal–metal bond in $[Cr_2(hpp)_4]$ and $[Cr_2(DPPC)_4]$ were measured to be 1.8517(7) and 1.904(1) Å, respectively, which can be considered as a chromium–chromium quadruple bond. The latter complex was further reacted with $AgPF_6$ to yield an one–electron reduction product, $[Cr_2(DPPC)_4][PF_6]$.[17b] The chromium–chromium bond length in $[Cr_2(DPPC)_4][PF_6]$ was measured to be 1.9249(9) Å, which is slightly longer than that of $[Cr_2(DPPC)_4]$. The reaction was suggested to

be a ligand oxidation reaction. The molecular orbital from which the electron has been removed spanned entirely over the ligands and has very little contribution from the chromium atomic orbitals.

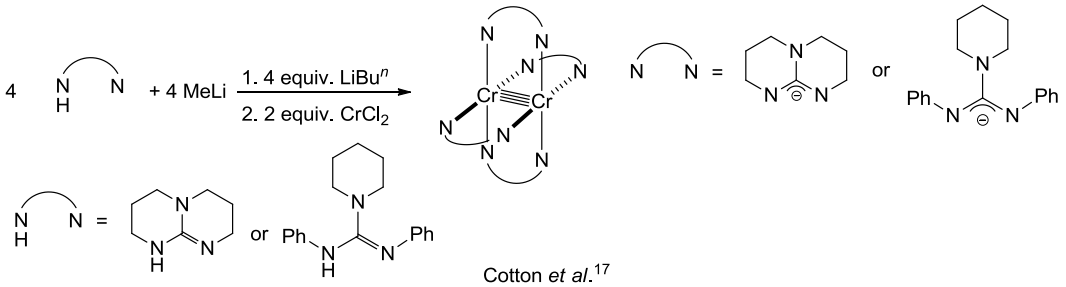

Cotton *et al*.[17]

Scheme 2—6

Recently, Gambarotta *et al*. have reported on a monomeric Cr(II) complex supported by the bulky $[(Me_3Si)_2NC(NCy)_2]^-$ ligand. Reaction of $CrCl_2$ with two molar equivalents of $Li[(Me_3Si)_2NC(NCy)_2]$ gave homoleptic chromium(II) complex $[Cr\{(Me_3Si)_2NC(NCy)_2\}_2]$ (Scheme 2–7).[18] By adding an alkylating agent, $AlMe_3$, one of the guanidinate ligands in $[Cr\{(Me_3Si)_2NC(NCy)_2\}_2]$ is replaced by an alkyl group to form dimeric $[\{[(Me_3Si)_2NC(NCy)_2]CrMe\}_2]$. The chromium–chromium bond length in the latter dimeric complex was measured to be 1.773(2) Å, which is shorter than those reported for $[Cr_2(hpp)_4]$[17a] and $[Cr_2(DPPC)_4]$.[17b] Each methyl group in $[\{[(Me_3Si)_2NC(NCy)_2]CrMe\}_2]$ is terminally bonded to one chromium atom with an orientation towards another chromium atom. This suggests the presence of a Cr–C–H···Cr agostic interaction.

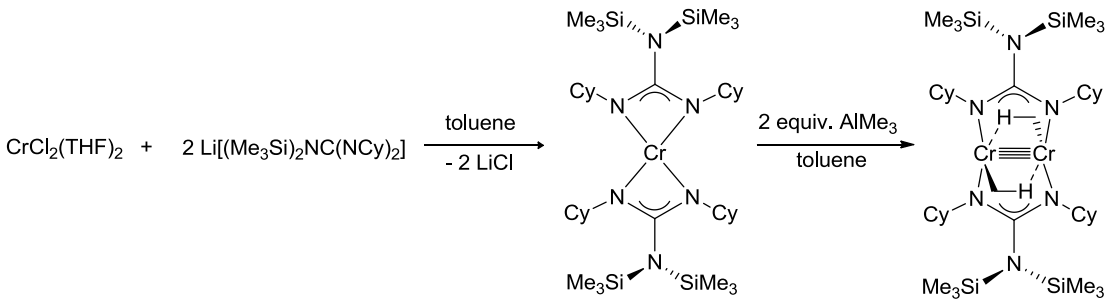

Gambarotta *et al*.[18]

Scheme 2—7

More recently, Kempe and co–workers have successfully isolated the first di–chromium(I) guanidinate complex, $[Cr\{Me_2NC(NAr)_2\}]_2$ (Ar = $C_6H_3Pr^i_2$–2,6), by adding excess KC_8 to the dimeric guanidinate–chloride complex $[Cr\{Me_2NC(NAr)_2\}(\mu\text{–}Cl)]_2$ (Scheme 2–8).[19] The chromium(I)–chromium(I) bond in $[Cr\{Me_2NC(NAr)_2\}]_2$ was measured to be 1.729(1) Å, which is the shortest chromium(I)–chromium(I) bond reported so far (Chart 2–7).[10,20a–f] It has been proposed that the two methyl groups on the non–coordinating nitrogen atom can push the two phenyl rings closer to the metals. This facilitated the formation of a short chromium(I)–chromium(I) bond.

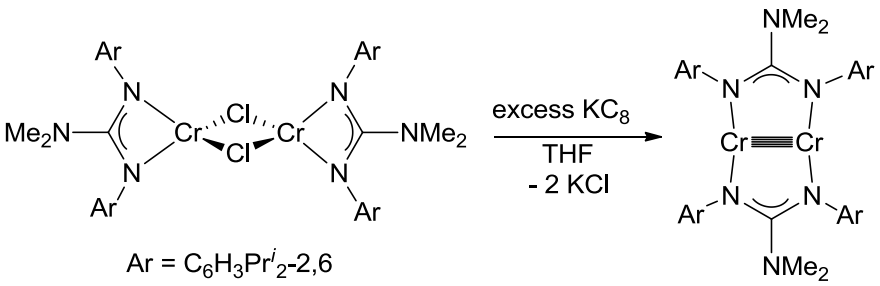

Kempe *et al*.[19]

Scheme 2—8

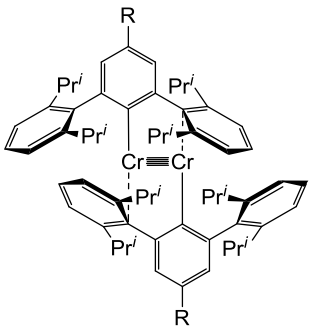

R = H, Cr—Cr = 1.8351(4) Å
R = $SiMe_3$, Cr—Cr = 1.8077(7) Å
R = OMe, Cr—Cr = 1.8160(5) Å
R = F, Cr—Cr = 1.831(2) Å

Power *et al*.[20a,c]

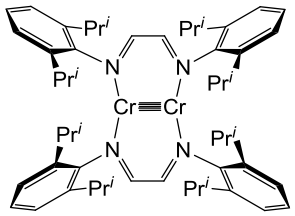

Cr—Cr = 1.8028(9) Å

Theopold *et al*.[20b]

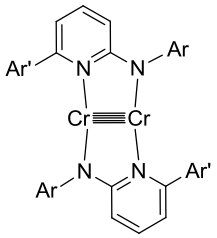

Ar = 2,6-$Pr^i_2C_6H_3$, Ar' = 2,6-$Me_2C_6H_3$
Cr—Cr = 1.750(1) Å
Ar = 2,4,6-$Me_3C_6H_2$, Ar' = 2,4,6-$Pr^i_3C_6H_2$
Cr—Cr = 1.749(2) Å

Kempe *et al*.[10]

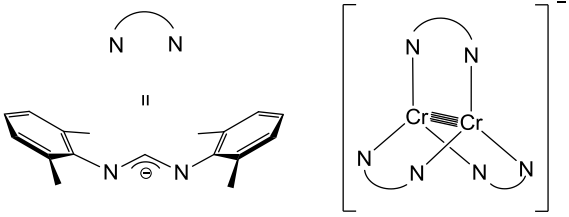

Cr—Cr = 1.7397(9) Å

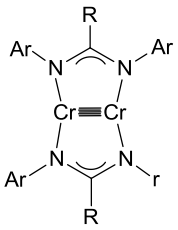

R = H, Ar = 2,4,6-$Me_3C_6H_2$, Cr—Cr = 1.7404(8) Å
R = H, Ar = 2,6-$Et_2C_6H_3$, Cr—Cr = 1.7454(1) Å
R = H, Ar = 2,6-$Pr^i_2C_6H_3$, Cr—Cr = 1.747(1) Å
R = Me, Ar = 2,6-$Pr^i_2C_6H_3$, Cr—Cr = 1.7395(7) Å

Tsai *et al*.[20d,e]

Chart 2—7

2.2 Results and Discussion

2.2.1 Synthesis and Structure of Potassium Derivative of $[(2,6\text{–}Me_2C_6H_3N)C(NHPr^i)(NPr^i)]^-$ (L^1) and Lithium Derivative of $[(2,6\text{–}Pr^i_2C_6H_3N)C\{N(SiMe_3)_2\}(NC_6H_3Pr^i_2\text{–}2,6)]^-$ (L^4)

Preparation

In this work, the potassium salt of $[(2,6\text{–}Me_2C_6H_3N)C(NHPr^i)(NPr^i)]^-$ (L^1) and lithium salt of $[(2,6\text{–}Pr^i_2C_6H_3N)C\{N(SiMe_3)_2\}(NC_6H_3Pr^i_2\text{–}2,6)]^-$ (L^4) were used as ligand transfer reagents for the synthesis of chromium(II) complexes. Deprotonation of $2,6\text{–}Me_2C_6H_3NH_2$ by KH, followed by the addition of *N*,*N*′–diisopropylcarbodiimide (DIC) led to the potassium guanidinate $[KL^1 \cdot 0.5PhMe]_n$ (**1**) in 76% yield (Scheme 2–9). On the other hand, direct lithiation of hexamethyldisilazane (HMDS) with $LiBu^n$ in Et_2O, followed by the addition of bis(2,6–diisopropylphenyl)carbodiimide (DIPPC)[21] yielded $[LiL^4(Et_2O)]$ (**2**) in 65% yield (Scheme 2–10). One of the silyl groups underwent 1,3–silyl migration to the nitrogen atom attached to the arene group. A similar silyl migration has been reported for $[LiCyNC\{N(SiMe_3)Py\}NCy]$ [Py = 2–(6–MeC_5H_3N)] by Junk and co–workers.[22]

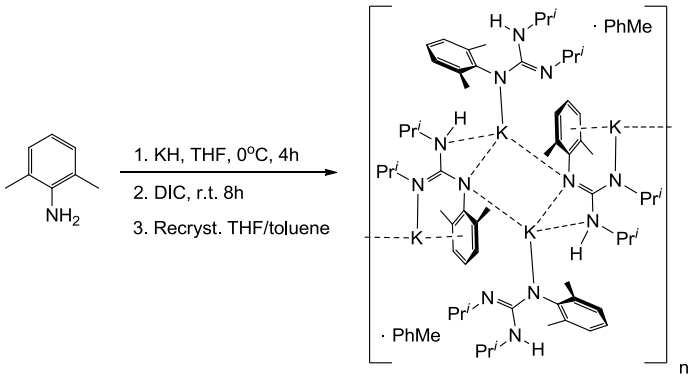

1 (76%)

Scheme 2—9

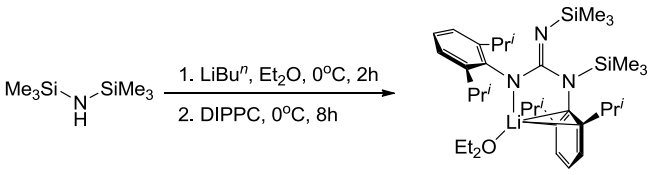

2 (65%)

Scheme 2—10

Physical Characterization of Complexes **1** and **2**

The molecular formula of complexes **1** and **2** were confirmed by elemental analysis, NMR spectroscopy, and X–ray diffraction analysis. Complexes **1** and **2** are soluble in THF, but insoluble in other common organic solvents, such as, hexane, toluene and Et_2O. Complex **1** melts with decomposition at 249–250 ^oC, whilst complex **2** melts at 137–140 ^oC. Table 2–1 summarizes the appearance and melting points of complexes **1** and **2**.

Table 2–1. Appearance and melting points of complexes **1** and **2**

Compound	Appearance	M.p. (^oC)
$[KL^1 \cdot 0.5PhMe]_n$ (**1**)	Colorless crystals	249–250 (dec.)
$[LiL^4(Et_2O)]$ (**2**)	Colorless crystals	137–140

NMR Spectra of Complexes **1** and **2**

The NMR spectra of complexes **1** and **2** are shown in Appendix 2 (Figures A2–1, A2–2, A2–4 and A2–6). Owing to a poor solubility of **1** in C_6D_6, the NMR spectra were measured in a THF–d_8 solution. The ^{1}H NMR of complex **1** shows one set of resonance signal due to the L^1 ligand and the solvated toluene molecules. The L^1:toluene ratio was found to be 3:1, which is consistent with the results of elemental analysis. A broad peak at 0.99 ppm is assignable to the four isopropyl methyl substituents and the signals at 3.25 and 3.78 ppm are assignable to the isopropyl methine protons. The ^{13}C NMR spectrum of **1** also shows broad resonance signals due to the isopropyl methyl groups (26.4 ppm) and the isopropyl methine carbons (44.5 and 46.4 ppm), respectively. Broadening of the resonance signals may be attributed to an exchange process due to delocalization of the negative charge between the coordinated N^{iso} (nitrogen atom with isopropyl substituent) atom and non–coordinated N^{iso} atom. In order to prove the presence of this exchange process, variable temperature ^{1}H NMR studies of complex **1** was carried out at 30^{o}C to –80^{o}C (Figure A2–3). The broad peak at 0.99 ppm separated into two sets of resonance signals (0.92 and 1.05 ppm) below –30^{o}C. This suggested that the exchange process was slowed down at low temperatures, and the two isopropyl substituents have different chemical environments.

The ^{1}H and ^{13}C NMR spectra of complex **2** shows one set of resonance signals assignable to the L^4 ligand and diethyl ether in a ratio of 1:1. Three singlet signals (–0.81, –0.18 and 0.13 ppm) were observed in the ^{1}H NMR, which are assignable to the silyl substituent of the L^4 ligand. Two doublet signals (1.12 and 1.24 ppm) are assignable to the isopropyl methyl groups. The ^{13}C NMR shows two broad signals at 4.8 and 5.0 ppm and two singlets at 25.0 and 25.4 ppm. They are assignable to carbon atoms of the silyl and isopropyl substituents, respectively. The ^{1}H NMR suggests that the methyl groups on each $SiMe_3$ substituent have different chemical environment. Therefore, a variable temperature ^{1}H NMR study of complex **2** (in toluene–d_8) was carried out at 20°C to 65°C (Figure A2–7). At 55°C, the signals due to the silyl substituents and isopropyl methyl substituents started to coalesce to a singlet resonance signal and a doublet resonance signal, respectively. The two sets of signals become more intense at 66°C.

Crystal Structures of Complexes **1** and **2**

Single crystals of **1** was obtained from a mixed THF/toluene (1:2) solution, whereas those of **2** was obtained from Et_2O. Figures 2–2 and 2–3 show the X–ray structures of polymeric potassium complex **1** and monomeric lithium complex **2**, respectively. Selected bond lengths and angles are listed in Tables 2–2 and 2–3. Selected crystallographic data are listed in Table A3–1 (Appendix 3).

1. $[KL^1 \cdot 0.5PhMe]_n$ (**1**)

Complex **1** crystallizes in the orthorhombic space group *Pbca*. In the solid state, it crystallizes as a one–dimensional polymer made up of linked binuclear $K_2L^1_2$ subunits. The two potassium atoms [K(1) and K(2)] exhibit different binding modes. K(1) is bound by two η^1–amide L^1 ligands [N(1) and N(4)] and one η^3–guanidinate L^1 ligand [N(4)A and N(5)A]. Similar binding modes have already been reported in the lithium guanidinate complexes $[\{(Et_2O)LiN(SiMe_3)C(NMe_2)N(Ph)\}_2]$[23] and $[\{LiPr^iNC(NPr^i_2)NPr^i(THF)\}_2]$.[24] On the other hand, K(2) is bound by two η^1–amide:η^6–arene L^1 ligands [N(6), N(2)B and the two phenyl rings]. A similar η^1:η^6 binding mode has been reported in the symmetrical potassium guanidinate complex $[\{K(Priso)\}_\infty]$ ($Priso^-$ = $[(2,6\text{–}Pr^i_2C_6H_3N)_2C(NPr^i_2)]^-$).[25] The potassium–nitrogen bond distances fall within the range of 2.806(4)–2.962(4) Å, which are slightly longer than those in $[\{K[CyNC(N(SiMe_3)_2)NCy]\}_2 \cdot C_6H_6]$ [2.765(2)–2.806(2) Å][26] and $[\{K(Priso)\}_\infty]$ [2.755(3) Å].[25] The observed K(2)–Centroid(1) [Centroid(1) = center position of the phenyl ring formed by C(16)–C(21)] distance in **1** is 2.895 Å, which is slightly shorter than the corresponding distances of 2.945 and 3.077 Å in $[\{K(Priso)\}_\infty]$.[25] The almost identical C–N distances, namely C(9)–N(1) [1.337(6) Å], C(9)–N(2) [1.308(6) Å], C(24)–N(4) [1.337(6) Å] and C(24)–N(6) [1.308(6) Å], in **1** indicate a delocalization

of the anionic charge over the N(1)–C(9)–N(2) and N(4)–C(24)–N(6) ligand moieties. The C(9)–N(3) [1.410(6) Å] and C(24)–N(5) [1.424(6) Å] distances are longer, suggesting that the anionic charge mainly delocalizes on the N(1)–C(9)–N(2) and N(4)–C(24)–N(6) moieties. The bite angle formed by Centroid(1)–K(2)–N(6) is measured to be 79.2°, which is similar to that in [{K(Priso)}$_\infty$] (79.0°).[25]

2. [LiL^4(Et$_2$O)] (**2**)

Complex **2** crystallizes in the monoclinic space group $P2_1/c$. The Li(1) center is bound by one coordinated Et$_2$O molecule and one L^4 ligand. The latter bonds to the lithium in an η^1–amide:η^3–arene mode. The observed N(3)–Li(1)–O(1), O(1)–Li(1)–Centroid(1) [Centroid(1) = center position of C(1), C(2) and C(6)] and N(3)–Li(1)–Centroid(1) angles are 138.4(4), 133.6 and 88.0°, respectively, with the sum of bond angles around Li(1) being 360.0°. If the η^3–arene binding is considered as a single coordination point, the geometry around the Li(I) center can be described as trigonal planar. A similar η^1:η^3 coordination mode has been reported for the lithium guanidinate complex [Li(THF)Giso] (Giso$^-$ = [ArNC(NCy$_2$)NAr]$^-$; Ar = 2,6–Pr$^i_2$C$_6$H$_3$)[25] and lithium triazenide complex [Li]$^+$[Li(N$_3$Tph$_2$)$_2$]$^-$ (Tph = 2–TripC$_6$H$_4$; Trip = 2,4,6–^{i}Pr$_3$C$_6$H$_2$).[27] The Li(1)–C(arene) distances of 2.377(7)–2.654(8) Å in **2** are longer than those of 2.290(3)–2.591(3) Å in [Li(THF)Giso],[25] but are comparable to those of 2.343(7)–2.605(7) Å in

[Li][Li($N_3Tph_2)_2$].[27] The C(16)–N(2) distance of 1.296(4) Å is shorter than the C–N double bond in [Li(THF)Giso] [1.315(2) Å],[25] [{K(Priso)}$_\infty$] [1.340(5) Å][25] and [{K(THF)$_2$}{Pip(Giso)$_2$}{K(THF)$_3$}] (Pip(Giso)$_2^{2-}$ = [{ArNCNAr}$_2${μ–N(C_2H_4)$_2$N}]$^{2-}$; Ar = 2,6–$Pr^i_2C_6H_3$) [1.322 Å (av.)].[25]

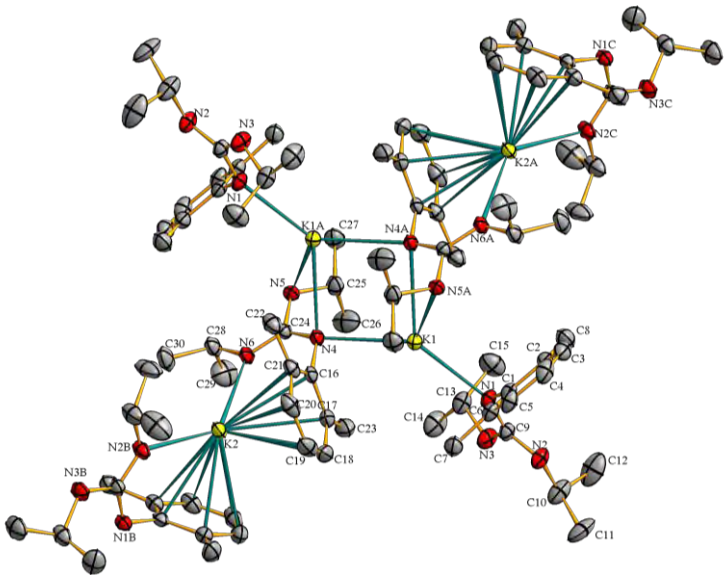

Figure 2–2. Molecular structure of polymeric $[KL^{1}\cdot 0.5PhMe]_n$ (**1**). The toluene solvate molecule is omitted for clarity.

Table 2–2. Selected bond distances (Å) and angles (deg.) for compound **1**

$[KL^{1}\cdot 0.5PhMe]_n$ (**1**)			
K(1)–N(1)	2.812(4)	K(1)–N(4)	2.928(4)
K(1)–N(4)A	2.962(4)	K(1)–N(5)A	2.872(4)
K(2)–N(6)	2.817(4)	K(2)–N(2)B	2.805(4)
C(24)–N(4)	1.337(6)	C(24)–N(5)	1.424(6)
C(24)–N(6)	1.308(6)	C(9)–N(1)	1.337(6)
C(9)–N(2)	1.308(6)	C(9)–N(3)	1.410(6)
K(2)–Centroid(1)*	2.895		
N(4)–K(1)–N(4)A	87.5(1)	N(4)A–K(1)–N(5)A	46.6(1)
N(1)–K(1)–N(4)	137.9(1)	N(4)–C(24)–N(5)	113.6(4)
N(1)–C(9)–N(3)	115.5(4)	N(1)–C(9)–N(2)	124.3(5)
N(6)–K(2)–N(2)B	134.3(1)		

Symmetry code: A –x, –y, –z+1; B –x+1/2, –y, z+1/2; C –x+1/2, –y, z–1/2

* Centroid(1) = center position of the phenyl ring formed by C(16)–C(21).

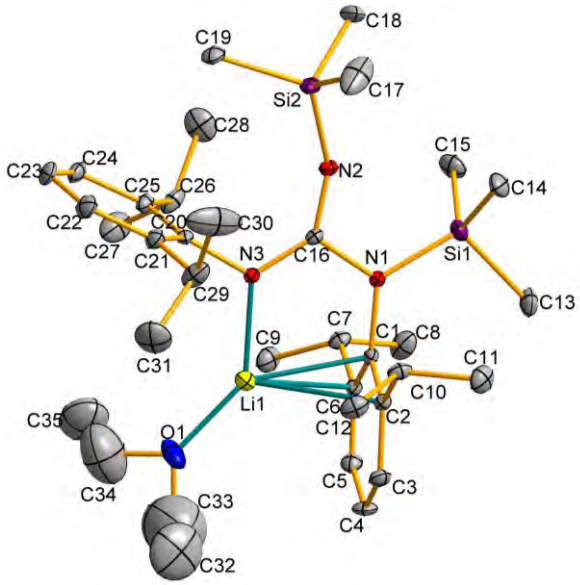

Figure 2–3. Molecular structure of [LiL^4(Et$_2$O)] (**2**).

Table 2–3. Selected bond distances (Å) and angles (deg.) for compound **2**

[LiL^4(Et$_2$O)] (**2**)			
Li(1)–N(3)	1.932(8)	Li(1)–O(1)	1.885(8)
Li(1)–C(1)	2.377(8)	Li(1)–C(2)	2.605(8)
Li(1)–C(6)	2.654(8)	C(16)–N(1)	1.431(4)
C(16)–N(2)	1.296(4)	C(16)–N(3)	1.345(4)
Si(1)–N(1)	1.756(3)	Si(2)–N(2)	1.671(3)
Li(1)–Centroid(1)*	2.318		
C(16)–N(2)–Si(2)	152.1(3)	C(16)–N(1)–Si(1)	116.3(2)
N(1)–C(16)–N(2)	113.4(3)	N(1)–C(16)–N(3)	114.2(3)
N(2)–C(16)–N(3)	132.4(3)	C(1)–N(1)–Si(1)	123.9(2)
C(1)–N(1)–C(16)	119.8(3)	C(16)–N(3)–C(20)	118.2(3)
C(16)–N(3)–Li(1)	125.0(3)	C(20)–N(3)–Li(1)	116.7(3)
N(3)–Li(1)–O(1)	138.4(4)	N(3)–Li(1)–Centroid(1)	88.0
O(1)–Li(1)–Centroid(1)	133.6		

* Centroid(1) = Center position formed by C(1), C(2) and C(6).

2.2.2 Synthesis and Structure of Cr(II) Guanidinate Complexes of L^1 and L^4

Preparation

Salt metathesis reaction of anhydrous $CrCl_2$ with two molar equivalents of potassium reagent **1** in THF yielded the mononuclear, purple crystalline Cr(II) bis(guanidinate) complex $[Cr(L^1)_2]$ (**3**) (Scheme 2–11). On the other hand, treatment of anhydrous $CrCl_2$ with one molar equivalent of lithium reagent **2** yielded the heterobimetallic ate complex* $[Cr(L^4)(\mu\text{–}Cl)_2Li(THF)(Et_2O)]$ (**4**), which was isolated as pale blue crystals (Scheme 2–12). Recrystallization of **4** from toluene gave dimeric $[\{Cr(L^4)(\mu\text{–}Cl)\}_2]$ (**5**) as dark blue crystals (Scheme 2–13).

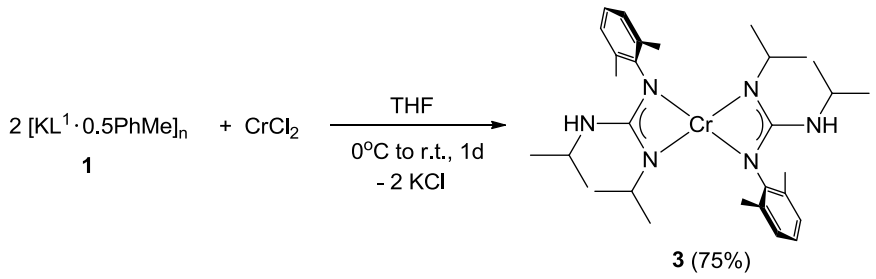

Scheme 2—11

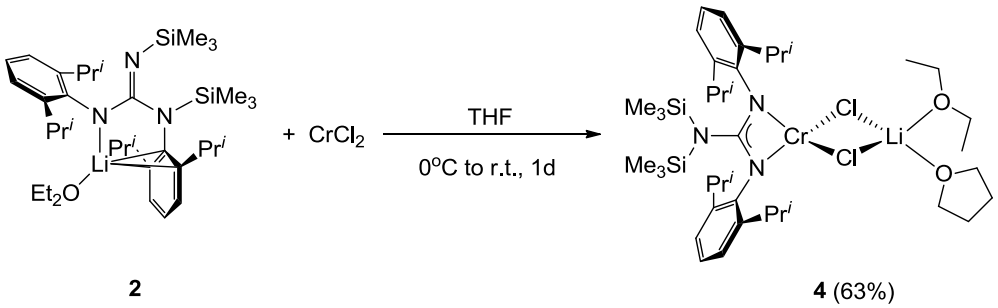

Scheme 2—12

* An ate complex is a salt formed by the reaction of a Lewis acid with a base whereby the central atom increases its valence.

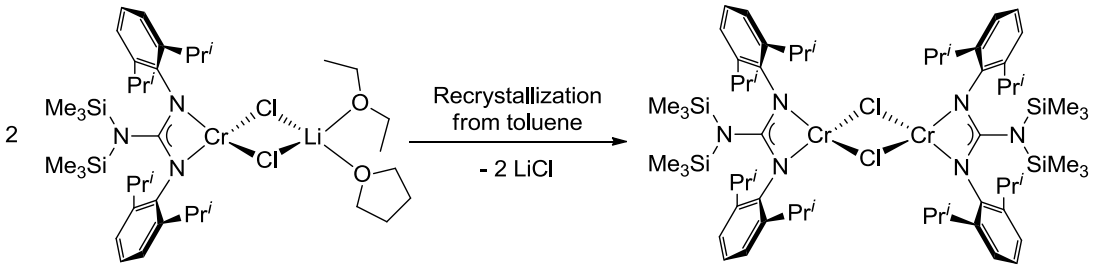

Scheme 2—13

Physical Characterization of Complexes **3**–**5**

All of the complexes **3**–**5** are extremely sensitive to air and moisture. Complex **3** is soluble in all common organic solvents, whereas complexes **4** and **5** are soluble in THF, toluene and diethyl ether, but only sparingly soluble in hexane. The appearance and melting points of complexes **3**–**5** are summarized in Table 2–4.

Complexes **3**–**5** have been characterized by elemental analysis and single–crystal X–ray diffraction analysis. Results of elemental analysis for complexes **3**–**5** are consistent with their empirical formula. In addition, an UV–Vis spectrum of complex **3** has also been measured.

Table 2–4. Appearance and melting points of complexes **3**–**5**

Compound	Appearance	M.p. (^{o}C)
$[Cr(L^1)_2]$ (**3**)	Purple crystals	168–172
$[Cr(L^4)(\mu\text{–}Cl)_2Li(THF)(Et_2O)]$ (**4**)	Pale blue crystals	185–187
$[\{Cr(L^4)(\mu\text{–}Cl)\}_2]$ (**5**)	Deep blue crystals	161–163

The solid–state structures of complexes **3**–**5** were determined by X-ray diffraction (*vide infra*). The Cr(II) center in **3** shows a distorted square planar

geometry, while that of complexes **4** and **5** displays a distorted tetrahedral geometry. Figures 2–4 and 2–5 show the splitting of d orbitals in a square planar field and a tetrahedral field, respectively.

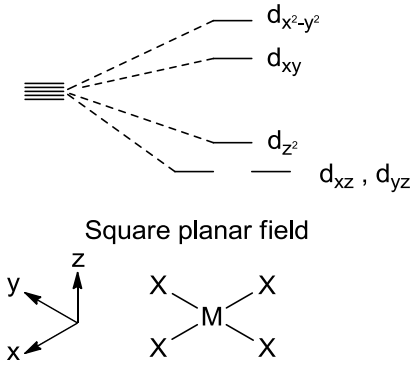

Figure 2—4

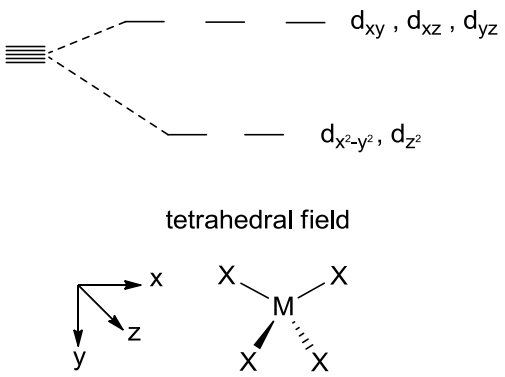

Figure 2—5

The solution magnetic moments of complexes **3**–**5** were determined by the Evans NMR method in C_6D_6 at 298 K.[28] Complexes **3** and **4** were found to be high–spin complexes. The solution magnetic moments of 4.83 μ_B (for **3**) and 4.84 μ_B (for **4**), are closed to the spin–only value of a high–spin d^4 electronic configuration (4.90 μ_B). The solution magnetic moment of 5.08 μ_B (2.54 μ_B per chromium center) for complex **5** is smaller than the spin–only value of a high–spin d^4 electronic configuration. This may be attributed to antiferromagnetic coupling between the two Cr(II) center in the [Cr(μ–Cl)$_2$] core. A similar result was also reported for the Cr(II) β–diketiminate chloride complex [(nacnac)Cr(μ–Cl)]$_2$ (nacnac = [ArNC(Bu^t)]$_2$CH$^-$, Ar = $C_6H_3Pr^i_2$–2,6) [μ_{eff} = 2.95 μ_B per chromium center].[9c]

UV–Vis spectrum of Complex **3**

The UV–Vis spectrum of complex **3** is shown in Figure A5–1 in Appendix 5. Complex **3** dissolved in THF to give a purple solution. The UV–Vis spectrum of complex **3** shows five absorption maxima at λ_{max} ($\varepsilon/M^{-1}cm^{-1}$): 375 (sh, 1500), 405 (sh, 1300), 466 (1100), 531 (sh, 940), 671 (sh, 490), respectively.

Crystal Structures of Complexes **3**–**5**

1. $[Cr(L^1)_2]$ (**3**)

The molecular structure of complex **3** with atom labeling is shown in Figure 2–6. Selected bond distances and angles are listed in Table 2–5.

Single crystals of complex **3** suitable for X–ray crystallographic analysis were obtained from Et_2O. Complex **3** crystallizes in a monoclinic crystal system with space group *Pc*. The Cr(II) center is coordinated by two κ^2–bound L^1 ligands. The observed N(1)–Cr(1)–N(4) and N(3)–Cr(1)–N(6) angles are 178.7(2) and 179.0(1)^o, respectively, with the sum of bond angles around Cr(1) being 360^o. Hence, the coordination geometry around the Cr(1) center can be described as distorted square planar.* A similar coordination geometry has been reported for other Cr(II) complexes such as $[Cr\{(pz)_2BEt_2\}]$ (pz = $C_2H_3N_2^-$),[29] $[Cr(DXylF)_2]$ (DXylF = *N*,*N*′–bis(2,6–xylyl)–formamidinate),[5b] $[\{(2,6\text{–}Pr^i{}_2C_6H_3)N{=}CH(C_4H_3N\text{–}2)\}_2Cr]$[8] and

* The dihedral angle formed by the N(1)–Cr(1)–N(3) and N(4)–Cr(1)–N(6) planes is measured to be 1.4^o.

$[(\eta^1\text{–}2,5\text{–}Me_2C_4H_2N)_2Cr(py)_2]$.[30] Apparently, the sterically bulky L^1 ligand helps to stabilize a square planar structure, instead of a dinuclear paddlewheel structure. It has been reported that $[Cr(DXylF)_2]$ exists as a monomer in the solid state due to the presence of the bulky 2,6–xylyl groups.[15b] In the latter complex, a difficulty to accommodate sixteen methyl groups on the two axial planes prevents the formation of a paddlewheel conformation (the two axial planes would accommodate twenty four methyl groups if complex **3** had a dinuclear structure). A minor modification in the steric bulkiness of supporting ligands can also lead to a different solid state structure. For example, $[(CyNC(CH_3)NCy)_2Cr]$[12] is mononuclear whereas $[\{(CyNC(H)NCy)_2Cr\}_2\cdot C_7H_8]$[12] is dinuclear in the solid–state. It is believed that a slight increase in the size of the substituent on the central carbon would force the cyclohexyl groups pointing down with a consequence of reducing the bite angle of the amidinates. As a result, the ligands prefer to chelate rather than span over two Cr(II) centers.

The Cr–N distances of 2.037(4)–2.070(3) Å in **3** are marginally shorter than the corresponding distances of 2.069(4)–2.085(4) Å in $[\{(2,6\text{–}Pr^i_2C_6H_3)N{=}CH(C_4H_3N\text{–}2)\}_2Cr]$,[8] but comparable to that of 2.045(2) and 2.075(2) Å in $[Cr(DXylF)_2]$.[15b] Delocalization of the anionic charge over the N–C–N moiety of L^1 is revealed from the nearly identical C–N bond distances [C(9)–N(1)

1.338(5) Å, C(9)–N(2) 1.356(6), C(9)–N(3) 1.319(5) Å, C(24)–N(4) 1.349(5) Å, C(24)–N(5) 1.368(5) Å and C(24)–N(6) 1.327(5) Å]. These C–N bond lengths in **3** are all shorter than a C–N single bond (1.47 Å), but longer than a C=N double bond (1.28 Å).[31] The N–C–N bond angles of 111.8(3) and 111.5(3)^{o} are comparable to those in the closely related Cr(II) amidinate complexes [Cr(DXylF)$_2$] [113.9(2)^{o}],[15b] [Cr{PhC(NSiMe$_3$)(NAr)}$_2$] (Ar = 2,6–Me$_2$C$_6$H$_3$) [113.7(6) and 114.5(6)^{o}][32] and [Cr(Bu^{t}NC(CH$_3$NEt)$_2$]$_2$ [114.5(2)^{o}].[13] The N–Cr–N bite angle in complex **3** fall within the range of 64.7(1)–65.2(1)^{o}, which are similar to those of 64.7(2)–65.0(2)^{o} in [Cr{PhC(NSiMe$_3$)(NAr)}$_2$],[32] but smaller than those of 81.8(2)–82.1(2)^{o} reported for the five–membered metallocyclic [Cr{(2,6–Pr$^i_2$C$_6$H$_3$)N=CH(C$_4$H$_3$N–2)}$_2$][8] and much smaller than those of 88.5(1)–89.4(1)^{o} in the six–membered metallocyclic [Cr{(Ph)$_2$nacnac}$_2$] ((Ph)$_2$nacnac = *N*,*N*′–diphenyl–2,4–pentanediimine anion).[7a] The trend of increasing N–Cr–N bite angles can be ascribed to an increase in the size of the metallocyclic ring in these complexes.

2. [Cr(L^4)(μ–Cl)$_2$Li(THF)(Et$_2$O)] (**4**) and [{Cr(L^4)(μ–Cl)}$_2$] (**5**)

The molecular structures of complexes **4** and **5** are shown in Figures 2–7 and 2–8, respectively. Selected bond lengths and angles are listed in Tables 2–6 and 2–7.

X–Ray quality crystals of complex **4** were obtained form diethyl ether. Single crystals of complex **5** suitable for X–ray diffraction studies were obtained from

toluene. Complex **4** crystallizes in the monoclinic space group $P2_1/c$, while complex **5** crystallizes in the triclinic space group $P\bar{1}$. The chromium metal in each complex is coordinated by one κ^2–bound L^4 ligand and two chloride ligands. The coordination geometry around the chromium atom in complexes **4** and **5** are best described as distorted tetrahedral.

The Cr–N bond lengths in **4** [2.044(4)–2.045(3) Å] are longer than the corresponding distances in **5** [2.005(4)–2.031(4) Å], but shorter than those of 2.059(3)–2.063(3) Å in $[(nacnac)Cr(\mu\text{–}Cl)]_2$[9c] and 2.072(2)–2.078(2) Å in $[Cr_2(\mu\text{–}Cl)_2(DXylF)_2(THF)_2]$.*[15b] The anionic charge on each amidinate ligand in $[Cr_2(\mu\text{–}Cl)_2(DXylF)_2(THF)_2]$ is shared by two chromium metals. The Cr–Cl distances of 2.369(2) and 2.371(2) Å in **4** are slightly shorter than the corresponding distances in **5** [2.374(2)–2.398(2) Å]. The Cr–Cl distances in both complexes **4** [2.369(2) and 2.371(2) Å] and **5** [2.374(2)–2.398(2) Å] are similar to the corresponding distances reported in $[(nacnac)Cr(\mu\text{–}Cl)]_2$ [2.4182(4) and 2.4316(4) Å],[9c] $[Cr_2(\mu\text{–}Cl)_2(DXylF)_2(THF)_2]$ [2.370(1) and 2.596(1) Å],[15b] $[Cr_2(\mu\text{–}Cl)_2L_2(THF)_2]$ (L = [6–(2,4,6–triisopropyphenyl)pyridin–2–yl] (2,4,6–trimethylphenyl)amide) [2.3773(5) and 2.6219(5) Å][10a] and $[Cr\{Me_2NC(NAr)_2\}(\mu\text{–}Cl)]_2$ [2.366(2)–2.389(3) Å].[19] The C(13)–N(1) and C(13)–N(3) distances [1.339(6) and 1.322(6) Å,

* The DxylF ligands coordinate to the Cr(II) center in $[Cr_2(\mu\text{–}Cl)_2(DXylF)_2(THF)_2]$ in a $\mu\text{–}\eta^1\text{:}\eta^1$ bridging mode.

respectively] in complex **4** are shorter than the C(13)–N(2) distance [1.434(6) Å], indicating the delocalization of the anionic charge over the N(1)–C(13)–N(2) moiety. Delocalization of anionic charge over the N(4)–C(44)–N(6) moiety is also noted in complex **5**: C(13)–N(1) 1.344(6) Å, C(13)–N(2) 1.412(6) Å, C(13)–N(3) 1.336(6) Å, C(44)–N(4) 1.339(6) Å, C(44)–N(5) 1.416(6) Å, and C(44)–N(6) 1.349(6) Å.

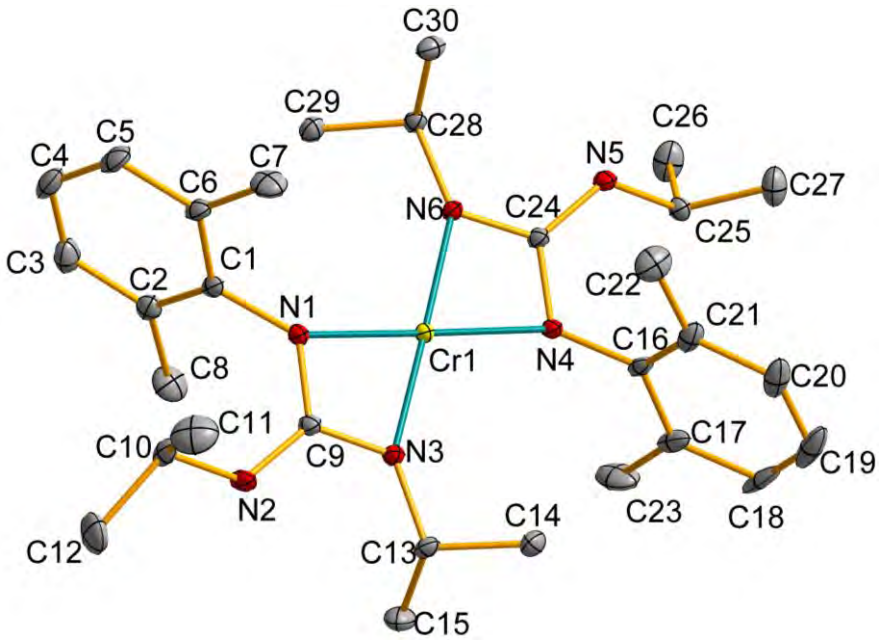

Figure 2–6. Molecular structure of $[Cr(L^1)_2]$ (**3**).

Table 2–5. Selected bond distances (Å) and angles (deg.) for compound **3**

$[Cr(L^1)_2]$ (**3**)			
Cr(1)–N(1)	2.060(3)	Cr(1)–N(3)	2.051(4)
Cr(1)–N(4)	2.070(3)	Cr(1)–N(6)	2.037(4)
C(9)–N(1)	1.338(5)	C(9)–N(2)	1.356(6)
C(9)–N(3)	1.319(5)	C(24)–N(4)	1.349(5)
C(24)–N(5)	1.368(5)	C(24)–N(6)	1.327(5)
N(1)–Cr(1)–N(3)	64.7(1)	N(1)–Cr(1)–N(6)	114.3(1)
N(4)–Cr(1)–N(3)	115.8(1)	N(4)–Cr(1)–N(6)	65.2(1)
N(1)–Cr(1)–N(4)	178.7(2)	N(3)–Cr(1)–N(6)	179.0(1)
N(1)–C(9)–N(3)	111.8(3)	N(4)–C(24)–N(6)	111.5(3)
C(9)–N(2)–C(10)	127.3(4)	C(24)–N(5)–C(25)	125.7(3)

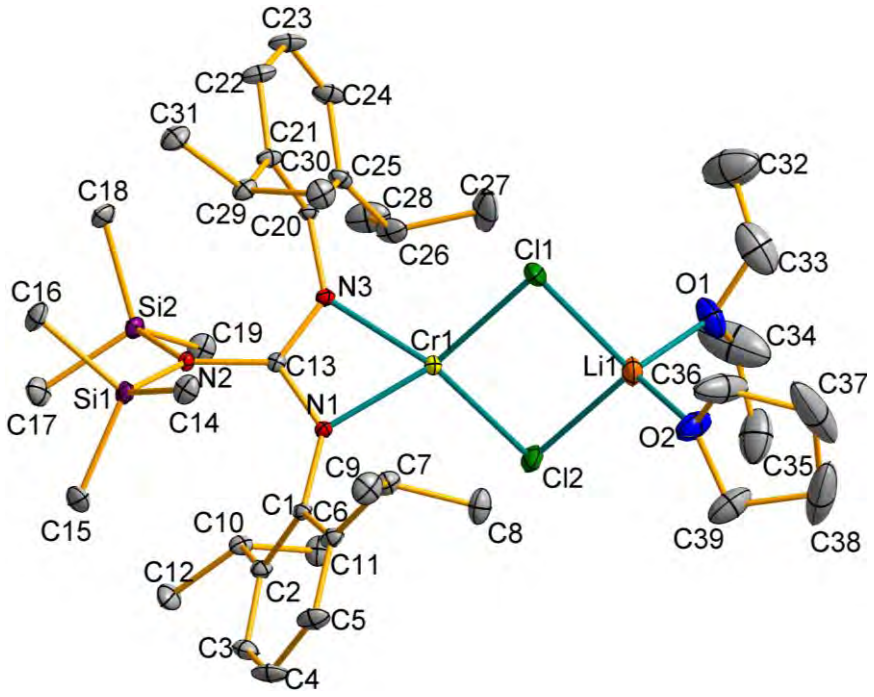

Figure 2–7. Molecular structure of $[Cr(L^4)(\mu\text{–}Cl)_2Li(THF)(Et_2O)]$ (**4**)

Table 2–6. Selected bond distances (Å) and angles (deg.) for compound **4**

$[Cr(L^4)(\mu\text{–}Cl)_2Li(THF)(Et_2O)]$ (**4**)			
Cr(1)–N(1)	2.045(3)	Cr(1)–N(3)	2.044(4)
Cr(1)–Cl(1)	2.369(2)	Cr(1)–Cl(2)	2.371(2)
Li(1)–Cl(1)	2.36(1)	Li(1)–Cl(2)	2.35(1)
Li(1)–O(1)	1.94(1)	Li(1)–O(2)	1.90(1)
N(1)–C(13)	1.339(6)	N(2)–C(13)	1.434(6)
N(3)–C(13)	1.322(6)		
N(1)–Cr(1)–N(3)	64.2(2)	Cl(1)–Cr(1)–Cl(2)	94.9(6)
N(1)–Cr(1)–Cl(1)	147.2(1)	N(1)–Cr(1)–Cl(2)	107.9(1)
N(3)–Cr(1)–Cl(1)	107.2(1)	N(3)–Cr(1)–Cl(2)	147.9(1)
O(1)–Li(1)–O(2)	108.6(5)	Cl(1)–Li(1)–Cl(2)	95.8(3)
O(1)–Li(1)–Cl(1)	111.1(5)	O(1)–Li(1)–Cl(2)	116.2(5)
O(2)–Li(1)–Cl(1)	111.9(5)	O(2)–Li(1)–Cl(2)	112.8(5)
Cr(1)–Cl(1)–Li(1)	84.5(3)	Cr(1)–Cl(2)–Li(1)	84.6(3)
N(1)–C(13)–N(3)	109.5(4)		

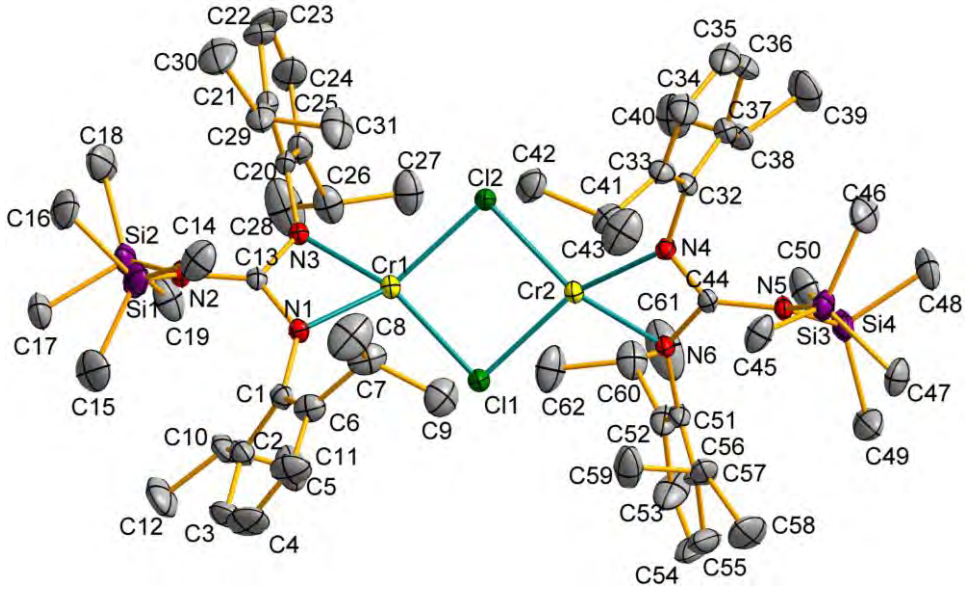

Figure 2–8. Molecular structure of [{Cr(L^4)(μ–Cl)$_2$}] (**5**)

Table 2–7. Selected bond distances (Å) and angles (deg.) for compound **5**

[{Cr(L^4)(μ–Cl)$_2$}] (**5**)			
Cr(1)–N(1)	2.029(4)	Cr(1)–N(3)	2.005(4)
Cr(2)–N(4)	2.031(4)	Cr(2)–N(6)	2.012(4)
Cr(1)–Cl(1)	2.374(2)	Cr(1)–Cl(2)	2.389(2)
Cr(2)–Cl(1)	2.398(2)	Cr(2)–Cl(2)	2.374(2)
N(1)–C(13)	1.344(6)	N(2)–C(13)	1.412(6)
N(3)–C(13)	1.336(6)	N(4)–C(44)	1.339(6)
N(5)–C(44)	1.416(6)	N(6)–C(44)	1.349(6)
N(1)–Cr(1)–N(3)	64.9(2)	Cl(1)–Cr(1)–Cl(2)	88.87(5)
N(4)–Cr(2)–N(6)	65.3(2)	Cl(1)–Cr(2)–Cl(2)	88.67(5)
N(1)–Cr(1)–Cl(1)	107.6(1)	N(1)–Cr(1)–Cl(2)	155.8(1)
N(3)–Cr(1)–Cl(1)	157.7(1)	N(3)–Cr(1)–Cl(2)	105.7(1)
N(4)–Cr(2)–Cl(1)	153.4(1)	N(4)–Cr(2)–Cl(2)	109.4(1)
N(6)–Cr(2)–Cl(1)	105.5(1)	N(6)–Cr(2)–Cl(2)	156.0(1)
Cr(1)–Cl(1)–Cr(2)	90.60(5)	Cr(1)–Cl(2)–Cr(2)	90.83(5)
N(1)–C(13)–N(3)	107.9(4)	N(4)–C(44)–N(6)	

2.2.3 Reaction Chemistry of $[Cr(L^1)_2]$ (3) and $[Cr(L^4)(\mu\text{–}Cl)_2Li(THF)(Et_2O)]$ (4)

The four–coordinated Cr(II) complex **3** is expected to be a reactive species due to its low oxidation state. By adding suitable oxidizing reagents to complex **3**, higher valent chromium complexes can be isolated. In addition, complex **4** contains a chloride ligand which can undergo metathesis reactions with suitable ligand–transfer reagents.

Reaction of **3** with iodine

Direct reaction of iodine with two equivalents of Cr(II) guanidinate **3** gave the Cr(III) guanidinate iodide complex $[Cr(L^1)_2I]$ (**6**) as red crystals (Scheme 2–14).

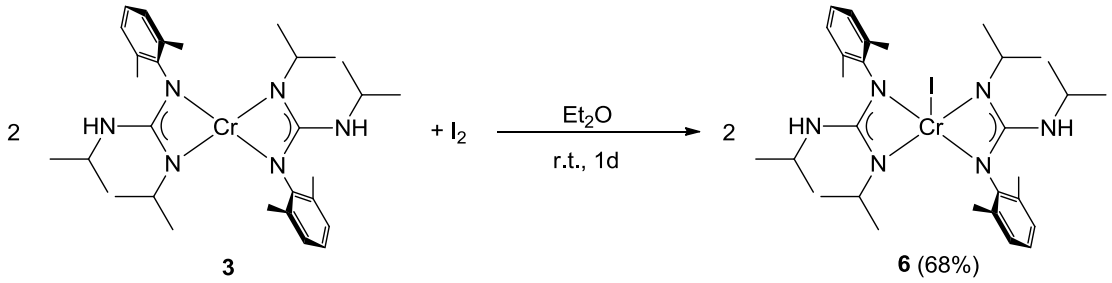

3 **6** (68%)

Scheme 2—14

Reactions of **3** with PhEEPh (E = S, Se, Te)

Treatment of diphenyl dichalcogenides PhEEPh (E = S, Se, Te) with two molar equivalents of complex **3** led to a reductive cleavage of the E–E bond to form the

corresponding Cr(III) chalcogenate complexes [Cr(L^1)$_2$(EPh)] [E = S (**7**), Se (**8**), Te (**9**)]. Complexes **7**–**9** were isolated as deep brown crystals (Scheme 2–15).

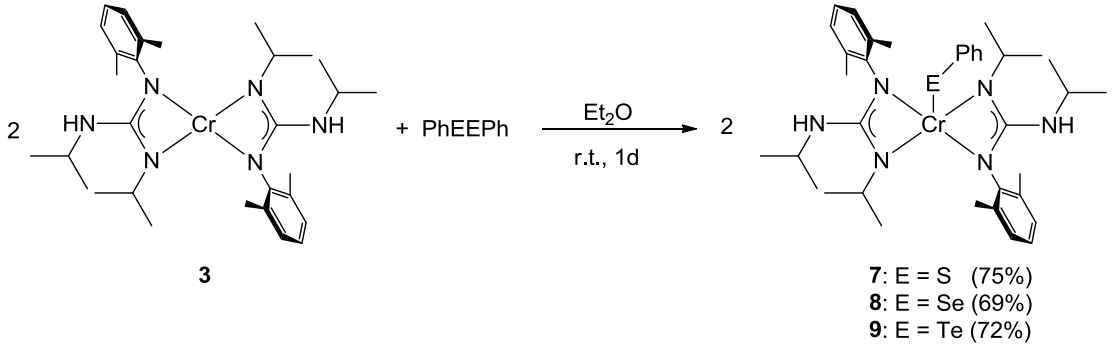

Scheme 2—15

Reaction of **3** with 1–azidoadamantane

Addition of one equivalent of 1–azidoadamantane to a solution of **3** in THF led to a color change of the reaction mixture from purple to deep green. Gas bubbles were generated at the beginning of the reaction, which may be attributed to the generation of N_2 from 1–azidoadamantane. After work–up, a deep green crystalline product was isolated, which was identified as [Cr(L^1)$_2${N(1–Ad)}] (1–Ad = 1–adamantyl) (**10**) (Scheme 2–16).

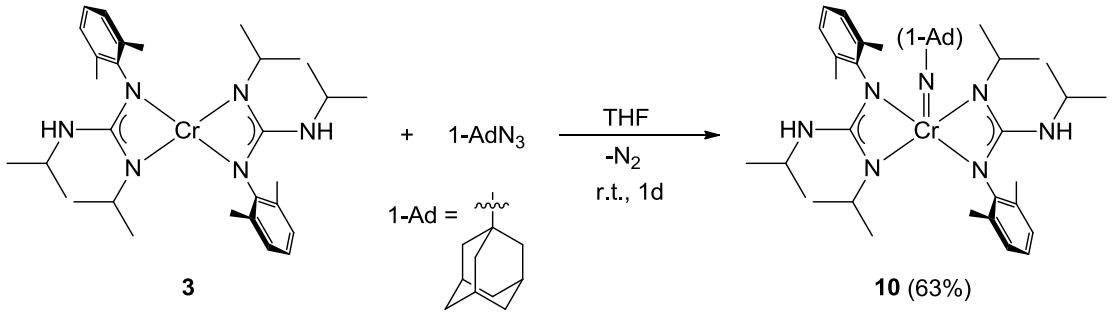

Scheme 2—16

Reaction of **4** with sodium methoxide

Treatment of complex **4** with one molar equivalent of NaOMe in THF yielded dinuclear Cr(II) guanidinate–methoxide complex [{Cr(L^4)(μ–OMe)}$_2$] (**11**) in 93% yield (Scheme 2–17). Complex **11** were isolated as purple crystals.

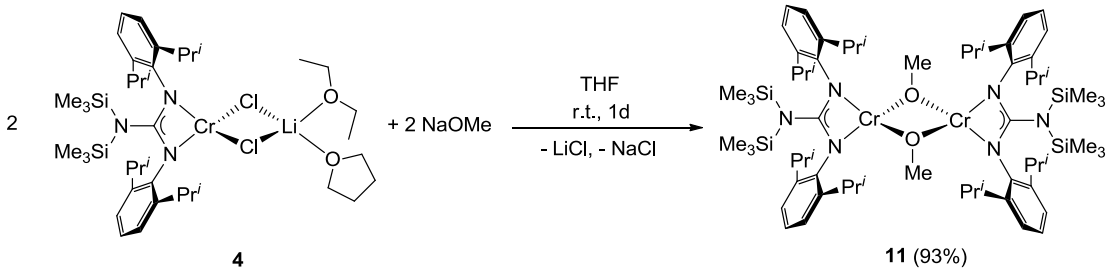

Scheme 2—17

Physical Characterization of Complexes **6–11**

All of the complexes **6–11** are extremely sensitive to air. They are soluble in common organic solvents except complex **10**, which is only soluble in THF and sparingly soluble in toluene.

The formulation of complexes **6–11** has been confirmed by elemental analysis and single–crystal X–ray diffraction studies. Table 2–8 summarizes the appearance and melting points of complexes **6–11**. In addition, UV–Vis spectra of complexes **7–9** have also been measured.

X–Ray diffraction studies revealed a distorted trigonal bipyramidal geometry around the metal center in complexes **6–10** (*vide infra*). Figure 2–9 shows the splitting of d orbitals in a trigonal bipyramidal field.

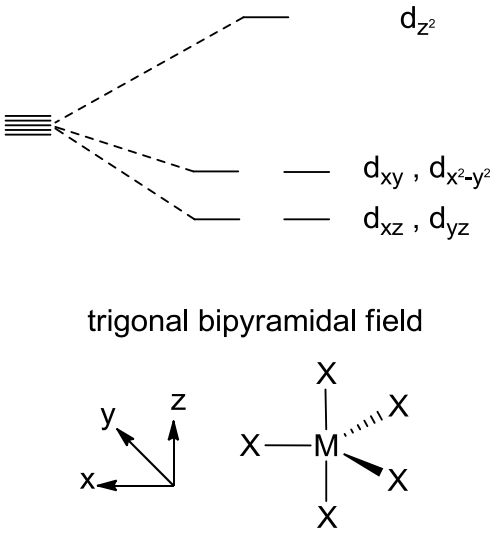

Figure 2—9

The solution magnetic moments of complexes **6**–**11** were measured by the Evans NMR method in C_6D_6 solutions at 298 K.[28] The solution magnetic moments of 3.68 μ_B for **6**, 3.83 μ_B for **7**, 3.88 μ_B for **8**, and 3.91 μ_B for **9** are all consistent with the spin–only value calculated for a high–spin d^3 electronic configuration (3.87 μ_B). The solution magnetic moment of 2.70 μ_B for the Cr(IV) complex **10** is consistent with a d^2 electronic configuration (spin–only value = 2.83 μ_B). For the dimeric Cr(II) complex **11**, the solution magnetic–moment of 2.40 μ_B per chromium center is smaller than the spin–only value of a high–spin d^4 electronic configuration, but is close to the value measured for complex **5**. This may be attributed to an antiferromagnetic coupling between the two Cr(II) centers in the $[\{Cr(L^4)(\mu\text{–}OMe)\}_2]$ complex.

Table 2–8. Appearance and melting points of complexes **6–11**

Compound	Appearance	M.p. (^{o}C)
$[Cr(L^1)_2I]$ (**6**)	Red crystals	195–197
$[Cr(L^1)_2(SPh)]$ (**7**)	Deep green crystals	171–172
$[Cr(L^1)_2(SePh)]$ (**8**)	Deep green crystals	168–170
$[Cr(L^1)_2(TePh)]$ (**9**)	Deep green crystals	175–177
$[Cr(L^1)_2\{N(1–Ad)\}]$ (**10**)	Deep green crystals	193–196 (dec.)
$[\{Cr(L^4)(\mu–OMe)\}_2]$ (**11**)	Purple crystals	182–183

UV–Vis spectra of Complexes **7–9**

The UV–Vis spectra of complexes **7–9** are shown in Figures A5–2 to A5–4, respectively, in Appendix 5. Complexes **7–9** dissolved in THF to give a greenish yellow solution. The UV–Vis spectra of complexes **7** and **8** show only one absorption maximum at λ_{max} (ε/$M^{-1}cm^{-1}$) 658 (130) and 674 (140), respectively. On the other hand, the UV–Vis spectrum of complex **9** shows two absorption maxima at λ_{max} (ε/$M^{-1}cm^{-1}$) 382 (sh, 640) and 674 (140), respectively.

Crystal Structures of Complexes **6–11**

Single crystals of **6** and **11** suitable for X–ray diffraction analysis were obtained from toluene. Those of **7–9** were obtained from Et_2O. Single crystals of **10** were obtained from THF. Selected crystallographic data of these complexes are listed in Appendix 3.

1. $[Cr(L^1)_2I]$ (**6**)

The molecular structure of complex **6** with atom labeling is shown in Figure 2–10. Selected bond lengths and angles are listed in Table 2–8.

Crystals of **6** belong to the orthorhombic space group $Pca2_1$. The chromium(III) center is coordinated by two κ^2–bound L^1 ligands and one iodide ligand. The coordination geometry around the metal center is best described as distorted trigonal bipyramidal, with the two axial positions being occupied by N(3) and N(6) [N(3)–Cr(1)–N(6) = 165.5(2)^o], whereas the equatorial plane consisting of N(1), N(4) and I(1) (sum of bond angles around Cr(1) = 360.0^o). The observed Cr–N distances in complex **6** [1.994(6)–2.009(5) Å] are necessarily shorter than those in the Cr(II) precursor complex **3** [2.037(4)–2.070(3) Å], since the ionic radii of Cr^{2+} and Cr^{3+} are 87 pm and 75.5 pm, respectively.[33] They are also shorter than the corresponding distances in the four–coordinated [CpCr{$(ArNCMe)_2CH$}(I)] (Ar = $C_6H_3Pr^i_2$–2,6) [2.034(2) and 2.041(2)Å][34] and the six–coordinated [Cr{$(Me_3SiN)_2CPh$}$_2$(I)(THF)] [2.023(3)–2.083(3) Å].[16] The C–N bond distances around C(9) [also for C(24)] are almost identical. This suggests that the electron density delocalizes in the CN_3 moiety of the guanidinate ligand. The Cr(1)–I(1) distance of 2.674(1) Å is slightly shorter than the terminal Cr–I distances in [CpCr{$(ArNCMe)_2CH$}(I)] [2.6813(5) Å],[34] [$Cp^*Cr(\mu$–OR)I]$_2$ (R = Me, Et) [2.6960(8) and 2.6979(4) Å][35] and [Cr{$(Me_3SiN)_2CPh$}$_2$(I)(THF)] [2.7664(5) Å].[16]

2. $[Cr(L^1)_2(EPh)]$ [E = S (**7**), Se (**8**), Te (**9**)]

The molecular structures of complexes **7**–**9** are shown in Figures 2–11 to 2–13, respectively. Selected bond lengths and angles are presented in Tables 2–9 to 2–11.

Complexes **7**, **8** and **9** are isostructural. All of them crystallize in the monoclinic space group $P2_1$. The chromium metal center in each complex is bound by two L^1 ligands and one terminal phenyl chalcogenide ligand. If the phenyl chalcogenide ligand is considered as a single point donor, each complex consists of a two–fold rotational axis passing through the Cr–E bond. Table 2–12 summarizes the Cr–E bond lengths, and important bond angles around the Cr(III) center in these complexes.

Table 2–12. The Cr–E distances (Å), the $N^{(isopropyl)}$–Cr–$N^{(isopropyl)}$ angles, the $N^{(aryl)}$–Cr–$N^{(aryl)}$ angles and the Cr–E–$C^{(phenyl)}$ angles (°) for complexes **7**–**9**.

$[Cr(L^1)_2(EPh)]$	E = S (**7**)	E = Se (**8**)	E = Te (**9**)
Cr–E (Å)	2.309(1)	2.424(1)	2.652(1)
$N^{(isopropyl)}$–Cr–$N^{(isopropyl)}$ (°)	157.8(2)	157.0(3)	152.8(3)
$N^{(aryl)}$–Cr–$N^{(aryl)}$ (°)	149.6(2)	153.7(3)	160.3(3)
Cr–E–$C^{(phenyl)}$ (°)	115.3(2)	113.0(2)	110.2(2)

The geometry around the chromium atom can be best described as distorted trigonal bipyramid. The two axial positions are occupied by the two $N^{(isopropyl)}$ atoms [N(3) and N(6)] in complexes **7** and **8**. The observed N(3)–Cr(1)–N(6) angles are 157.8(2)^o (for **7**) and 157.0(3)^o (for **8**). However, in complex **9**, the axial positions are occupied by the two $N^{(aryl)}$ atoms [N(1) and N(4)] with N(1)–Cr(1)–N(4) angle being 160.3(3)^o. The steric bulkiness of the ligand substituents increase in the order of Pr^i < EPh < Ar. According to the VSEPR theory, the equatorial plane of complexes **7** and **8** is consisting of one EPh ligand and two $N^{(aryl)}$ atoms. Complex **9** has the longest Cr–E distance (among the three complexes). Therefore, steric repulsion between the PhTe ligand and the two aryl groups is reduced. This is also consistent with a reduction in the Cr–E–$C^{(phenyl)}$ angle from complex **7** [115.3(2)^o] to complex **9** [110.2(2)^o]. In complex **9**, the two $N^{(aryl)}$ atoms occupy the axial positions, keeping the TePh ligand on the equatorial plane.

The observed Cr–E bond distance increases from complex **7** to complex **9**, which is consistent with an increasing ionic radius of S < Se < Te.

The terminal Cr–S distance in complex **7** [2.309(1) Å] is shorter than the corresponding distances in the five–coordinated [{CpCr(SPh)}$_2$S] [2.365(1)–2.383(1) Å].[36] The Cr(1)–S(1)–C(31) angle of 115.3(2)^o is comparable to the corresponding angles in [{CpCr(SPh)}$_2$S] [109.6(1)–115.6(2)^o].[36]

The terminal Cr–Se distance in **8** [2.414(1) Å] is shorter than the corresponding bond length of 2.473(2)–2.500(2) Å in [{CpCr(SePh)}$_2$Se].[37] The Cr(1)–Se(1)–C(31) angle of 113.0^o is larger than the corresponding angles in [{CpCr(SePh)}$_2$Se] [106.5(2)–113.1(3)^o].[37]

The terminal Cr–Te distance in **9** of 2.652(1) Å falls within the range of 2.642(1)–2.661(1) Å in [{CpCr(TePh)}$_2$Te].[38] The Cr(1)–Te(1)–C(31) angle of 110.2(2)^o is comparable to the corresponding angles of 107.6(3)–109.7(3)^o in [{CpCr(TePh)}$_2$Te].[38]

3. [Cr(L^1)$_2${N(1–Ad)}] (**10**)

The molecular structure of complex **10** with the atom labeling scheme is shown in Figure 2–14. Selected bond distances and angles of complex **10** is listed in Table 2–13.

Complex **10** crystallizes in the monoclinic space group $P2_1/c$. The coordination geometry around the chromium atom can also be described as distorted trigonal bipyramid: nitrogen atoms N(1), N(4) and N(7) form the equatorial plane, whereas, N(3) and N(6) occupy the axial sites [N(3)–Cr(1)–N(6) = 151.3(4)^o]. The sum of bond angles around Cr(1) on the trigonal plane is measured to be of 360.0^o. It is noted that the sterically bulky aromatic and adamantyl groups occupying the equatorial positions to give a sterically stable configuration.

The Cr(1)–N(7) distance of 1.661(8) Å is comparable to the Cr=N double bond in [(^{t}Bu$_3$SiO)$_2$Cr=N(2,6–Ph$_2$C$_6$H$_3$)] [1.649(2) Å][39] and [(L$^{\cdot}$)$_2$Cr(NAd)] [1.667(2) Å] (where L$^{\cdot}$ represents a monoanionic π radical of the α–iminopyrid ligand 2,6–bis(1–methylethyl)–*N*–(2–pyridinylmethylene)phenylamine).[40] Based on a comparison with these complexes, the Cr(1)–N(7) bond can be considered as a double bond.

The imido nitrogen atom N(7) adopts an almost linear geometry [Cr(1)–N(7)–C(31) = 175.3(8)^o], indicating an sp hybridization. A similar observation was also reported for the chromium(IV) imido complexes [(^{t}Bu$_3$SiO)$_2$Cr=N(2,6–Ph$_2$C$_6$H$_3$)] [175.9(2)^o][39] and [(L$^{\cdot}$)$_2$Cr(NAd)] [163.6(1)^o].[40]

4. [{Cr(L^4)(μ–OMe)}$_2$] (**11**)

The molecular structure of complex **11** with the atom labeling scheme is shown in Figure 2–15. Selected bond distances and angles of complex **11** are listed in Table 2–14.

Complex **11** crystallizes in the monoclinic space group $P2_1/c$. The binuclear complex consists of a planar Cr_2O_2 core [angle sum of the Cr(1)–O(1)–Cr(2)–O(2) square plane is 358.9^o]. The coordination geometry around each chromium atom can be described as distorted tetrahedral with each Cr(II) center being coordinated by one κ^2–bound L^4 ligand and two bridging methoxide ligands. The O atom in each

methoxide ligand adopts a trigonal planar geometry (sum of bond angles around O(1) and O(2) are both 359.9°), indicating an sp^2 hybridized oxygen atom.

The observed Cr–N distances of 2.038(3)–2.065(3) Å in **11** are comparable to the corresponding distances of 2.037(4)–2.070(3) Å in the Cr(II) bis(guanidinate) complex $[Cr(L^1)_2]$ (**3**) and 2.044(4)–2.045(3) Å in the Cr(II) chloride precursor $[Cr(L^4)(\mu\text{–}Cl)_2Li(THF)(Et_2O)]$ (**4**). They are slightly longer than that of 2.005(4)–2.031(4) Å in the dimeric Cr(II) guanidinate complex $[\{Cr(L^4)(\mu\text{–}Cl)_2\}]$ (**5**). On the other hand, it is relatively long as compared with those terminal Cr–N(amido) distances observed in the two–coordinate Cr(II) amides $[Cr\{N(H)Ar^{Pr^i_6}\}_2]$ ($Ar^{Pr^i_6}$ = C_6H_3–2,6–(C_6H_2–2,4,6–Pr^i_3)$_2$) [1.997(1) Å],[6c] $[Cr\{N(H)Ar^{Pr^i_4}\}_2]$ ($Ar^{Pr^i_4}$ = C_6H_3–2,6–(C_6H_2–2,6–Pr^i_2)$_2$) [1.978(1) Å],[6c] $[Cr\{N(H)Ar^{Me_6}\}_2]$ (Ar^{Me_6} = C_6H_3–2,6–(C_6H_2–2,4,6–Me_3)$_2$) [1.977(3) Å][6c] and the three–coordinate $[Cr\{N(H)Ar^{Me_6}\}_2(THF)]$ [1.978(1) Å].[6c]

The Cr–O distances of 1.988(2)–1.994(3) Å in **11** fall within the range of 1.987(8)–2.036(8) Å in $[\{Cr(\mu\text{–}Cl)(\mu\text{–}OSi^tBu_3)\}_4]$[41] and 1.835(4)–2.013(4) Å in $[(^tBu_3SiO)Cr]_2(\mu\text{–}OSi^tBu_3)_2$.[39] However, they are slightly longer than the corresponding distances in $[(^tBu_3SiO)Cr(\mu\text{–}OSi^tBu_3)_2]Na\cdot C_6H_6$ [1.891(2)–1.972(1) Å][41] and $[(^tBu_3SiO)_3Cr][Na(dibenzo\text{–}18\text{–}crown\text{–}6)]$ [1.891(3)–1.942(3) Å].[41]

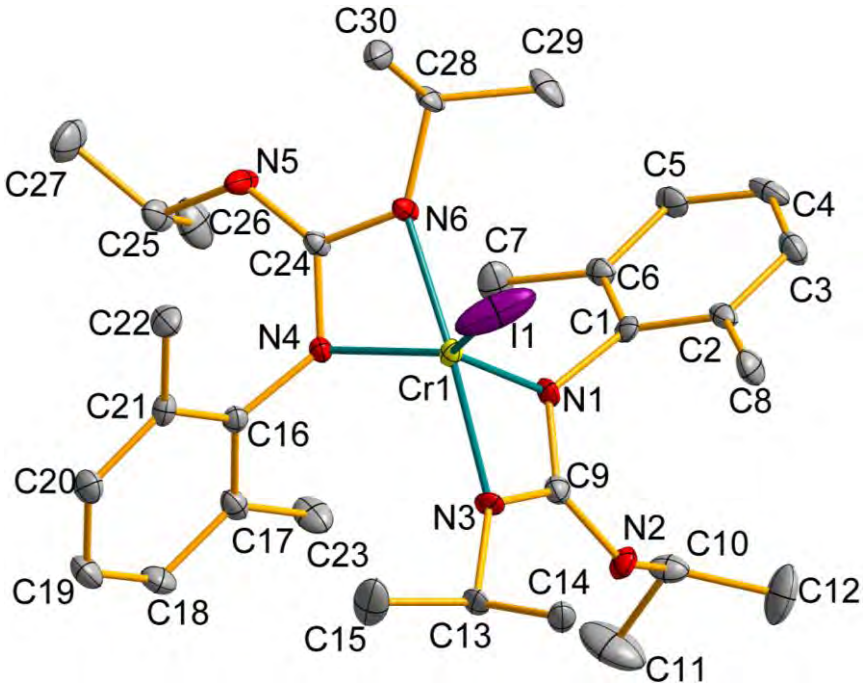

Figure 2–10. Molecular structure of $[Cr(L^1)_2I]$ (**6**)

Table 2–8. Selected bond distances (Å) and angles (deg.) for compound **6**

$[Cr(L^1)_2I]$ (**6**)			
Cr(1)–N(1)	1.996(6)	Cr(1)–N(3)	2.009(5)
Cr(1)–N(4)	1.976(6)	Cr(1)–N(6)	1.994(5)
Cr(1)–I(1)	2.674(1)	N(1)–C(9)	1.36(1)
N(2)–C(9)	1.34(1)	N(3)–C(9)	1.33(1)
N(4)–C(24)	1.364(9)	N(5)–C(24)	1.35(1)
N(6)–C(24)	1.32(1)		
N(1)–Cr(1)–N(3)	66.4(2)	N(4)–Cr(1)–N(6)	66.4(2)
N(3)–Cr(1)–N(6)	165.5(2)	N(1)–Cr(1)–N(4)	99.4(3)
N(1)–Cr(1)–I(1)	128.2(2)	N(4)–Cr(1)–I(1)	132.4(2)
N(3)–Cr(1)–N(4)	103.5(3)	N(1)–Cr(1)–N(6)	103.9(3)
N(3)–Cr(1)–I(1)	97.7(2)	N(6)–Cr(1)–I(1)	96.8(2)

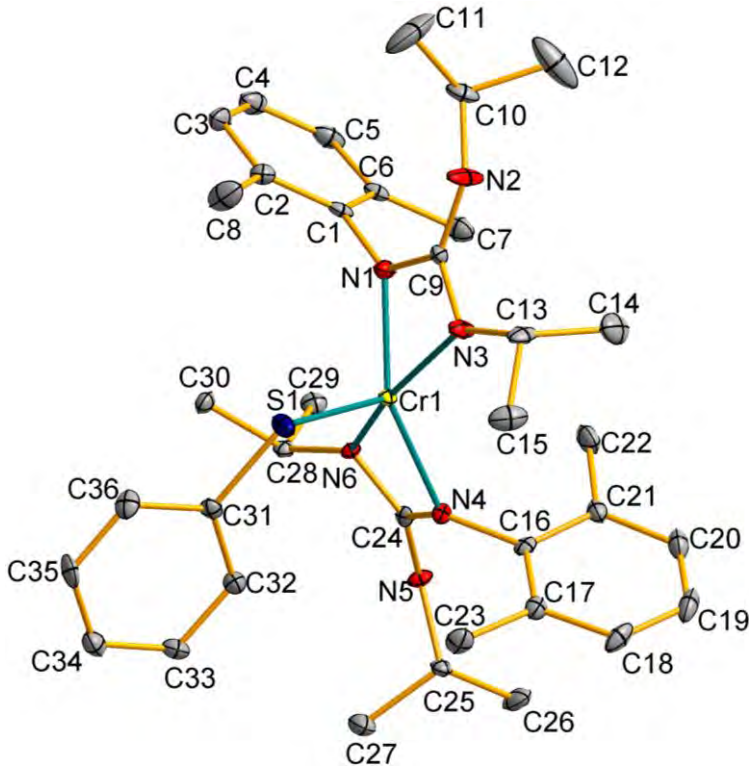

Figure 2–11. Molecular structure of $[Cr(L^1)_2(SPh)]$ (**7**)

Table 2–9. Selected bond distances (Å) and angles (deg.) for compound **7**

$[Cr(L^1)_2(SPh)]$ (**7**)			
Cr(1)–N(1)	2.016(5)	Cr(1)–N(3)	2.015(5)
Cr(1)–N(4)	2.028(4)	Cr(1)–N(6)	2.003(4)
Cr(1)–S(1)	2.309(1)	N(1)–C(9)	1.345(7)
N(2)–C(9)	1.348(7)	N(3)–C(9)	1.338(7)
N(4)–C(24)	1.346(7)	N(5)–C(24)	1.356(6)
N(6)–C(24)	1.333(7)	S(1)–C(31)	1.762(5)
N(1)–Cr(1)–N(3)	66.0(2)	N(4)–Cr(1)–N(6)	66.2(2)
N(3)–Cr(1)–N(6)	157.8(2)	N(1)–Cr(1)–N(4)	149.6(2)
N(1)–Cr(1)–S(1)	106.2(1)	N(4)–Cr(1)–S(1)	104.2(1)
N(3)–Cr(1)–N(4)	110.4(2)	N(1)–Cr(1)–N(6)	105.2(2)
N(3)–Cr(1)–S(1)	93.9(2)	N(6)–Cr(1)–S(1)	108.3(1)
Cr(1)–S(1)–C(31)	115.3(2)		

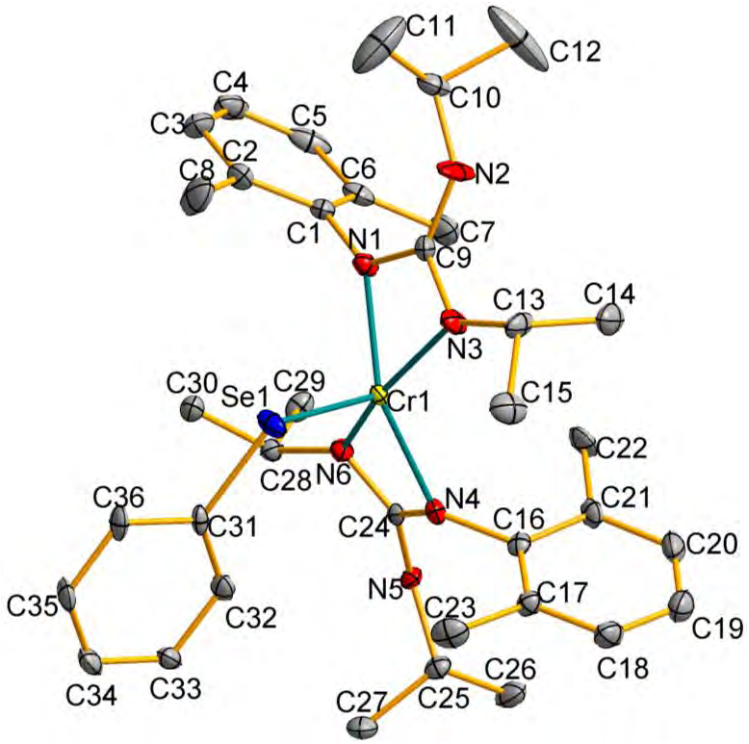

Figure 2–12. Molecular structure of $[Cr(L^1)_2(SePh)]$ (**8**)

Table 2–10. Selected bond distances (Å) and angles (deg.) for compound **8**

$[Cr(L^1)_2(SePh)]$ (**8**)			
Cr(1)–N(1)	2.034(7)	Cr(1)–N(3)	2.018(7)
Cr(1)–N(4)	2.033(7)	Cr(1)–N(6)	1.981(7)
Cr(1)–Se(1)	2.414(1)	N(1)–C(9)	1.31(1)
N(2)–C(9)	1.33(1)	N(3)–C(9)	1.35(1)
N(4)–C(24)	1.34(1)	N(5)–C(24)	1.34(1)
N(6)–C(24)	1.31(1)	Se(1)–C(31)	1.896(7)
N(1)–Cr(1)–N(3)	65.3(3)	N(4)–Cr(1)–N(6)	65.9(3)
N(3)–Cr(1)–N(6)	157.0(3)	N(1)–Cr(1)–N(4)	153.7(3)
N(1)–Cr(1)–Se(1)	101.6(2)	N(4)–Cr(1)–Se(1)	104.6(2)
N(3)–Cr(1)–N(4)	110.8(3)	N(1)–Cr(1)–N(6)	106.9(3)
N(3)–Cr(1)–Se(1)	93.8(3)	N(6)–Cr(1)–Se(1)	109.2(2)
Cr(1)–Se(1)–C(31)	113.0(2)		

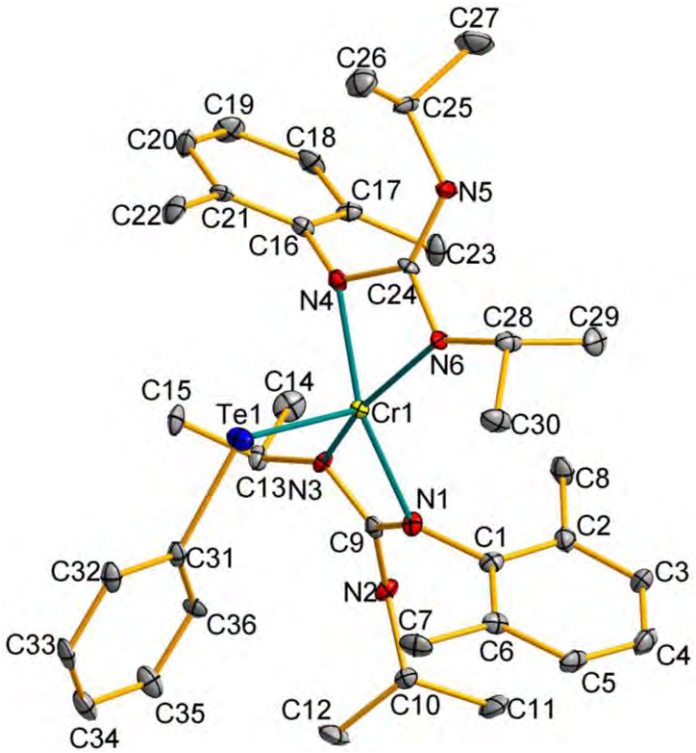

Figure 2–13. Molecular structure of $[Cr(L^1)_2(TePh)]$ (**9**)

Table 2–11. Selected bond distances (Å) and angles (deg.) for compound **9**

$[Cr(L^1)_2(TePh)]$ (**9**)			
Cr(1)–N(1)	2.035(8)	Cr(1)–N(3)	2.026(7)
Cr(1)–N(4)	2.062(7)	Cr(1)–N(6)	2.020(7)
Cr(1)–Te(1)	2.652(1)	N(1)–C(9)	1.34(1)
N(2)–C(9)	1.37(1)	N(3)–C(9)	1.32(1)
N(4)–C(24)	1.35(1)	N(5)–C(24)	1.37(1)
N(6)–C(24)	1.35(1)	Te(1)–C(31)	2.120(9)
N(1)–Cr(1)–N(3)	65.6(3)	N(4)–Cr(1)–N(6)	65.9(3)
N(3)–Cr(1)–N(6)	152.8(3)	N(1)–Cr(1)–N(4)	160.3(3)
N(1)–Cr(1)–Te(1)	105.2(2)	N(4)–Cr(1)–Te(1)	94.5(2)
N(3)–Cr(1)–N(4)	109.1(3)	N(1)–Cr(1)–N(6)	109.4(3)
N(3)–Cr(1)–Te(1)	108.3(2)	N(6)–Cr(1)–Te(1)	98.8(2)
Cr(1)–Te(1)–C(31)	110.2(2)		

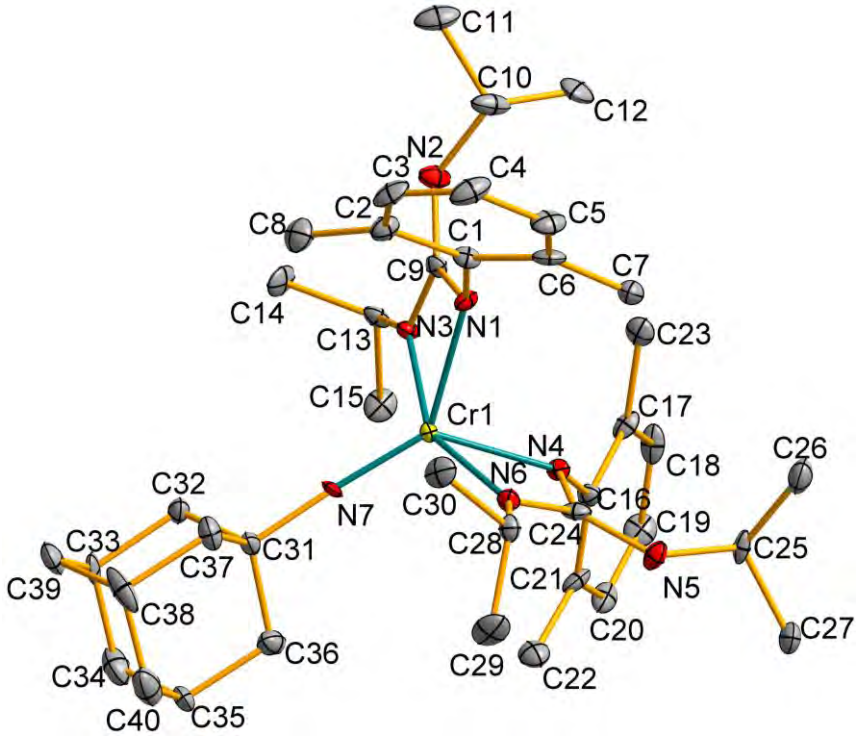

Figure 2–14. Molecular structure of [Cr(L^1)$_2${N(1–Ad)}] (**10**)

Table 2–13. Selected bond distances (Å) and angles (deg.) for compound **10**

[Cr(L^1)$_2${N(1–Ad)}] (**10**)			
Cr(1)–N(1)	2.129(9)	Cr(1)–N(3)	2.033(9)
Cr(1)–N(4)	2.111(9)	Cr(1)–N(6)	2.044(9)
Cr(1)–N(7)	1.661(8)	N(1)–C(9)	1.34(1)
N(2)–C(9)	1.36(1)	N(3)–C(9)	1.33(1)
N(4)–C(24)	1.34(1)	N(5)–C(24)	1.38(2)
N(6)–C(24)	1.32(1)	N(7)–C(31)	1.46(1)
N(1)–Cr(1)–N(3)	63.7(3)	N(4)–Cr(1)–N(6)	63.4(3)
N(3)–Cr(1)–N(6)	151.3(4)	N(1)–Cr(1)–N(4)	96.0(3)
N(1)–Cr(1)–N(7)	132.8(4)	N(4)–Cr(1)–N(7)	131.2(4)
N(3)–Cr(1)–N(4)	97.3(3)	N(1)–Cr(1)–N(6)	95.9(4)
N(3)–Cr(1)–N(7)	105.7(4)	N(6)–Cr(1)–N(7)	103.0(4)
Cr(1)–N(7)–C(31)	175.3(8)		

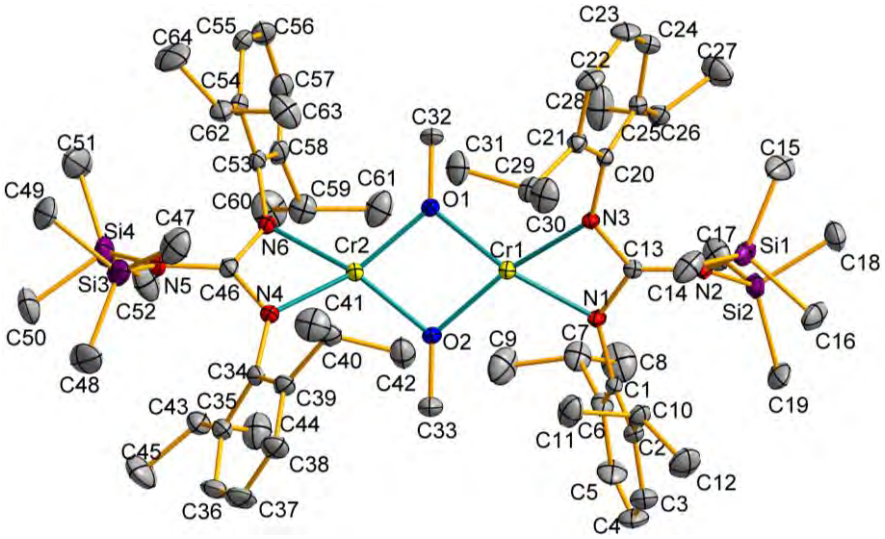

Figure 2–15. Molecular structure of [{Cr(L^4)(μ–OMe)}$_2$] (**11**)

Table 2–14. Selected bond distances (Å) and angles (deg.) for compound **11**

[{Cr(L^4)(μ–OMe)}$_2$] (**11**)			
Cr(1)–N(1)	2.048(3)	Cr(1)–N(3)	2.065(3)
Cr(2)–N(4)	2.042(3)	Cr(2)–N(6)	2.038(3)
Cr(1)–O(1)	1.988(2)	Cr(1)–O(2)	1.994(3)
Cr(2)–O(1)	1.990(3)	Cr(2)–O(2)	1.993(3)
N(1)–C(13)	1.348(4)	N(2)–C(13)	1.420(4)
N(3)–C(13)	1.340(4)	N(4)–C(46)	1.340(5)
N(5)–C(46)	1.432(5)	N(6)–C(46)	1.345(5)
N(1)–Cr(1)–N(3)	64.2(1)	O(1)–Cr(1)–O(2)	79.6(1)
N(4)–Cr(2)–N(6)	64.2(1)	O(1)–Cr(2)–O(2)	79.65(1)
N(1)–Cr(1)–O(1)	162.4(1)	N(1)–Cr(1)–O(2)	110.1(1)
N(3)–Cr(1)–O(1)	111.3(1)	N(3)–Cr(1)–O(2)	160.4(1)
N(4)–Cr(2)–O(1)	157.2(1)	N(4)–Cr(2)–O(2)	113.0(1)
N(6)–Cr(2)–O(1)	109.7(1)	N(6)–Cr(2)–O(2)	161.8(1)
Cr(1)–O(1)–Cr(2)	100.0(1)	Cr(1)–O(2)–Cr(2)	99.7(1)
N(1)–C(13)–N(3)	108.7(3)	N(4)–C(46)–N(6)	107.7(3)

2.2.4 Attempted Reactions of $[Cr(L^4)(\mu\text{–}Cl)_2Li(THF)(Et_2O)]$ (4)

Attempted reactions of **4** with LiC≡C(TMS), $NaNH_2$ and MeMgI, respectively

Attempts to react complex **4** with LiC≡C(TMS), $NaNH_2$ and MeMgI, respectively, were unsuccessful. Although an immediate color change of the solution from blue to brown was observed, only a brown intractable oil was obtained after work–up. The latter remained unidentified in this work.

Attempted reactions of **4** with Na, K and Mg metals, respectively

Reactions of complex **4** with strongly reducing Na, K and Mg metals, respectively, were examined in this work. Complex **4** was found to be unreactive towards Mg even at an elevated temperature of 50^{o}C. On the other hand, reactions of complex **4** with excess Na or K metal only led to the isolation of a brown intractable oil.

2.3 Summary

Divalent chromium complexes supported by the two unsymmetrical guanidinate ligands, namely $[(2,6\text{–}Me_2C_6H_3N)C(NHPr^i)(NPr^i)]^-$ (L^1) and $[(2,6\text{–}Pr^i{}_2C_6H_3N)C\{N(SiMe_3)_2\}(NC_6H_3Pr^i{}_2\text{–}2,6)]^-$ (L^4), have been synthesized and structurally characterized. A direct reaction of $CrCl_2$ with two molar equivalents of $[KL^1 \cdot 0.5PhMe]_n$ (**1**) gave the neutral, mononuclear Cr(II) bis(guanidinate) complex $[Cr(L^1)_2]$ (**3**). Treatment of $CrCl_2$ with one molar equivalent of $[LiL^4(Et_2O)]$ (**2**) led to the isolation of an ate–complex, $[Cr(L^4)(\mu\text{–}Cl)_2Li(THF)(Et_2O)]$ (**4**). Recrystallization of **4** from toluene gave neutral, dimeric $[\{Cr(L^4)(\mu\text{–}Cl)\}_2]$ (**5**).

The reaction chemistry of **3** and **4** was examined. Reaction of **3** with iodine resulted in the Cr(III) mono (iodo) complex $[Cr(L^1)_2I]$ (**6**). The Cr(III) chalcogenide complexes $[Cr(L^1)_2(EPh)]$ [E = S (**7**), Se (**8**), Te (**9**)] were prepared by the reactions of **3** with the corresponding diphenyl dichalcogenide (PhEEPh) in a 2:1 ratio. Treatment of **3** with 1–azidoadamantane yielded the mononuclear Cr(IV) bis(guanidinate)–imido complex $[Cr(L^1)_2\{N(1\text{–}Ad)\}]$ (**10**). Complex **4** underwent ligand substitution with NaOMe, leading to dimeric Cr(II) methoxide complex, $[\{Cr(L^4)(\mu\text{–}OMe)\}_2]$ (**11**).

2.4 Experimental Section for Chapter 2

Starting Materials:

Anhydrous $CrCl_2$ was purchased from Strem and used as received. Potassium hydride, *N*,*N*'–diisopropylcarbodiimide, n–butyllithium (1.6 M in hexane), sodium methoxide, PhSSPh, PhSeSePh, PhTeTePh, iodine and 1–azidoadamantane were purchased from Aldrich and used without further purification. 2,6–Dimethylaniline and hexamethyldisilazane were dried over and distilled from sodium hydroxide under reduced pressure. Bis(2,6–diisopropylphenyl)carbodiimide was prepared according to literature procedure.[21]

Synthesis of $[KL^1 \cdot 0.5PhMe]_n$ (1). To a slurry of potassium hydride (0.61 g, 15.2 mmol) in THF (20 ml) at 0 °C was added dropwise a solution of 2,6–dimethylaniline (1.84 g, 15.2 mmol) in THF (20 ml). The reaction mixture was allowed to warm slowly to room temperature and stirred for another period of 2 h. The solution was filtered and the filtrate was treated with *N*,*N*'–diisopropylcarbodiimide (2.3 ml, 14.8 mmol) at room temperature. The pale yellow reaction mixture was stirred at 45 °C for 8 h. All the volatiles were removed in *vacuo* and the brown residue was extracted with toluene (20 ml). Standing the solution at room temperature for 1 d gave complex **1** as colorless crystals. Yield: 3.66 g, 11.5 mmol, 76%. M.p.: 249–250 ℃ (dec.). ^{1}H NMR (400.13 MHz, THF–d_8): δ 0.99 (br, 12H, NCH(CH_3)$_2$), 2.08 (s, 6H,

ArCH_3), 2.31 (s, 1H, $C_6H_5CH_3$)*, 3.25 (br, 1H, NCH(CH_3)$_2$) 3.78 (br, 1H, NHCH(CH_3)$_2$), 6.37 (br, 1H, *p*–ArH), 6.77 (d, J = 7.2 Hz, 2H, *m*–ArH), 7.06–7.12 (m, 1.6H, $C_6H_5CH_3$)*. ^{13}C NMR (100.62 MHz, THF–d_8): δ 19.8, 21.5, 26.4, 44.5, 46.4, 116.5, 126.0, 128.0, 128.9, 129.7, 131.5, 133.3, 138.4, 156.6. Anal. Found: C, 65.85; H, 8.44; N, 13.30%. Calc. for $C_{37}H_{56}K_2N_6$: C, 67.02; H, 8.51; N, 12.67%.†

Synthesis of [LiL$_4$(Et$_2$O)] (2). To a solution of hexamethyldisilazane (1.61 g, 10 mmol) in diethyl ether (30 ml) was added a solution of LiBu^n (1.6 M, 7.5 ml, 12 mmol) in hexane at 0 ^{o}C. The resulting solution was stirred at room temperature for 2 h. A solution of bis(2,6–diisopropylphenyl)carbodiimide (3.63 g, 10 mmol) in diethyl ether (30 ml) was added at 0^{o}C. The reaction mixture was stirred at room temperature for 8 h. The solution was filtered and the filtrate was concentrated under reduced pressure to *ca*. 10 ml. Standing the solution at room temperature yielded complex **2** as colorless crystals. Yield: 3.92 g, 6.5 mmol, 65%. M.p.: 137–140 ^{o}C. ^{1}H NMR (400.13 MHz, THF–d_8): δ –0.81 (s, 6H, Si(CH_3)$_3$), –0.18 (s, 6H, Si(CH_3)$_3$), 0.13 (s, 6H, Si(CH_3)$_3$), 1.10–1.13 (br, 18H, CH(CH_3)$_2$ and OCH$_2$CH_3), 1.24 (dd, J = 5.6 Hz, 12H, CH(CH_3)$_2$), 3.39 (quartet, J = 7.2 Hz, 4H, OCH_2CH$_3$), 3.75 (br, 4H, CH(CH_3)$_2$), 6.67 (br, 2H, *p*–ArH), 6.83 (br, 4H, *m*–ArH). ^{13}C NMR (100.62

* Integration of resonance signals due to the solvated $C_6H_5CH_3$ molecules was not consistent with the formula of complex **1** as revealed by X-ray crystallography probably due to loss of $C_6H_5CH_3$ molecules during the preparation of NMR samples.

† Satisfactory results of elemental analysis could not be obtained for this compound.

MHz, THF–d_8): δ 4.8, 5.0, 15.5, 25.0, 25.4, 28.2, 66.0, 120.7, 121.6, 122.6, 146.1, 149.2. Anal. Found: C, 69.00; H, 10.25; N, 7.27%. Calc. for $C_{35}H_{62}LiN_3OSi_2$: C, 69.60; H, 10.35; N, 6.95%.

Synthesis of [Cr(L^1)$_2$] (3). To a slurry of $CrCl_2$ (0.42 g, 3.4 mmol) in THF (20 ml) at 0 ^oC was added dropwise a solution of $[KL^1 \cdot 0.5PhMe]_n$ (2.20 g, 6.6 mmol) in THF (20 ml). The resulting blue solution was allowed to warm slowly to room temperature and stirred for 1 d. All the volatiles were removed in *vacuo* and the blue residue was extracted with Et_2O (40 ml). The solution was filtered and then concentrated to *ca*. 5 ml to give complex **3** as purple crystals. Yield: 1.35 g, 2.5 mmol, 75%. M.p.: 168–172 ^oC. μ_{eff} = 4.83 μ_B. UV–Vis (THF) λ_{max} ($\varepsilon/M^{-1}cm^{-1}$): 375 (sh, 1500), 405 (sh, 1300), 466 (1100), 531 (sh, 940), 671 (sh, 490). Anal. Found: C, 66.15; H, 9.51; N, 15.69%. Calc. for $C_{30}H_{48}CrN_6$: C, 66.15; H, 8.88; N, 15.42%.

Synthesis of [Cr(L^4)(μ–Cl)$_2$Li(THF)(Et$_2$O)] (4). To a slurry of $CrCl_2$ (0.37 g, 3.0 mmol) in THF (20 ml) at 0 ^oC was slowly added a colorless solution of $[LiL^4(Et_2O)]$ (1.80 g, 3.0 mmol) in THF (10 ml). The resulting blue solution was allowed to warm slowly to room temperature and stirred for 1 d. The solution was concentrated to *ca*. 5 ml and the blue suspension was extracted with Et_2O (30 ml). The solution was filtered and concentrated under reduced pressure to *ca*. 10 ml. Upon standing

the solution at room temperature for one day gave complex **4** as pale blue crystals. Yield: 1.56 g, 2.0 mmol, 65%. 185–187 ^{o}C. μ_{eff} = 4.84 μ_B. Anal. Found: C, 57.92; H, 9.29; N, 5.56%. Calc. for $C_{39}H_{70}Cl_2CrLiN_3O_2Si_2$: C, 58.63; H, 8.83; N, 5.26%.

Preparation of [{Cr(L^4)(μ–Cl)}$_2$] (5). Complex **4** (1.56 g, 2.0 mmol) was dissolved in toluene (30 ml) at r.t. and stirred for 2 h, during which a white suspension was observed. The deep blue solution was filtered and concentrated to *ca*. 10 ml to give complex **5** as deep blue crystals. Yield: 1.10 g, 1.8 mmol, 88%. M.p.: 161–163 ^{o}C. μ_{eff} = 5.08 μ_B (2.54 μ_B per chromium center). Anal. Found: C, 60.93; H, 8.67; N, 7.50%. Calc. for $C_{62}H_{104}Cl_2Cr_2N_6Si_4$: C, 61.00; H, 8.59; N, 6.88%.

Reaction of [Cr(L^1)$_2$] (3) with I$_2$. To a solution of complex **3** (1.08 g, 1.97 mmol) in Et_2O (20 ml) at r.t. was slowly added a solution of I_2 (0.25 g, 0.99 mmol) in the same solvent (20 ml). The color of the solution changed immediately from purple to red. The reaction mixture was allowed to stir for 1 d. All the volatiles were removed in *vacuo*. The red residue was extracted with toluene (40ml). The solution was filtered and concentrated to give [Cr(L^1)$_2$I] (**6**) as red crystals. Yield: 0.90 g, 1.33 mmol, 68%. M.p.: 195–197 ^{o}C. μ_{eff} = 3.68 μ_B. Anal. Found: C, 53.49; H, 7.42; N, 12.95%. Calc. for $C_{30}H_{48}CrN_6I$: C, 53.65; H, 7.20; N, 12.51%.

General procedure for the synthesis of [Cr(L^1)$_2$(EPh)] [E = S (7), Se (8), Te (9)].

To a solution of complex **3** in Et_2O (20 ml) was slowly added a solution of PhEEPh in the same solvent (20 ml) at r.t. The reaction mixture immediately turned brown. Stirring was continued at r.t. for 1 d. The solution was filtered and then concentrated to *ca*. 10 ml to give a deep green crystalline product.

Synthesis of [Cr(L^1)$_2$(SPh)] (7). [Cr(L^1)$_2$] (**3**): 0.93 g, 1.70 mmol; PhSSPh: 0.19 g, 0.85 mmol. Yield: 0.83 g, 1.28 mmol, 75%. M.p.: 171–172 ^oC. μ_{eff} = 3.83 μ_B. UV–Vis (THF) λ_{max} (ε/$M^{-1}cm^{-1}$): 658 (130). Anal. Found: C, 65.71; H, 8.61; N, 13.32%. Calc. for $C_{36}H_{53}CrN_6S$: C, 66.12; H, 8.17; N, 12.85%.

Synthesis of [Cr(L^1)$_2$(SePh)] (8). [Cr(L^1)$_2$] (**3**): 1.03 g, 1.89 mmol; PhSeSePh: 0.30 g, 0.95 mmol. Yield: 0.91 g, 1.30 mmol, 69%. M.p.: 168–170 ^oC. μ_{eff} = 3.88 μ_B. UV–Vis (THF) λ_{max} (ε/$M^{-1}cm^{-1}$): 674 (140). Anal. Found: C, 61.46; H, 7.67; N, 12.65%. Calc. for $C_{36}H_{53}CrN_6Se$: C, 61.70; H, 7.62; N, 11.99%.

Synthesis of [Cr(L^1)$_2$(TePh)] (9). [Cr(L^1)$_2$] (**3**): 1.21 g, 2.22 mmol; PhTeTePh: 0.45 g, 1.10 mmol. Yield: 1.19 g, 1.58 mmol, 72%. M.p.: 175–177 ^oC. μ_{eff} = 3.91 μ_B. UV–Vis (THF) λ_{max} (ε/$M^{-1}cm^{-1}$): 382 (sh, 640), 674 (140). Anal. Found: C, 57.55; H, 7.49; N, 11.50%. Calc. for $C_{36}H_{53}CrN_6Te$: C, 57.70; H, 7.13; N, 11.21%.

Reaction of [Cr(L^1)$_2$] (3) with 1–azidoadamantane. To a solution of complex **3** (1.37 g, 2.50 mmol) in THF (20 ml) at r.t. was slowly added a solution of 1–azidoadamantane in the same solvent (20 ml). The reaction mixture turned deep

green within 10 minutes. Effervescence was observed in the first 15 minutes. The reaction mixture was allowed to stir for 1 d. The solution was filtered and concentrated to *ca*. 20 ml to give [Cr(L^1)$_2${N(1–Ad)}] (1–Ad = 1–adamantyl) (**10**) as deep green crystals. Yield: 1.10 g, 1.58 mmol, 63%. M.p.: 193–196 ^oC (dec.). μ_{eff} = 2.70 μ_B. Anal. Found: C, 68.62; H, 9.30; N, 14.60%. Calc. for $C_{40}H_{63}CrN_7$: C, 69.23; H, 9.15; N, 14.13%.

Reaction of [Cr(L^4)(μ–Cl)$_2$Li(THF)(Et$_2$O)] (4) with NaOMe. A solution of complex **4** (1.16 g, 1.45 mmol) in THF (30 ml) at r.t. was slowly added to a slurry of NaOMe (0.10 g, 1.82 mmol) in the same solvent (10 ml). The resulting purple solution was allowed to stir for 1 d. All the volatiles were removed in *vacuo*. The purple residue was extracted with toluene (40ml). The solution was filtered and concentrated to give [{Cr(L^4)(μ–OMe)}$_2$] (**11**) as purple crystals. Yield: 0.82 g, 1.35 mmol, 93%. M.p.: 182–183 ^oC. μ_{eff} = 4.81 μ_B (2.40 μ_B per chromium center). Anal. Found: C, 63.44; H, 9.81; N, 7.12%. Calc. for $C_{64}H_{110}Cr_2N_6O_2Si_4$: C, 63.43; H, 9.15; N, 6.93%.

2.5 References for Chapter 2

1. Pearson, R. G. *J. Am. Chem. Soc*. **1963**, *85*, 3533–3539.

2. Lappert, M. F.; Power, P. P.; Sanger, A. R.; Srivastave, R. C. *Metal and Metalloid Amides*; Ellis Horwood: Chichester, U. K., 1980.

3. Lappert, M; Protchenko, A.; Power, P.; Seeber, A. *Metal Amide Chemistry*; John Wiley and Sons, Ltd., 2009.

4. Bradley, D. C.; Hursthouse, M. B.; Newing, C. W.; Welch, A. J. *J. Chem. Soc*., *Chem. Commun*. **1972**, 567–568.

5. a) Edema, J. J. H.; Gambarotta, S.; Spek, A. L. *Inorg. Chem*. **1989**, *28*, 811–813.

   b) Edema, J. J. H.; Gambarotta, S.; Meetsma, A.; Spek, A. L.; Smeets, W. J. J.; Chiang, M. Y. *J. Chem. Soc*., *Dalton Trans*. **1993**, 789–797.

   c) Ruppa, K. B. P.; Feghili, K.; Kovacs, I.; Aparna, K.; Gambarotta, S.; Yap, G. P. A.; Besimon, C. *J. Chem. Soc*., *Dalton Trans*. **1998**, 1595–1606.

6. a) Bartlett, R. A.; Chen, H.; Power, P. P. *Angew. Chem*., *Int. Ed*. **1989**, *28*, 316–317.

   b) Chen, H.; Bartlett, R. A.; Olmstead, M. M.; Power, P. P.; Shoner, S. C. *J. Am. Chem. Soc*. **1990**, *112*, 1048–1055.

   c) Boynton, J. N.; Alexander Merrill, W.; Reiff, W. M.; Fettinger, J. C.;

Power, P. P. *Inorg*. *Chem*. **2012**, *51*, 3212–3219.

7. a) MacAdams, L. A.; Kim, W. -K.; Liable-Sands, L. M.; Guzei, I. A.; Rheingold, A. L.; Theopold, K. H. *Organometallics* **2002**, *21*, 952–960.

   b) Monillas, W. H.; Yap, G. P. A.; Theopold, K. H. *J. Chem*. *Cryst*. **2009**, *39*, 73–77.

8. Gibson, V. C.; Newton, C.; Redshaw, C.; Solan, G. A.; White, A. J. P.; Williams, D. J. *J. Chem*. *Soc*., *Dalton Trans*. **2002**, 4017–4023.

9. a) Monillas, W. H.; Yap, G. P. A.; Theopold, K. H. *J. Chem*. *Cryst*. **2009**, *39*, 377–379.

   b) Monillas, W. H.; Yap, G. P. A.; Theopold, K. H. *J. Chem*. *Cryst*. **2010**, *40*, 67–71.

   c) Fan, H.; Adhikari, D.; Saleh, A. A.; Clark, R. L.; Zuno-Cruz, F. J.; Cabrera, G. S.; Huffman, J. C.; Pink, M.; Mindiola, D. J.; Baik, M. -H. *J. Am*. *Chem*. *Soc*. **2008**, *130*, 17351–17361.

10. a) Noor, A.; Wagner, F. R.; Kempe, R. *Angew*. *Chem*. *Int*. *Ed*. **2008**, *47*, 7246–7249.

    b) Noor, A.; Glatz, G.; Müller, R.; Kaupp, M.; Demeshko, S.; Kempe, R. *Nat*. *Chem*. **2009**, *1*, 322–325.

11. Buijink, J. -K.; Noltemeyer, M.; Edelmann, F. T. *Z. Naturforsch*. **1991**, *46b*,

1328–1332.

12. Hao, S.; Gambarotta, S.; Bensimon, C.; Edema, J. J. H. *Inorg. Chim. Acta*. **1993**, *213*, 65–74.

13. Sadique, A. R.; Heeg, M. J.; Winter, C. H. *J. Am. Chem. Soc*. **2003**, *125*, 7774–7775.

14. Nijhuis, C. A.; Jellema, E.; Sciarone, T. J. J.; Meetsma, A.; Budzelaar, P. H. M.; Hessen, B. *Eur. J. Inorg. Chem*. **2005**, 2089–2099.

15. a) Cotton, F. A.; Ren, T. *J. Am. Chem. Soc*. **1992**, *114*, 2237–2242.

    b) Cotton, F. A.; Daniels, L. M.; Murillo, C. A.; Schooler, P. *J. Chem. Soc*., *Dalton Trans*. **2000**, 2001–2005.

    c) Cotton, F. A.; Li, Z.; Murillo, C. A. *Eur. J. Inorg. Chem*. **2007**, 3509–3513.

16. Dykerman, B. A.; Smith, J. J.; McCarvill, E. M.; Gallant, A. J.; Doiron, N. D.; Wagner, B. D.; Jenkins, H. A.; Patrick, B. O.; Smith, K. M. *J. Organomet. Chem*. **2007**, *692*, 3183–3190.

17. a) Cotton, F. A.; Timmons, D. J. *Polyhedron* **1998**, *17*, 179–184.

    b) Cotton, F. A.; Daniels, L. M.; Huang, P.; Murillo, C. A. *Inorg. Chem*. **2002**, *41*, 317–320.

18. Horvath, S.; Gorelsky, S. I.; Gambarotta, S.; Korobkov, I. *Angew. Chem. Int*.

Ed. **2008**, *47*, 9937–9940.

19. Noor, A.; Glatz, G.; Müller, R.; Kaupp, M.; Demshko, S.; Kempe, R. *Z. Anorg. Allog. Chem*. **2009**, *635*, 1149–1152.

20. a) Nguyen, T.; Sutton, A. D.; Brynda, M.; Fettinger, J. C.; Long, G. J.; Power, P. P. *Science*, **2005**, *310*, 844–847.

    b) Kreisel, K. A.; Yap, G. P. A.; Dmitrenko, O.; Landis, C. R.; Theopold, H. *J. Am. Chem. Soc*. **2007**, *129*, 14162–14163.

    c) Wolf, R.; Ni, C.; Nguyen, T.; Brynda, M.; Long, G. J.; Sutton, A. D.; Fischer, R. C.; Fettinger, J. C.; Hellman, M.; Pu, L.; Power, P. P. *Inorg. Chem*. **2007**, *46*, 11277–11290.

    d) Tsai, Y. -C.; Hsu, C. -W.; Yu, J. -S. K.; Lee, G.-H.; Wang, Y.; Kuo, T. -S. *Angew. Chem. Int. Ed*. **2008**, *47*, 7250–7253.

    e) Hsu, C. -W.; Yu, J. -S. K.; Yen, C. -H.; Lee, G. -H.; Wang, Y.; Tsai, Y. -C. *Angew. Chem. Int. Ed*. **2008**, *47*, 9933–9936.

21. Findlater, M.; Hill, N. J.; Cowley, A. H. *Dalton Trans*. **2008**, 4419–4423.

22. Cole, M. L.; Junk, P. C. *Dalton Trans*. **2003**, 2109–2111.

23. Zhou, M.; Tong, H.; Wei, X.; Liu, D. *J. Organomet. Chem*. **2007**, *692*, 5195–5202.

24. Pang, X.; Yao, Y.; Wang, J.; Sheng, H.; Zhang, Y.; Shen, Q. *Chin. J. Chem*.

2005, *23*, 1193–1197.

25. Jin, G.; Jones, C.; Junk, P. C.; Lippert, K. -A.; Rose, R. P.; Stasch, A. *New J. Chem*. **2009**, *33*, 64–75.

26. Giesbrecht, G. R.; Shafir, A.; Arnold, J. *J. Chem. Soc., Dalton Trans*. **1999**, 3601–3604.

27. Lee, H. S.; Niemeyer, M. *Inorg. Chem*. **2006**, *45*, 6126–6128.

28. Schubert, E. M. *J. Chem. Educ*. **1992**, *69*, 62.

29. Cotton, F. A.; Mott, G. N. *Inorg. Chem*. **1983**, *22*, 1136–1139.

30. Edema, J. J. H.; Gambarotta, S.; Meetsma, A.; van Bolhuis, F.; Spek, A. L.; Smeets, W. J. J. *Inorg. Chem*. **1990**, *29*, 2147–2153.

31. Weast, R. C. *Handbook of chemistry and physics*, 53rd ed., CRC Press, 1972–1973.

32. Lam, P. C. *M. Phil. Thesis*, The Chinese University of Hong Kong, 2006.

33. Shannon, R. D. *Acta Cryst*. **1976**, *A32*, 751–767.

34. Doherty, J. C.; Ballem, K. H. D.; Patrick, B. O.; Smith, K. M. *Organometallics* **2004**, *23*, 1487–1489.

35. Shin, R. Y. C.; Tan, G. K. Koh, L. L.; Goh, L. Y.; Webster, R. D. *Organometallics* **2005**, *24*, 1401–1403.

36. Goh, L. Y.; Tay, M. S.; Mak, T. C. W.; Wang, R. -J. *Organometallics* **1992**, *11*,

1711–1717.

37. Goh, L. Y.; Tay, M. S.; Lim, Y. Y.; Chen, W.; Zhou, Z. -Y.; Mak, T. C. W. *J. Organomet. Chem.* **1992**, *441*, 51–61.

38. Goh, L. Y.; Tay, M. S.; Wei, C. *Organometallics* **1994**, *13*, 1813–1820.

39. Sydora, O. L.; Kuiper, D. S.; Wolczanski, P. T.; Lobkovsky, E. B.; Dinescu, A.; Cundari, T. R. *Inorg. Chem.* **2006**, *45*, 2008–2021.

40. Lu, C. C.; George, S. D.; Weyhermüller, T.; Bill, E.; Bothe, E.; Wieghardt, K. *Angew. Chem. Int. Ed.* **2008**, *47*, 6384–6387.

41. Sydora, O. L.; Wolczanski, P. T.; Lobkovsky, E. B.; Buda, C.; Cundari, T. R. *Inorg. Chem.* **2005**, *44*, 2606–2618.

Chapter 3

Synthesis and Reactivity of Divalent Lanthanide Guanidinate Complexes

3.1 The Development of Lanthanide(II) Guanidinate Complexes

Sm, Eu and Yb are readily accessible in their +2 oxidation state. The reduction potentials of Ln^{3+}/Ln^{2+} vs NHE (Ln = Sm: –1.55 V; Eu: –0.35 V; Yb: –1.15 V)[1] show that Sm^{2+}, Eu^{2+}, Yb^{2+} are the three most stable Ln^{2+} metal ions among the fifteen lanthanide metal ions. According to Pearson's hard and soft acid base concept,[2] lanthanide metal ions are classified as hard Lewis acids. They form stable metal complexes with hard ligands (hard bases).

Lanthanide(II) amide complexes

N–donor ligands are hard base ligands. Early development of organolanthanide(II) chemistry involved the use of the monodentate N–donor ligand $[N(SiMe_3)_2]^-$, as demonstrated by the pioneering work of Andersen,[3] Lappert,[4] and Evans.[5] The first structurally authenticated lanthanide(II) amides, $[Eu\{N(SiMe_3)_2\}_2(Sol)_2]$ (Sol = THF, DME) were prepared by reduction of its chloro derivative $[Eu\{N(SiMe_3)_2\}_2Cl]$ with sodium naphthalene [Na(naph)] in tetrahydrofuran or 1,2–dimethoxyethane (DME) (Scheme 3–1).[3a] The reactions of LnI_2 (Ln = Sm, Eu, Yb) with $MN(SiMe_3)_2$ (M = Na, K) in an appropriate solvent gave the neutral $[Ln\{N(SiMe_3)_2\}_2(Sol)_n]$ [Ln = Sm, Sol = THF, n = 2; Ln = Yb, Sol = Et_2O, n = 2; Ln = Yb, Sol = DMPE, n = 1; Ln = Eu, Yb, Sol = DME) and the anionic complexes $[NaLn\{(SiMe_3)_2\}_3]$ (Ln = Eu, Yb) and $[KSm\{(SiMe_3)_2\}_3]$.[3b,c,5]

Alternatively, the Yb(II) complex $[Yb\{N(SiMe_3)_2\}_2(DME)_2]$ can also be prepared by the reaction of Yb metal with $Sn[N(SiMe_3)_2]_2$ in refluxing THF.[4a] The solvent free $[Yb\{N(SiMe_3)_2\}\{\mu\text{–}N(SiMe_3)_2\}]_2$ complex was prepared by desolvating $[Yb\{N(SiMe_3)_2\}_2(Et_2O)_2]$ in *vacuo* at 20 °C.[4b]

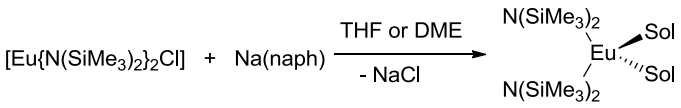

Sol = THF, DME

Andersen *et al*.[3a]

Scheme 3—1

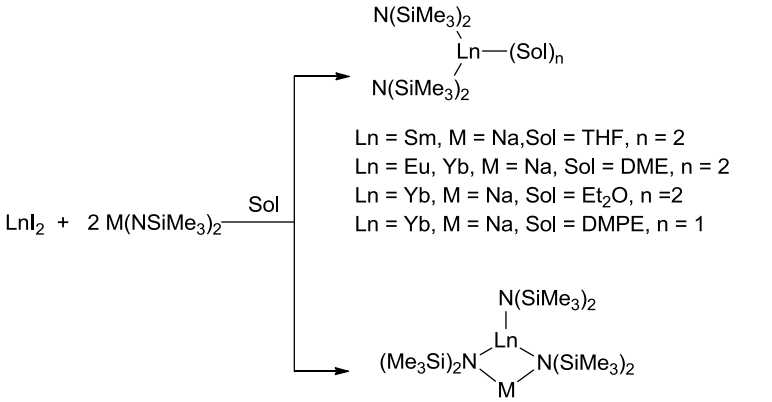

Andersen *et al*.[3b,c]
Evans *et al*.[5]

Scheme 3—2

Treatment of an equimolar amount of $SmI_2(THF)_2$ with $[\{(Me_3Si)_2N\}_2Sm(THF)_2]$ in DME/THF gave the heteroleptic Sm(II) amide, $[\{(Me_3Si)_2N\}Sm(\mu\text{–}I)(DME)(THF)]_2$ (Scheme 3–3).[5a] Heteroleptic Yb(II) amide, $[Yb\{N(SiMe_3)_2\}(\mu\text{–}OCBu^t_3)]_2$, was prepared by protolytic ligand exchange between $[Yb\{N(SiMe_3)_2\}\{\mu\text{–}N(SiMe_3)_2\}]_2$ and Bu^t_3COH in hexane (Scheme 3–4).[4b]

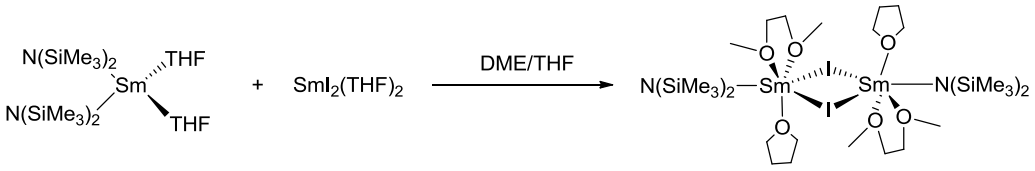

Evans *et al*.[5a]

Scheme 3—3

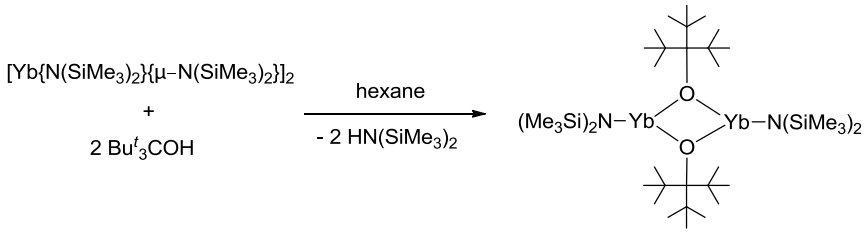

Lappert *et al*.[4b]

Scheme 3—4

Lanthanide(II) amidinate complexes

Compared with monodentate ligands, bidentate ligands can better stabilize metal complexes because of chelation effect. Bulky bidentate ligands can reduce the coordination number of a metal, and, hence, increase its reactivity (the metal center becomes more exposed). Amidinates and guanidinates are closely related bidentate N–donor ligands. By varying the substituents on the N–C–N backbone, several lanthanide(II) amidinate and guanidinate complexes have been reported.[6-8] Edelmann and co–workers have reported on the first Yb(II) amidinate complexes $[Yb\{RC_6H_4C(NSiMe_3)_2\}_2(THF)_n]$ (R = H, OMe, n = 2; R = Ph, n = 0), which were prepared by salt metathesis of $YbI_2(THF)_2$ with an appropriate sodium *N*,*N*′–bis(trimethylsilyl)benzamidinate in THF (Scheme 3–5).[6a] Reactions of $[Yb\{C_6H_5C(NSiMe_3)_2\}_2(THF)_2]$ with $[Me_2NC(S)S]_2$ and PhSeSePh led to the

cleavage of S–S and Se–Se bonds, yielding [Yb{$C_6H_5C(NSiMe_3)_2$}$_2$(S_2CNMe_2)] and [Yb{$C_6H_5C(NSiMe_3)_2$}$_2$(SePh)(THF)], respectively (Scheme 3–6).[6a] The same research group has also reported on the reactions of [{$RC_6H_4C(NSiMe_3)_2$}$_2$Yb(THF)$_n$] (R = H, OMe) with diaryl diselenides and ditellurides, which led to the isolation of [Yb{$RC_6H_4C(NSiMe_3)_2$}$_2$(SeR')(THF)] (R = H, R' = Ph, Mes) and [Yb{$RC_6H_4C(NSiMe_3)_2$}$_2$(TeR')(THF)] (R = OMe, R' = Mes), respectively (Scheme 3–7).[6b]

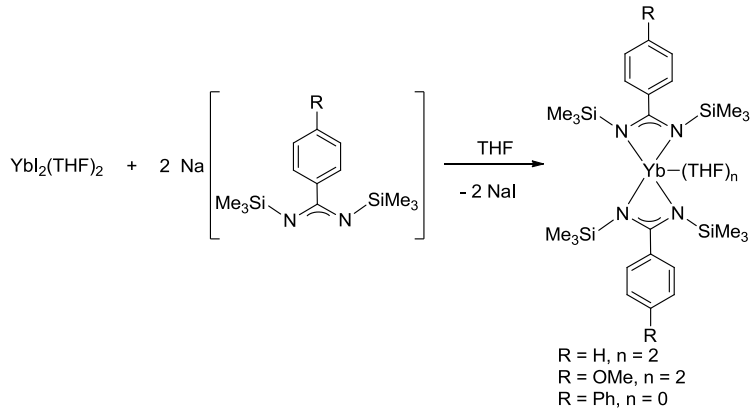

Edelmann *et al*.[6a]

Scheme 3—5

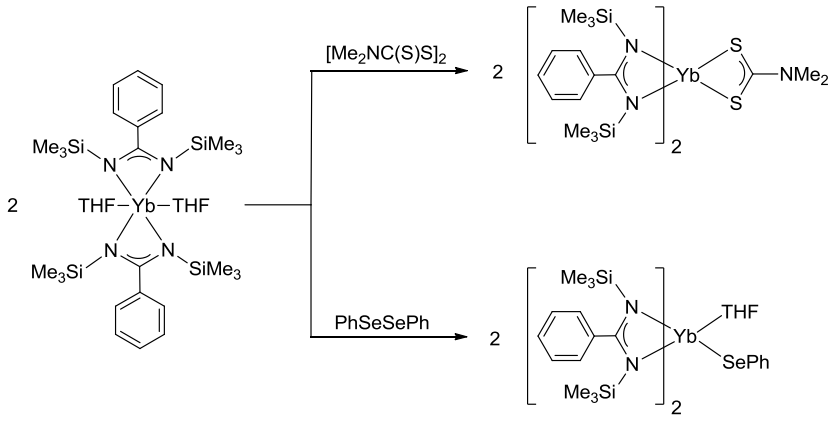

Edelmann *et al*.[6a]

Scheme 3—6

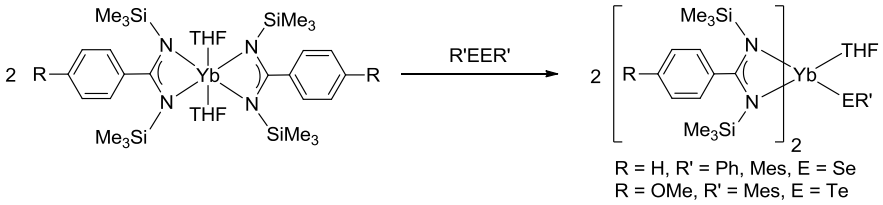

Edelmann *et al*.[6b]

Scheme 3—7

The first Sm(II) amidinate complex $[Sm(DippForm)_2(THF)_2]$ [DippForm = $\{(2,6\text{–}Pr^i_2C_6H_3)NC(H)N(2,6\text{–}Pr^i_2C_6H_3)\}^-$] have been prepared by three different methods, namely (i) the reaction of $SmI_2(THF)_2$ with Na(DippForm), (ii) the reaction of excess samarium metal with $[(C_6F_5)_2Hg]$ and DippFormH, and (iii) transamination of $[Sm\{N(SiMe_3)_2\}(THF)_2]$ with DippFormH (Scheme 3–8), respectively.[7] The reaction of $[Sm(DippForm)_2(THF)_2]$ with half equivalents of $SmI_2(THF)_2$ in the presence of one equivalent of NaI gave ion–paired $[Na(THF)_5][Sm(I)_2(DippForm)_2(THF)]$. On the other hand, treatment of $[Sm(DippForm)_2(THF)_2]$ with half molar equivalents of $[(C_6F_5)_2Hg]$ and DippFormH led to C–F bond activation and the formation of complex $[Sm(F)(DippForm)_2(THF)]$.

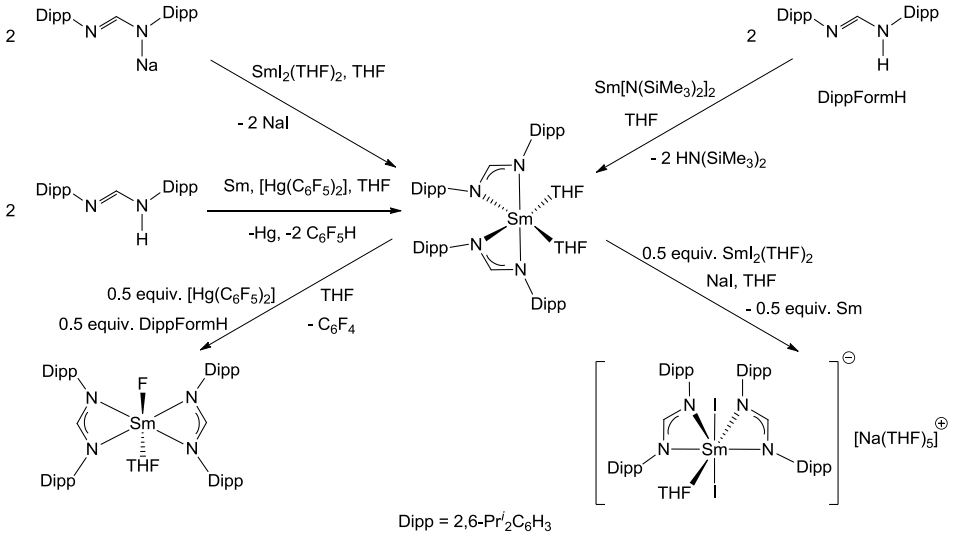

Junk *et al*.[7]

Scheme 3—8

Recently, a series of lanthanide(II) amidinate complexes have been reported by our research group.[8] Utilizing the unsymmetrical $[PhC(NSiMe_3)(NC_6H_3Pr^i_2\text{–}2,6)]^-$ ligand, the corresponding lanthanide(II) amidinate complexes $[LnL_2(THF)_n]$ [Ln = Sm, Eu, n = 2; Ln = Yb, n = 1; L = $\{PhC(NSiMe_3)(NC_6H_3Pr^i_2\text{–}2,6)\}^-$] have been isolated (Scheme 3–9). Subsequent reactions of $[LnL_2(THF)_2]$ (Ln = Sm, Eu) with diphenyl dichalcogenides PhEEPh (E = Se, Te) led to the binuclear lanthanide(III) amidinate–chalcogenolate complexes $[LnL_2(\mu\text{–}EPh)]_2$ (Ln = Sm, E = Se, Te; Ln = Eu, E = Se), whereas reactions of $[YbL_2(THF)]$ with PhSeSePh and iodine yielded the mononuclear $[YbL_2(SePh)(THF)]$ and $[YbL_2(I)(THF)]$, respectively. Treatment of $[SmL_2(THF)_2]$ with *N*,*N*′–dicyclohexylcarbodiimide afforded the mixed–ligand Sm(III) tris(amidinate) $[SmL_2\{CyNC(H)NCy\}]$.

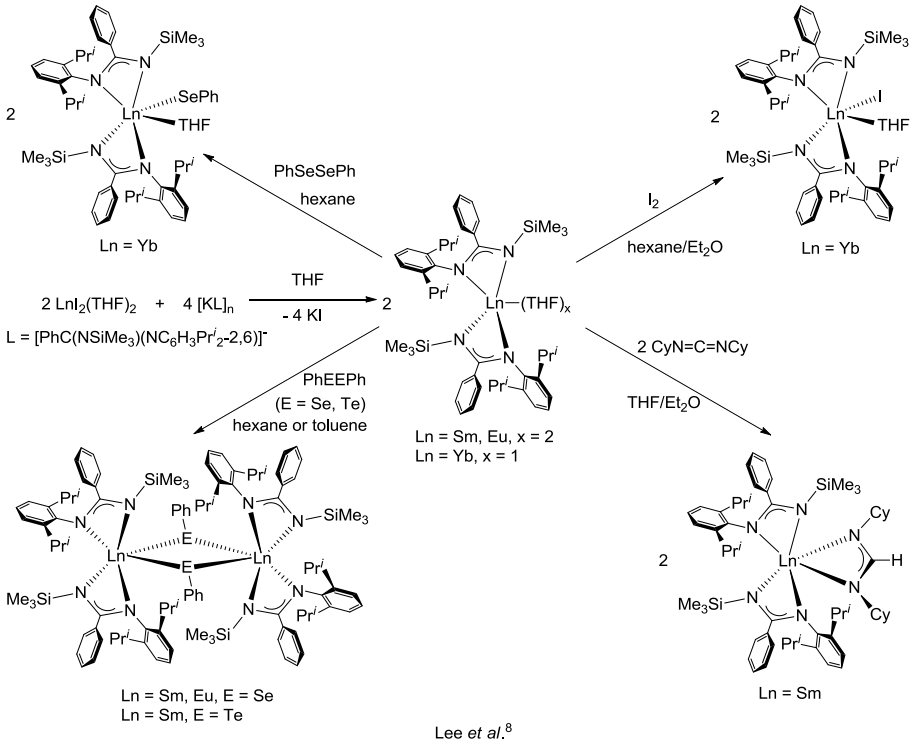

Lee *et al*.[8]

Scheme 3—9

Lanthanide(II) guanidinate complexes

The first lanthanide(II) guanidinate complex, [{CyNC(N(SiMe$_3$)$_2$)NCy}$_2$Yb(TMEDA)], was reported by Richeson and co–workers.[9] This complex can be prepared by (i) salt elimination reaction of YbI_2 with Li{CyNC(N(SiMe$_3$)$_2$)NCy} (Scheme 3–10), and (ii) reduction of the Yb(III) complex [Yb{CyNC(N(SiMe$_3$)$_2$)NCy}$_2$(μ–Cl)$_2$Li(TMEDA)] with excess Na/K in benzene.

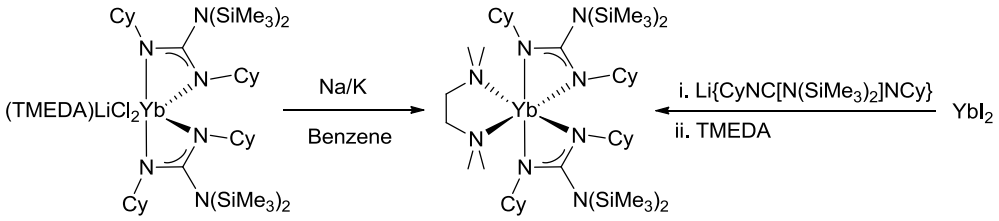

Richeson *et al*.[9]

Scheme 3—10

Recently, Jones and co–workers have successfully prepared a few homoleptic lanthanide(II) guanidinate complexes, [Ln(Giso)$_2$] [Ln = Sm, Eu, Yb; Giso = {(2,6–Pr$^i_2$C$_6$H$_3$N)$_2$CNCy$_2$}$^-$] (Scheme 3–11), as well as heteroleptic ytterbium(II) complexes [{Yb(Giso)(μ–I)(THF)}$_2$] and [{Yb(η^1–N:η^6–Ar–Giso}$_2$]. The Sm(II) and Eu(II) complexes have the unprecedented planar 4–coordinate lanthanide centers.

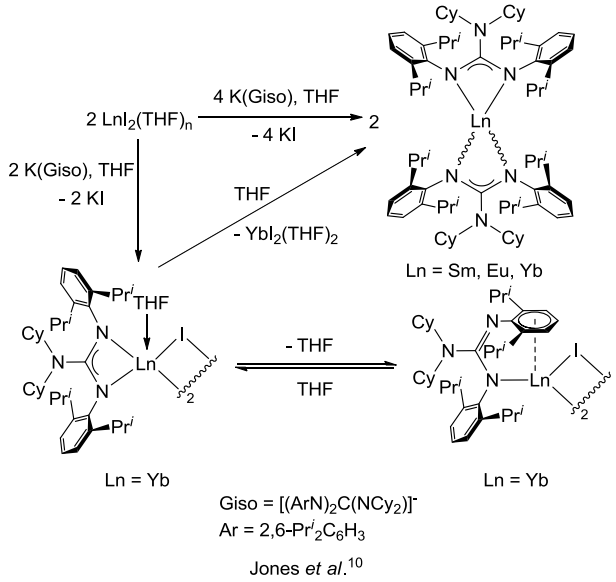

Jones *et al*.[10]

Scheme 3—11

More recently, the same research group have isolated new lanthanide(II) complexes using bulky amidinate ligand, $[(2,6\text{–}Pr^{i}{}_{2}C_{6}H_{3}N)_{2}CBu^{t}]^{-}$ (Piso) and guanidinate ligand, $[(2,6\text{–}Pr^{i}{}_{2}C_{6}H_{3}N)_{2}CNPr^{i}{}_{2}]^{-}$ (Priso).[11] Salt metathetical reactions of potassium guanidinate, K(Priso), with LnI_2 (Ln = Sm, Eu, Yb) in THF, led to the isolation of homoleptic $[Ln(Priso)_2]$ (Ln = Sm, Eu, Yb) (Scheme 3–12).[11] Co–crystallization of free guanidine (PrisoH) was observed in the above reactions. Besides, the reaction that gave $[Yb(Priso)_2]$ also led to a few crystals of heteroleptic Yb(II) complex, $[\{Yb(Priso)(\mu\text{–}I)\}_2]$. Treatment of SmI_2 with two equivalents of potassium amidinate, K(Piso), gave a few crystals of heteroleptic Sm(II) $[(\eta^1\text{–}N{:}\eta^6\text{–}Ar\text{–}Piso)Sm(THF)(\mu\text{–}I)_2Sm(\eta^1\text{–}N{:}\eta^6\text{–}Ar\text{–}Piso)]$ as the only isolable product. Repeating the experiment in a 1:1 ratio gave only little improvement to the product yield (14%). Reaction of the Sm(II) guanidinate complex $[Sm(Giso)_2]$ with CS_2 led to the isolation of unsymmetrical coupling product,

$[(Giso)_2Sm(\mu–\eta^3–:\eta^2–S_2CSCS)Sm(Giso)_2]$ (Scheme 3–13).[11]

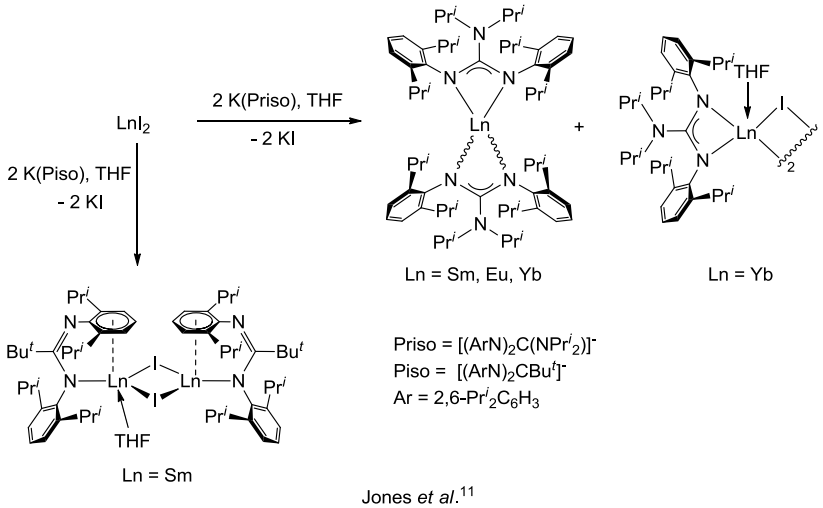

Jones *et al*.[11]

Scheme 3—12

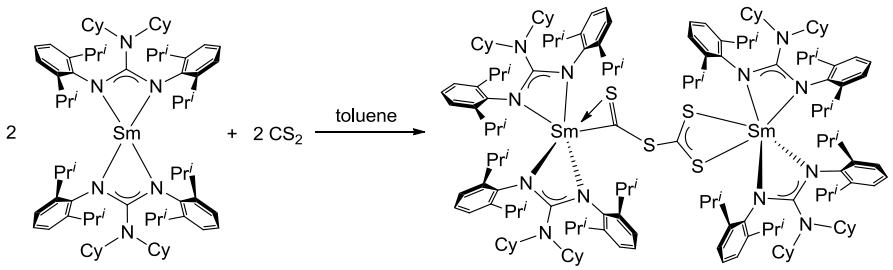

Jones *et al*.[11]

Scheme 3—13

3.2 Results and Discussion

3.2.1 Synthesis and Structure of Potassium Complexes of $[(2,6\text{–}Me_2C_6H_3N)C(NHCy)(NCy)]^-$ (L^2), $[(2,6\text{–}Me_2C_6H_3N)C\{N(SiMe_3)Cy\}(NCy)]^-$ (L^3) and $[(2,6\text{–}Pr^i{}_2C_6H_3N)C(NEt_2)(NC_6H_3Pr^i{}_2\text{–}2,6)]^-$ (L^5)

Preparation

Potassium complexes of $[(2,6\text{–}Me_2C_6H_3N)C(NHCy)(NCy)]^-$ (L^2), $[(2,6\text{–}Me_2C_6H_3N)C\{N(SiMe_3)Cy\}(NCy)]^-$ (L^3) and $[(2,6\text{–}Pr^i{}_2C_6H_3N)C(NEt_2)(NC_6H_3Pr^i{}_2\text{–}2,6)]^-$ (L^5) were used as ligand transfer reagents for the synthesis of lanthanide(II) guanidinate complexes in this work. Lithium complexes of the L^2, L^3 and L^5 ligands were readily prepared by deprotonation of an appropriate aniline or amine with $LiBu^n$/TMEDA (TMEDA = *N*,*N*,*N*′,*N*′–tetramethylethylenediamine), followed by the addition of substituted carbodiimides RN=C=NR (R = Cy or $C_6H_3Pr^i{}_2$–2,6) (Scheme 3–14).[12,13]

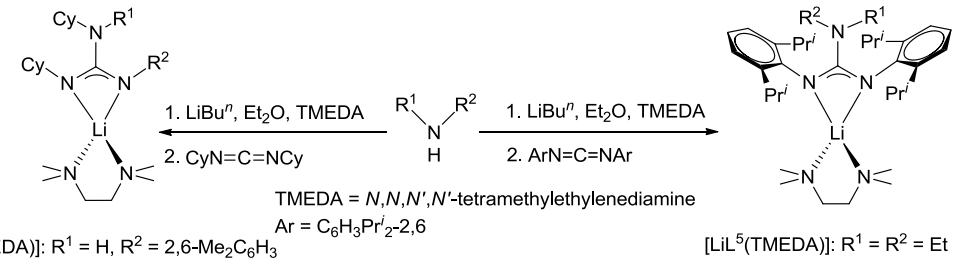

[LiL^2(TMEDA)]: R^1 = H, R^2 = 2,6-Me$_2$C$_6$H$_3$
[LiL^3(TMEDA)]: R^1 = SiMe$_3$, R^2 = 2,6-Me$_2$C$_6$H$_3$

[LiL^5(TMEDA)]: R^1 = R^2 = Et

Yeung L. F.[12]
Wong, G. F.[13]

Scheme 3—14

Potassium complexes of L^2, L^3 and L^5 were obtained by transmetallation reactions of lithium complexes [LiL^n(TMEDA)] (n = 2, 3, 5) with potassium tert–butoxide in THF (Scheme 3–15). The [$KL^2(THF)_{0.5}]_n$ (**12**), KL^3 (**13**) and [$KL^5(THF)_2$] (**14**) complexes were isolated in good yields.

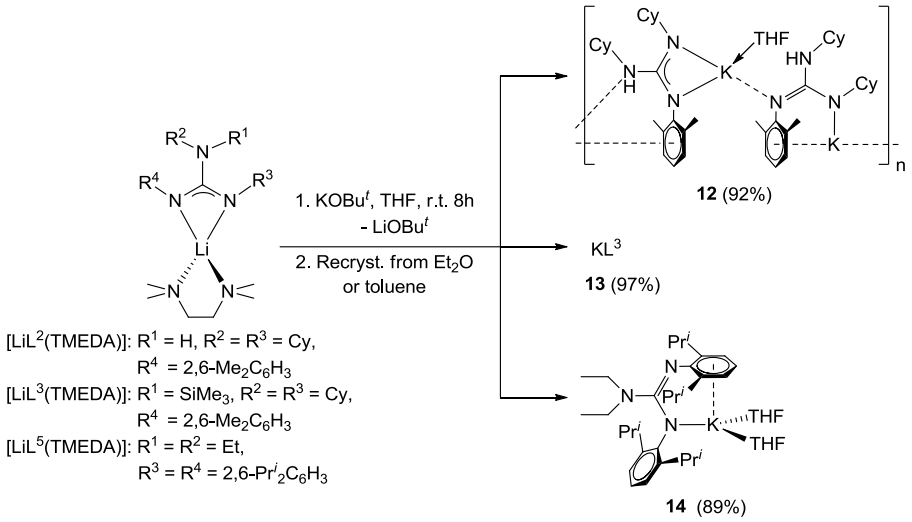

Scheme 3—15

Physical Characterization of Complexes **12–14**

All of the complexes **12–14** are sensitive to air and moisture. They are soluble in THF and sparingly soluble in toluene, but insoluble in Et_2O and hexane. The molecular formula of complexes **12–14** has been confirmed by elemental analysis, NMR spectroscopy (^{1}H and ^{13}C) and X–ray diffraction analysis (for **12** and **14**). Table 3–1 summarizes the appearance and melting points of complexes **12–14**.

Table 3–1. Appearance and melting points of complexes **12**–**14**

Compound	Appearance	M.p. (^{o}C)
$[KL^{2}(THF)_{0.5}]_{n}$ (**12**)	Colorless crystals	229–231 (dec.)
KL^{3} (**13**)	White solid	215–216 (dec.)
$[KL^{5}(THF)_{2}]$ (**14**)	Colorless crystals	245–247 (dec.)

NMR Spectra of Complexes **12**–**14**

The NMR spectra of complexes **12**–**14** are shown in Figures A2–8 to A2–13 (Appendix 2). Owing to a poor solubility of **12**–**14** in C_6D_6, their NMR spectra were measured in THF–d_8 solutions. The ^{1}H and ^{13}C NMR spectra of complex **12** show one set of resonance signals which are assignable to the L^{2} ligand and the THF molecule (L^{2}:THF = 4:1). In the ^{1}H NMR, one singlet signal at 2.07 ppm is assignable to the ortho methyl groups on the aryl substituent. This suggests that the two methyl groups are chemically equivalent. Protons on the cyclohexyl substituents occur as broad signals at 0.9–1.9 and 3.4 ppm. The broadness of these signals may be attributed to the ring flipping process of the cyclohexyl groups. Similar peak broadening has also been observed in the precursor complex $[LiL^{2}(TMEDA)]$.[12]

The ^{1}H and ^{13}C NMR spectra of complex **13** show one set of resonance signals which are assignable to the L^{3} ligand. A singlet signal at 0.10 ppm is observed in the

^{1}H NMR, which is assignable to the silyl substituent of the L^3 ligand. The ^{1}H NMR suggests that the three methyl groups in the silyl substituent have similar chemical environment. One set of broad signals in the range of 0.9–3.1 ppm are assignable to the cyclohexyl protons. Similar peak broadening has also been observed for the precursor compound [LiL^3(TMEDA)].[12] A singlet signal at 10.0 ppm is observed in the ^{13}C NMR, which is assignable to the three carbon atoms in the silyl substituent. A similar downfield shift has been observed for [LiL^3(TMEDA)] (5.6 ppm). A singlet signal at 20.3 ppm, and four singlet signals at 26.3, 27.4, 35.2 and 54.6 ppm are assignable to the ortho methyl groups on the aryl substituent and the chyclohexyl groups, respectively. Four singlet signals at 115.1, 127.5, 128.8 and 154.4 ppm, and one singlet signal at 158.7 ppm are assignable to the aryl carbons and central carbon on the N–C–N backbone, respectively.

The ^{1}H and ^{13}C NMR spectra of complex **14** show one set of resonance signals which are assignable to the L^4 ligand and the THF molecule (L^4:THF = 2:1). The two doublet signals at 1.09 and 1.18 ppm and a septet signal at 3.66 ppm are assignable to the isopropyl methyl protons and methine protons, respectively. These indicate that the two isopropyl groups on each phenyl ring are chemically non–equivalent. This may be attributed to a hindered rotation of the isopropyl groups. Two singlet signals at 13.6 and 28.3 ppm are observed in the ^{13}C NMR

spectrum, which are assignable to the methyl and methylene carbons on the ethyl groups, respectively. Another two singlet signals at 24.4 and 43.9 ppm are assignable to the methyl and methine carbons on the isopropyl groups of the aryl substituents. Four singlet peaks at 118.1, 122.9, 141.8 and 154.4 ppm, and one singlet peak at 158.2 ppm are assignable to the carbons on the aryl substituent and the N–C–N backbone, respectively.

Crystal Structures of Complexes **12** and **14**

Single crystals of complexes **12** and **14** were obtained from a mixed THF/Et_2O (1:1) solution. Figures 3–1 and 3–2 show the X–ray structures of potassium complexes **12** and **14**, respectively. Selected bond lengths and angles are listed in Tables 3–2 and 3–3. Selected crystallographic data are listed in Table A3–5 (Appendix 3).

1. $[KL^2(THF)_{0.5}]_n$ (**12**)

Complex **12** crystallizes in the monoclinic space group $P2_1/c$. It exists as a one–dimensional polymer made up of linked binuclear $K_2L^2_2$ subunits. The two potassium atoms [K(1) and K(2)] exhibit different binding modes. The K(1) center is bound by two L^2 ligands, each of which is coordinated in an η^1–amide:η^6–arene mode. A similar coordination mode has been observed in $[KL^1 \cdot 0.5PhMe]_n$ (**1**). The K(2) center is bound by one THF molecule, and two L^2 ligands in η^1–amide and

η^3–guanidinate modes, respectively. If the η^6–arene is considered as a single coordination point, the coordination geometry around the K(1) and K(2) centers can be described as distorted tetrahedral. The K–N distances fall within the range of 2.722(4)–2.993(4) Å, which are comparable to the corresponding distances in complex **1** [2.806(4)–2.962(4) Å], and other reported potassium complexes, such as, $[\{K[CyNC(N(SiMe_3)_2)NCy]\}_2 \cdot C_6H_6]$ [2.765(2)–2.806(2) Å][14] and $[\{K(Priso)\}_\infty]$ (Priso = $[(2,6\text{–}Pr^i_2C_6H_3N)_2CNPr^i_2]^-$) [2.755(3) Å].[15] The almost identical C(9)–N(1) [1.327(6) Å] {C(30)–N(4) [1.330(6) Å]} and C(9)–N(3) [1.325(5) Å] {C(30)–N(5) [1.312(5) Å]} distances indicate delocalization of the anionic charge in between the two nitrogen atoms through the N–C–N backbone in **12**. The observed K(1)–Centroid(1) and K(1)–Centroid(2) (centroid = center position of phenyl ring) distances in **12** are 2.934 and 2.903 Å, respectively, which are slightly longer than that of 2.895 Å in complex **1**, but comparable to the corresponding distances of 2.945 and 3.077 Å in $[\{K(Priso)\}_\infty]$.[15] The potassium–oxygen bond distance of 2.729(5) Å in **12**, falls within the range of 2.646(3)–2.780(3) Å in $[\{K(THF)_2\}\{Pip(Giso)_2\}\{K(THF)_3\}]$ [$Pip(Giso)_2$ = $[\{ArNCNAr\}_2\{\mu\text{–}N(C_2H_4)_2N\}]^{2-}$; Ar = $2,6\text{–}Pr^i_2C_6H_3$].[15] The bite angles formed by N(3)–K(1)–Centroid(1) and N(5)–K(1)–Centroid(2) are measured to be 80.5 and 81.2°, respectively. They are similar to that in $[\{K(Priso)\}_\infty]$ [79.0°].[15]

2. $[KL^5(THF)_2]$ (**14**)

Complex **14** crystallizes in the orthorhombic space group *Pbcn*. The K(1) center is bound by two THF molecules and one L^5 ligand. The latter binds to the metal in an η^1–amide:η^6–arene coordination mode. If the η^6–arene is considered as a single coordination point, the coordination geometry around K(1) metal is best described as distorted tetrahedral. The potassium–nitrogen bond distance in **14** [2.7404 Å] is shorter than the corresponding distances of 2.778(3) and 2.852(4) Å in complex **12**. This suggests that the steric repulsion exerted by the two THF molecules and one L^5 ligand around K(1) in complex **14** is smaller than that due to two L^2 ligands around K(1) in complex **12**. The nearly identical C(13)–N(1) [1.338(6)] and C(13)–N(3) [1.324(6)] distances indicate delocalization of the anionic charge on the N–C–N backbone. The observed K(1)–Centroid(1) distance of 2.889 Å in **14**, is shorter than the corresponding distances of 2.934 and 2.903 Å in **12**. This may be due to a shorter K–N bond distance in the former complex. The K(1)–O(1) and K(1)–O(2) bond distances of 2.666(4) and 2.690(4) Å, respectively, are shorter than the corresponding distance of 2.729(5) Å in complex **12**. The N(1)–C(13)–N(3) bond angle of 122.9(4)^o in **14** is comparable to the corresponding angles of 124.2(4) and 125.9(4)^o in **12**.

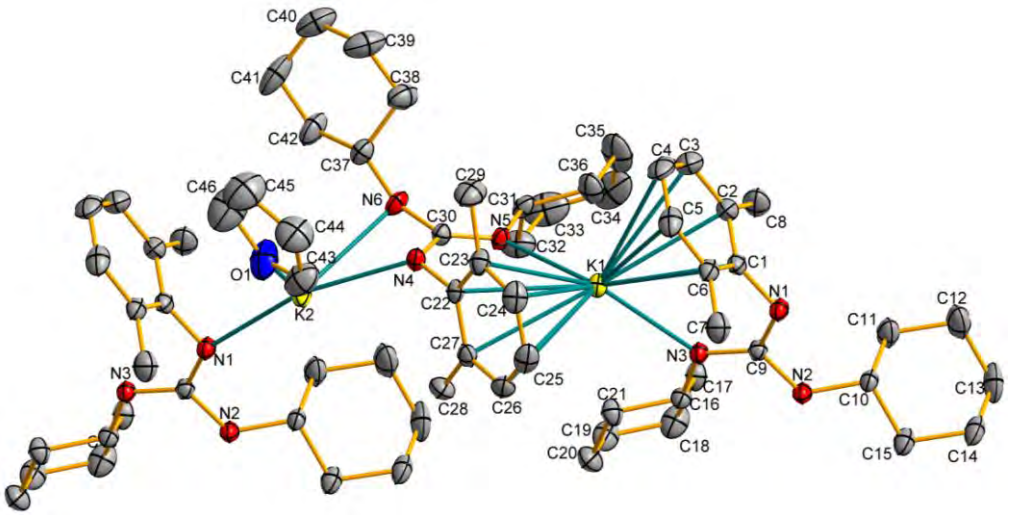

Figure 3–1. Molecular structure of $[KL^2(THF)_{0.5}]_n$ (**12**).

Table 3–2. Selected bond distances (Å) and angles (deg.) for compound **12**

$[KL^2(THF)_{0.5}]_n$ (**12**)			
K(1)–N(3)	2.778(3)	K(1)–N(5)	2.852(4)
K(2)–N(4)	2.722(4)	K(2)–N(6)	2.993(4)
C(9)–N(1)	1.327(6)	C(9)–N(2)	1.407(4)
C(9)–N(3)	1.325(5)	C(30)–N(4)	1.330(6)
C(30)–N(5)	1.312(5)	C(30)–N(6)	1.446(6)
K(1)–Centroid(1)*	2.934	K(1)–Centroid(2)*	2.903
K(2)–O(1)	2.729(5)		
N(3)–K(1)–Centroid(1)	80.5	N(5)–K(1)–Centroid(2)	81.2
Centroid(1)–K(1)–Centroid(2)	119.6	N(3)–K(1)–N(5)	123.9(1)
N(1)–C(9)–N(3)	124.2(4)	N(4)–C(30)–N(5)	125.9(4)
N(4)–C(30)–N(6)	112.8(4)		

* Centroid(1) = center position of phenyl ring formed by C(1)–C(6).
* Centroid(2) = center position of phenyl ring formed by C(22)–C(27).

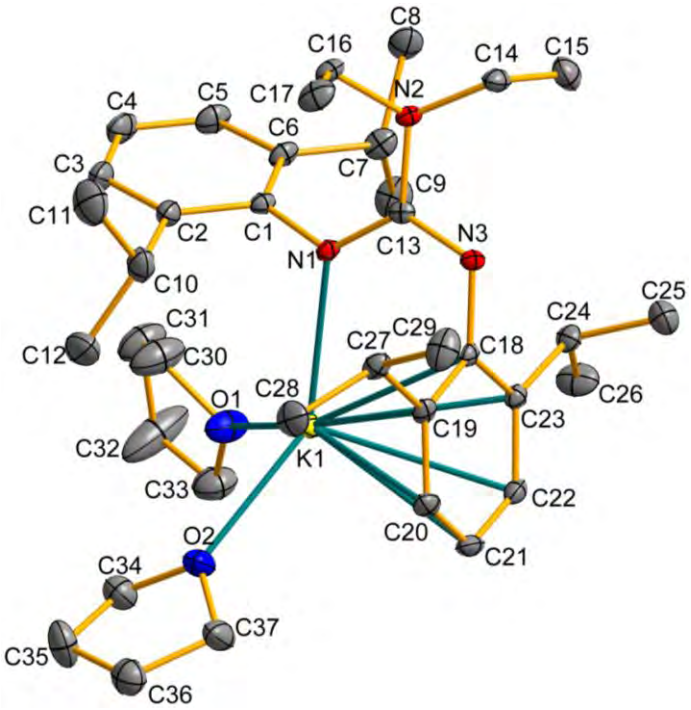

Figure 3–2. Molecular structure of $[KL^5(THF)_2]$ (**14**).

Table 3–3. Selected bond distances (Å) and angles (deg.) for compound **14**

$[KL^5(THF)_2]$ (**14**)			
K(1)–N(1)	2.740(4)	K(1)–O(1)	2.690(4)
K(1)–O(2)	2.666(4)	K(1)–Centroid(1)*	2.889
C(13)–N(1)	1.338(6)	C(13)–N(2)	1.421(6)
C(13)–N(3)	1.324(6)		
N(1)–K(1)–Centroid(1)	81.2	O(1)–K(1)–O(2)	85.9(1)
N(1)–K(1)–O(1)	110.3(1)	N(1)–K(1)–O(2)	133.6(1)
N(1)–C(13)–N(3)	122.9(4)	O(1)–K(1)–Centroid(1)	150.4
O(2)–K(1)–Centroid(1)	105.4		

* Centroid(1) = center position of phenyl ring formed by C(18)–C(23).

3.2.2 Synthesis and Structure of Ln(II) (Ln = Sm, Eu, Yb) Complexes of the L^1, L^2, L^3 and L^5 Ligands

Preparation

Reaction of $EuI_2(THF)_2$ with two equivalents of $[KL^1 \cdot 0.5PhMe]_n$ (**1**)† in THF yielded dimeric $[\{Eu(L^1)(\mu\text{–}L^1)\}_2]$ (**15**) (Scheme 3–16). Metathesis reactions of $LnI_2(THF)_2$ (Ln = Yb, Eu) with potassium guanidinates **12** and **13** in THF, led to the isolation of $[\{Ln(L^2)(\mu\text{–}L^2)\}_2 \cdot nC_6H_{14}]$ [Ln = Eu, n = 2 (**16**); Ln = Yb, n = 0 (**17**)], $[Yb(L^2)_2(THF)_2]$ (**18**) (Scheme 3–17) and $[Ln(L^3)_2(THF)_2 \cdot 0.25C_6H_{14}]$ [Ln = Eu (**19**), Yb (**20**)], respectively (Scheme 3–18). Treatment of $SmI_2(THF)_2$ with one molar equivalent of **13** in THF yielded the iodide bridged Sm(II) complex $[\{Sm(L^3)(\mu\text{–}I)(THF)\}_2]$ (**21**). Salt metathesis reaction of $SmI_2(THF)_2$ with two equivalents of **14** gave the mononuclear Sm(II) complex $[Sm(L^5)_2]$ (**22**) (Scheme 3–19).

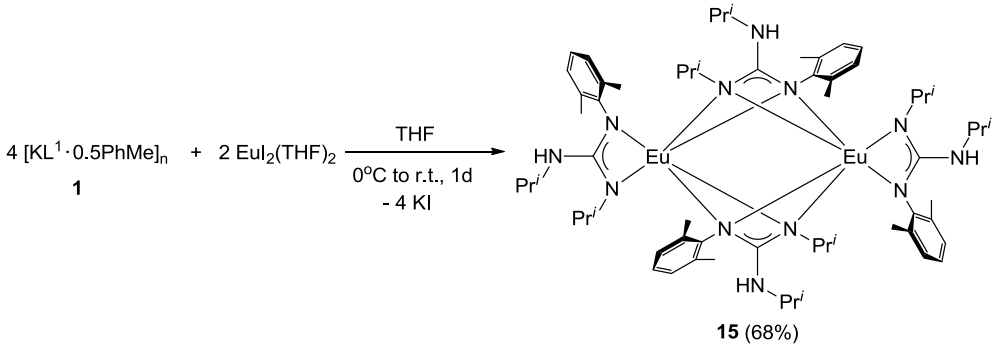

Scheme 3—16

† The preparation of complex **1** has been described in Chapter 2.

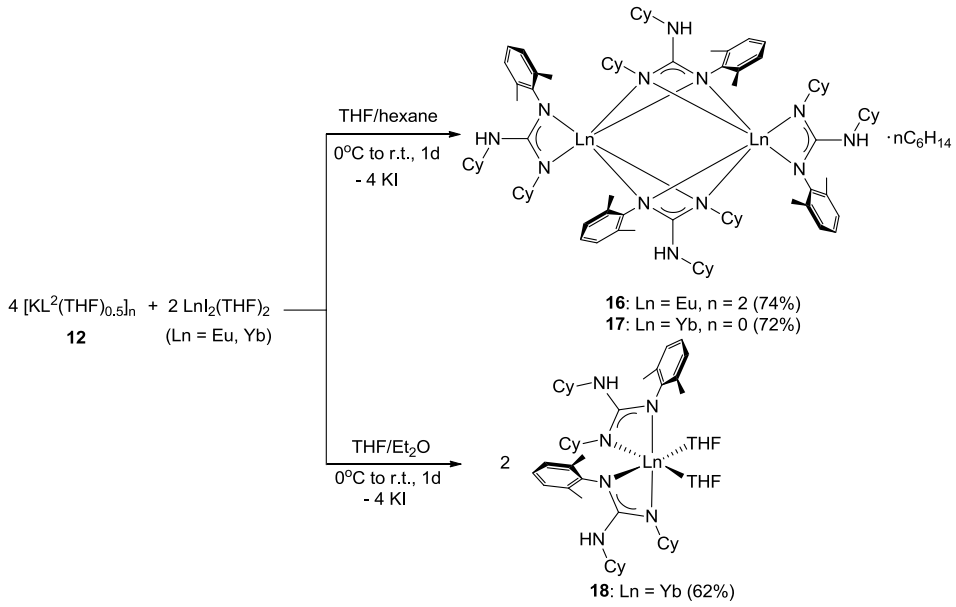

Scheme 3—17

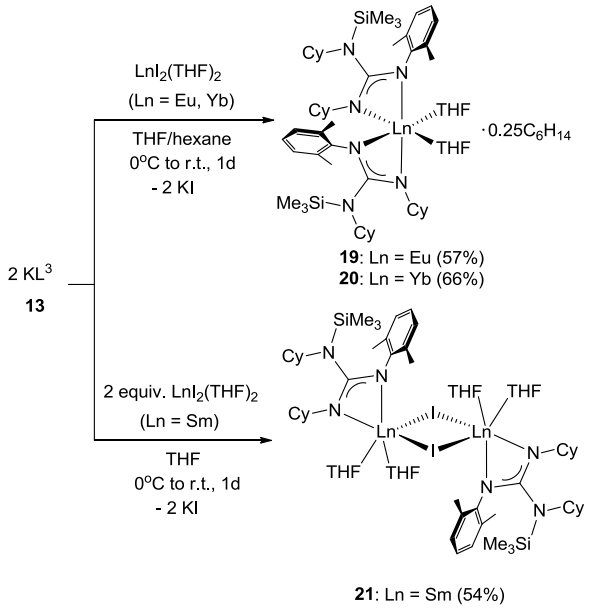

Scheme 3—18

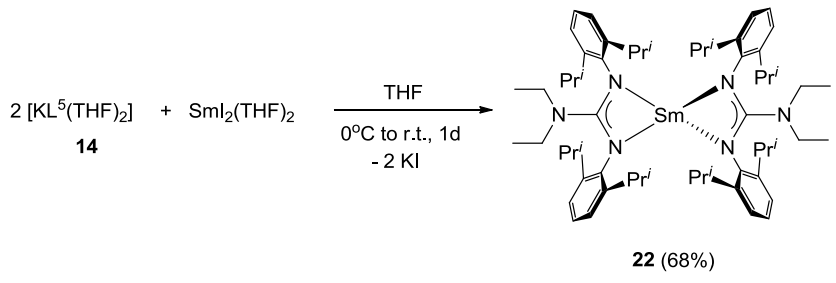

Scheme 3—19

Physical Characterization of Complexes **15**–**22**

The molecular formula of complexes **15**–**22** was confirmed by elemental analysis

and X–ray diffraction analysis. NMR spectroscopy were also carried out for the diamagnetic Yb(II) complexes **17**, **18** and **20**. All of the complexes (except **21**) are soluble in THF, toluene, Et_2O and hexane. However, complex **21** is only soluble in THF. The appearance and melting points of complexes **15**–**22** are summarized in Table 3–4.

Table 3–4. Appearance and melting points of complexes **15**–**22**

Compound	Appearance	M.p. (^oC)
$[\{Eu(L^1)(\mu\text{–}L^1)\}_2]$ (**15**)	Orange crystals	211–212 (dec.)
$[\{Eu(L^2)(\mu\text{–}L^2)\}_2 \cdot 2C_6H_{14}]$ (**16**)	Orange crystals	241–243 (dec.)
$[\{Yb(L^2)(\mu\text{–}L^2)\}_2]$ (**17**)	Red crystals	185–186 (dec.)
$[Yb(L^2)_2(THF)_2]$ (**18**)	Red crystals	174–175 (dec.)
$[Eu(L^3)_2(THF)_2 \cdot 0.25C_6H_{14}]$ (**19**)	Orange crystals	252–253 (dec.)
$[Yb(L^3)_2(THF)_2 \cdot 0.25C_6H_{14}]$ (**20**)	Red crystals	178–179 (dec.)
$[\{Sm(L^3)(\mu\text{–}I)(THF)_2\}_2]$ (**21**)	Dark green crystals	168–169 (dec.)
$[Sm(L^5)_2]$ (**22**)	Purple crystals	161–162 (dec.)

NMR Spectra of Yb(III) Complexes **17**, **18** and **20**

The ^1H and ^{13}C NMR spectra of complexes **17**, **18** and **20** are shown in Figures A2–14, A2–15 and A2–17 to A2–20 (Appendix 2), respectively. The ^1H NMR spectrum of complex **17** shows three broad signals at 2.18, 2.30 and 2.41 ppm, respectively, which are assignable to the ortho methyl groups on the aryl substituent.

These indicate that the methyl groups on each phenyl ring are chemically non–equivalent. This may be attributed to a hindered rotation of the methyl groups. Broadening of the resonance signals may be attributed to the equilibrium process between monomer and dimer, therefore variable temperature ^{1}H NMR studies of complex **17** were carried out at 25^{o}C to 90^{o}C (Figure A2–16). However, no significant change was observed in the ^{1}H NMR of **17** over the above temperature range. Apparently, the peak broadening of complex **17** is not due to fluxional behavior. The ^{13}C NMR spectrum of complex **17** shows two sets of resonance signals corresponding to the L^2 ligands. This is consistent with the solid–state structure of complex **17** (vide infra), in which one terminal L^2 ligand is bonded to each Yb center in a κ^2 coordination mode, while another L^2 ligand bridges two Yb centers in a μ–η^3:η^3 coordination mode.

The ^{1}H NMR spectrum of complex **18** shows one set of signal, corresponding to two L^2 ligands and three THF solvent molecules, indicating that the two L^2 ligands are chemically equivalent. A broad singlet signal at 2.47 ppm is assignable to the ortho methyl groups on the aryl substituent. Two sets of broad resonance signals are observed for the cyclohexyl substituents in both ^{1}H and ^{13}C NMR spectra. These spectroscopic behaviors suggest that the two cyclohexyl substituents in each L^2 ligand are chemically non–equivalent.

The ^{1}H NMR spectrum of complex **20** shows one set of resonance signal assignable to the L^3 ligand, THF and hexane molecules with an integral ratio of L^3:THF:hexane = 8:8:1. The two L^3 ligands in each monomeric unit are chemically equivalent. In the ^{1}H NMR spectrum, two broad signals at 0.46 and 2.46 ppm are assignable to $SiMe_3$ and the *ortho* methyl groups on the aryl substituent, respectively. Similar to complex **18**, the two cyclohexyl substituents in each L^3 ligand in complex **20** are chemically non–equivalent. The cyclohexyl substituents exist as two sets of resonance signals in both ^{1}H and ^{13}C NMR spectra.

Crystal Structures of Complexes **15**–**22**

Single crystals of **15** suitable for X–ray diffraction analysis were obtained from toluene. Those of **16**, **17**, **19**, **20** and **22** were obtained from hexane. Single crystals of **18** and **21** were obtained from Et_2O and THF, respectively. Selected crystallographic data of these complexes are listed in Tables A3–6 to A3–8 (Appendix 3), respectively.

1. $[\{Eu(L^1)(\mu\text{–}L^1)\}_2]$ (**15**)

The molecular structure of complex **15** with atom labeling is shown in Figure 3–3. Selected bond lengths and angles are listed in Table 3–5.

Complex **15** crystallizes in the monoclinic space group $P\bar{1}$. The europium

center in complex **15** is coordinated by one κ^2–bound L^1 ligand and two μ–η^3:η^3–bound L^1 ligands. A similar μ–η^3:η^3 binding mode has been reported for Eu(II) bis(pyrazolate) complex [{Eu(^{t}Bu$_2$pz)$_2$(THF)}$_2$].[16] The coordination geometry around the Eu(1) atom in complex **15** is best described as distorted octahedral, with the two axial positions being occupied by N(3) and N(6)# [N(3)–Eu(1)–N(6)# = 154.83(8)^o], whereas the equatorial plane consisting of N(1), N(4), N(4)# and N(6) [sum of bond angles around Eu(1) = 344.0^o]. A similar heavily distorted octahedral geometry has also been observed for complexes **16** and **17** (vide infra). Besides, complex **15** (also for complexes **16** and **17**) consists of an inversion center in each dimeric unit. Compare to the monomeric Cr(II) derivative, [Cr(L^1)$_2$] (**3**), complex **15** crystallizes as a dimer. This results in an increase in the coordination number in the latter complex (the coordination number of complex **3** is 4, whereas the coordination number of **15** is 6), which may be attributed to a difference in the ionic radius of Cr^{2+} [0.80 (Å)] and Eu^{2+} [1.17 (Å)].[17]

The Eu···Eu distance in **15** [3.4241(3) Å] is longer than the sum of ionic radii of two Eu(II) metals (2.34 Å).[17] Therefore, no metal–metal bond is expected to be observed in **15**.

The Eu–N distances of the terminal L^1 ligands [Eu(1)–N(3) = 2.560(2) Å and Eu(1)–N(1) = 2.561(2) Å] are necessarily shorter than those of the bridging L^1 ligands

[Eu(1)–N(6) = 2.635(2) Å and Eu(1)–N(4) = 2.822(3) Å]. The measured Eu(1)–$N^{(isopropyl)}$ distances [$N^{(isopropyl)}$ = N(3) and N(6)] are shorter than the Eu(1)–$N^{(aryl)}$ distances [$N^{(aryl)}$ = N(1) and N(4)]. On the other hand, the C–$N^{(isopropyl)}$ distances [C(9)–N(3) = 1.325(4) Å and C(24)–N(6) = 1.334(4) Å] on the $N^{(aryl)}$–C–$N^{(isopropyl)}$ backbone of the terminal and bridging L^1 ligands are shorter than the C–$N^{(aryl)}$ distances [C(9)–N(1) = 1.340(4) Å and C(24)–N(4) = 1.350(4) Å]. This may be ascribed to the presence of a relatively stronger electron–donating Pr^i substituent as compared to that of the aryl substituent. Moreover, the almost identical C–N bonds in the terminal L^1 ligand [C(9)–N(1) 1.340(4) Å and C(9)–N(3) 1.325(4) Å] and the bridging L^1 ligand [C(24)–N(4) 1.350(4) Å and C(24)–N(6) 1.334(4) Å] indicates the delocalization of the anionic charge over the N(1)–C(9)–N(3) and N(4)–C(24)–N(6) ligand moieties, respectively. A similar trend on the C–N bond distances has also been observed in complexes **16** and **17**.

The terminal Eu–N distances of 2.560(2) and 2.561(2) Å in **15** are comparable to the corresponding distances of 2.525(2)–2.563(2) Å in [Eu(Giso)$_2$] [Giso = {(2,6–$Pr^i{}_2C_6H_3N)_2CNCy_2$}$^-$],[10] 2.496(2) and 2.503(2) Å in complex [Eu(Priso)$_2$] [Priso = {(2,6–$Pr^i{}_2C_6H_3N)_2CNPr^i{}_2$}$^-$],[11] 2.526(4)–2.768(4) Å in [Eu{PhC(NSiMe$_3$)($NC_6H_3Pr^i{}_2$–2,6)}$_2$(THF)$_2$][8] and 2.473(1) and 2.518(1) Å in the bis(pyrazolate) complex [{Eu(^{t}Bu$_2$pz)$_2$(THF)}$_2$].[16] On the other hand, they are

reasonably longer than the Eu(II) bis(amide) complexes such as $[Eu\{N(SiMe_3)_2\}_2(DME)_2]$ [2.530(4) Å][3a] and $[NaEu\{N(SiMe_3)_2\}_3]$ [2.448(4) Å].[3c]

The bridging Eu–N distances of 2.635(2) and 2.822(3) Å in **15** are comparable to the corresponding distances of 2.552(1)–2.792(1) Å in $[\{Eu(^tBu_2pz)_2(THF)\}_2]$.[16]

The sum of bond angles around C(9) and C(24) are 360.0°, indicating that the central carbon atoms on the terminal and bridging L^1 ligands are sp^2 hybridized. A similar observation has also been noted in the corresponding carbon atoms in complexes **16** and **17**.

The N(4)–Eu(1)–N(6) (bridging) and N(1)–Eu(1)–N(3) (terminal) bite angles are acute, namely 48.99(8) and 52.80(8)°, which are similar to those reported for the four–membered metallacyclic ring complexes such as $[Eu\{PhC(NSiMe_3)(NC_6H_3Pr^i_2\text{–}2,6)\}_2(THF)_2]$ [50.9(1) and 51.6(1)°],[8] $[Eu(Giso)_2]$ [52.41(6) and 52.81(6)°][10] and $[Eu(Priso)_2]$ [53.33(9) and 53.96(9)°].[11]

2. $[\{Eu(L^2)(\mu\text{–}L^2)\}_2\cdot 2C_6H_{14}]$ (**16**)

The molecular structure of complex **16** with atom labeling is shown in Figure 3–4. Selected bond lengths and angles are listed in Table 3–6.

Complex **16** crystallizes in the monoclinic space group *C*2/*c*. Similar to complex **15**, each Eu(II) center in complex **16** is coordinated by one κ^2–bound L^2 ligand and two $\mu\text{–}\eta^3\text{:}\eta^3$ bound L^2 ligands. The coordination geometry around Eu(1)

is best described as distorted octahedral, with the two axial positions being occupied by N(3) and N(6) [N(3)–Eu(1)–N(6) = 154.8(1)^{o}], whereas the equatorial plane consisting of N(1), N(1)#, N(3)# and N(4) (sum of bond angles around Eu(1) = 381.6^{o}).

The Eu···Eu distance in **16** [3.4297(5) Å] is similar to the corresponding distance in **15** [3.4241(3) Å], indicating that no metal–metal bond is present in the dinuclear complex.

The Eu–N distances of the terminal L^2 ligand [Eu(1)–N(4) = 2.580(4) Å and Eu(1)–N(6) = 2.554(4) Å] in **16** are comparable to the corresponding distances in **15** [2.560(2) and 2.561(2) Å]. They are also comparable to the corresponding distances in other Eu(II) complexes such as [Eu(Giso)$_2$] [2.525(2)–2.563(2) Å],[10] [Eu(Priso)$_2$] [2.496(2) and 2.503(2) Å],[11] [Eu{PhC(NSiMe$_3$)(NC$_6$H$_3$Pr$^i_2$–2,6)}$_2$(THF)$_2$] [2.526(4)–2.768(4) Å][8] and [{Eu(^{t}Bu$_2$pz)$_2$(THF)}$_2$] [2.473(1) and 2.518(1) Å].[16]

The Eu–N distances of the bridging L^2 ligand [Eu(1)–N(1) = 2.653(4) Å and Eu(1)–N(3) = 2.714(4) Å] in **16** are slightly shorter than the corresponding distances in **15** [2.635(2) and 2.822(3) Å]. Although L^1 is a sterically more demanding ligand than L^2, the increases in the Eu–N distances in the latter complex may be due to other factors besides steric effect.

The N(1)–Eu(1)–N(3) and N(4)–Eu(1)–N(6) bite angles in **16** are measured to be

49.6(1) and 52.5(1)^{o}, which are similar to the corresponding angles in **15** [48.99(8) and 52.80(8)^{o}]. The terminal bite angle is also similar to the corresponding angles reported for other Eu(II) complexes such as [Eu{PhC(NSiMe$_3$)(NC$_6$H$_3$Pr$^{i}_2$–2,6)}$_2$(THF)$_2$] [50.9(1) and 51.6(1)^{o}],[8] [Eu(Giso)$_2$] [52.41(6) and 52.81(6)^{o}][10] and [Eu(Priso)$_2$] [53.33(9) and 53.96(9)^{o}].[11]

3. [{Yb(L^2)(μ–L^2)}$_2$] (**17**)

The molecular structure of complex **17** with atom labeling is shown in Figure 3–5. Selected bond lengths and angles are listed in Table 3–7.

Complex **17** crystallizes in the monoclinic space group *C*2/*c*. It is isotypic to its Eu(II) analogue **16**. Each Yb(II) center in the dimeric unit is coordinated by one κ^2–bound L^2 ligand and two μ–η^3:η^3 bound L^2 ligands. The coordination geometry around Yb(1) is best described as distorted octahedral, with the two axial positions being occupied by N(3)# and N(6) [N(3)#–Yb(1)–N(6) = 154.3(1)^{o}], whereas the equatorial plane consisting of N(1), N(1)#, N(3) and N(4) (sum of bond angles around Yb(1) = 379.6^{o}).

The observed Yb···Yb distance in **17** [3.2719(4) Å] is longer than the sum of ionic radii of two Yb(II) ions (2.04 Å).[17] Apparently, no metal–metal bond is present in the dinuclear complex.

The measured Yb(1)–N$^{(cyclohexyl)}$ distances [N$^{(cyclohexyl)}$ = N(3) and N(6)] are

shorter than the Yb(1)–$N^{(aryl)}$ distances [$N^{(aryl)}$ = N(1) and N(4)] [Yb(1)–N(1) = 2.787(4) Å, Yb(1)–N(3) = 2.552(4) Å, Yb(1)–N(4) = 2.475(4) Å, Yb(1)–N(6) = 2.451(4) Å]. On the other hand, the C–$N^{(cyclohexyl)}$ distances [C(9)–N(3) = 1.338(6) Å and C(30)–N(6) = 1.328(6) Å] on the $N^{(aryl)}$–C–$N^{(cyclohexyl)}$ backbone of the terminal and bridging L^1 ligands are shorter than the C–$N^{(aryl)}$ distances [C(9)–N(1) = 1.342(6) Å and C(30)–N(4) = 1.354(5) Å]. A similar trend is also observed in complex **15**, which suggests that the electron density is not equally distributed in the unsymmetrical L^2 ligand.

The observed terminal Yb–N distances [Yb(1)–N(4) and Yb(1)–N(6)] in complex **17** of 2.4551(4) and 2.475(4) Å are slightly longer than the Yb–$N^{(amide)}$ bonds in the Yb(II) bis(2–pyridylamide) complexes [$Yb(Ap^{Me})_2(THF)_2$] [Ap^{Me} = $N(C_6H_2Me_3–2,4,6)\{2–C_5H_3N–6–(C_6H_2Me_3–2,4,6)\}$] [2.396(5) Å],[18] [$Yb(Ap')_2(THF)$] [Ap' = $N(C_6H_3Pr^i_2–2,6)\{2–C_5H_3N–6–(C_6H_3Me_2–2,6)\}$] [2.380(4) and 2.384(3) Å],[18] [$Yp(Ap')_2$] [2.371(1) and 2.404(2) Å][18] and [$Yb(Ap^*)_2(THF)_2$] [Ap^* = $N(C_6H_3Pr^i_2–2,6)\{2–C_5H_3N–6–(C_6H_2Pr^i_3–2,4,6)\}$] [2.431(6) and 2.464(7) Å].[19] However, they are comparable to the Yb–$N^{(pyridyl)}$ bonds in [$Yb(Ap^{Me})_2(THF)_2$] [2.544(4) Å],[18] [$Yb(Ap')_2(THF)$] [2.466(4) and 2.479(4) Å],[18] [$Yp(Ap')_2$] [2.432(2) and 2.449(2) Å][18] and [$Yb(Ap^*)_2(THF)_2$] [2.511(5) and 2.511(6) Å].[19] A longer Yb–$N^{(pyridyl)}$ bond has been observed comparing to the Yb–$N^{(amide)}$ bond in the above

Yb(II) bis(2–pyridylamide) complexes, which can be explained by a localized anionic charge at the $N^{(amide)}$ atom.[18] The terminal Yb–N distances are also comparable to the Yb(II) bis(amidinate) complexes [Yb{PhC($NSiMe_3$)$_2$}$_2$(THF)$_2$] [2.468(2) and 2.478(2) Å][6a] and [Yb{PhC($NSiMe_3$)($NC_6H_3Pr^i_2$–2,6)}$_2$(THF)] [2.399(3)–2.453(4) Å],[8] Yb(II) guanidinate–iodo complexes [{Yb(Giso)(μ–I)(THF)}$_2$] [2.373(3) and 2.426(3) Å][10] and [{Yb(Priso)(μ–I)}$_2$] [2.36(1) and 2.425(9) Å][11] and Yb(II) bis(guanidinate) complexes [Yb($Giso$)$_2$] [2.378(2)–2.430(2) Å][10] and [Yb($Priso$)$_2$] [2.376(3) and 2.390(3) Å].[11]

The N–Yb–N bite angles of the bridging [N(4)–Yb(1)–N(6)] and terminal [N(1)–Yb(1)–N(3)] L^2 ligands in **17** are acute, namely 49.5(1) and 54.6(1)°. The terminal N–Yb–N bite angle is similar to the corresponding angles in the four–membered metallacyclic complexes such as [Yb(Ap^{Me})$_2$(THF)$_2$] [54.8(2)°],[18] [Yb(Ap')$_2$(THF)] [55.8(2) and 56.2(1)°],[18] [Yb(Ap')$_2$] [56.02(6) and 56.05(6)°],[18] [Yb(Ap^*)$_2$(THF)$_2$] [54.4(2) and 55.1(2)°],[19] [Yb{PhC($NSiMe_3$)$_2$}$_2$(THF)$_2$] [55.6(1)°],[6a] [Yb{PhC($NSiMe_3$)($NC_6H_3Pr^i_2$–2,6)}$_2$(THF)] [55.8(1) and 56.3(1)°],[8] [Yb($Giso$)$_2$] [55.79(8) and 56.48(8)°][10] and [Yb($Priso$)$_2$] [55.8(1)°].[11]

4. [Yb(L^2)$_2$(THF)$_2$] (**18**)

The molecular structure of complex **18** with atom labeling is shown in Figure 3–6. Selected bond lengths and angles are listed in Table 3–8.

Complex **18** crystallizes in the monoclinic space group $P2_1/c$. The Yb(II) center in complex **18** is coordinated by two κ^2–bound L^2 ligand and two THF molecules, which formed a six–coordinate environment around the metal center. The two THF ligands coordinate in a cis–manner with O(1)–Yb(1)–O(2) = 82.2(2)^o. The coordination geometry around Yb(1) can be described as distorted octahedral, with the two axial positions being occupied by N(1) and N(4) [N(1)–Yb(1)–N(4) = 163.8(2)^o], whereas the equatorial plane being occupied by N(3), N(6), O(1) and O(2) [sum of bond angles around Yb(1) = 380.9^o]. Beside, the complex consists of a two–fold rotational axis passing through the metal center and bisecting the O(1)–Yb(1)–O(2) angle. A similar two–fold rotational axis has also been found in complexes **19** and **20**.

The observed Yb–$N^{(cyclohexyl)}$ distances in complex **18** [Yb(1)–N(3) = 2.422(4) Å, Yb(1)–N(6) = 2.412(5) Å] are shorter than the Yb–$N^{(aryl)}$ distances [Yb(1)–N(1) = 2.470(4) Å, Yb(1)–N(4) = 2.479(4) Å], indicates a more localized anionic charge on the $N^{(cyclohexyl)}$ atom. The Yb–N distances in **18** [2.412(5)–2.479(4) Å] are comparable to the terminal Yb–N distances in **17** [2.451(4) and 2.475(4) Å], which suggests a less steric congestion environment around the Yb(II) center in the former complex. They are also similar to the corresponding distances in other six–coordinate Yb(II) complexes such as [Yb(Ap^{Me})$_2$(THF)$_2$] [Yb–$N^{(amide)}$ = 2.396(5)

Å, Yb–$N^{(aryl)}$ = 2.544(4) Å][18] and [Yb{PhC($NSiMe_3$)$_2$}$_2$($THF)_2$] [2.468(2) and 2.478(2) Å],[6a] as well as five–coordinate complexes [Yb(Ap')$_2$(THF)] [Yb–$N^{(amide)}$ = 2.380(4) and 2.3843 Å, Yb–$N^{(aryl)}$ = 2.4664 and 2.479(4) Å][18] and [Yb{PhC($NSiMe_3$)($NC_6H_3Pr^i_2$–2,6)}$_2$(THF)] [2.399(3)–2.453(4) Å].[8] Besides, they are comparable to the corresponding distances in the four–coordinate complex [Yb(Giso)$_2$] [2.378(2)–2.430(2) Å],[10] but marginally longer than the corresponding distances in [Yb(Priso)$_2$] [2.376(3) and 2.390(3) Å].[11]

The Yb(1)–O(2) and Yb(1)–O(1) distances in **18** are measured to be 2.429(4) and 2.452(4) Å, respectively, which are comparable to those reported in the six–coordinate complexes [Yb(Ap^{Me})$_2$($THF)_2$] [2.428(4) Å][18] and [Yb{PhC($NSiMe_3$)$_2$}$_2$($THF)_2$] [2.406(3) and 2.424(3) Å].

The N(4)–Yb–N(6) and N(1)–Yb–N(3) bite angles in **18** [55.0(2) and 55.1(1)^o] are similar to those of 54.8(2)^o in [Yb(Ap^{Me})$_2$($THF)_2$],[18] 54.4(2) and 55.1(2)^o in [Yb(Ap^*)$_2$($THF)_2$][19] and 55.6(1)^o in [Yb{PhC($NSiMe_3$)$_2$}$_2$($THF)_2$].[6a]

5. [Eu(L^3)$_2$($THF)_2$·0.25C_6H_{14}] (**19**)

The molecular structure of complex **19** with atom labeling is shown in Figure 3–7. Selected bond lengths and angles are listed in Table 3–9.

The hexane solvated complex **19** crystallizes in the monoclinic space group $P2_1/c$. The Eu(II) center in complex **19** is coordinated by two κ^2–bound L^3 ligand

and two THF molecules. The two coordinated THF molecules bind to the Eu(II) center in a cis–manner [O(1)–Eu(1)–O(2) = 81.2(1)^{o}]. The coordination geometry around Eu(1) can be described as distorted octahedral, with the two axial positions being occupied by N(1) and N(4) [N(1)–Eu(1)–N(4) = 166.9(1)^{o}], whereas the equatorial plane being occupied by N(3), N(6), O(1) and O(2) [sum of bond angles around Eu(1) = 385.7^{o}].

The Eu–N distances in complex **19** [Eu(1)–N(1) = 2.558(3) Å, Eu(1)–N(3) = 2.565(4) Å, Eu(1)–N(4) = 2.582(4) Å and Eu(1)–N(6) = 2.556(4) Å] are similar to the Eu–N bond distances of the terminal L^1 ligand in **15** [2.560(2) and 2.561(2) Å] and those of the terminal L^2 ligand in **16** [2.554(4) and 2.580(4) Å]. They are also comparable to the corresponding distances of 2.526(4)–2.768(4) Å in $[Eu\{PhC(NSiMe_3)(NC_6H_3Pr^i_2\text{–}2,6)\}_2(THF)_2]$[8] and 2.518(1)–2.792(1) Å in $[\{Eu(^tBu_2pz)_2(THF)\}_2]$.[16]

The Eu(1)–O(2) and Eu(1)–O(1) bond distances are measured to be 2.594(4) and 2.599(4) Å, respectively, which are comparable to those reported in the Eu(II) complexes $[\{Eu(^tBu_2pz)_2(THF)\}_2]$ [2.583(1) Å][16] and $[Eu\{PhC(NSiMe_3)(NC_6H_3Pr^i_2\text{–}2,6)\}_2(THF)_2]$ [*transoid*: 2.604(4) Å; *cisoid*: 2.527(4) and 2.570(4) Å].

The N(1)–Eu(1)–N(3) and N(4)–Eu(1)–N(6) bite angles are acute, namely 52.3(1)

and 51.7(1)^{o}.

The C–N–C angles on the $N^{(cyclohexyl)}$ atoms [C(9)–N(3)–C(19) = 122.2(4)^{o} and C(33)–N(6)–C(43) = 123.1(4)^{o} and the $N^{(aryl)}$ atoms [C(9)–N(1)–C(1) = 123.7(4)^{o} and C(33)–N(4)–C(25) = 125.5(4)^{o}] in **19** are larger than the corresponding angles in **18** [C(30)–N(6)–C(37) = 119.9(4)^{o} and C(30)–N(4)–C(22) = 121.4(4)^{o}]. This suggests that an additional $SiMe_3$ substituent on L^3 leads to an increase in steric bulkiness of the ligand environment, and, hence, the cyclohexyl and aryl substituents on the $N^{(cyclohexyl)}$ and $N^{(aryl)}$ atoms are pushed towards the Eu(II) center. The Eu(II) center in **19** is now more hindered as compared to complex **18**, which only allows the coordination of small molecules (such as THF) to the metal center in the former complex.

6. $[Yb(L^3)_2(THF)_2 \cdot 0.25C_6H_{14}]$ (**20**)

The molecular structure of complex **20** with atom labeling is shown in Figure 3–8. Selected bond lengths and angles are listed in Table 3–10.

The hexane solvated complex **20** is isostructural to its Eu(II) analogue **19**. It crystallizes in the monoclinic space group $P2_1/c$. The Yb(II) center is coordinated by two κ^2–bound L^3 ligands and two THF molecules. The two coordinated THF molecules bind to the Yb(II) center in a cis–manner with O(1)–Yb(1)–O(2) = 81.7(1)^{o}. The coordination geometry around Yb(1) can be described as distorted octahedral,

with the two axial positions being occupied by N(1) and N(4) [N(1)–Yb(1)–N(4) = 168.1(1)^{o}], whereas the equatorial plane being occupied by N(3), N(6), O(1) and O(2) [sum of bond angles around Yb(1) = 383.1^{o}].

The Yb–N bond distances in complex **20** [Yb(1)–N(1) = 2.475(3) Å, Yb(1)–N(3) = 2.451(4) Å, Yb(1)–N(4) = 2.451(3) Å and Yb(1)–N(6) = 2.474(3) Å] are similar to the corresponding distances in **18** [2.412(5)–2.479(4) Å]. On the other hand, they are reasonably shorter than the Eu–N bond distances in **19** [2.556(4)–2.582(4) Å] (ionic radius of Eu^{2+} = 1.17 Å ,Yb^{2+} = 1.02 Å).[17]

The Yb(1)–O(2) and Yb(1)–O(1) distances of 2.484(3) and 2.485(3) Å in **20** are slightly longer than the corresponding distances of 2.429(4) and 2.452(4) Å in **18**. This may be attributed to a more bulky ligand environment generated by ligand L^3 as compared to that of L^2.

The N(1)–Yb(1)–N(3) and N(4)–Yb(1)–N(6) bite angles are acute, namely 53.6(1) and 54.5(1)^{o}.

7. [{Sm(L^3)(μ–I)$(THF)_2$}$_2$] (**21**)

The molecular structure of complex **21** with atom labeling is shown in Figure 3–9. Selected bond lengths and angles are listed in Table 3–11.

Complex **21** crystallizes in the triclinic space group $P\bar{1}$. The Sm(II) center is coordinated by one κ^2–bound L^3 ligand, two μ–bridging iodide ligands and two THF

molecules. The two coordinated THF molecules attach to the Sm(II) center in a cis–manner with O(1)–Sm(1)–O(2) = 80.2(2)^{o}. The coordination geometry around Sm(1) can be best described as distorted octahedral, with the two axial positions being occupied by N(1) and I(1)# [N(1)–Sm(1)–I(1)# = 154.9(1)^{o}], whereas the equatorial plane consists of I(1), N(3), O(1) and O(2) [sum of bond angles around Sm(1) = 373.3^{o}]. Besides, the complex consists of an inversion center.

The Sm(1)–N(3) and Sm(1)–N(1) distances of 2.510(4) and 2.544(4) Å in complex **21** are similar to the corresponding distances in the amidinate complexes [Sm(DippForm)$_2$(THF)$_2$] [2.529(3) and 2.617(3) Å],[7] [Sm{PhC(NSiMe$_3$)(NC$_6$H$_3$Pr$^i_2$–2,6)}$_2$(THF)$_2$] [2.49(1)–2.67(1) Å][8] and [(η^1–N:η^6–Ar–Piso)Sm(THF)(μ–I)$_2$Sm(η^1–N:η^6–Ar–Piso)] [2.483(4) and 2.552(4) Å][11] and the guanidinate complexes [Sm(Giso)$_2$] [2.529(2)–2.570(2) Å][10] and [Sm(Priso)$_2$] [2.507(2) and 2.515(3) Å].[11]

The Sm(1)–O(2) and Sm(1)–O(1) distances of 2.576(5) and 2.582(5) Å are comparable to the corresponding distances in [Sm(DippForm)$_2$(THF)$_2$] [2.560(3) and 2.599(3) Å],[7] [Sm{PhC(NSiMe$_3$)(NC$_6$H$_3$Pr$^i_2$–2,6)}$_2$(THF)$_2$] [2.61(1)–2.64(1) Å][8] and [(η^1–N:η^6–Ar–Piso)Sm(THF)(μ–I)$_2$Sm(η^1–N:η^6–Ar–Piso)] [2.605(4) Å].[11]

The Sm(1)–I(1)# and Sm(1)–I(1) distances of 3.3045(6) and 3.3343(6) Å in **21** are comparable to the corresponding distances of 3.356(2) and 3.459(2) Å in

$[\{(C_5Me_5)Sm(\mu\text{–}I)(THF)_2\}_2]$,[20] 3.275(2) and 3.299(2) Å in $[\{Sm(Ap^*)(\mu\text{–}I)(THF)_2\}_2]$[21] and 3.1972(8)–3.3218(8) Å in $[(\eta^1\text{–}N{:}\eta^6\text{–}Ar\text{–}Piso)Sm(THF)(\mu\text{–}I)_2Sm(\eta^1\text{–}N{:}\eta^6\text{–}Ar\text{–}Piso)]$.[11]

The N(1)–Sm(1)–N(3) bite angle in **21** [52.5(1)^o] is similar to the corresponding angles in the six–coordinate complexes $[Sm(DippForm)_2(THF)_2]$ [52.9(1)^o][7] and $[Sm\{PhC(NSiMe_3)(NC_6H_3Pr^i_2\text{–}2,6)\}_2(THF)_2]$ [52.3(4) and 53.7(4)^o].[8]

8. $[Sm(L^5)_2]$ (**22**)

The molecular structure of complex **22** with atom labeling is shown in Figure 3–10. Selected bond lengths and angles are listed in Table 3–12.

Complex **22** crystallizes in the orthorhombic space group $Pna2_1$. Atom Sm(1) exhibits positional disorder with Sm(1') at a minor site, the occupancy ratio being 0.6:0.4. Each Sm(II) center in complex **22** is coordinated by two κ^2–bound L^5 ligands. The coordination geometry around each metal center can be best described as distorted square planar, with the square plane consists of N(1), N(2), N(4) and N(5) [sum of bond angles around Sm(1) and Sm(1') are 334.1 and 331.7^o, respectively]. A similar coordination geometry has been reported for the Sm(II) bis(guanidinate) complex $[Sm(Giso)_2]$ [sum of bond angle around Sm(II) center has been reported to be 357.6^o].[10] It has been proposed that the formation of the square planar geometry in the latter complex, $[Sm(Giso)_2]$, may be ascribed to the $Sm^{2+}\cdots$Me agostic

interaction (the shortest Sm···C interaction is measured to be 3.64 Å).[10] In complex **22**, the Sm(1)···C(42) and Sm(1')···C(24) interactions are measured to be 3.452(8) and 3.35(1) Å, respectively. They are also comparable to the Sm···C interaction in $[Sm\{N(SiMe_3)_2\}_2(THF)_2]$ [3.32(1) Å].[5a] Based on a comparison with these two complexes, Sm^{2+}···Me agostic interaction exists in complex **22**.

The C–N distances on the N–C–N backbone are similar to each other [C(1)–N(1) = 1.340(8) Å, C(1)–N(2) = 1.338(8) Å, C(30)–N(4) = 1.342(8) Å and C(30)–N(5) = 1.333(8) Å], which indicate a delocalization of the anionic charge over the N–C–N backbone.

The Sm–N distances of 2.496(5)–2.551(5) Å in complex **22** are similar to the corresponding distances in complex **21** [2.510(4) and 2.544(4) Å] and other Sm(II) bis(guanidinate) complexes, such as $[Sm(Giso)_2]$ [2.529(2)–2.570(2) Å][10] and $[Sm(Priso)_2]$ [2.507(2) and 2.515(3) Å].[11]

The N–Sm–N bite angles in **22** [53.1(2)–53.9(2)^o] are comparable to the corresponding angles in **21** [52.5(1)^o] and other Sm(II) bis(guanidinate) complexes $[Sm(Giso)_2]$ [52.55(7) and 52.18(7)^o][10] and $[Sm(Priso)_2]$ [52.8(1) and 53.8(1)^o].[11]

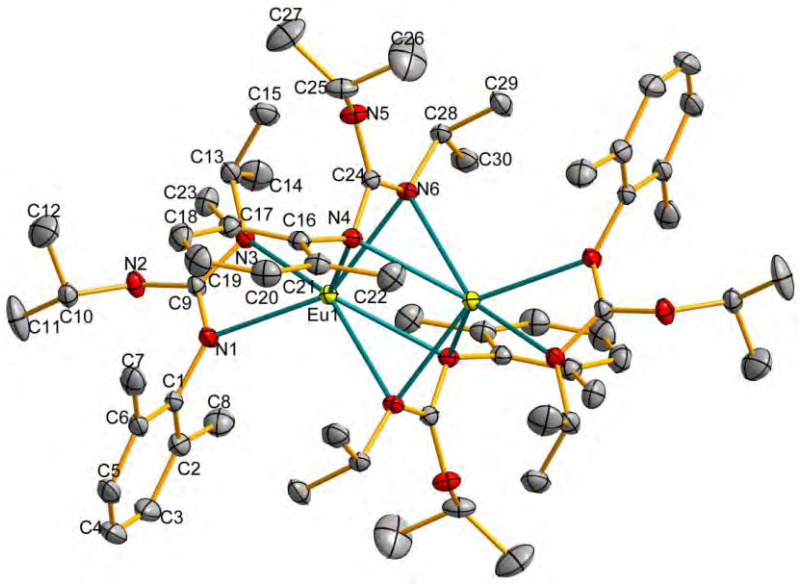

Figure 3–3. Molecular structure of [{Eu(L^1)(μ–L^1)}$_2$] (**15**)

Table 3–5. Selected bond distances (Å) and angles (deg.) for compound **15**

[{Eu(L^1)(μ–L^1)}$_2$] (**15**)			
Eu(1)–N(1)	2.561(2)	Eu(1)–N(3)	2.560(2)
Eu(1)–N(4)	2.822(3)	Eu(1)–N(6)	2.635(2)
C(9)–N(1)	1.340(4)	C(9)–N(2)	1.405(4)
C(9)–N(3)	1.325(4)	C(24)–N(4)	1.350(4)
C(24)–N(5)	1.375(4)	C(24)–N(6)	1.334(4)
Eu(1)···Eu(1)#	3.4241(3)		
N(1)–Eu(1)–N(3)	52.80(8)	N(1)–C(9)–N(3)	117.3(3)
Eu(1)–N(4)–Eu(1)#	76.99(6)	Eu(1)–N(6)–Eu(1)#	78.95(6)
N(4)–C(24)–N(6)	113.9(2)	N(4)–Eu(1)–N(6)	48.99(8)
N(3)–Eu(1)–N(6)#	154.83(8)	N(1)–Eu(1)–N(4)	125.92(8)
N(1)–Eu(1)–N(4)#	120.52(8)	N(4)#–Eu(1)–N(6)	48.56(8)

Symmetry code: # –x+1, –y+1, –z

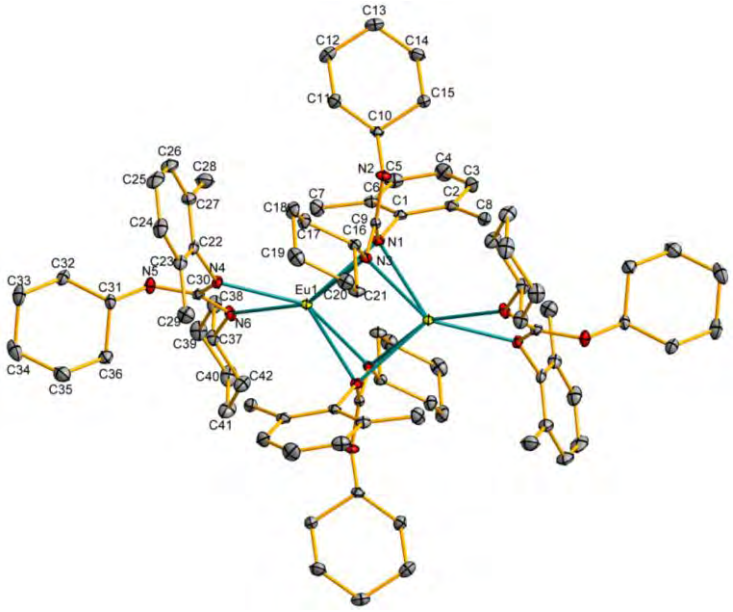

Figure 3–4. Molecular structure of $[\{Eu(L^2)(\mu\text{–}L^2)\}_2 \cdot 2C_6H_{14}]$ (**16**). The hexane solvent molecule is omitted for clarity.

Table 3–6. Selected bond distances (Å) and angles (deg.) for compound **16**

$[\{Eu(L^2)(\mu\text{–}L^2)\}_2 \cdot 2C_6H_{14}]$ (**16**)			
Eu(1)–N(1)	2.653(4)	Eu(1)–N(3)	2.714(4)
Eu(1)–N(4)	2.580(4)	Eu(1)–N(6)	2.554(4)
C(9)–N(1)	1.348(6)	C(9)–N(2)	1.369(6)
C(9)–N(3)	1.346(5)	C(30)–N(4)	1.359(6)
C(30)–N(5)	1.375(6)	C(30)–N(6)	1.334(6)
Eu(1)···Eu(1)#	3.4297(5)		
N(1)–Eu(1)–N(3)	49.6(1)	N(1)–C(9)–N(3)	113.5(4)
Eu(1)–N(1)–Eu(1)#	77.98(9)	Eu(1)–N(3)–Eu(1)#	79.7(1)
N(4)–C(30)–N(6)	115.0(4)	N(4)–Eu(1)–N(6)	52.5(1)
N(3)–Eu(1)–N(6)	154.8(1)	N(1)–Eu(1)–N(4)	125.4(1)
N(4)–Eu(1)–N(1)#	123.4(1)	N(1)–Eu(1)–N(3)#	83.2(1)
C(30)–N(4)–C(22)	121.4(4)	C(30)–N(6)–C(37)	119.9(4)

Symmetry code: # –x, –y+1, –z+1

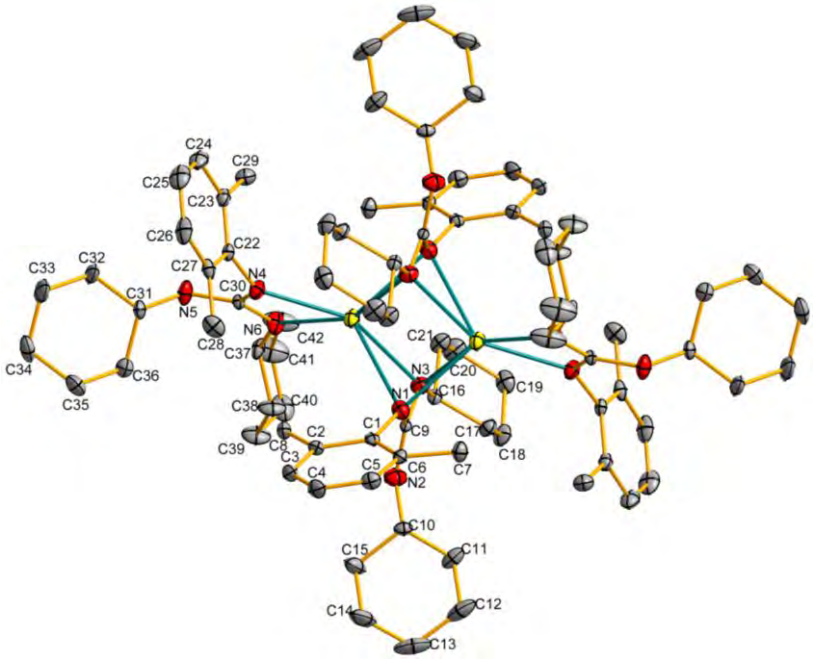

Figure 3–5. Molecular structure of [{Yb(L^2)(μ–L^2)}$_2$] (**17**)

Table 3–7. Selected bond distances (Å) and angles (deg.) for compound **17**

[{Yb(L^2)(μ–L^2)}$_2$] (**17**)			
Yb(1)–N(1)	2.787(4)	Yb(1)–N(3)	2.552(4)
Yb(1)–N(4)	2.475(4)	Yb(1)–N(6)	2.451(4)
C(9)–N(1)	1.342(6)	C(9)–N(2)	1.368(6)
C(9)–N(3)	1.338(6)	C(30)–N(4)	1.354(5)
C(30)–N(5)	1.373(5)	C(30)–N(6)	1.328(6)
Yb(1)–Yb(1)#	3.2719(4)		
N(1)–Yb(1)–N(3)	49.5(1)	N(1)–C(9)–N(3)	113.8(4)
Yb(1)–N(1)–Yb(1)#	75.8(1)	Yb(1)–N(3)–Yb(1)#	78.6(1)
N(4)–C(30)–N(6)	114.7(4)	N(4)–Yb(1)–N(6)	54.6(1)
N(3)#–Yb(1)–N(6)	154.3(1)	N(1)#–Yb(1)–N(4)	121.6(1)
N(1)–Yb(1)–N(4)	123.5(1)	N(1)#–Yb(1)–N(3)	85.0(1)

Symmetry code: # –x, –y+1, –z+1

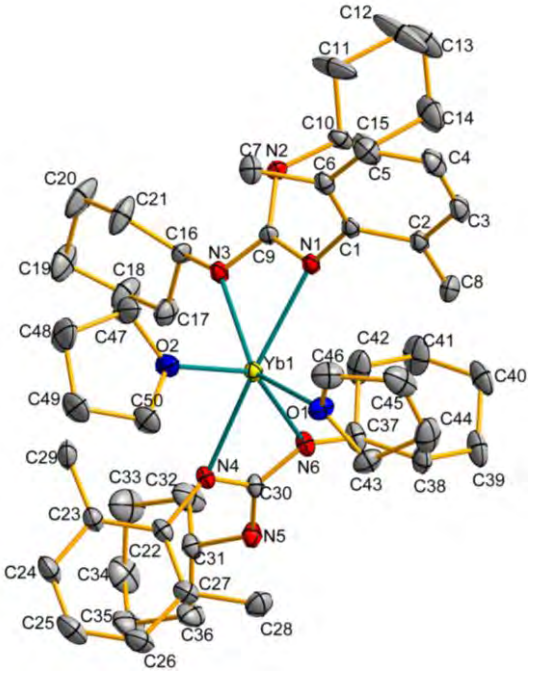

Figure 3–6. Molecular structure of [{Yb(L^2)$_2$(THF)$_2$] (**18**)

Table 3–8. Selected bond distances (Å) and angles (deg.) for compound **18**

[{Yb(L^2)$_2$(THF)$_2$] (**18**)			
Yb(1)–N(1)	2.470(4)	Yb(1)–N(3)	2.422(4)
Yb(1)–N(4)	2.479(4)	Yb(1)–N(6)	2.412(5)
Yb(1)–O(1)	2.452(4)	Yb(1)–O(2)	2.429(4)
C(9)–N(1)	1.350(6)	C(9)–N(2)	1.380(7)
C(9)–N(3)	1.322(6)	C(30)–N(4)	1.341(7)
C(30)–N(5)	1.386(7)	C(30)–N(6)	1.323(7)
N(1)–Yb(1)–N(3)	55.1(1)	N(1)–C(9)–N(3)	115.9(5)
N(4)–Yb(1)–N(6)	55.0(2)	N(4)–C(30)–N(6)	115.9(5)
O(1)–Yb(1)–O(2)	82.2(2)	N(1)–Yb(1)–N(4)	163.8(2)
N(3)–Yb(1)–O(2)	95.3(2)	O(1)–Yb(1)–N(6)	95.9(2)
N(3)–Yb(1)–N(6)	107.5(2)		

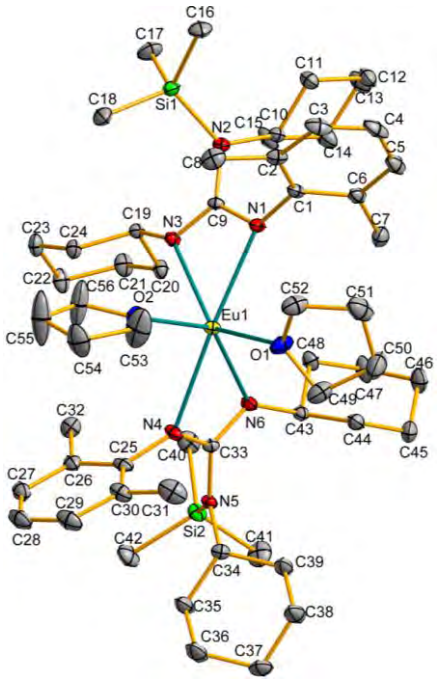

Figure 3–7. Molecular structure of $[Eu(L^3)_2(THF)_2 \cdot 0.25C_6H_{14}]$ (**19**). The hexane solvent molecule is omitted for clarity.

Table 3–9. Selected bond distances (Å) and angles (deg.) for compound **19**

$[Eu(L^3)_2(THF)_2 \cdot 0.25C_6H_{14}]$ (**19**)			
Eu(1)–N(1)	2.558(3)	Eu(1)–N(3)	2.565(4)
Eu(1)–N(4)	2.582(4)	Eu(1)–N(6)	2.556(4)
Eu(1)–O(1)	2.599(4)	Eu(1)–O(2)	2.594(4)
C(9)–N(1)	1.342(5)	C(9)–N(2)	1.444(5)
C(9)–N(3)	1.321(5)	C(33)–N(4)	1.333(6)
C(33)–N(5)	1.442(5)	C(33)–N(6)	1.326(6)
N(1)–Eu(1)–N(3)	52.3(1)	N(1)–C(9)–N(3)	115.8(4)
N(4)–Eu(1)–N(6)	51.7(1)	N(4)–C(33)–N(6)	114.7(4)
O(1)–Eu(1)–O(2)	81.2(1)	N(1)–Eu(1)–N(4)	166.9(1)
N(3)–Eu(1)–O(2)	93.6(1)	O(1)–Eu(1)–N(6)	102.1(1)
N(3)–Eu(1)–N(6)	108.8(1)	C(9)–N(1)–C(1)	123.7(4)
C(9)–N(3)–C(19)	122.2(4)	C(33)–N(4)–C(25)	125.5(4)
C(33)–N(6)–C(43)	123.1(4)		

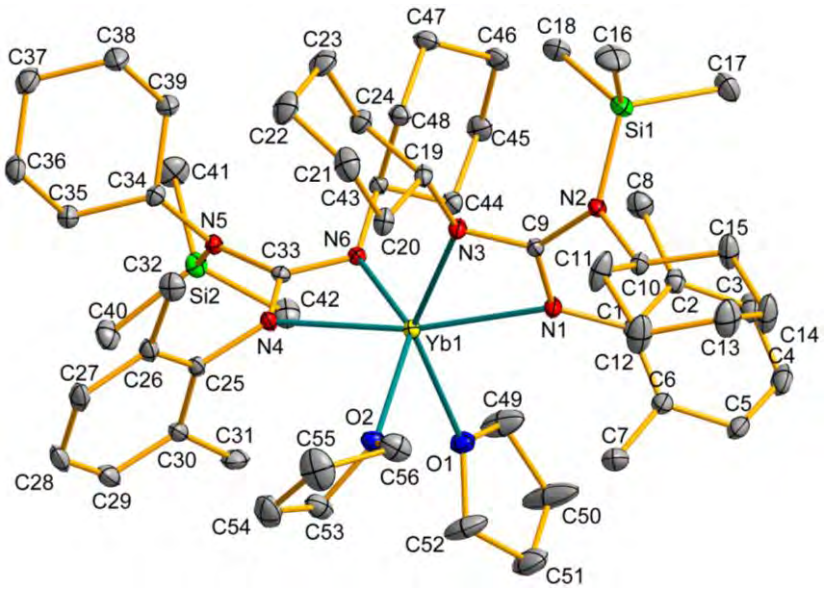

Figure 3–8. Molecular structure of $[Yb(L^3)_2(THF)_2 \cdot 0.25C_6H_{14}]$ (**20**). The hexane solvent molecule is omitted for clarity.

Table 3–10. Selected bond distances (Å) and angles (deg.) for compound **20**

$[Yb(L^3)_2(THF)_2 \cdot 0.25C_6H_{14}]$ (**20**)			
Yb(1)–N(1)	2.475(3)	Yb(1)–N(3)	2.451(4)
Yb(1)–N(4)	2.451(3)	Yb(1)–N(6)	2.474(3)
Yb(1)–O(1)	2.485(3)	Yb(1)–O(2)	2.484(3)
C(9)–N(1)	1.328(5)	C(9)–N(2)	1.448(5)
C(9)–N(3)	1.315(5)	C(33)–N(4)	1.344(5)
C(33)–N(5)	1.435(5)	C(33)–N(6)	1.318(5)
N(1)–Yb(1)–N(3)	53.6(1)	N(1)–C(9)–N(3)	114.5(4)
N(4)–Yb(1)–N(6)	54.5(1)	N(4)–C(33)–N(6)	115.7(4)
O(1)–Yb(1)–O(2)	81.7(1)	N(1)–Yb(1)–N(4)	168.1(1)
N(3)–Yb(1)–N(6)	107.8(1)	N(3)–Yb(1)–O(2)	100.5(1)
N(6)–Yb(1)–O(1)	93.1(1)		

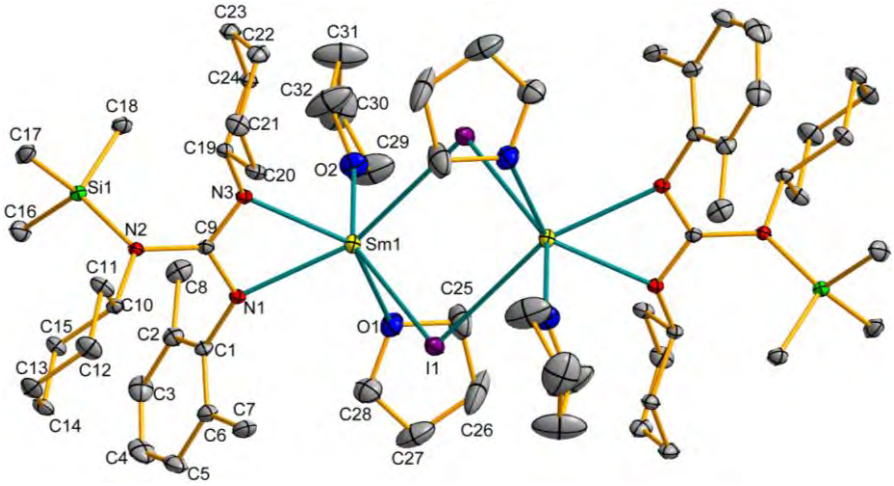

Figure 3–9. Molecular structure of [{Sm(L^3)(μ–I)$(THF)_2$}$_2$] (**21**).

Table 3–11. Selected bond distances (Å) and angles (deg.) for compound **21**

[{Sm(L^3)(μ–I)$(THF)_2$}$_2$] (**21**)			
Sm(1)–N(1)	2.544(4)	Sm(1)–N(3)	2.510(4)
Sm(1)–I(1)	3.3343(6)	Sm(1)–I(1)#	3.3045(6)
Sm(1)–O(1)	2.582(5)	Sm(1)–O(2)	2.576(5)
C(9)–N(1)	1.326(7)	C(9)–N(2)	1.433(7)
C(9)–N(3)	1.326(6)		
N(1)–Sm(1)–N(3)	52.5(1)	N(1)–C(9)–N(3)	115.0(5)
N(1)–Sm(1)–I(1)#	154.9(1)	O(1)–Sm(1)–I(1)	83.1(2)
O(1)–Sm(1)–O(2)	80.2(2)	I(1)–Sm(1)–N(3)	118.4(1)
N(3)–Sm(1)–O(2)	91.6(2)	I(1)–Sm(1)–I(1)#	82.12(2)
Sm(1)–I(1)–Sm(1)#	97.88(2)		

Symmetry code: # –x+1, –y+2, –z+1

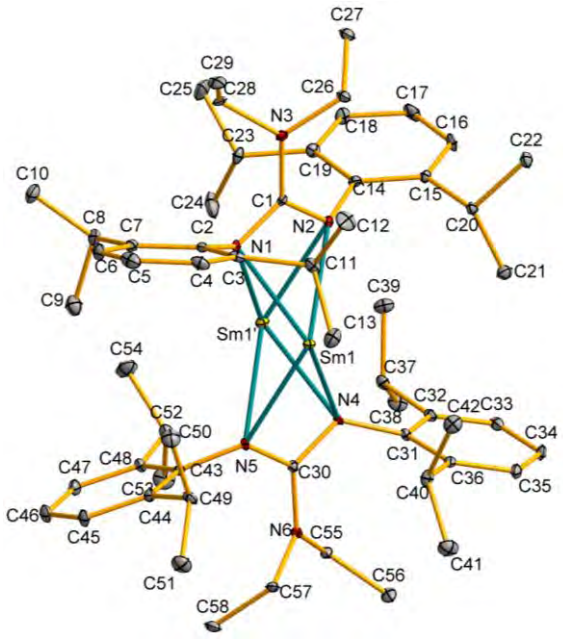

Figure 3–10. Molecular structure of $[Sm(L^5)_2]$ (**22**). Atom Sm1 exhibits positional disorder with Sm1' at a minor site, the occupancy ratio being 0.6:0.4.

Table 3–12. Selected bond distances (Å) and angles (deg.) for compound **22**

$[Sm(L^5)_2]$ (**22**)			
Sm(1)–N(1)	2.530(5)	Sm(1)–N(2)	2.509(5)
Sm(1)–N(4)	2.505(5)	Sm(1)–N(5)	2.475(5)
Sm(1')–N(1)	2.526(5)	Sm(1')–N(2)	2.496(5)
Sm(1')–N(4)	2.551(5)	Sm(1')–N(5)	2.497(5)
Sm(1)–C(42)	3.452(8)	Sm(1')–C(24)	3.35(1)
C(1)–N(1)	1.340(8)	C(1)–N(2)	1.338(8)
C(1)–N(3)	1.381(7)	C(30)–N(4)	1.342(8)
C(30)–N(5)	1.333(8)	C(30)–N(6)	1.385(8)
N(1)–Sm(1)–N(2)	53.4(2)	N(4)–Sm(1)–N(5)	53.9(2)
N(1)–Sm(1)–N(5)	113.9(2)	N(2)–Sm(1)–N(4)	112.9(2)
N(1)–Sm(1')–N(2)	53.6(2)	N(4)–Sm(1')–N(5)	53.1(2)
N(1)–Sm(1')–N(5)	113.2(2)	N(2)–Sm(1')–N(4)	111.8(2)
N(1)–C(1)–N(2)	115.5(5)	N(4)–C(30)–N(5)	115.0(5)

3.2.3 Reactivity Studies

Lanthanide(II) complexes are strong reducing agents. The reduction potentials of Eu^{3+}/Eu^{2+}, Yb^{3+}/Yb^{2+} and Sm^{3+}/Sm^{2+} were reported to be –0.35, –1.15 and –1.55, respectively.[1] They are good starting materials for the preparation of heteroleptic lanthanide(III) complexes.

Reaction of [{Eu(L^1)(μ–L^1)}$_2$] (**15**) with iodine

Treatment of Eu(II) guanidinate **15** with one molar equivalent of I_2 gave purple crystalline Eu(III) guanidinate–iodide complex [{Eu(L^1)$_2$(μ–I)}$_2$] (**23**) in 72% yield (Scheme 3–20).

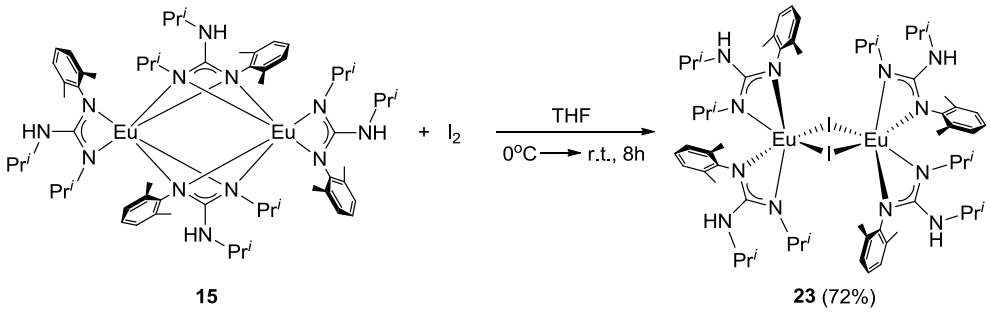

15 **23** (72%)

Scheme 3—20

Reaction of [{Yb(L^2)$_2$(THF)$_2$] (**18**) with PhEEPh (E = S, Se)

Addition of diphenyl dichalcogenides PhEEPh (E = S, Se) to two molar equivalents of **18** led to reductive cleavage of the E–E bond, yielding the corresponding Yb(III) chalcogenate complexes [{Yb(L^2)$_2$(μ–EPh)}$_2$] [E = S (**24**), Se(**25**)] (Scheme 3–21). Both complexes **24** and **25** were isolated as a yellow crystalline solid from diethyl ether.

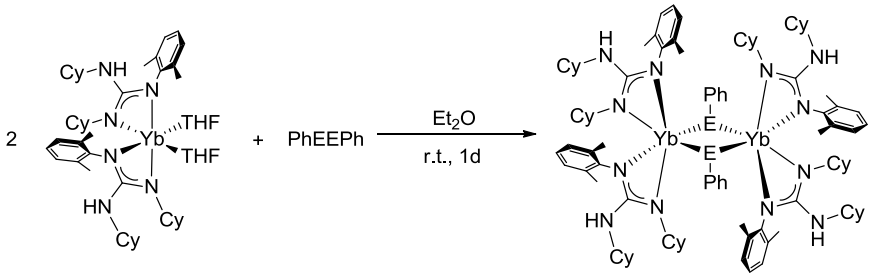

18

Scheme 3—21

Reaction of **18** with CuCl

Oxidation of complex **18** by CuCl led to the Yb(III) guanidinate–chloride complex [{Yb(L^2)$_2$(μ–Cl)}$_2$] (**26**), with concomitant reduction of Cu(I) to Cu(0). Complex **26** was obtained as a yellow crystalline solid (Scheme 3–22).

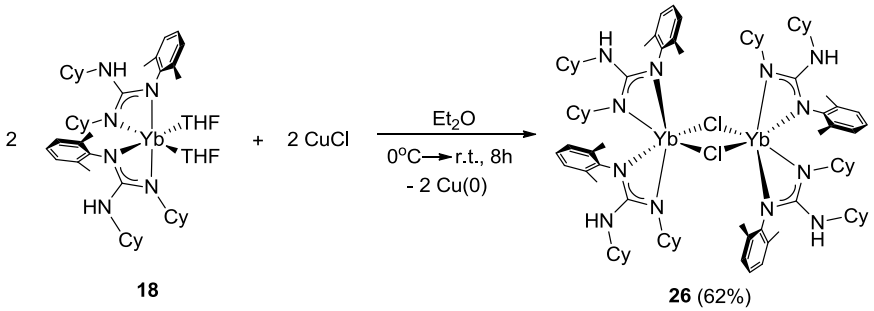

18

Scheme 3—22

Reaction of **18** with azobenzene

Treatment of complex **18** with one molar equivalent of PhNNPh led to the isolation of [{Yb(L^2)$_2$}$_2$(μ–η^2:η^2–PhNNPh)] (**27**) in 37% yield (Scheme 3–23). In a separate experiment, a 2:1 reaction of **18** with PhNNPh under similar reaction conditions (solvent and temperature) also yielded **27** as orange crystalline solid in 30% yield.

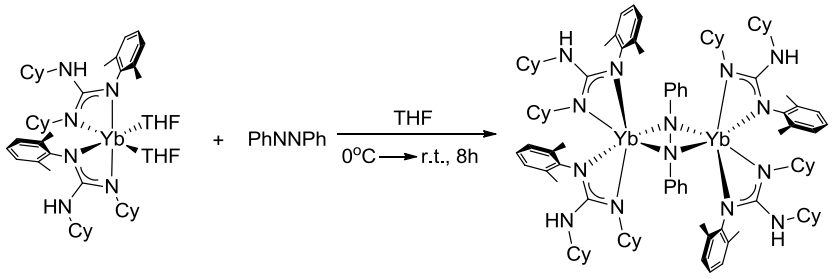

18 **27** (37%)

Scheme 3—23

Reaction of [Yb(L^3)$_2$(THF)$_2$·0.25C_6H_{14}] (**20**) with azobenzene

Treatment of complex **20** with one molar equivalent of PhNNPh in toluene yielded the blue, crystalline mononuclear Yb(III) complex [Yb(L^3)$_2$(η^2–PhNNPh)·PhMe] (**28**), which was isolated as a toluene solvated compound in 64% yield (Scheme 3–24).

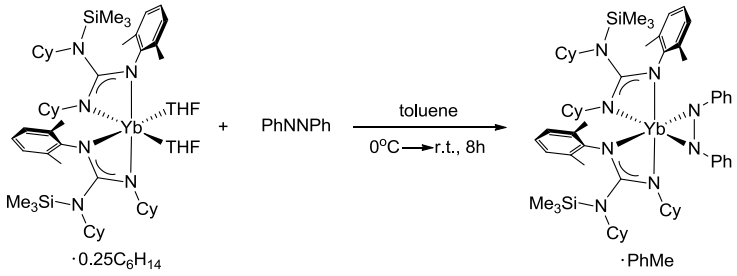

20 **28** (64%)

Scheme 3—24

Reaction of [Sm(L^5)$_2$] (**22**) with CS_2

Reaction of **22** with CS_2 in toluene afforded the coupling product [(L^5)$_2$Sm(μ–η^3:η^2–S_2CSCS)Sm(L^5)$_2$] (**29**) as green crystals in 66% yield (Scheme 3–25). It is interesting to note that two molecules of CS_2 was reduced by Sm(II) metal together with the formation of a C–S bond as a coupled $[S_2CSCS]^{2-}$ ligand. A

similar reaction of [Sm(Giso)$_2$] with CS_2 has been reported by Jones and co–workers. In the latter study, a binuclear Sm(III) complex [(Giso)$_2$Sm(μ–η^3:η^2–S_2CSCS)Sm(Giso)$_2$] was isolated and characterized.[11]

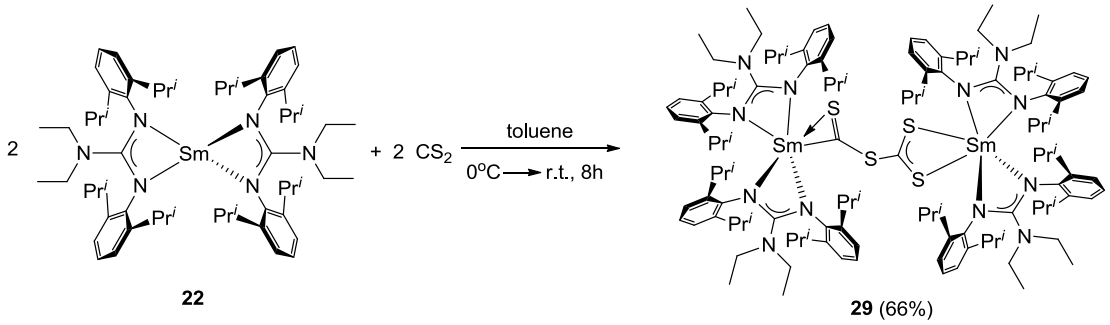

Scheme 3—25

Physical Characterization of Complexes **23**–**29**

Table 3–13 lists the appearance and melting points of complexes **23**–**29**. The molecular formula of these complexes was confirmed by elemental analysis and X–ray diffraction analysis. IR and UV–Vis spectra of complexes **27** and **28** were also measured.

Table 3–13. Appearance and melting points of complexes **23**–**29**

Compound	Appearance	M.p. (°C)
[{Eu(L^1)$_2$(μ–I)}$_2$] (**23**)	Purple crystals	162–163 (dec.)
[{Yb(L^2)$_2$(μ–SPh)}$_2$] (**24**)	Yellow crystals	185–187 (dec.)
[{Yb(L^2)$_2$(μ–SePh)}$_2$] (**25**)	Yellow crystals	200–201 (dec.)
[{Yb(L^2)$_2$(μ–Cl)}$_2$] (**26**)	Yellow crystals	212 (dec.)
[{Yb(L^2)$_2$}$_2$(μ–η^2:η^2–PhNNPh)] (**27**)	Orange crystals	199–202 (dec.)
Yb(L^3)$_2$(η^2–PhNNPh)·PhMe] (**28**)	Blue crystals	185–187 (dec.)
[(L^5)$_2$Sm(μ–η^3:η^2–S_2CSCS)Sm(L^5)$_2$] (**29**)	Green crystals	181–182 (dec.)

IR spectra of complexes **27** and **28**

The IR spectra of complexes **27** and **28** are shown in Figures A4–1 and A4–2 (Appendix 4), respectively. The stretching frequency of the N–N bond of the $[PhNNPh]^{2-}$ ligand in complex **27** is measured to be 1070 (m) cm^{-1}, which is comparable to the ν_{N-N} stretching of hydrazine (1077 cm^{-1}).[22] A similar ν_{N-N} stretching was also reported for $[(C_5Me_5)(THF)Sm]_2[N_2Ph_2]_2$ [1080 (m) and 1020 (s) cm^{-1}].[23] The IR spectrum of complex **28** shows a strong absorption at 1534 cm^{-1}, which is not observed in the spectrum of complex **27**. This absorption peak belongs to the $\nu_{N=N}$ stretching of the $[PhNNPh]^{-}$ ligand. It is similar to the $\nu_{N=N}$ stretching of cis–azobenzene (1512 cm^{-1}).[24] Besides, it is also comparable to the absorption peaks at 1575 (m), 1470 (m) and 1445 (s) cm^{-1} reported for $[(C_5Me_5)_2Sm(N_2Ph_2)(THF)]$.[23] Based on the above comparison, the N–N bond of the $[PhNNPh]^{2-}$ ligand (complex **27)** and the $[PhNNPh]^{-}$ ligand (complex **28**) has 1 and 1.5 bond order, respectively.

UV–Vis spectra of complexes **27** and **28**

The UV–Vis spectra of complexes **27** and **28** are shown in Figures A5–5 and A5–6 (Appendix 5), respectively. Complexes **27** and **28** dissolved in THF to give a yellow and blue solution, respectively. The UV–Vis spectrum of complex **27** shows one absorption maximum at λ_{max} ($\varepsilon/M^{-1}cm^{-1}$): 443 (200), whereas that of complex **28**

shows two absorption maxima at λ_{max} ($\varepsilon/M^{-1}cm^{-1}$): 585 (br, 800) and 378 (2700), respectively.

Crystal Structures of Complexes **23**–**29**

Single crystals of **24**–**26** suitable for X–ray diffraction analysis were obtained from Et_2O. Those of **23**, **27** and **28** were obtained from hexane. Single crystals of **29** were obtained from toluene. Selected crystallographic data of these complexes are listed in Tables A3–8 to A3–10 (Appendix 3), respectively.

1. $[\{Eu(L^1)_2(\mu\text{–}I)\}_2]$ (**23**)

The molecular structure of complex **23** with atom labeling is shown in Figure 3–11. Selected bond lengths and angles are listed in Table 3–14.

Complex **23** crystallizes in the monoclinic space group $P2_1$. Each Eu(III) center in the binuclear complex is coordinated by two κ^2–bound L^1 ligands and two bridging iodide ligands.

The observed Eu–N bond distances of 2.34(1)–2.39(1) Å in **23**, are much shorter than the terminal Eu–N bond distances of 2.560(2) and 2.561(2) Å in the Eu(II) precursor **15**, but are comparable to the corresponding distances in the six–coordinate Eu(III) tris(amidinate) complex $[Eu\{Bu^tNC(CH_3)NBu^t\}_3]$ [2.423(8)–2.469(7) Å][25] and the seven–coordinate Eu(III) tris(amidinate) complex $[Eu\{PhC(NSiMe_3)_2\}_3(NCPh)]$ [2.423(4)–2.528(4) Å].[26]

The N–Eu–N bite angles of 56.0(4)–56.5(4)^{o} in **23** are similar to the corresponding angles in [Eu{Bu^{t}NC(CH$_3$)NBu^{t}}$_3$] [54.1(3) and 54.7(3)^{o}][25] and [Eu{PhC(NSiMe$_3$)$_2$}$_3$(NCPh)] [55.0(1)–55.3(1)^{o}].[26]

2. [{Yb(L^2)$_2$(μ–SPh)}$_2$] (**24**)

The molecular structure of complex **24** with atom labeling is shown in Figure 3–12. Selected bond lengths and angles are listed in Table 3–15.

Complex **24** crystallizes in the triclinic space group $P\bar{1}$. The binuclear complex consists of a planar Yb$_2$S$_2$ core. Each Yb(III) ion is coordinated by two κ^2–bound L^2 ligands and two bridging phenyl sulphide ligands. The coordination geometry around Yb(1) can be described as distorted octahedral: the two axial positions are occupied by N(6) and S(1) [N(6)–Yb(1)–S(1) = 155.4(2)^{o}], whereas the equatorial plane is formed by N(1), N(3), N(4) and S(1)#. The sum of bond angles around Yb(1) on the equatorial plane is measured to be 368.9^{o}.

The Yb–N distances of 2.239(5)–2.339(9) Å in complex **24** are shorter than the corresponding distances of 2.412(5)–2.479(4) Å in the Yb(II) precursor **18**, but are comparable to the corresponding distances in other Yb(III) sulphide or thiolate complexes such as [{Yb[(Me$_3$Si)$_2$NC(NCy)$_2$]$_2$}$_2$(μ–η^2:η^2–S$_2$)] [2.299(6) and 2.306(6) Å],[27] [{Yb[(Me$_3$Si)$_2$NC(NCy)$_2$]$_2$(μ–SBu^{n})}$_2$] [2.309(8) and 2.320(9) Å][27] and [{Yb[(Me$_3$Si)$_2$NC(NCy)$_2$]$_2$(μ–SPh)}$_2$] [2.320(7) and 2.354(8) Å].[27]

The Yb(1)–S(1)# and Yb(1)–S(1) distances of 2.7539(7) and 2.7698(9) Å are slightly longer than the corresponding distances in $[\{Yb[(Me_3Si)_2NC(NCy)_2]_2\}_2(\mu–\eta^2:\eta^2–S_2)]$ [2.645(3)–2.671(3) Å].[27] However, they are slightly shorter than those reported for $[\{Yb[(Me_3Si)_2NC(NCy)_2]_2(\mu–SBu^n)\}_2]$ [2.784(4) and 2.808(4) Å][27] and $[\{Yb[(Me_3Si)_2NC(NCy)_2]_2(\mu–SPh)\}_2]$ [2.804(4) and 2.826(4) Å].[27]

The S(1)–Yb(1)–S(1)# and S(1)–Yb(1)#–S(1)# angles of 65.65(2)^o are comparable to the corresponding angles in $[\{Yb[(Me_3Si)_2NC(NCy)_2]_2(\mu–SBu^n)\}_2]$ [64.5(1) and 65.1(1)^o][27] and $[\{Yb[(Me_3Si)_2NC(NCy)_2]_2(\mu–SPh)\}_2]$ [63.1(1) and 63.6(1)^o].[27]

3. $[\{Yb(L^2)_2(\mu–SePh)\}_2]$ (**25**)

The molecular structure of complex **25** with atom labeling is shown in Figure 3–13. Selected bond lengths and angles are listed in Table 3–16.

Complex **25** crystallizes in the orthorhombic space group *Pnma*. Similar to complex **24**, the binuclear complex consists of a planar Yb_2Se_2 core. Each Yb(III) center in the dimeric unit is coordinated by two κ^2–bound L^2 ligands and two bridging phenyl selenide ligands. The coordination geometry around Yb(1) can be described as distorted octahedral: the two axial positions are occupied by N(3) and Se(1) [N(3)–Yb(1)–Se(1) = 148.2(5)^o], whereas the equatorial plane is formed by N(1),

N(1)#1, N(3)#1 and Se(1)#2. The sum of bond angles around Yb(1) on the equatorial plane is measured to be 373.9°.

The average Yb–N distance of 2.31 Å in **25** is slightly longer than the correspond distance of 2.30 Å in **24**, this may be ascribed to the coordination of the sterically more bulky ligand ($SePh^-$) to the Yb(III) center in **25** as compared to the SPh^- ligand in **24**. The Yb–N distances of 2.30(2)–2.31(2) Å in **25** are similar to the corresponding distances of 2.265(7)–2.366(7) Å in $[Yb\{PhC(NSiMe_3)_2\}_2(SePh)(THF)]$[6a] and 2.277(4)–2.406(4) Å in $[Yb\{PhC(NSiMe_3)(NC_6H_3Pr^i_2\text{–}2,6)\}_2(SePh)(THF)]$.[8]

The Yb–Se distances in complex **25** [2.910(2) Å] are reasonably longer than the Yb–S distances in complex **24** [2.7539(7) and 2.7698(9) Å]. They are also longer than the terminal Yb–Se distance in $[Yb\{PhC(NSiMe_3)_2\}_2(SePh)(THF)]$ [2.805(1) Å][6a] and $[Yb\{PhC(NSiMe_3)(NC_6H_3Pr^i_2\text{–}2,6)\}_2(SePh)(THF)]$ [2.7604(7) Å]. Apparently, sharing of the phenyl selenide anion by two Yb(III) centers in **25** lengthens the Yb–Se bonds.

The Se(1)–Yb(1)–Se(1)#2 bite angle of 65.1(1)° in **25** is similar to the S–Yb–S bite angles of 65.65(2)° in **24**.

4. $[\{Yb(L^2)_2(\mu\text{–}Cl)\}_2]$ (**26**)

The molecular structure of complex **26** with atom labeling is shown in Figure

3–14. Selected bond lengths and angles are listed in Table 3–17.

Complex **26** crystallizes in the triclinic space group $P\bar{1}$. The binuclear complex consists of a planar Yb_2Cl_2 core. Each Yb(III) center is coordinated by two κ^2–bound L^2 ligands and two bridging chloride ligands.

The Yb–N distances of 2.249(8)–2.299(6) Å in **26** are comparable to the corresponding distances of 2.295(3)–2.332(3) Å in the Yb(III) chloride complex $[Yb\{(SiMe_3)_2NC(NPr^i)_2\}(\mu\text{–}Cl)_2Li(THF)]$[28] and 2.266(2)–2.271(1) Å in $[\{Yb\{(Me_3Si)_2NC(NCy)_2\}Cl_2\}_2(LiCl)_2(THF)_4]$.[29]

The Yb–Cl distances of 2.668(2)–2.680(2) Å in **26** are comparable to the corresponding distances of 2.608(1) and 2.631(1) Å in $[Yb\{(SiMe_3)_2NC(NPr^i)_2\}(\mu\text{–}Cl)_2Li(THF)]$[28] and 2.5944(7)–2.6727(7) Å in $[\{Yb\{(Me_3Si)_2NC(NCy)_2\}Cl_2\}_2(LiCl)_2(THF)_4]$.[29]

The Cl(1)–Yb(2)–Cl(2) and Cl(1)–Yb(1)–Cl(2) bite angles of 80.18(6) and 80.27(6)^o are similar to the corresponding angle of 84.42(4)^o in $[Yb\{(SiMe_3)_2NC(NPr^i)_2\}(\mu\text{–}Cl)_2Li(THF)]$,[28] and 78.16(2) and 84.93(2)^o in $[\{Yb\{(Me_3Si)_2NC(NCy)_2\}Cl_2\}_2(LiCl)_2(THF)_4]$.[29]

5. $[\{Yb(L^2)_2\}_2(\mu\text{–}\eta^2\text{:}\eta^2\text{–}PhNNPh)]$ (**27**)

The molecular structure of complex **27** with atom labeling is shown in Figure 3–15. Selected bond lengths and angles are listed in Table 3–18.

Complex **27** crystallizes in the triclinic space group $P\bar{1}$. Each Yb(III) center in the dinuclear complex is coordinated by two κ^2–bound L^2 ligands and one $[\mu–\eta^2:\eta^2–Ph_2N_2]^{2–}$ ligand. A two–fold rotational axis is located at the center of N(13)–N(14). The two phenyl rings on the $[Ph_2N_2]^{2–}$ ligand are oriented cis to each other. A similar di-ytterbium(II) complex of the formula $[Me_2Si(C_5Me_4)(NPh)Yb(THF)(\mu–\eta^2:\eta^3–Ph_2N_2)Yb(NPh)(C_5Me_4)SiMe_2]$ has been reported and shown to be a one–electron reductant.[30]

The $Yb–N_{(guanidinate)}$ [$N_{(guanidinate)}$ are nitrogen atoms N(1), N(3), N(4), N(6), N(7), N(9), N(10) and N(12) on the L^2 ligands] distances of 2.315(4)–2.3504 Å in **27** are similar to the corresponding distances observed in Yb(III) complexes **24** [2.239(5)–2.339(9) Å], **25** [2.30(2)–2.31(2) Å] and **26** [2.249(8)–2.299(6) Å].

The $Yb–N_{(hydrazenide)}$ [$N_{(hydrazenide)}$ are nitrogen atoms N(13) and N(14) on the $[Ph_2N_2]^{2–}$ ligand] distances fall within the range of 2.259(4)–2.515(4) Å, which are comparable to the corresponding distances of 2.188(5)–2.572(5) Å in $[\{Yb(C_5H_5)(THF)\}_2(Ph_2N_2)_2]$[23] and 2.271(5)–2.367(5) Å in $[Me_2Si(C_5Me_4)(NPh)Yb(THF)(\mu–\eta^2:\eta^3–Ph_2N_2)Yb(NPh)(C_5Me_4)SiMe_2]$.[30] The N(13)–N(14) bond distance of 1.503(5) Å is close to the bond length of a N–N single bond (1.47 Å).[31] It is also comparable to the corresponding distance of 1.470(6) Å in $[\{Yb(C_5H_5)(THF)\}_2(Ph_2N_2)_2]$,[23] 1.44(1) Å in $[\{Sm(C_5Me_5)(THF)\}_2(Ph_2N_2)_2]$[23] and

1.468(7) Å in [$Me_2Si(C_5Me_4)(NPh)Yb(THF)(\mu–\eta^2:\eta^3–Ph_2N_2)Yb(NPh)(C_5Me_4)SiMe_2$].[30] Based on the above comparison, the N(13)–N(14) bond has a bond order of 1, which is consistent to the result of the IR spectrum.

The N(13)–Yb(1)–N(14) [36.6(1)°] and N(13)–Yb(2)–N(14) [36.2(1)°] angles are close to the corresponding angles reported for [$\{Yb(C_5H_5)(THF)\}_2(Ph_2N_2)_2$] [34.8(3) and 35.9(3)°][23] and [$\{Sm(C_5Me_5)(THF)\}_2(Ph_2N_2)_2$] [33.8(3)°].[23]

6. [$Yb(L^3)_2(\eta^2–PhNNPh)\cdot PhMe$] (**28**)

The molecular structure of complex **28** with atom labeling is shown in Figure 3–16. Selected bond lengths and angles are listed in Table 3–19.

Complex **28** crystallizes in the monoclinic space group $P2_1/c$. In the solid state, the toluene solvated complex **28** consists of a mononuclear, six–coordinate Yb(III) center, which is coordinated by two κ^2–bound L^3 ligands and one $[\eta^2–Ph_2N_2]^-$ ligand. Each molecule consists of a two–fold rotational axis bisecting the N(7)–Yb(1)–N(8) angle. The two phenyl rings on the $[Ph_2N_2]^-$ ligand are cis to each other. The $Yb–N_{(guanidinate)}$ [$N_{(guanidinate)}$ are nitrogen atoms N(1), N(3), N(4) and N(6) on the L^3 ligands] distances of 2.280(6)–2.336(6) Å in **28** are comparable to the corresponding distances observed in Yb(III) complexes **24**–**27**. The Yb(1)–N(7) and Yb(1)–N(8) distances of 2.268(6) and 2.275(7) Å, respectively, fall within the range of

2.259(4)–2.515(4) Å in **27** and 2.188(5)–2.572(5) Å in $[\{Yb(C_5H_5)(THF)\}_2(Ph_2N_2)_2]$.[23]

The observed N(7)–N(8) distance of 1.382(9) Å in **28** is much shorter than the corresponding distance of 1.503(5) Å in **27**. It falls within the bond distance range of 1.47 Å for an N–N single bond and 1.25 Å for an N=N double bond.[31] Similar N–N bond distances of 1.32(1) and 1.39(2) Å have been reported for the Sm(II) complex $[\{Sm(C_5Me_5)(THF)\}_2(Ph_2N_2)_2]$.[23] From the above comparison, it is concluded that the N(7)–N(8) bond has a bond order of 1.5.

The N(7)–Yb(1)–N(8) angle of 35.4(2)^o is similar to those of 36.2(1) and 36.6(1)^o in **27**, 34.8(3) and 35.9(3)^o in $[\{Yb(C_5H_5)(THF)\}_2(Ph_2N_2)_2]$,[23] and 33.8(3)^o in $[\{Sm(C_5Me_5)(THF)\}_2(Ph_2N_2)_2]$.[23]

7. $[(L^5)_2Sm(\mu\text{–}\eta^3\text{:}\eta^2\text{–}S_2CSCS)Sm(L^5)_2]$ (**29**)

The molecular structure of complex **29** with atom labeling is shown in Figure 3–17. Selected bond lengths and angles are listed in Table 3–20.

Complex **29** crystallizes in the monoclinic space group $P2_1/n$. Each of the Sm(III) centers in the binuclear complex adopts different coordination geometry. Sm(1) is coordinated by two κ^2–bound L^5 ligands and S(1) and S(2) of the $[SCSCS_2]^{2-}$ ligand. The latter bind in an η^3–SCS coordination mode. Sm(2) is coordinated by two κ^2–bound L^5 ligands and C(60) and S(4) at the other end of the

$[SCSCS_2]^{2-}$ ligand. The latter bind in an η^2–SC coordination mode. A similar coordination mode has been reported for the Sm(III) complex $[(Giso)_2Sm(\mu–\eta^3:\eta^2–S_2CSCS)Sm(Giso)_2]$.[11] Reductive coupling of CS_2 through head–to–head C–C bond formation (yielding $[S_2CCS_2]^{2-}$) is commonly observed in reactions with transition metal complexes,[32] though a number of head–to–tail C–S coupling products have also been reported.[33] It has been proposed that the sterically hindered ligand environment generated by the Giso ligand only allows a head–to–tail C–S coupling of the linear CS_2 substrate in $[(Giso)_2Sm(\mu–\eta^3:\eta^2–S_2CSCS)Sm(Giso)_2]$.[11] Conceivably, a similar steric bulkiness of the L^5 ligands in **29** (as compared to that of Giso) does not favor a head–to–head C–C coupling of two CS_2 molecules.

The $Sm–N_{(guanidinate)}$ [$N_{(guanidinate)}$ are nitrogen atoms N(1), N(2), N(4), N(6), N(7), N(9), N(10) and N(12) on the L^5 ligands] distances of 2.383(5)–2.461(5) Å in **29** are similar to the corresponding distances of 2.386(5)–2.486(5) Å in $[(Giso)_2Sm(\mu–\eta^3:\eta^2–S_2CSCS)Sm(Giso)_2]$,[11] 2.378(3)–2.434(3) Å in $[Sm\{(SiMe_3)_2NC(NCy)_2\}_2(\mu–Cl)_2Li(THF)_2]$,[34] 2.425(6)–2.460(6) Å in $[Sm\{Ph_2NC(NCy)_2\}_3]$[35] and 2.395(4)–2.426(4) Å in $[Sm\{CyNC[N(SiMe_3)_2]NCy\}_2\{CH(SiMe_3)_2\}]$.[9]

The Sm–S distances of 2.790(2)–2.870(2) Å in **29** are comparable to the

corresponding distances of 2.813(8)–2.998(5) Å in $[(Giso)_2Sm(\mu–\eta^3:\eta^2–S_2CSCS)Sm(Giso)_2]$.[11] The S(1)–Sm(1)–S(2) angle of 63.04(5)^o is slightly larger than that of 59.9(2)^o in $[(Giso)_2Sm(\mu–\eta^3:\eta^2–S_2CSCS)Sm(Giso)_2]$,[11] whereas the S(4)–Sm(2)–C(60) angle of 35.8(1)^o is comparable to the corresponding angle of 34.7(3)^o in $[(Giso)_2Sm(\mu–\eta^3:\eta^2–S_2CSCS)Sm(Giso)_2]$.[11]

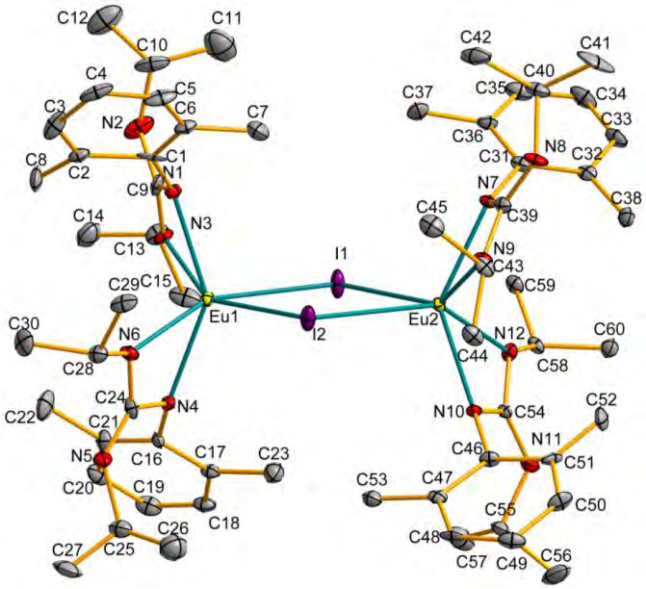

Figure 3–11. Molecular structure of [{Eu(L^1)$_2$(μ–I)}$_2$] (**23**).

Table 3–14. Selected bond distances (Å) and angles (deg.) for compound **23**

[{Eu(L^1)$_2$(μ–I)}$_2$] (**23**)			
Eu(1)–N(1)	2.37(1)	Eu(1)–N(3)	2.38(1)
Eu(1)–N(4)	2.37(1)	Eu(1)–N(6)	2.39(1)
Eu(2)–N(7)	2.39(1)	Eu(2)–N(9)	2.35(1)
Eu(2)–N(10)	2.34(1)	Eu(2)–N(12)	2.389(9)
Eu(1)–I(1)	3.169(1)	Eu(1)–I(2)	3.158(1)
Eu(2)–I(1)	3.159(1)	Eu(2)–I(2)	3.190(1)
N(1)–Eu(1)–N(3)	56.3(4)	N(1)–C(9)–N(3)	116(1)
N(4)–Eu(1)–N(6)	56.5(4)	N(4)–C(24)–N(6)	113(1)
N(7)–Eu(2)–N(9)	56.5(4)	N(7)–C(39)–N(9)	113(1)
N(10)–Eu(2)–N(12)	56.0(4)	N(10)–C(54)–N(12)	112(1)
Eu(1)–I(1)–Eu(2)	101.63(3)	Eu(1)–I(2)–Eu(2)	101.21(3)
I(1)–Eu(1)–I(2)	78.74(3)	I(1)–Eu(2)–I(2)	78.41(3)

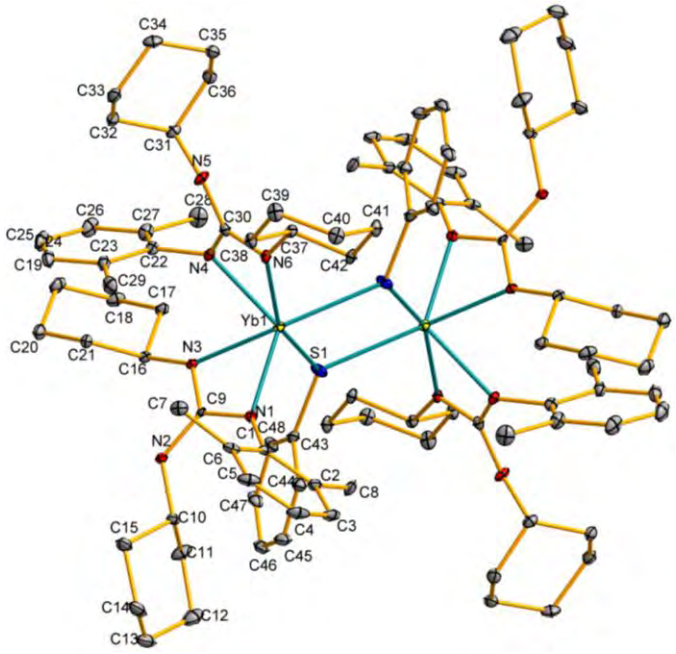

Figure 3–12. Molecular structure of [{Yb(L^2)$_2$(μ–SPh)}$_2$] (**24**).

Table 3–15. Selected bond distances (Å) and angles (deg.) for compound **24**

[{Yb(L^2)$_2$(μ–SPh)}$_2$] (**24**)			
Yb(1)–N(1)	2.286(7)	Yb(1)–N(4)	2.321(6)
Yb(1)–N(6)	2.339(9)	Yb(1)–N(9)	2.239(5)
Yb(1)–S(1)	2.7698(9)	Yb(1)–S(1)#	2.7539(7)
S(1)–C(43)	1.75(1)	C(9)–N(1)	1.30(2)
C(9)–N(2)	1.39 (2)	C(9)–N(3)	1.34(2)
C(30)–N(4)	1.34(1)	C(30)–N(5)	1.38 (1)
C(30)–N(6)	1.33(2)		
N(1)–Yb(1)–N(3)	59.1(3)	N(4)–Yb(1)–N(6)	57.9(3)
Yb(1)–S(1)–Yb(1)#	114.36(3)	S(1)–Yb(1)–S(1)#	65.65(2)
Yb(1)–S(1)#–Yb(1)#	114.36(3)	S(1)–Yb(1)#–S(1)#	65.65(2)
N(1)–C(9)–N(3)	115(1)	N(4)–C(30)–N(6)	116.0(9)
N(6)–Yb(1)–S(1)	155.4(2)	N(4)–Yb(1)–N(3)	68.8(2)
N(1)–Yb(1)–S(1)#	133.0(2)	N(4)–Yb(1)–S(1)#	108.0(1)

Symmetry code: # –x+1, –y+2, –z+1

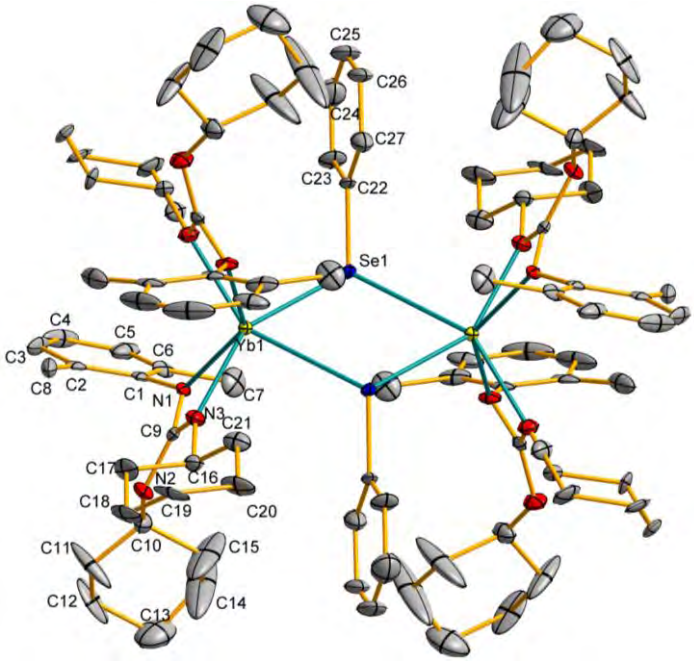

Figure 3–13. Molecular structure of [{Yb(L^2)$_2$(μ–SePh)}$_2$] (**25**).

Table 3–16. Selected bond distances (Å) and angles (deg.) for compound **25**

[{Yb(L^2)$_2$(μ–SePh)}$_2$] (**25**)			
Yb(1)–N(1)	2.31(2)	Yb(1)–N(1)#1	2.31(2)
Yb(1)–N(3)	2.30(2)	Yb(1)–N(3)#1	2.30(2)
Yb(1)–Se(1)	2.910(2)	Yb(1)–Se(1)#2	2.910(2)
Se(1)–C(22)	1.89(3)	C(9)–N(1)	1.38(3)
C(9)–N(2)	1.38(3)	C(9)–N(3)	1.32(3)
N(1)–Yb(1)–N(3)	59.0(8)	N(1)#1–Yb(1)–N(3)#1	59.0(8)
Yb(1)–Se(1)–Yb(1)#2	114.9(1)	Se(1)–Yb(1)–Se(1)#2	65.1(1)
N(1)–C(9)–N(3)	115(2)	N(3)–Yb(1)–Se(1)	148.2(5)
N(1)–Yb(1)–Se(1)#2	108.3(5)	N(1)#1–Yb(1)–Se(1)#2	108.8(6)
N(1)–Yb(1)–N(3)#1	97.8(7)		

Symmetry code: #1 x, –y, –z+1 #2 –x, –y, –z+1

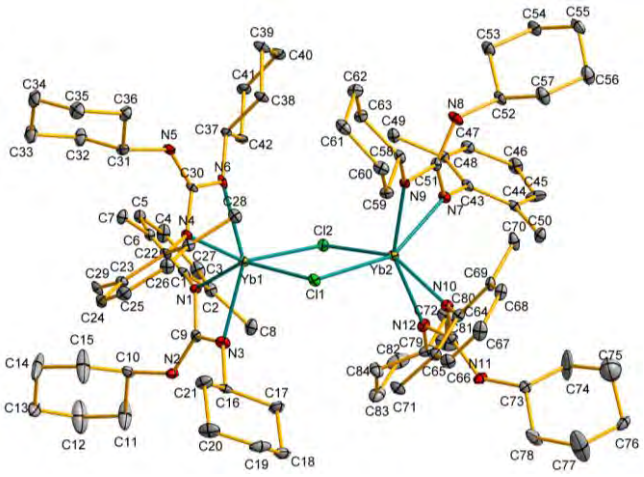

Figure 3–14. Molecular structure of [{Yb(L^2)$_2$(μ–Cl)}$_2$] (**26**).

Table 3–17. Selected bond distances (Å) and angles (deg.) for compound **26**

[{Yb(L^2)$_2$(μ–Cl)}$_2$] (**26**)			
Yb(1)–N(1)	2.279(6)	Yb(1)–N(3)	2.290(7)
Yb(1)–N(4)	2.299(6)	Yb(1)–N(6)	2.253(8)
Yb(2)–N(7)	2.292(7)	Yb(2)–N(9)	2.249(8)
Yb(2)–N(10)	2.283(7)	Yb(2)–N(12)	2.282(7)
Yb(1)–Cl(1)	2.675(2)	Yb(1)–Cl(2)	2.668(2)
Yb(2)–Cl(1)	2.669(2)	Yb(2)–Cl(2)	2.680(2)
N(1)–C(9)	1.34(1)	N(2)–C(9)	1.35(1)
N(3)–C(9)	1.34(1)	N(4)–C(30)	1.35(1)
N(5)–C(30)	1.35(1)	N(6)–C(30)	1.35(1)
N(7)–C(51)	1.36(1)	N(8)–C(51)	1.36(1)
N(9)–C(51)	1.36(1)	N(10)–C(72)	1.34(1)
N(11)–C(72)	1.34(1)	N(12)–C(72)	1.34(1)
N(1)–Yb(1)–N(3)	58.4(2)	N(1)–C(9)–N(3)	112.2(7)
N(4)–Yb(1)–N(6)	58.7(2)	N(4)–C(30)–N(6)	111.9(7)
N(7)–Yb(2)–N(9)	59.2(2)	N(7)–C(51)–N(9)	111.2(7)
N(10)–Yb(2)–N(12)	58.1(2)	N(10)–C(72)–N(12)	111.3(7)
Yb(1)–Cl(1)–Yb(2)	99.59(6)	Yb(1)–Cl(2)–Yb(2)	99.49(6)
Cl(1)–Yb(1)–Cl(2)	80.27(6)	Cl(1)–Yb(2)–Cl(2)	80.18(6)
N(3)–Yb(1)–N(6)	150.9(3)	N(9)–Yb(2)–N(12)	151.0(3)

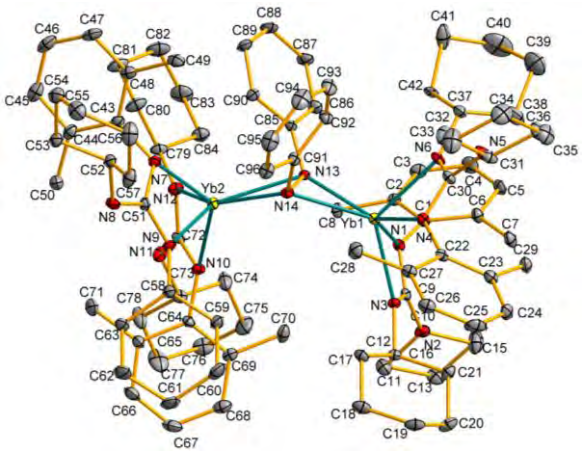

Figure 3–15. Molecular structure of [{Yb(L^2)$_2$}$_2$(μ–η^2:η^2–PhNNPh)] (**27**).

Table 3–18. Selected bond distances (Å) and angles (deg.) for compound **27**

[{Yb(L^2)$_2$}$_2$(μ–η^2:η^2–PhNNPh)] (**27**)			
Yb(1)–N(1)	2.315(4)	Yb(1)–N(3)	2.330(4)
Yb(1)–N(4)	2.350(4)	Yb(1)–N(6)	2.330(4)
Yb(2)–N(7)	2.344(4)	Yb(2)–N(9)	2.328(4)
Yb(2)–N(10)	2.336(4)	Yb(2)–N(12)	2.335(4)
Yb(1)–N(13)	2.259(4)	Yb(1)–N(14)	2.481(4)
Yb(2)–N(13)	2.515(4)	Yb(2)–N(14)	2.268(4)
N(1)–C(9)	1.358(6)	N(3)–C(9)	1.323(6)
N(4)–C(30)	1.338(7)	N(6)–C(30)	1.336(7)
N(7)–C(51)	1.354(6)	N(9)–C(51)	1.331(6)
N(10)–C(72)	1.345(7)	N(12)–C(72)	1.341(7)
N(13)–N(14)	1.503(5)		
N(1)–Yb(1)–N(3)	57.7(1)	N(1)–C(9)–N(3)	113.5(4)
N(4)–Yb(1)–N(6)	57.9(2)	N(4)–C(30)–N(6)	115.7(5)
N(7)–Yb(2)–N(9)	57.9(2)	N(7)–C(51)–N(9)	114.7(4)
N(10)–Yb(2)–N(12)	58.0(2)	N(10)–C(72)–N(12)	114.8(5)
Yb(1)–N(13)–Yb(2)	126.4(2)	Yb(1)–N(14)–Yb(2)	127.7(2)
N(13)–Yb(1)–N(14)	36.6(1)	N(13)–Yb(2)–N(14)	36.2(1)

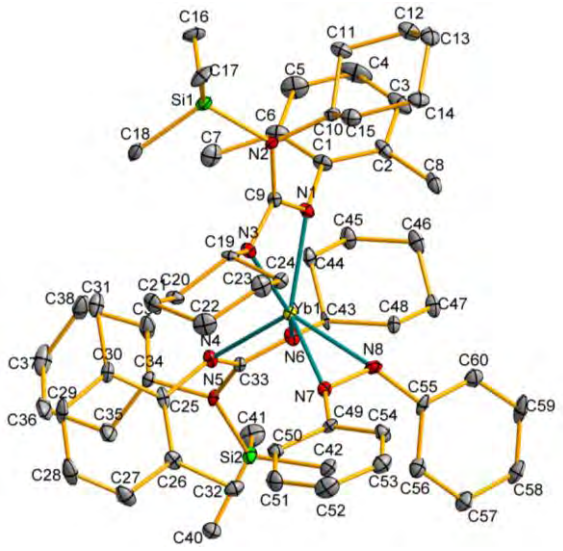

Figure 3–16. Molecular structure of $[Yb(L^3)_2(\eta^2\text{–PhNNPh})\cdot PhMe]$ (**28**). The toluene solvent molecule is omitted for clarity.

Table 3–19. Selected bond distances (Å) and angles (deg.) for compound **28**

$[Yb(L^3)_2(\eta^2\text{–PhNNPh})\cdot PhMe]$ (**28**)			
Yb(1)–N(1)	2.301(7)	Yb(1)–N(3)	2.322(7)
Yb(1)–N(4)	2.280(6)	Yb(1)–N(6)	2.336(6)
Yb(1)–N(7)	2.268(6)	Yb(1)–N(8)	2.275(7)
N(1)–C(9)	1.378(9)	N(2)–C(9)	1.40(1)
N(3)–C(9)	1.35(1)	N(4)–C(33)	1.37(1)
N(5)–C(33)	1.43(1)	N(6)–C(33)	1.31(1)
N(7)–N(8)	1.382(9)		
N(1)–Yb(1)–N(3)	58.3(2)	N(1)–C(9)–N(3)	111.6(7)
N(4)–Yb(1)–N(6)	57.9(2)	N(4)–C(33)–N(6)	112.9(7)
N(7)–Yb(1)–N(8)	35.4(2)	N(3)–Yb(1)–N(6)	144.9(2)
N(4)–Yb(1)–N(7)	101.8(2)	N(1)–Yb(1)–N(8)	112.8(2)
N(1)–Yb(1)–N(4)	123.9(2)		

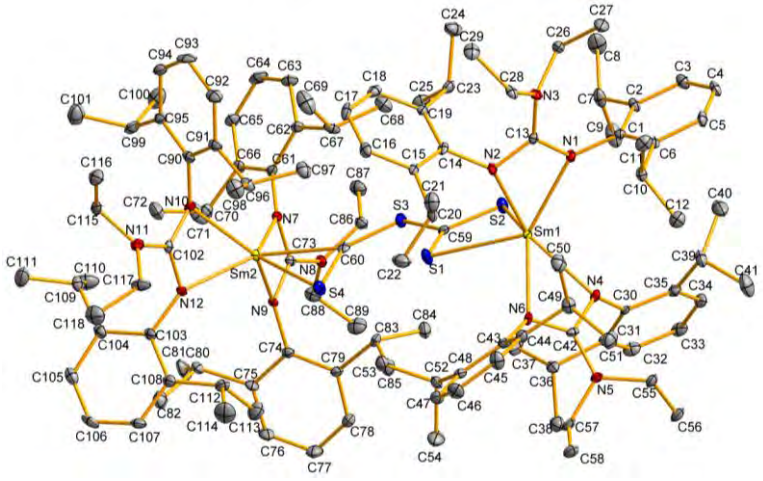

Figure 3–17. Molecular structure of $[(L^5)_2Sm(\mu–\eta^3:\eta^2–S_2CSCS)Sm(L^5)_2]$ (**29**).

Table 3–20. Selected bond distances (Å) and angles (deg.) for compound **29**

$[(L^5)_2Sm(\mu–\eta^3:\eta^2–S_2CSCS)Sm(L^5)_2]$ (**29**)			
Sm(1)–N(1)	2.433(5)	Sm(1)–N(2)	2.405(5)
Sm(1)–N(4)	2.424(5)	Sm(1)–N(6)	2.452(5)
Sm(2)–N(7)	2.383(5)	Sm(2)–N(9)	2.461(5)
Sm(2)–N(10)	2.448(5)	Sm(2)–N(12)	2.442(5)
Sm(1)–S(1)	2.870(2)	Sm(1)–S(2)	2.860(2)
Sm(2)–S(4)	2.790(2)	Sm(2)–C(60)	2.522(6)
C(59)–S(1)	1.655(6)	C(59)–S(2)	1.711(6)
C(60)–S(3)	1.676(6)	C(60)–S(4)	1.654(6)
N(1)–C(13)	1.343(7)	N(2)–C(13)	1.359(7)
N(4)–C(42)	1.368(7)	N(6)–C(42)	1.316(7)
N(7)–C(73)	1.363(7)	N(9)–C(73)	1.336(7)
N(10)–C(102)	1.316(7)	N(12)–C(102)	1.354(7)
N(1)–Sm(1)–N(2)	55.3(2)	N(1)–C(13)–N(2)	112.4(5)
N(4)–Sm(1)–N(6)	55.0(2)	N(4)–C(42)–N(6)	113.9(5)
N(7)–Sm(2)–N(9)	55.5(2)	N(7)–C(73)–N(9)	113.6(5)
N(10)–Sm(2)–N(12)	54.4(2)	N(10)–C(102)–N(12)	113.8(5)
S(1)–Sm(1)–S(2)	63.04(5)	S(4)–Sm(2)–C(60)	35.8(1)

3.2.4 Other Attempted Reactions in This Work

Attempted reactions of [{Eu(L^1)(μ–L^1)}$_2$] (**15**) with CuCl and Br_2, respectively

Treatment of complex **15** with CuCl and Br_2, respectively, led to an immediate color change of the solution from orange to red and purple, respectively. Unfortunately, only an intractable oil was obtained after work–up. The latter remained unidentified in this work.

Attempted reactions of [{Eu(L^2)(μ–L^2)}$_2$ · $2C_6H_{14}$] (**16**) and [Eu(L^3)$_2$(THF)$_2$ · $0.25C_6H_{14}$] (**19**) with PhNNPh

The reactions of **16** and **19**, respectively, with PhNNPh were examined in this work. These reactions only resulted in a brown intractable oil after work–up. The product remained unidentified in this work.

Attempted reactions of [{Yb(L^2)$_2$(THF)$_2$] (**18**) with Br_2, I_2 and PhTeTePh, respectively

Attempts to prepare mixed–ligand Yb(III) guanidinate–bromide, guanidinate–iodide and guanidinate–telluride complexes by treatment of complex **18** with Br_2, I_2 and PhTeTePh, respectively, have been unsuccessful. In all these reactions, only a yellow intractable oil was obtained after work–up. The latter remained unidentified in this work.

3.3 Summary

The coordination chemistry of a series of related bulky guanidinate ligands, namely $[(2,6\text{–}Me_2C_6H_3N)C(NHPr^i)(NPr^i)]^-$ (L^1), $[(2,6\text{–}Me_2C_6H_3N)C(NHCy)(NCy)]^-$ (L^2), $[(2,6\text{–}Me_2C_6H_3N)C\{N(SiMe_3)Cy\}(NCy)]^-$ (L^3) and $[(2,6\text{–}Pr^i{}_2C_6H_3N)C(NEt_2)(NC_6H_3Pr^i{}_2\text{–}2,6)]^-$ (L^5) with divalent Eu, Sm and Yb ions was examined in this work. The reaction of $EuI_2(THF)_2$ with $[KL^1 \cdot 0.5PhMe]_n$ (**1**) gave the neutral, binuclear Eu(II) bis(guanidiante) complex $[\{Eu(L^1)(\mu\text{–}L^1)\}_2]$ (**15**). Treatment of $LnI_2(THF)_2$ (Ln = Eu, Yb) with $[KL^2(THF)_{0.5}]_n$ (**12**) and KL^3 (**13**) led to the isolation of dimeric $[\{Ln(L^2)(\mu\text{–}L^2)\}_2 \cdot nC_6H_{14}]$ [Ln = Eu, n = 2 (**16**); Ln = Yb, n = 0 (**17**)], $[Yb(L^2)_2(THF)_2]$ (**18**) and monomeric $[Ln(L^3)_2(THF)_2 \cdot 0.25C_6H_{14}]$ [Ln = Eu (**19**), Yb (**20**)]. The heteroleptic Sm(II) complex $[\{Sm(L^3)(\mu\text{–}I)(THF)\}_2]$ (**21**) was prepared by treatment of $SmI_2(THF)_2$ with one molar equivalent of **13**. While the reaction of $SmI_2(THF)_2$ with $[KL^5(THF)_2]$ (**14**) gave the homoleptic Sm(II) complex $[Sm(L^5)_2]$ (**22**).

The reaction chemistry of complexes **15**, **18**, **20** and **22** has been studied in this work. Oxidation of **15** with iodine yielded the Eu(III) guanidinate–iodide complex $[\{Eu(L^1)_2(\mu\text{–}I)\}_2]$ (**23**). Reactions of **18** with PhEEPh (E = S, Se) gave the corresponding Yb(III) guanidinate–chalcogenato complexes $[\{Yb(L^2)_2(\mu\text{–}SPh)\}_2]$ (**24**) and $[\{Yb(L^2)_2(\mu\text{–}SePh)\}_2]$ (**25**). Complex **18** was readily oxidized by CuCl to yield

the corresponding Yb(III) guanidinate–chloride complex [{Yb(L^2)$_2$(μ–Cl)}$_2$] (**26**). The reactions of complexes **18** and **20** with PhNNPh resulted in the isolation of binuclear [{Yb(L^2)$_2$}$_2$(μ–η^2:η^2–PhNNPh)] (**27**) and mononuclear [Yb(L^3)$_2$(η^2–PhNNPh)·PhMe] (**28**), respectively. The N–N bond of the [PhNNPh]$^{2-}$ ligand (complex **27)** and the [PhNNPh]$^{-}$ ligand (complex **28**) has 1 and 1.5 bond order, respectively. Direct reaction of **22** with CS_2 led to a head–to–tail coupling of CS_2 and the formation of the unsymmetrical [(L^5)$_2$Sm(μ–η^3:η^2–S_2CSCS)Sm(L^5)$_2$] (**29**).

3.4 Experimental Section for Chapter 3

Reagents:

Potassium tert–butoxide (Aldrich), azobenzene (Aldrich), carbon disulphide (5 M in THF) (Aldrich), copper(I) chloride (Strem), samarium (Strem), europium (Strem) and ytterbium (Strem) metals were used as received. $LnI_2(THF)_2$ (Ln = Sm, Eu, Yb) were prepared according to literature procedures.[35] The potassium reagent $[KL^1 \cdot 0.5PhMe]_n$ (**1**) was prepared according to the procedure as described in Chapter 2. The lithium guanidinates $[LiL^n(TMEDA)]$ (n = 2, 3, 5) were prepared as described previously by former members of our research group.[12,13]

Synthesis of $[KL^2(THF)_{0.5}]_n$ (12). To a slurry of $KOBu^t$ (1.2 g, 10.7 mmol) in THF (20 ml) at room temperature was added a colorless solution of $[LiL^2(TMEDA)]$ (4.8 g, 10.7 mmol) in the same solvent (20 ml). The reaction mixture was allowed to stir for 1 d. All the volatiles were removed in *vacuo* and the residue was extracted with Et_2O (50 ml). Standing the milky suspension at room temperature for 1d gave **12** as colorless crystals. Yield: 3.93 g, 9.8 mmol, 92%. M.p.: 229–231 ^oC (dec.). ^1H NMR (400.13 MHz, THF–d_8): δ 0.94–1.03 (m, 4H, C_6H_{11}), 1.09–1.15 (m, 2H, C_6H_{11}), 1.23–1.32 (m, 4H, C_6H_{11}), 1.54–1.57 (m, 2H, C_6H_{11}), 1.63–1.66 (m, 4H, C_6H_{11}), 1.76–1.79 (m, 1H, THF), 1.94 (br, 4H, C_6H_{11}), 2.07 (s, 6H, CH_3), 3.43 (br, 2H, C_6H_{11}), 3.60–3.63 (m, 1H, THF), 6.45 (br, 1H, *p*–Ar*H*), 6.80 (d, *J* = 6.8 Hz, 2H, *m*–Ar*H*).

^{13}C NMR (100.62 MHz, THF–d_8): δ 19.7, 26.2, 26.5, 27.2, 35.8, 51.6, 68.0, 115.8, 127.8, 130.8, 156.8. Anal. Found: C, 68.77; H, 8.89; N, 10.15%. Calc. for $C_{46}H_{72}K_2N_6O$: C, 68.78; H, 9.03; N, 10.46%.

Synthesis of KL^3 (13). Complex **13** was prepared by a procedure similar to that of **12**, starting with 6.91 g (13.2 mmol) of [LiL^3(TMEDA)] and 1.56 g (13.9 mmol) of KOBu^t. Complex **13** was recrystallized as a white solid from toluene. Yield: 5.64 g, 12.9 mmol, 97%. M.p.: 215–216 ^{o}C (dec.). ^{1}H NMR (400.13 MHz, THF–d_8): δ 0.10 (s, 9H, Si(CH_3)$_3$), 0.97 (br, 6H, C$_6H_{11}$), 1.40–1.42 (m, 6H, C$_6H_{11}$), 1.56 (br, 8H, C$_6H_{11}$), 2.11 (s, 6H, ArCH_3), 3.06 (br, 2H, C$_6H_{11}$), 6.25 (br, 1H, *p*–Ar*H*), 6.68 (d, *J* = 4.8 Hz, 2H, *m*–Ar*H*). ^{13}C NMR (100.62 MHz, THF–d_8): δ 10.0, 19.7, 20.3, 26.3, 27.4, 35.2, 54.6, 115.1, 127.5, 127.7, 128.7, 129.4, 131.3, 154.4, 158.7. Anal. Found: C, 64.41; H, 9.78; N, 9.63%. Calc. for $C_{24}H_{40}KN_3Si$: C, 65.85; H, 9.21; N, 9.59%.[†]

Synthesis of [KL^4(THF)$_2$] (14). This compound was prepared by a procedure similar to that of **12**, starting with 5.57 g (10.0 mmol) of [LiL^4(TMEDA)] and 1.12 g (10.0 mmol) of KOBu^t. Complex **14** was isolated as colorless crystals. Yield: 5.50 g, 8.9 mmol, 89%. M.p.: 245–247 ^{o}C (dec.). ^{1}H NMR (400.13 MHz, THF–d_8): 0.92 (t, *J* = 6.8 Hz, 6H, CH$_2$CH_3), 1.09 (d, *J* = 7.2 Hz, 12H, CH(CH_3)$_2$), 1.18 (d, *J* = 6.8 Hz, 12H, CH(CH_3)$_2$), 1.76–1.80 (m, 2H, THF), 2.99 (q, *J* = 6.8Hz, 4H, CH_2CH$_3$),

[†] Satisfactory results of elemental analysis could not be obtained for this compound.

3.60–3.63 (m, 2H, THF), 3.66 (septet, J = 6.8 Hz, 4H, C*H*(CH_3)$_2$), 6.62 (t, J = 7.5 Hz, 2H, *p*–Ar*H*), 6.92 (d, J = 7.5 Hz, 4H, *m*–Ar*H*). ^{13}C NMR (100.62 MHz, THF–d_8): δ 13.6, 24.4, 26.4, 28.3, 43.9, 68.2, 118.1, 122.9, 141.8, 154.4, 158.2. Anal. Found: C, 71.45; H, 10.04; N, 7.15%. Calc. for $C_{37}H_{60}KN_3O_2$: C, 71.91; H, 9.79; N, 6.80%.

Synthesis of [{Eu(L^1)(μ–L^1)}$_2$] (15). To a pale green solution of $EuI_2(THF)_2$ (1.81 g, 3.29 mmol) in THF (20 ml) at 0 ^{o}C was added dropwise a colorless solution of **1** (2.20 g, 6.6 mmol) in the same solvent (20 ml). The yellow reaction mixture was allowed to warm slowly to room temperature and stirred for 1 d. All the volatiles were removed in *vacuo*. The yellow residue was extracted with toluene (40 ml). The orange toluene extract was filtered and then concentrated to *ca*. 10 ml to give complex **15** as orange crystals. Yield: 1.44 g, 1.1 mmol, 68%. M.p.: 211–212 ℃ (dec.). Anal. Found: C, 56.44; H, 7.08; N, 13.51%. Calcd. for $C_{60}Eu_2H_{96}N_{12}$: C, 55.89; H, 7.50; N, 13.03%.

Synthesis of [{Eu(L^2)(μ–L^2)}$_2$ · 2C$_6$H$_{14}$] (16). To a pale green solution of $EuI_2(THF)_2$ (1.29 g, 2.35 mmol) in THF (20 ml) at 0 ^{o}C was added dropwise a colorless solution of **12** (1.8 g, 4.5 mmol) in the same solvent (20 ml). The yellow reaction mixture was allowed to warm slowly to room temperature and stirred for 1 d. The yellow solution was concentrated under reduced pressure to *ca*. 5 ml, followed by extraction with hexane (20 ml). The orange solution was filtered and concentrated to

ca. 10 ml to give complex **16** as orange crystals. Yield: 1.46 g, 0.82 mmol, 74%. M.p.: 241–243 ℃ (dec.). Anal. Found: C, 64.31; H, 8.96; N, 9.92%. Calcd. for $C_{84}Eu_2H_{128}N_{12}$+2C_6H_{14}: C, 64.69; H, 8.82; N, 9.43%.

Synthesis of [{Yb(L^2)(μ–L^2)}$_2$] (17). This compound was prepared by a procedure similar to that of **16**, starting with 1.66 g (2.90 mmol) of $YbI_2(THF)_2$ and 1.97 g (4.91 mmol) of complex **12**. Complex **17** was isolated as red crystals. Yield: 1.44 g, 0.87 mmol, 72%. M.p.: 185–186 ℃ (dec.). ^{1}H NMR (400.13 MHz, toluene–d_8): 0.86 (br, 12H, C_6H_{11}), 0.93–1.03 (br, 8H, C_6H_{11}), 1.23 (br, 10H, C_6H_{11}), 1.41 (br, 16H, C_6H_{11}), 1.53 (br, 10H, C_6H_{11}), 1.67 (br, 8H, C_6H_{11}), 1.83 (br, 4H, C_6H_{11}), 2.00 (br, 4H, C_6H_{11}), 2.11 (overlapping with toluene–d_8) (br, 7H, C_6H_{11}), 2.18 (br, 3H, CH_3), 2.30 (br, 12H, CH_3), 2.41 (br, 9H, CH_3), 2.83 (br, 3H, C_6H_{11}), 3.10 (br, 1H, C_6H_{11}), 3.26 (br, 2H, C_6H_{11}), 3.36 (br, 1H, C_6H_{11}), 3.64–3.66 (br, 1H, C_6H_{11}), 4.02 (br, 1H, C_6H_{11}), 6.74–6.75 (br, 4H, Ar*H*), 6.82 (br, 3H, Ar*H*), 6.99–7.09 (overlapping with toluene–d_8) (br, 5H, Ar*H*). ^{13}C NMR (100.62 MHz, C_6D_6): 18.9, 19.9, 20.9, 23.2, 23.7, 25.3, 25.9, 26.6, 30.3, 34.3, 35.6, 36.3, 37.8, 50.5, 51.6, 52.4, 56.1, 57.5, 120.7, 121.8, 130.8, 132.5, 147.2, 148.1, 150.6, 151.3, 161.3, 163.0. Anal. Found: C, 60.39; H, 8.38; N, 10.49%. Calcd. for $C_{84}H_{128}N_{12}Yb_2$: C, 61.07; H, 7.81; N, 10.17%.

Synthesis of [{Yb(L^2)$_2$(THF)$_2$] (18). To a yellow solution of $YbI_2(THF)_2$ (1.66 g, 2.90 mmol) in THF (20 ml) at 0°C was added dropwise a colorless solution of **12**

(1.97 g, 4.90 mmol) in the same solvent (20 ml). The brick red reaction mixture was allowed to warm slowly to room temperature and stirred for 1 d. The solution was concentrated under reduced pressure to *ca*. 5 ml, followed by extraction with Et_2O (20 ml). The brick red solution was filtered and concentrated to *ca*. 10 ml to give complex **18** as red crystals. Yield: 1.47 g, 1.52 mmol, 62%. M.p.: 174–175 °C (dec.). ^{1}H NMR (400.13 MHz, toluene–d_8): 0.81–1.04 (m, 12H, C_6H_{11}), 1.36 (overlapping with THF) (br, 2H, C_6H_{11}), 1.36 (br, 12H, THF), 1.44–1.62 (m, 12H, C_6H_{11}), 1.74–1.76 (m, 4H, C_6H_{11}), 1.88–1.91 (m, 4H, C_6H_{11}), 2.09–2.13 (m, 4H, C_6H_{11}), 2.47 (s, 12H, CH_3), 2.80–2.83 (m, 2H, C_6H_{11}), 3.19–3.22 (m, 2H, C_6H_{11}), 3.51 (br, 12H, THF), 3.70 (d, J = 10.2 Hz, N*H*), 6.78 (t, J = 7.2 Hz, 2H, *p*–Ar*H*), 7.06 (d, J = 7.6 Hz, 4H, *m*–Ar*H*). ^{13}C NMR (100.62 MHz, toluene–d_8): 25.5, 26.0, 26.1, 26.6, 35.6, 37.6, 51.6, 52.2, 52.4, 55.8, 68.1, 118.7, 131.0, 147.9, 152.2, 162.6. Anal. Found: C, 61.06; H, 8.90; N, 9.08%. Calcd. for $C_{50}H_{80}N_6O_2Yb$: C, 61.07; H, 7.81; N, 10.17%.[†]

Synthesis of [Eu(L^3)$_2$(THF)$_2$·0.25C_6H_{14}] (19). To a pale green solution of $EuI_2(THF)_2$ (1.43 g, 2.60 mmol) in THF (20 ml) at 0 °C was added dropwise a colorless solution of **13** (2.30 g, 5.20 mmol) in the same solvent (20 ml). The yellow reaction mixture was stirred at room temperature for 8 h. The solution was

[†] Results of elemental analysis of complex **18** is consistent to the formula Yb(L^2)$_2$(THF)$_{1.5}$. This may be attributed to the partial evaporation of coordinated THF during the preparation process.

concentrated under reduced pressure to *ca*. 5 ml, followed by extraction with hexane (30 mL). The resulting orange solution was filtered and concentrated to *ca*. 10 ml to give complex **19** as orange crystals. Yield: 1.65 g, 1.50 mmol, 57%. M.p.: 252–253 ℃ (dec.). Anal. Found: C, 60.99; H, 9.31; N, 8.23%. Calcd. for $C_{56}EuH_{96}N_6O_2Si_2$+0.25C_6H_{14}: C, 61.94; H, 8.99; N, 7.53%.‡

Synthesis of [Yb(L^3)$_2$(THF)$_2$·0.25C_6H_{14}] (20). This complex was prepared by a procedure similar to that of **19**, starting with 1.34 g (2.35 mmol) of $YbI_2(THF)_2$ and 1.77 g (4.28 mmol) of complex **13**. Complex **20** was isolated as red crystals. Yield: 1.60 g, 1.41 mmol, 66%. M.p.: 178–179 ℃ (dec.). ^{1}H NMR (400.13 MHz, C_6D_6) δ 0.46 (br, 18H, Si(C*H*$_3$)$_3$)), 0.89 (br, 1.5H, hexane), 0.97 (br, 4H, C_6H_{11}), 1.25 (br, 10H, hexane and THF), 1.37–1.79 (br, 30H, NC_6H_{11}), 1.96 (br, 4H, C_6H_{11}), 2.18 (br, 4H, NC_6H_{11}), 2.46(br, 12H, C*H*$_3$), 3.13 (br, 2H, C_6H_{11}), 3.52 (br, 8H, THF), 6.91–6.98 (br, 3H, Ar*H*), 7.11 (br, 3H, Ar*H*). ^{13}C NMR (100.62 MHz, C_6D_6): 5.4, 14.4, 21.4, 23.1, 25.0, 26.5, 26.7, 27.9, 32.0, 36.2, 38.3, 56.6, 60.5, 68.7, 120.3, 132.1, 151.5, 167.8. Anal. Found: C, 60.92; H, 9.14; N, 7.54%. Calcd. for $C_{56}H_{96}N_6O_2Si_2Yb$+0.25C_6H_{14}: C, 60.78; H, 8.83; N, 7.40%.

Synthesis of [{Sm(L^3)(μ–I)(THF)$_2$}$_2$] (21). To a dark blue solution of $SmI_2(THF)_2$ (1.40 g, 2.56 mmol) in THF (20 ml) at 0 ^{o}C was added dropwise a colorless solution

‡ Results of elemental analysis of complex **19** is consistent to the formula Eu(L^3)$_2$(THF)$_2$. This may be attributed to the evaporation of solvated hexane during the preparation process.

of **13** (0.99 g, 2.27 mmol) in the same solvent (20 ml). The dark green reaction mixture was stirred at room temperature for 8 h. The solution was filtered and concentrated under reduced pressure to *ca*. 5 ml. The dark green solution was kept at –30 ^{o}C to give complex **21** as dark green crystals. Yield: 1.01 g, 0.61 mmol, 54%. M.p.: 168–169 ^{o}C (dec.). Anal. Found: C, 48.81; H, 6.93; N, 6.70%. Calcd. for $C_{64}H_{112}I_2N_6O_4Si_2Sm_2$: C, 46.86; H, 6.88; N, 5.12%.[†]

Synthesis of [Sm(L^5)$_2$] (22). To a dark blue solution of $SmI_2(THF)_2$ (2.05 g, 3.74 mmol) in THF (20 ml) at 0 ^{o}C was added dropwise a colorless solution of **14** (4.62 g, 7.48 mmol) in the same solvent (20 ml). The purple reaction mixture was stirred at room temperature for 8 h. All the volatiles were removed in *vacuo*. The purple residue was extracted with hexane (40 ml). The purple solution was filtered and then concentrated to *ca*. 10 ml to give complex **22** as purple crystals. Yield: 2.59 g, 2.54 mmol, 68%. M.p.: 161–162 ^{o}C (dec.). Anal. Found: C, 67.66; H, 8.68; N, 8.47%. Calcd. for $C_{58}H_{88}N_6Sm$: C, 68.31; H, 8.70; N, 8.24%.

Reaction of [{Eu(L^1)(μ–L^1)}$_2$] (15) with I$_2$. To an orange solution of complex **15** (1.2 g, 1.8 mmol) in THF (20 ml) at 0 °C was added dropwise a solution of I_2 (0.22 g, 1.8 mmol) in the same solvent (20 ml). The purple reaction mixture was stirred at room temperature for 8 h. All the volatiles were removed in *vacuo*. The purple

[†] Satisfactory results of elemental analysis could not be obtained for this compound.

residue was extracted with hexane (30 ml). The purple solution was filtered and concentrated to *ca*. 10 ml to give [{Eu(L^1)$_2$(μ–I)}$_2$] (**23**) as purple crystals. Yield: 1.00 g, 1.30 mmol, 72%. M.p.: 162–163 ℃ (dec.). Anal. Found: C, 46.38; H, 6.68; N, 10.63%. Calcd. for $C_{60}Eu_2H_{96}I_2N_{12}$: C, 46.70; H, 6.27; N, 10.89%.

General procedure for the synthesis of [{Yb(L^2)$_2$(μ–EPh)}$_2$] [E = S (24), Se (25)]. To a solution of complex **18** in Et_2O (20 ml) was slowly added a solution of PhEEPh in the same solvent (20 ml) at room temperature. The reaction mixture immediately turned yellow. Stirring was continued at room temperature for 1 d. The solution was filtered and then concentrated to *ca*. 10 ml to give a yellow crystalline product.

Synthesis of [{Yb(L^2)$_2$(μ–SPh)}$_2$] (24). [{Yb(L^2)$_2$(THF)$_2$] (**18**): 0.61g, 0.63 mmol; PhSSPh: 0.07g, 0.32 mmol. Yield: 0.38 g, 0.20 mmol, 63%. M.p.: 185–187 ℃ (dec.). Anal. Found: C, 61.06; H, 7.60; N, 9.42%. Calcd. for $C_{96}H_{138}N_{12}S_2Yb_2$: C, 61.65; H, 7.44; N, 8.98%.

Synthesis of [{Yb(L^2)$_2$(μ–SePh)}$_2$] (25). [{Yb(L^2)$_2$(THF)$_2$] (**18**): 1.68g, 1.73 mmol; PhSeSePh: 0.27g, 0.87 mmol. Yield: 1.23 g, 0.63 mmol, 72%. M.p.: 200–201 ℃ (dec.). Anal. Found: C, 58.16; H, 7.78; N, 8.90%. Calcd. for $C_{96}H_{138}N_{12}Se_2Yb_2$: C, 58.70; H, 7.08; N, 8.55%.

Reaction of [Yb(L^2)$_2$(THF)$_2$] (18) with CuCl. To a slurry of CuCl (0.09g, 0.94 mmol) in Et_2O (10 ml) at 0 °C was added dropwise a solution of complex **18** (0.92g,

0.94 mmol) in the same solvent (20 ml). The reaction mixture was stirred at room temperature for 8 h to afford a dark suspension. Standing the dark suspension at room temperature for 10 minutes, a yellow solution with brown precipitate was observed. The yellow solution was filtered and concentrated to give [{Yb(L^2)$_2$(μ–Cl)}$_2$] (**26**) as yellow crystals. Yield: 0.50 g, 0.29 mmol, 62%. M.p.: 212 °C (dec.). Anal. Found: C, 58.36; H, 7.66; N, 9.73%. Calcd. for $C_{84}Cl_2H_{128}N_{12}Yb_2$: C, 58.56; H, 7.49; N, 9.75%.

Reaction of [Yb(L^2)$_2$(THF)$_2$] (18) with PhNNPh. To a solution of complex **18** (1.28g, 1.3 mmol) in THF (20 ml) at 0 °C was added dropwise an orange solution of PhNNPh (0.25g, 1.3 mmol) in the same solvent (20 ml). The brown reaction mixture was warmed slowly to room temperature and stirred for 8 h. All the volatiles were removed in *vacuo* and the brown residue was extracted with hexane (30 ml). The brown solution was filtered and concentrated to *ca*. 10 ml to give [{Yb(L^2)$_2$}$_2$(μ–η^2:η^2–PhNNPh)] (**27**) as orange crystals. Yield: 0.44 g, 0.24 mmol, 37%. M.p.: 199–202 °C (dec.). IR (KBr) 3394 (w br), 2930 (s), 2853 (m), 2373 (w), 2345(w), 1630 (m br), 1448 (s), 1261 (s), 1228 (s), 1070 (m), 841(s) cm^{-1}. UV–Vis (THF) λ_{max} (ε/M^{-1}cm^{-1}): 443 (200). Anal. Found: C, 63.24; H, 7.89; N, 10.74%. Calcd. for $C_{96}H_{138}N_{14}Yb_2$: C, 62.86; H, 7.58; N, 10.69%.

Reaction of [Yb(L^3)$_2$(THF)$_2$·0.25C_6H_{14}] (20) with PhNNPh. To a solution of

complex **20** (1.66 g, 1.46 mmol) in toluene (20 ml) at 0 °C was added dropwise an orange solution of PhNNPh (0.27 g, 1.46 mmol) in the same solvent (20 ml). The blue reaction mixture was warmed slowly to room temperature and stirred for 8 h. The blue solution was filtered and concentrated to *ca*. 10 ml to give $[Yb(L^3)_2(\eta^2\text{–PhNNPh})\cdot PhMe]$ (**28**) as blue crystals. Yield: 1.18 g, 0.94 mmol, 64%. M.p.: 185–187°C (dec.). IR (KBr) 3419 (w br), 2925 (s), 2853 (s), 2346 (w), 1638 (m), 1534 (s), 1452–1467 (s), 1269 (s), 1239 (s), 1150 (m), 1090 (s), 760 (s) cm^{-1}. UV–Vis (THF) λ_{max} ($\varepsilon/M^{-1}cm^{-1}$): 585 (br, 800), 378 (2700). Anal. Found: C, 64.81; H, 8.07; N, 9.30%. Calcd. for $C_{60}H_{90}N_8Si_2Yb+C_7H_8$: C, 64.65; H, 7.94; N, 9.00%.

Reaction of $[Sm(L^5)_2]$ (22) with CS_2. To a solution of complex **22** (1.58 g, 1.55 mmol) in toluene (20 ml) at 0 °C was added dropwise a solution of CS_2 (5 M in THF, 0.3 ml, 1.65 mmol). The green reaction mixture was warmed slowly to room temperature and stirred for 8 h. The green solution was filtered and concentrated to *ca*. 10 ml to give $[(L^5)_2Sm(\mu\text{–}\eta^3\text{:}\eta^2\text{–}S_2CSCS)Sm(L^5)_2]$ (**29**) as green crystals. Yield: 1.14 g, 0.51 mmol, 66%. M.p.: 181–182 ℃ (dec.). Anal. Found: C, 64.24; H, 8.42; N, 7.78%. Calcd. for $C_{118}H_{178}N_{12}S_4Sm_2$: C, 64.67; H, 8.09; N, 7.67%.

3.5 References for Chapter 3

1. Morss, L. R. *Chem*. *Rev*. **1976**, *76*, 827–841.

2. Pearson, R. G. *J*. *Am*. *Chem*. *Soc*. **1963**, *85*, 3533–3539.

3. a) Tilley, T. D.; Zalkin, A.; Andersen, R. A.; Templeton, D. H. *Inorg*. *Chem*. **1981**, *20*, 551–554.

   b) Tilley, T. D.; Andersen, R. A.; Zalkin, A. *J*. *Am*. *Chem*. *Soc*. **1982**, *104*, 3725–3727.

   c) Tilley, T. D.; Andersen, R. A.; Zalkin, A. *Inorg*. *Chem*. **1984**, *23*, 2271–2276.

4. a) Cetinkaya, B.; Hitchcock, P. B.; Lappert, M. F.; Smith, R. G. *J*. *Chem*. *Soc*., *Chem*. *Commun*. **1992**, 932–934.

   b) van den Hende, J. R.; Hitchock, P. B.; Lappert, M. F. *J*. *Chem*. *Soc*., *Dalton Trans*. **1995**, 2251–2258.

5. a) Evans, W. J.; Drummond, D. K.; Zhang, H.; Atwood, J. L. *Inorg*. *Chem*. **1988**, *27*, 575–579.

   b) Evans, W. J.; Johnston, M. A.; Clark, R. D.; Anwander, R.; Ziller, J. W. *Polyhedron* **2001**, *20*, 2483–2490.

6. a) Welder, M.; Noltemeyer, M.; Pieper, U.; Schmidt, H. -G.; Stalke, D.; Edelmann, F. T. *Angew*. *Chem*. *Int*. *Ed*. *Engl*. **1990**, *29*, 894–896.

b) Welder, M.; Recknagel, A.; Gilje, J. W.; Nottemeyer, M.; Edelmann, F. T. *J. Organomet. Chem.* **1992**, *426*, 295–306.

7. Cole, M. L.; Junk, P. C. *Chem. Commun.* **2005**, 2695–2697.
8. Yao, S.; Chan, H. -S.; Lam, C. -K.; Lee, H. K. *Inorg. Chem.* **2009**, *48*, 9936–9946.
9. Zhou, Y.; Yap, G. P. A.; Richeson, D. S. *Organometallics* **1998**, *17*, 4387–4391.
10. Heitmann, D.; Jones, C.; Junk, P. C.; Lippert, K. -A.; Stasch, A. *Dalton Trans.* **2007**, 187–189.
11. Heitmann, D.; Jones, C.; Mills, D. P.; Stasch, A. *Dalton Trans.* **2010**, *39*, 1877–1882.
12. Yeung, L. F. *M. Phil. Thesis*, The Chinese University of Hong Kong, 2010.
13. Wong, G. F. *PhD. Thesis*, The Chinese University of Hong Kong, 2013.
14. Giesbrecht, G. R.; Shafir, A.; Arnold, J. *J. Chem. Soc., Dalton Trans.* **1999**, 3601–3604.
15. Jin, G.; Jones, C.; Junk, P. C.; Lippert, K. -A.; Rose, R. P.; Stasch, A. *New J. Chem.* **2009**, *33*, 64–75.
16. Hitzbleck, J.; O'Brien, A. Y.; Deacon, G. B.; Ruhlandt-Senge, K. *Inorg. Chem.* **2006**, *45*, 10329–10337.
17. Shannon, R. D. *Acta Cryst.* **1976**, *A32*, 751–767.

18. Qayyum, S.; Haberland, K.; Forsyth, C. M.; Junk, P. C.; Deacon, G. B.; Kempe, R. *Eur. J. Inorg. Chem.* **2008**, 557–562.

19. Qayyum, S.; Noor, A.; Glatz, G.; Kempe, R. *Z. Anorg. Allg. Chem.* **2009**, *635*, 2455–2458.

20. Evans, W. J.; Grate, J. W.; Choi, H. W.; Bloom, I.; Hunter, W. E.; Atwood, J. L. *J. Am. Chem. Soc.* **1985**, *107*, 941–946.

21. Scott, N. M.; Kempe, R. *Eur. J. Inorg. Chem.* **2005**, 1319–1324.

22. Gulaczyk, I.; Kreglewski, M.; Valentin, A. *J. Mol. Spectrosc.* **2003**, *220*, 132–136.

23. Evans, W. J.; Drummond, D. K.; Chamberlain, L. R.; Doedens, R. J.; Bott, S. G.; Zhang, H.; Atwood, J. L. *J. Am. Chem. Soc.* **1988**, *110*, 4983–4994.

24. Hamm, S.; Ohline, S. M.; Zinth, W. *J. Chem. Phys.* **1997**, *106,* 519–529.

25. Päiväsaari, J.; Dezelah, IV, C. L.; Back, D.; EI-Kaderi, H. M.; Heeg, M. J.; Putkonen, M.; Niinistö, L.; Winter, C. H. *J. Mater. Chem.* **2005**, *15*, 4224–4233.

26. Richter, J.; Feiling, J.; Schmidt, H. -G.; Noltemeyer, M.; Brüser, W.; Edelmann, F. T. *Z. Anorg. Allg. Chem.* **2004**, *630*, 1269–1275.

27. Zhang, Z.; Zhang, L.; Li, Y.; Hong, L.; Chen, Z.; Zhou, X. *Inorg. Chem.* **2010**, *49*, 5715–5722.

28. Luo, Y.; Yao, Y.; Shen, Q.; Yu, K.; Weng, L. *Eur. J. Inorg. Chem.* **2003**, 318–323.

29. Zhang, Z.; Roskey, H. W.; Schulz, T.; Stalke, D.; Döring, A. *Eur. J. Inorg. Chem.* **2009**, 4864–4869.

30. Hou, Z.; Koizumi, T.; Nishiura, M.; Wakatsuki, Y. *Organometallics* **2001**, *20*, 3323–3328

31. Weast, R. C. *Handbook of Chemistry and Physics*, 53rd ed., CRC Press, **1972**, p.1972–1973.

32. a) Maj, J. J.; Rae, A. D.; Dahl, L. F. *J. Am. Chem. Soc.* **1982**, *104*, 4278–4280.

    b) North, T. E.; Thoden, J. B.; Bjarnason, A.; Dahl, L. F. *Organometallics* **1992**, *11*, 4338–4343.

    c) Christon, V.; Wuller, S. P.; Arnold, J. *J. Am. Chem. Soc.* **1993**, *115*, 10545–10552.

    d) Cromhout, N. L.; Manning, A. R.; McAdam, C. J.; Palmer, A. J.; Rieger, A. L.; Rieger, P. H.; Robinson, B. H.; Simpson, J. *Dalton Trans.* **2003**, 2224–2230.

33. a) Werner, H.; Kolb, O.; Feser, R. *J. Organomet. Chem.* **1980**, *191*, 283–293.

    b) Carmona, E.; Galindo, A.; Monge, A.; Muñoz, M. A.; Poveda, M. L.; Ruiz, C. *Inorg. Chem.* **1990**, *29*, 5074–5080.

c) Whited, M. T.; Grubbs, R. H. *Organometallics* **2009**, *28*, 161–166.

34. Yao, Y. -M.; Luo, Y. -J.; Shen, Q.; Yu, K. -B. *Chinese J. Struct. Chem.* **2004**, *23*, 391–394.

35. Zhou, L.; Yao, Y.; Zhang, Y.; Xue, M.; Chen, J.; Shen, Q. *Eur. J. Inorg. Chem.* **2004**, 2167–2172.

36. a) Namy, J. L.; Girard, P.; Kagan, H. B. *Nouv. J. Chim.* **1977**, *1*, 5–7.

b) Namy, J. L.; Girard, P.; Kagan, H. B. *Nouv. J. Chim.* **1981**, *5*, 479–484.

c) Watson, P. L.; Tulip, T. J.; Williams, I. *Organometallics* **1990**, *9*, 1999–2009.

Chapter 4

Trivalent Lanthanide Complexes Derived from the Unsymmetrical $[(2,6\text{–}Me_2C_6H_3N)C(NHPr^i)(NPr^i)]^-$ Ligand

4.1 The Development of Organolanthanide(III) Chemistry

The lanthanide metals refer to the fifteen elements from lanthanum (La) to lutetium (Lu). All lanthanide elements can exist in the oxidation state of +3 with electronic configurations $[Xe]4f^n$ (n = 0–14). The shielding effect of the orbitals decreases in the order s > p > d > f. Because of the poor shielding effect of the 4f orbitals, there is a steady increase in the effective nuclear charge of the metal across the row from La to Lu. This also results in a decrease in their ionic radii. This trend is called the lanthanide contraction.

The first organolanthanide(III) complexes, $[Ln(Cp)_3]$ (Ln = La, Ce, Pr, Nd, Sm, Gd, Dy, Er, Yb; Cp = $C_5H_5^-$), were reported by Wilkinson and Birmingham in the mid 1950's (Scheme 4–1).[1] These complexes were synthesized by metathetical reactions of an appropriate anhydrous lanthanide trichloride with sodium cyclopentadienide in THF. In the following decades, the coordination chemistry of cyclopentadienyl ligands with the lanthanide metals has been well studied.[2]

$$LnCl_3 + 3\ NaC_5H_5 \xrightarrow[-\ 3\ NaCl]{THF} Ln(C_5H_5)_3$$

Ln = La, Ce, Pr, Nd, Sm, Gd, Dy, Er, Yb

Wilkinson and Birmingham[1]

Scheme 4—1

Following an exhaustive study on cyclopentadienyl–type ligands, tremendous

research efforts have been devoted to develop alternative ligand sets that can sterically saturate the coordination sphere around the large lanthanide metal center, and at the same time, keep enough space for further reactions. The chemistry of various types of non–cyclopentadienyl ligand systems have been reviewed.[3] Some of them are depicted in Chart 4–1.

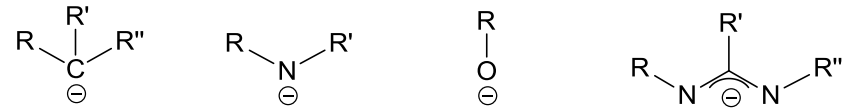

Chart 4—1

Guanidinates anions belong to a class of versatile ligands. They are flexible ligands due to their tunable steric and electronic properties through introduction of various substituents at the nitrogen atoms. The chemistry of lanthanide guanidinate complexes has been reviewed.[4] Beside their applications in various polymerization processes (see P.22 in Chapter 1), volatile lanthanide(III) tris(guanidinate) complexes have been reported to be suitable precursors for the deposition of lanthanide metals and lanthanide oxides (Ln_2O_3) thin layers by atomic layer deposition (ALD) and metal–organic chemical vapor deposition (MOCVD) processes.[5]

Recently, Devi and co–workers have reported on the preparations of Gd(III) and

Dy(III) tris(guanidinates), [M{(Pr^iN)$_2$C(NMe_2)}$_3$] (M = Gd, Dy).[5a] The latter complexes were found to be stable precursors for deposition of Gd_2O_3 and Dy_2O_3 thin films on Si(100) substrates. Gadolinium nitride (GdN), an emerging material, has attracted considerable attention due to its unique magnetic and electronic properties and, thus, its potential applications in spintronics.[6] Gadolinium nitride thin films can be grown by deposition of a volatile Gd(III) single–source precursors (SSP) on Al_2O_3 or Si(100) substrates, followed by purging nitrogen or ammonia as a reactive gas in the temperature range of 650–850 ^oC.[5b,c] Devi and co–workers have demonstrated the preparation of GdN thin film by using Gd(III) tris(guanidinate) [Gd{(Pr^iN)$_2$C(NMe_2)}$_3$] as SSP.[5b,c] Compared with other lanthanide complexes, lanthanide(III) tris(guanidinate) complexes were found to be better SSP for MOCVD of metal nitrides.

4.1.1 Lanthanide(III) Tris(guanidinate) Complexes

Lanthanide(III) tris(guanidinate) complexes were extensively studied by two research groups led independently by Devi[5] and Shen.[7] These complexes were readily prepared by (i) metathetical reactions of lanthanide trichlorides with an appropriate lithium guanidinate, and (ii) the reactions of a lanthanide triamide with a substituted carbodiimide (Chart 4–2). Lanthanide(III) tris(guanidinate) complexes

were shown to be active catalysts for the ring–opening polymerization of ε–caprolactone,[7a] trimethylene carbonate,[7b] amidation of aldehydes with amines,[7d,e] and single–source precursors for MOCVD of Ln_2O_3 (Ln = Gd, Dy).[5a]

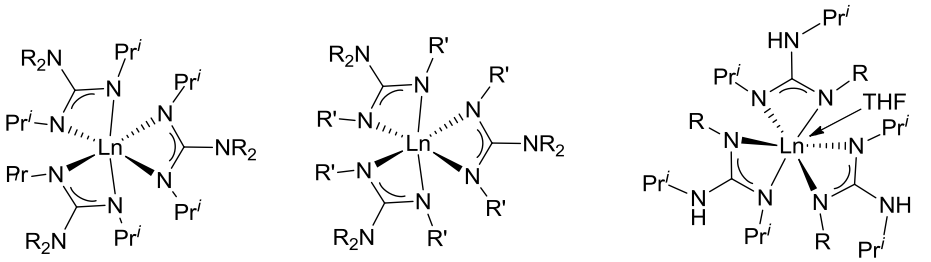

Devi *et al*.[5a] Shen *et al*.[7]

Chart 4—2

4.1.2 Lanthanide(III) Bis(guanidinate) Complexes

Richeson and co–workers have reported on the preparation of Sm(III) and Yb(III) bis(guanidinate) complexes of the type $[Ln\{CyNC[N(SiMe_3)_2]NCy\}_2(\mu\text{–}Cl)_2Li(X)_2]$ (Ln = Sm, Yb; Cy = cyclohexyl; X = Et_2O, 0.5 TMEDA) (Scheme 4–2).[8] Substitution of the chloro ligands in these complexes by $[CH(SiMe_3)_2]^-$ and $[N(SiMe_3)]^-$ gave the corresponding alkyl and amido compounds, respectively. Later on, Shen[9] and Trifonov[10] have used the same ligand to prepare similar Sm(III) and Lu(III) bis(guanidinate) complexes $Ln\{CyNC[N(SiMe_3)_2]NCy\}_2(\mu\text{–}Cl)_2Li(THF)_2$ (Ln = Sm, Lu),[9,10] as well as $Ln\{CyNC[N(SiMe_3)_2]NCy\}_2Cl(THF)$ (Ln = Nd, Sm,

Lu).[10] The latter complexes were prepared by the reactions of an appropriate $LnCl_3$ with two equivalents of sodium guanidinate Na{CyNC[N($SiMe_3$)$_2$]NCy}. It is noted that the use of sodium guanidinate may suppress the formation of ate–complexes. The Lu(III) complex [Lu{CyNC[N($SiMe_3$)$_2$]NCy}$_2$(μ–Cl)$_2$Li(THF)$_2$] underwent further reactions with $LiCH_2SiMe_3$, yielding the corresponding alkyl complex [Lu{CyNC[N($SiMe_3$)$_2$]NCy}$_2$(CH_2SiMe_3)] (Scheme 4–3).[11] Besides, addition of $PhSiH_3$ to [Lu{CyNC[N($SiMe_3$)$_2$]NCy}$_2$(CH_2SiMe_3)] gave the hydrido complex [Lu{CyNC[N($SiMe_3$)$_2$]NCy}$_2$(μ–H)$_2$]$_2$.[11] Results of a preliminary study showed that the latter hydrido complex could catalyze the hydrosilylation of 1–nonene with $PhSiH_3$ to give $PhSiH_2$(*n*–C_9H_{19}) as the only isolable product.

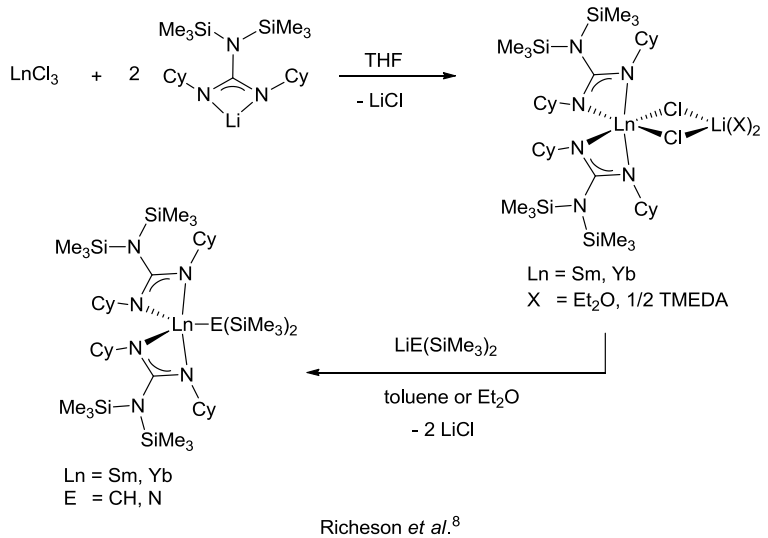

Richeson *et al.*[8]

Scheme 4—2

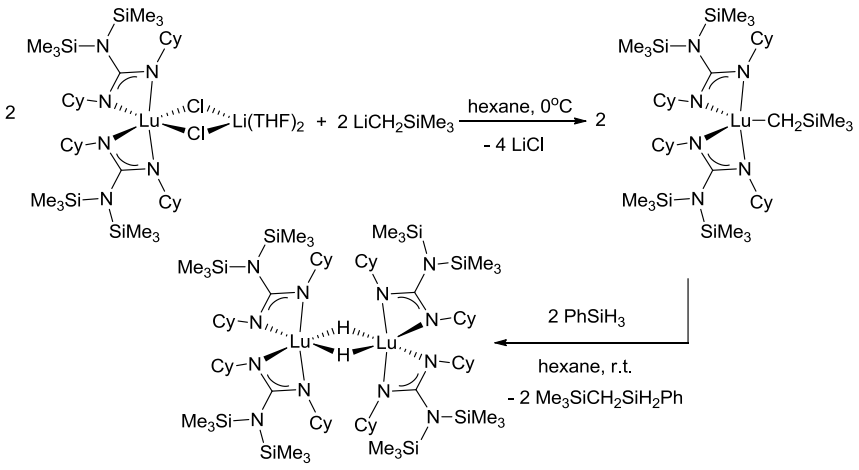

Trifonov *et al*.[11]

Scheme 4—3

More recently, Trifonov and co–workers have isolated a series of lanthanide(III) borohydride complexes of the type $[(Me_3Si)_2NC(NCy)_2]_2Ln(\mu\text{–}BH_4)_2Li(THF)_2$ (Ln = Nd, Sm, Yb)[12] by the reactions of an appropriate Ln(III) tris(borohydrides), $Ln(BH_4)_3(THF)_2$ (Ln = Nd, Sm, Yb), with a twofold molar excess of $Li[(Me_3Si)_2NC(NCy)_2]$ in toluene at 65 °C (Scheme 4–4). The borohydride complexes, especially the Nd(III) complex, acted as mono–initiators for the ring–opening polymerization of *rac*–lactide, yielding atactic polymers with controlled molecular weights and relatively narrow polydispersities ($1.09<M_w/M_n<1.77$).

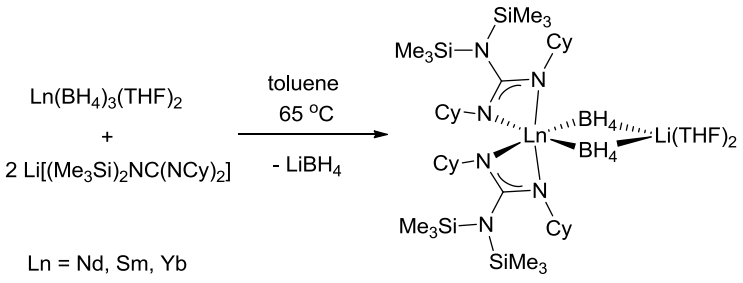

Trifonov *et al*.[12]

Scheme 4—4

The coordination properties of $[(Me_3Si)_2NC(NPr^i_2)_2]^-$ has been extensively studied by Shen[13] and Trifonov.[14] A few lanthanide(III) bis(guanidinate) complexes derived from the $[(Me_3Si)_2NC(NPr^i_2)_2]^-$ ligand have been isolated, e.g. $[Ln\{Pr^iNC[N(SiMe_3)_2]NPr^i\}_2(\mu\text{–}Cl)_2Li(THF)_2]$ (Ln = Nd, Yb, Lu)[13a,b,14a] and $[Ln\{Pr^iNC[N(SiMe_3)_2]NPr^i\}_2(\mu\text{–}Cl)]_2$ (Ln = Nd, Sm, Yb)[13c] (Chart 4–3). They were prepared by the reactions of $LnCl_3$ (Ln = Nd, Sm, Yb, Lu) with two molar equivalents of $Li[(Me_3Si)_2NC(NPr^i_2)_2]$ in an appropriate solvent. Subsequent reactions of these complexes with $LiN(Pr^i)_2$, LiMe, $NaOPr^i$, $KOBu^t$, $LiCH_2SiMe_3$ were also studied (Scheme 4–5 and Scheme 4–6). These complexes were proved to be efficient initiators for the polymerization of olefins,[13a,14b] ε–caprolactone,[13b,c,14c] methyl methacrylate,[13b,c] *rac*–lactide,[14a] *rac*–β–butyrolactone,[14a] as well as hydrosilylation of 1–nonene with $PhSiH_3$.[14c]

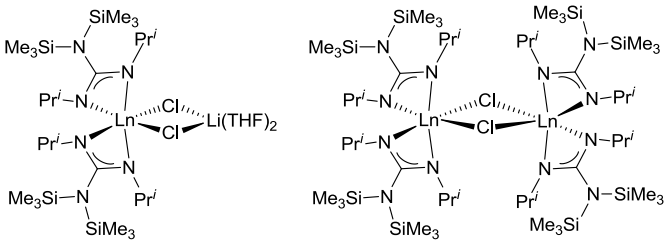

Ln = Nd, Yb, Lu

Ln = Nd, Sm, Yb

Shen *et al*.[13]
Trifonov *et al*.[14a]

Chart 4—3

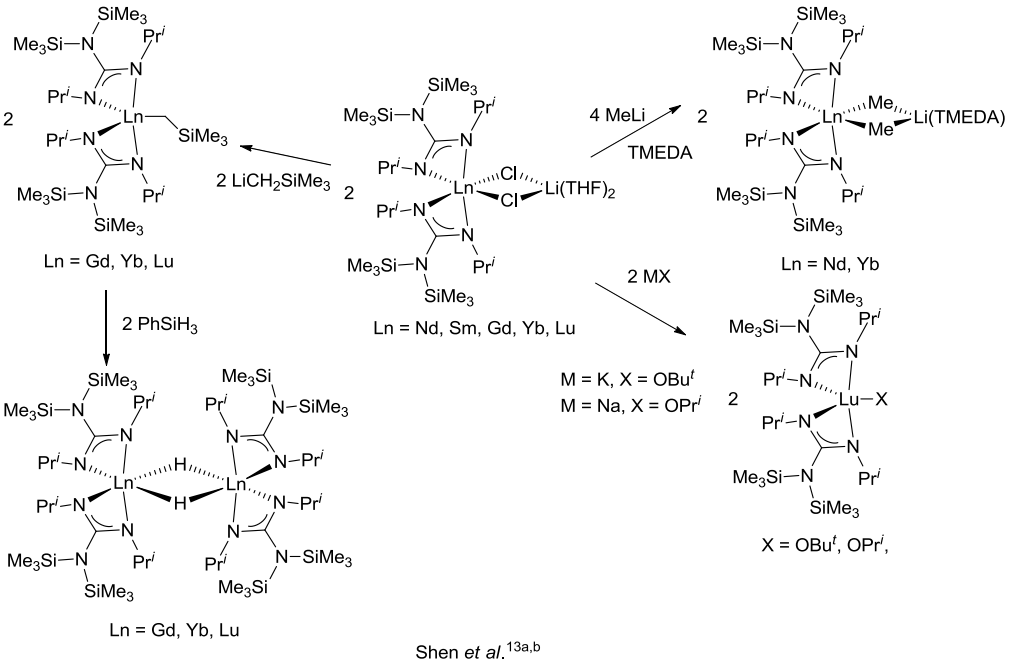

Shen *et al*.[13a,b]
Trifonov *et al*.[14]

Scheme 4—5

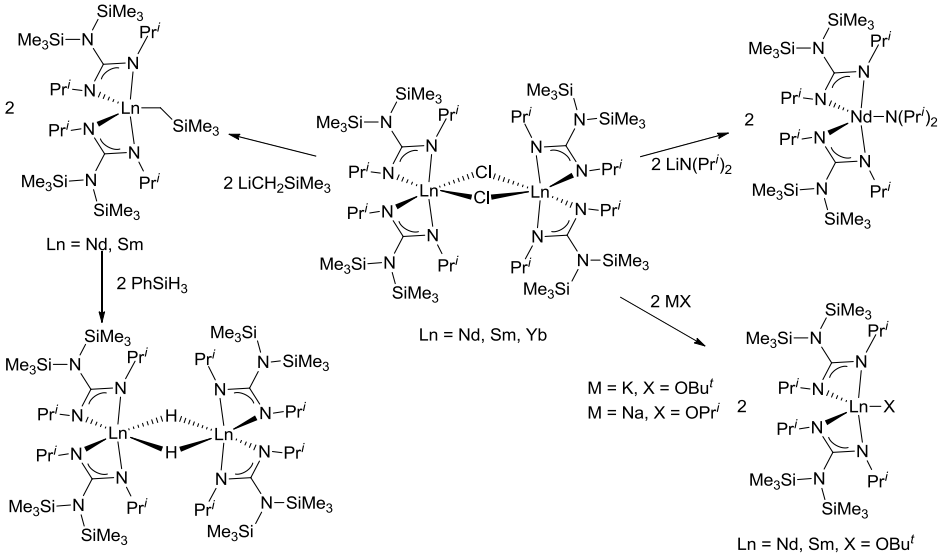

Shen *et al*.[13c]
Trifonov *et al*.[14]

Scheme 4—6

4.1.3 Lanthanide(III) Mono(guanidinate) Complexes

The first lanthanide(III) mono(guanidinate) complex, $[La\{CyNC(NSiMe_3)_2)NCy\}\{N(SiMe_3)_2\}_2]$, was reported by Arnold and co–workers.[15] This complex was synthesized by the reaction of $La[N(SiMe_3)_2]_3$ with

1,3–dicyclohexylcarbodiimide in refluxing toluene (Scheme 4–7). The corresponding bis(guanidinate) complex [La{CyNC(NSiMe$_3$)$_2$)NCy}$_2${N(SiMe$_3$)$_2$}] was also isolated in this reaction, but these two complexes could be separated by fractional crystallization. [La{CyNC(NSiMe$_3$)$_2$)NCy}$_2${N(SiMe$_3$)$_2$}] reacted cleanly with two equivalents of 2,6–di–tert–butylphenol in pentane to give the corresponding bis(phenoxide) complex [La{CyNC(NSiMe$_3$)$_2$)NCy}(OC$_6$H$_3$^{t}Bu$_2$–2,6)].

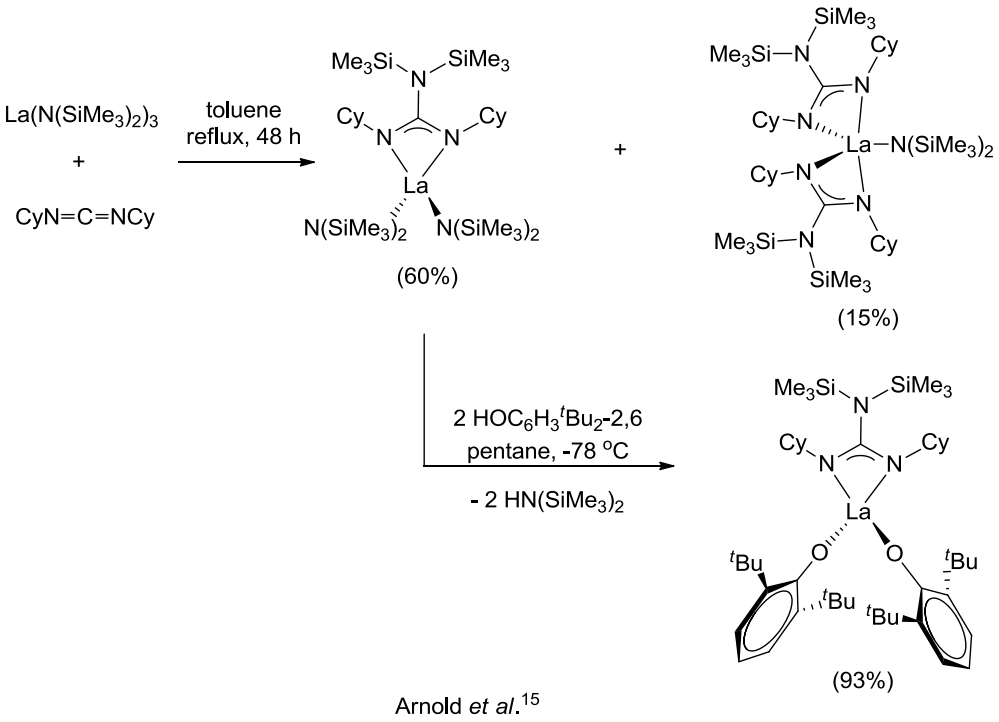

Arnold *et al*.[15]

Scheme 4—7

Mono(guanidinate) Er(III) and Yb(III) borohydride complexes [{(Me$_3$Si)$_2$NC(NCy)$_2$}Ln(BH$_4$)$_2$(THF)$_2$] (Ln = Er, Yb) were prepared by the reactions of Ln(BH$_4$)$_3$(THF)$_3$ (Ln = Er, Yb) with one molar equivalent of sodium guanidinate Na[(Me$_3$Si)$_2$NC(NCy)$_2$] in THF (Scheme 4–8).[16]

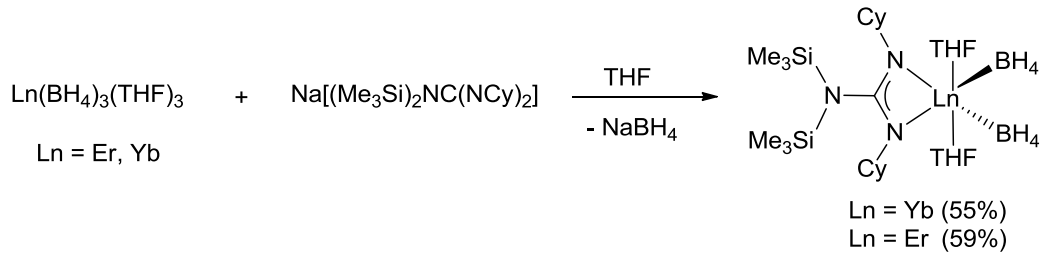

Yuan *et al*.[16]

Scheme 4—8

Treatment of [Ln(MBMP){$N(SiMe_3)_2$}$_2$($THF)_2$] [Ln = Nd, Yb; MBMP = 2,2'–methylene bis(6–tert–butyl–4–methyl–phenolate)] with Pr^iN=C=NPr^i gave the corresponding mixed ligand complexes [Nd(μ–O–MBMP){$(Pr^iN)_2CN(SiMe_3)_2$}]$_2$ and [Yb(MBMP){$(Pr^iN)_2CN(SiMe_3)_2$}] (Scheme 4–9).[17]

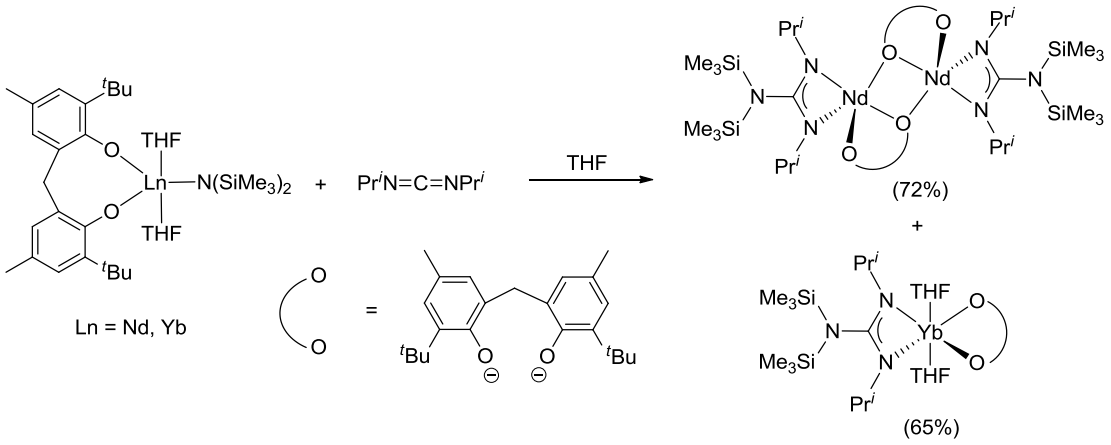

Shen *et al*.[17]

Scheme 4—9

Recently, Zhou and co–workers have reported on a number of bis(cyclopentadienyl) lanthanide guanidinates [Cp_2LnL] (Cp = $C_5H_5^-$, Ln = lanthanides, L = guanidinates) derived from various types of substituted guanidinate ligands (Chart 4–4).[18] These mixed–ligand guanidinate complexes were prepared by the reactions of [Cp_2LnL] (L = amides) with an appropriate carbodiimide, except for

$[(C_5H_5)_2Ln\{\mu\text{–}\eta^1\text{:}\eta^2\text{–}N{=}C(NMe_2)_2\}]_2$ (Ln = Gd, Er),[18e] which were prepared by salt metathesis reactions of Cp_2LnCl with lithium guanidinate $LiN{=}C(NMe_2)_2$.[18e]

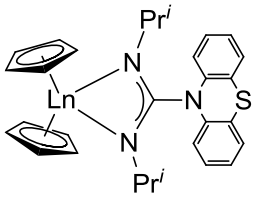

Ln = Dy, Er, Yb

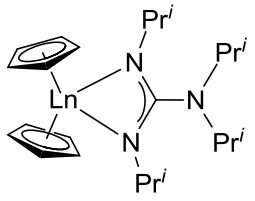

Ln = Gd, Dy, Yb

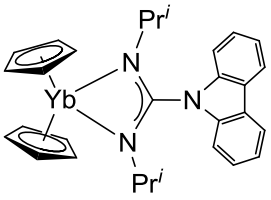

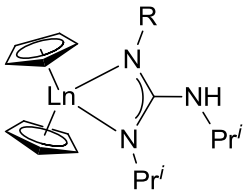

Ln = Dy, Er, Yb
R = ^{t}Bu, Ph

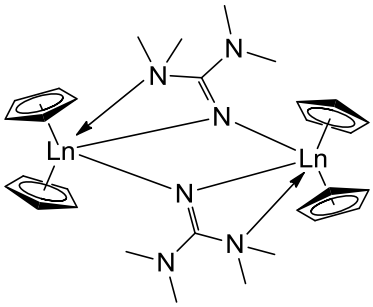

Ln = Gd, Er

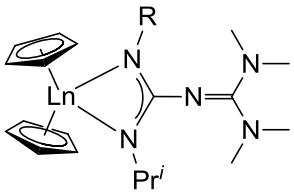

Ln = Dy, Er, Yb

Zhou *et al*.[18]

Chart 4—4

4.2 Results and Discussion

4.2.1 Synthesis and Structure of Lanthanide(III) Tris(guanidinate) and Bis(guanidinate) Complexes Derived from Ligand L^1

Preparation

The preparation of $[KL^1 \cdot 0.5PhMe]_n$ (**1**) have been described in Chapter 2. Salt metathesis reactions of an appropriate anhydrous $LnCl_3$ (Ln = Ce, Pr, Gd, Tb, Ho, Er, Tm) with three molar equivalents of potassium reagent **1** in THF yielded the corresponding homoleptic lanthanide(III) tris(guanidinate) complexes $[Ln(L^1)_3]$ [Ln = Ce (**30**), Pr (**31**), Gd (**32**), Tb (**33**), Ho (**34**), Er (**35**), Tm (**36**)] (Scheme 4–10).

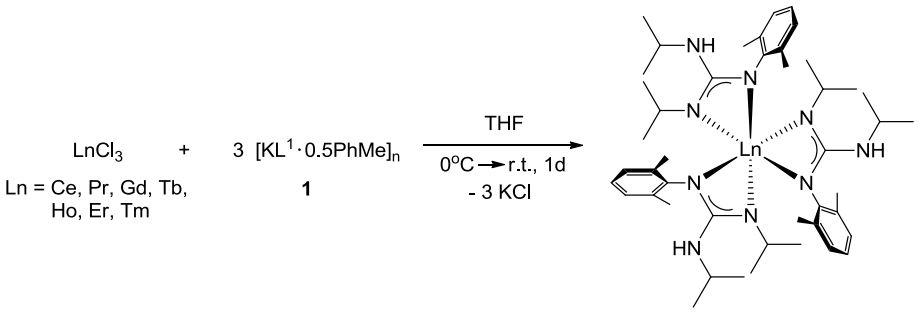

30: Ln = Ce (70%)
31: Ln = Pr (77%)
32: Ln = Gd (72%)
33: Ln = Tb (75%)
34: Ln = Ho (80%)
35: Ln = Er (78%)
36: Ln = Tm (82%)

Scheme 4—10

Treatment of $LnCl_3$ (Ln = Ce, Lu) with two molar equivalents of **1** in THF led to the isolation of binuclear lanthanide(III) bis(guanidinate) complexes $[\{Ln(L^1)_2(\mu\text{–}Cl)\}_2]$ [Ln = Ce (**37**), Lu (**38**)] (Scheme 4–11).

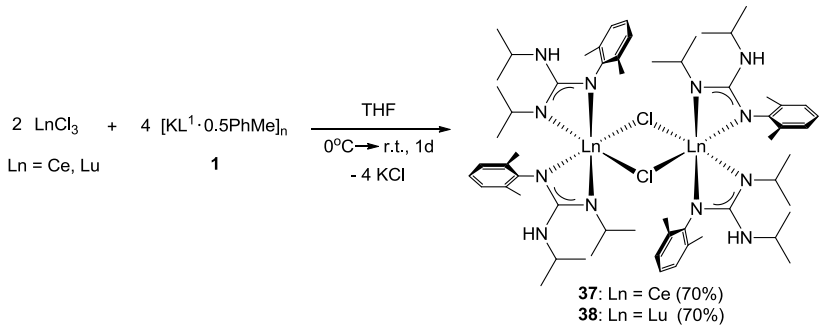

Scheme 4—11

Physical Characterization of Complexes **30–38**

All of the complexes **30–38** are sensitive to air and moisture. They are readily soluble in common organic solvents such as THF, toluene, Et_2O and hexane. The formulation of complexes **30–38** has been confirmed by elemental analysis, NMR spectroscopy (for **38**) and X–ray diffraction analysis. Table 4–1 summarizes the appearance and melting points of complexes **30–38**.

Table 4–1. Appearance and melting points of complexes **30–38**

Compound	Appearance	M.p. (^oC)
$[Ce(L^1)_3]$ (**30**)	Yellow crystals	174–176
$[Pr(L^1)_3]$ (**31**)	Pale green crystals	189–192
$[Gd(L^1)_3]$ (**32**)	Colorless crystals	176–178
$[Tb(L^1)_3]$ (**33**)	Colorless crystals	173–174
$[Ho(L^1)_3]$ (**34**)	Pink crystals	173–174
$[Er(L^1)_3]$ (**35**)	Colorless crystals	162–164
$[Tm(L^1)_3]$ (**36**)	Colorless crystals	175–176
$[\{Ce(L^1)_2(\mu\text{–}Cl)\}_2]$ (**37**)	Yellow crystals	180–181
$[\{Lu(L^1)_2(\mu\text{–}Cl)\}_2]$ (**38**)	Colorless crystals	189–190

NMR Spectra of Complex **38**

The NMR spectra of complex **38** are shown in Figures A2–21 and A2–22 (Appendix 2), respectively. Complex **38** was dissolved in C_6D_6 for NMR analysis. The ^{1}H and ^{13}C NMR spectra of complex **38** show only one set of resonance signals which are assignable to the L^1 ligand, indicating that the four L^1 ligands in each dimeric unit are chemically equivalent. Its ^{1}H NMR shows one broad signal and one doublet signal at 0.72 and 0.78 ppm, respectively, which are assignable to the isopropyl methyl groups. A doublet of septet signal at 2.83 ppm and one septet signal at 3.21 ppm are assignable to the methine proton on the isopropyl group attached to the non–coordinated amino nitrogen atom and the coordinated nitrogen atom, respectively. Besides, a singlet signal at 2.17 ppm is assignable to the ortho methyl groups on the aryl substituent. A triplet signal at 6.66 ppm and a doublet signal at 6.81 ppm are assignable to the para and meta protons on the aryl substituent, respectively. The ^{13}C NMR spectrum of **38** also shows broad resonance signals due to the isopropyl methyl groups (74.5 and 76.0 ppm) and the isopropyl methine carbons (95.1 and 96.6 ppm), respectively. One singlet signal at 70.3 ppm, four singlet signals at 172.7, 178.7, 184.1 and 197.1 ppm, and one singlet signal at 214.3 ppm are assignable to the ortho methyl groups on the aryl substituents, the carbon atoms on the aryl substituents and the central carbon atom on the N–C–N backbone, respectively.

Crystal Structures of Complexes **30–38**

Single crystals of complexes **30–36** were obtained from pentane, whereas those of complexes **37** and **38** were obtained from hexane. Figures 4–1 to 4–9 show the molecular structures of the homoleptic complexes **30–38**, respectively. Selected bond lengths and angles are listed in Tables 4–2 to 4–10. Selected crystallographic data are listed in Tables A3–11 to A3–13 (Appendix 3), respectively.

1. $[Ln(L^1)_3]$ [Ln = Ce (**30**), Pr (**31**), Gd (**32**), Tb (**33**), Ho (**34**), Er (**35**), Tm (**36**)]

Complexes **30–36** are isotypic, in which the metal center is coordinated by three κ^2–bound L^1 ligands. All of them crystallize in a triclinic crystal system with space group $P\bar{1}$. Each of them consists of a three–fold rotational axis passing through the metal center. The coordination geometry around the metal center can be best described as a distorted trigonal prism: one of the trigonal planes is consisted of nitrogen atoms N(1), N(4) and N(7), while the other trigonal plane is composed of nitrogen atoms N(3), N(6) and N(9). It is noteworthy that the solid–state structures of complexes **30–36** show that they are Λ–isomers, but, the possibility for both Λ– and Δ–isomers co–exist as a racemic mixture for each complex should not be excluded.[†] Table 4–11 summarizes important structural parameters for complexes **30–36**.

[†]Λ– and Δ–isomers are enantiomers. Both isomers have the same energy of crystallization in non–chiral solvents (e.g. pentane).

Table 4–11. The $C^{(center)}$–$N^{(aryl)}$† distances, $C^{(center)}$–$N^{(isopropyl)}$† distances, Ln–$N^{(aryl)}$ distances, Ln–$N^{(isopropyl)}$ distances (Å) and the $N^{(aryl)}$–Ln–$N^{(isopropyl)}$ angles (°) (Å) for complexes **30**–**36**.

$[Ln(L^1)_3]$	$C^{(center)}$–$N^{(aryl)}$ (Å)	$C^{(center)}$–$N^{(isopropyl)}$ (Å)	Ln–$N^{(aryl)}$ (Å)	Ln–$N^{(isopropyl)}$ (Å)	$N^{(aryl)}$–Ln–$N^{(isopropyl)}$ (°)
30 (Ln = Ce)	1.336(3)–1.338(3)	1.326(4)–1.335(3)	2.480(2)–2.514(2)	2.482(2)–2.504(2)	53.58(8)–53.71(7)
31 (Ln = Pr)	1.340(3)–1.347(3)	1.328(4)–1.335(3)	2.463(2)–2.503(2)	2.463(2)–2.489(2)	54.10(7)–54.15(8)
32 (Ln = Gd)	1.336(4)–1.346(4)	1.325(5)–1.332(4)	2.401(3)–2.428(3)	2.398(3)–2.411(3)	55.56(9)–55.87(9)
33 (Ln = Tb)	1.338(4)–1.341(4)	1.327(5)–1.335(4)	2.386(3)–2.417(2)	2.383(3)–2.402(2)	55.95(8)–56.07(8)
34 (Ln = Ho)	1.342(4)–1.350(4)	1.330(4)–1.338(4)	2.362(3)–2.392(3)	2.357(3)–2.377(3)	56.66(9)–56.81(9)
35 (Ln = Er)	1.335(3)–1.343(3)	1.332(3)–1.337(3)	2.352(2)–2.377(2)	2.343(3)–2.365(2)	56.96(8)–57.06(7)
36 (Ln = Tm)	1.331(4)–1.355(4)	1.324(4)–1.338(4)	2.332(2)–2.368(2)	2.331(2)–2.357(2)	57.05(8)–57.44(8)

† $C^{(center)}$ = carbon atoms C(9), C(24) and C(39) on the N–C–N backbone; $N^{(aryl)}$ = nitrogen atoms N(1), N(4) and N(7), each of them attached to the aryl substituent of the L^1 ligand; $N^{(isopropyl)}$ = nitrogen atoms N(3), N(6) and N(9), each of them attached to the isopropyl substituent of the L^1 ligand.

The observed $C^{(center)}$–$N^{(aryl)}$ and $C^{(center)}$–$N^{(isopropyl)}$ bond distances are almost identical in **30**–**36**, indicating a delocalization of the anionic charge over the guanidinate N–C–N moiety. Because of different steric and electronic properties of substituents on the N–C–N moiety, the $C^{(center)}$–$N^{(aryl)}$ and $C^{(center)}$–$N^{(isopropyl)}$ bond distances are slightly different in complexes **30**–**36**. The observed $C^{(center)}$–$N^{(isopropyl)}$ distances are marginally shorter than the $C^{(center)}$–$N^{(aryl)}$ distances. This may be ascribed to the presence of a relatively strong electron–donating Pr^{i} substituent as compared to that of the aryl substituent. A higher electron density on the $N^{(isopropyl)}$ atom resulted in a shorter Ln–$N^{(isopropyl)}$ bond, in which the observed Ln–$N^{(isopropyl)}$ bond distances listed in Table 4–10 are marginally shorter than the Ln–$N^{(aryl)}$ distances in the above complexes **30**–**36**. Both the Ln–$N^{(aryl)}$ and Ln–$N^{(isopropyl)}$ distances of complexes **30**–**36** decrease across the lanthanide series. This trend is consistent with the lanthanide contraction. Moreover, the $N^{(aryl)}$–Ln–$N^{(isopropyl)}$ bite angles increase across the lanthanide series. When the Ln–N distances decrease, an increase in steric repulsion forces the aryl and isopropyl substituents around the coordinated $N^{(aryl)}$ and $N^{(isopropyl)}$ atoms pointing away from the metal center, resulted in an increment of the bite angle.

The Ce–N distances of 2.480(2)–2.514(2) Å in **30** are slightly longer than the corresponding distances of 2.422(8)–2.507(2) Å in $[Ce\{Bu^{t}NC(CH_3)NBu^{t}\}_3]$.[19]

However, they are comparable to the corresponding distances of 2.487(5)–2.502(5) Å in $[Ce\{(PhC{\equiv}C)C(NPr^{i})_2\}_3]$[20] and 2.482(2)–2.492(2) Å in $[Ce\{Pr^{i}NC(Ph)NPr^{i}\}_3]$.[21]

The $N^{(aryl)}$–Ce–$N^{(isopropyl)}$ bite angles of 53.58(8)–53.71(7)° in **30** are similar to those of 52.44(7)–54.7(3)° in $[Ce\{Bu^{t}NC(CH_3)NBu^{t}\}_3]$,[19] 54.1(2) and 54.3(2)° in $[Ce\{(PhC{\equiv}C)C(NPr^{i})_2\}_3]$[20] and 53.95(5)–54.12(7)° in $[Ce\{Pr^{i}NC(Ph)NPr^{i}\}_3]$.[21]

The Pr–N distances of 2.463(2)–2.503(2) Å in **31** are similar to those of 2.460(4)–2.468(4) Å in the four–membered tris(guanidinate) complex $[Pr\{PhC(NCy)_2\}_3]$,[22] and 2.479(5)–2.536(5) Å in the six–membered tris(β–diketiminate) complex $[Pr\{(4\text{–}ClC_6H_4)NC(Me)\}_2CH\}_3]$.[23] However, they are reasonably longer than those of 2.423(8)–2.431(8) Å in the ate–complex $[\{\{(Me_3Si)_2N\}_4Pr\}\{K(THF)_6\}]$.[24] This suggests that an increase in the coordination number around the metal center resulted in a longer metal–ligand bond distance.

The $N^{(aryl)}$–Pr–$N^{(isopropyl)}$ bite angles of 54.10(7)–54.15(8)° in **31** are similar to the corresponding angles of 54.8(2)° in the four–membered $[Pr\{PhC(NCy)_2\}_3]$,[22] but are much smaller than those of 71.6(2)–74.9(2)° in the six–membered $[Pr\{(4\text{–}ClC_6H_4)NC(Me)\}_2CH\}_3]$.[23]

The Gd–N distances of 2.398(3)–2.428(3) Å in **32** are comparable to those reported for other Gd(III) tris(guanidinate) complexes such as, $[Gd\{(NPr^{i})_2CNMe_2\}_3]$ [2.410(7) Å],[19] $[Gd\{(NPr^{i})_2CNEt_2\}_3]$ [2.406(9) Å][19] and $[Gd\{(NPr^{i})_2CNPr^{i}_2\}_3]$

[2.405(4) Å][19] and Gd(III) tris(2–pyridylamide) complex [Gd{6–Me–2–($SiMe_3N$)C_5H_3N}$_3$] [2.334(7)–2.460(7) Å],[25] but they are slightly shorter than those of 2.415(5)–2.601(5) Å in the eight–coordinated Gd(III) dipyridylamide complex [Gd_2{$N(C_5H_4N)_2$}$_6$].[26]

The $N^{(aryl)}$–Gd–$N^{(isopropyl)}$ bite angles of 55.56(9)–55.87(9)^o in **32** are similar to those of 55.82(7)–55.90(7)^o in [Gd{$(NPr^i)_2CNMe_2$}$_3$],[19] 55.6(2) and 55.9(2)^o in [Gd{$(NPr^i)_2CNEt_2$}$_3$][19] and 55.69(7) and 55.0(1)^o in [Gd{$(NPr^i)_2CNPr^i_2$}$_3$],[19] but are slightly smaller than those of 56.5(2)–56.8(2)^o in [Gd{6–Me–2–($SiMe_3N$)C_5H_3N}$_3$].[25]

The Tb–N distances of 2.383(3)–2.417(2) Å in **33** are similar to the corresponding distances of 2.380(6)–2.411(6) Å in the six–coordinate complex [Tb{$Pr^iNC(NPr^i_2)NPr^i$}$_3$],[7c] but are reasonably longer than those of 2.23(1) Å in the three–coordinate complex [Tb{$N(SiMe_3)_2$}$_3$].[27]

The $N^{(aryl)}$–Tb–$N^{(isopropyl)}$ bite angles of 55.95(8)–56.07(8)^o in **33** are marginally smaller than those of 56.2(2)–56.6(2)^o in [Tb{$Pr^iNC(NPr^i_2)NPr^i$}$_3$].[7c]

The Ho–N distances of 2.357(3)–2.392(3) Å in **34** are reasonably longer than those of 2.235(2)–2.278(2) Å in the monodentate Ho(III) tris(amide) complex [Ho{$N(SiHMe_2)_2$}$_3$$(THF)_2$],[28] but are similar to the corresponding distances of 2.367(6)–2.386(7) Å in the six–coordinated Ho(III) tris(amidinate) complex [{$Ho(EtForm)_3$}·2THF].[29] On the other hand, they are marginally shorter than those

of 2.366(5)–2.516(5) Å in the eight–coordinated Ho(III) dipyridylamide complex $[Ho_2\{N(C_5H_4N)_2\}_6]$.[30]

The $N^{(aryl)}$–Ho–$N^{(isopropyl)}$ bite angles of 56.66(9)–56.81(9)^o in **34** are similar to the corresponding angles of 56.4(3)–57.4(3)^o in $[\{Ho(EtForm)_3\}\cdot 2THF]$,[28] but are smaller than those of 73.4(2)–87.3(2)^o in $[Ho_2\{N(C_5H_4N)_2\}_6]$.[30]

The Er–N distances of 2.343(3)–2.377(2) Å in **35** are similar to those in the six–coordinate complex $[Er\{Bu^tNC(CH_3)NBu^t\}_3]$ [2.35(1)–2.41(1) Å][19] and $[Er\{6\text{–}Me\text{–}2\text{–}(SiMe_3N)C_5H_3N\}_3]$ [2.279(4)–2.387(4) Å],[25] but are reasonably shorter than those in the eight–coordinate complex $[Er(PhNNNPh)_3(C_5H_5N)_2\cdot(C_5H_5N)_{1.0}\cdot(C_7H_8)_{0.5}]$ [2.378(6)–2.484(6) Å][31] and $[Er_2\{N(C_5H_4N)_2\}_6]$ [2.367(9)–2.513(9) Å].[30]

The $N^{(aryl)}$–Er–$N^{(isopropyl)}$ bite angles of 56.96(8)–57.06(7)^o in **35** are similar to the corresponding angles of 56.6(6) and 57.2(5)^o in $[Er\{Bu^tNC(CH_3)NBu^t\}_3]$,[19] but are smaller than those of 73.4(4)–88.8(4)^o in $[Er_2\{N(C_5H_4N)_2\}_6]$.[30]

The Tm–N distances of 2.331(2)–2.368(2) Å in **36** are comparable to the corresponding distances of 2.355(4)–2.517(4) Å in the eight–coordinated Tm(III) dipyridylamide complex $[Tm_2\{N(C_5H_4N)_2\}_6]$.[30]

The N(1)–Tm(1)–N(3), N(4)–Tm(1)–N(6) and N(7)–Tm(1)–N(9) bite angles are acute, namely 57.05(8), 57.11(9) and 57.44(8)^o.

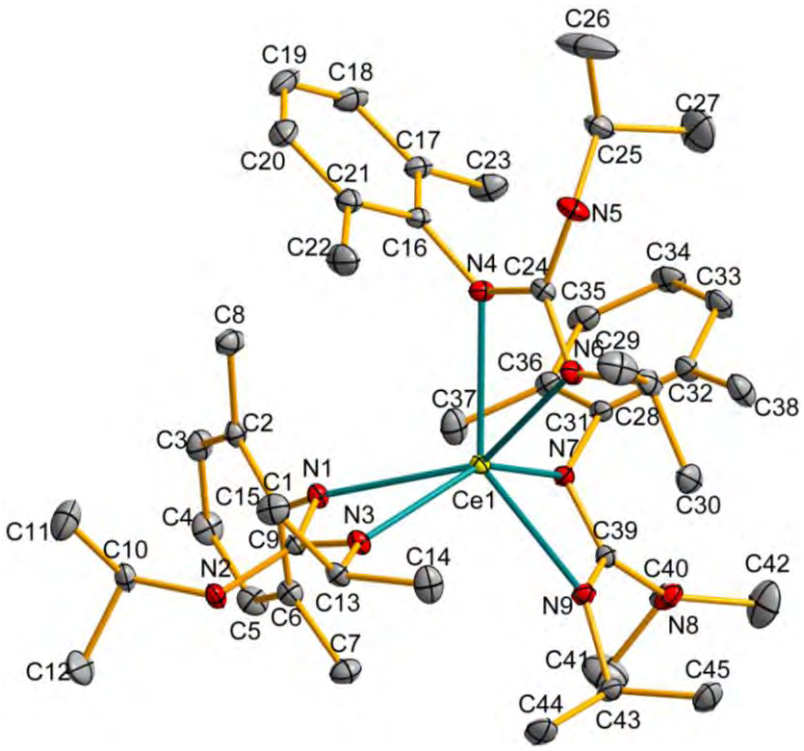

Figure 4–1. Molecular structure of $[Ce(L^1)_3]$ (**30**)

Table 4–2. Selected bond distances (Å) and angles (deg.) for compound **30**

$[Ce(L^1)_3]$ (**30**)			
Ce(1)–N(1)	2.480(2)	Ce(1)–N(3)	2.490(2)
Ce(1)–N(4)	2.514(2)	Ce(1)–N(6)	2.482(2)
Ce(1)–N(7)	2.503(2)	Ce(1)–N(9)	2.504(2)
N(1)–C(9)	1.336(3)	N(2)–C(9)	1.371(3)
N(3)–C(9)	1.334(3)	N(4)–C(24)	1.336(4)
N(5)–C(24)	1.378(4)	N(6)–C(24)	1.326(4)
N(7)–C(39)	1.338(3)	N(8)–C(39)	1.373(3)
N(9)–C(39)	1.335(3)		
N(1)–Ce(1)–N(3)	53.63(7)	N(4)–Ce(1)–N(6)	53.58(8)
N(7)–Ce(1)–N(9)	53.71(7)	N(1)–C(9)–N(3)	114.2(2)
N(4)–C(24)–N(6)	115.6(2)	N(7)–C(39)–N(9)	115.6(2)

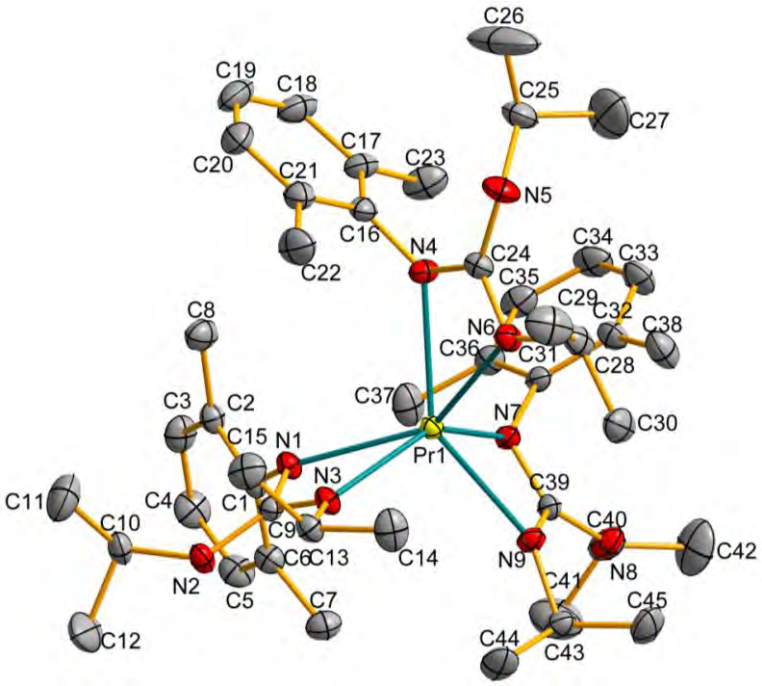

Figure 4–2. Molecular structure of $[Pr(L^1)_3]$ (**31**)

Table 4–3. Selected bond distances (Å) and angles (deg.) for compound **31**

$[Pr(L^1)_3]$ (**31**)			
Pr(1)–N(1)	2.463(2)	Pr(1)–N(3)	2.476(2)
Pr(1)–N(4)	2.503(2)	Pr(1)–N(6)	2.463(2)
Pr(1)–N(7)	2.478(2)	Pr(1)–N(9)	2.489(2)
N(1)–C(9)	1.347(3)	N(2)–C(9)	1.365(3)
N(3)–C(9)	1.335(3)	N(4)–C(24)	1.344(4)
N(5)–C(24)	1.380(4)	N(6)–C(24)	1.328(4)
N(7)–C(39)	1.340(3)	N(8)–C(39)	1.373(4)
N(9)–C(39)	1.333(3)		
N(1)–Pr(1)–N(3)	54.10(7)	N(4)–Pr(1)–N(6)	54.15(8)
N(7)–Pr(1)–N(9)	54.14(7)	N(1)–C(9)–N(3)	113.8(2)
N(4)–C(24)–N(6)	115.6(2)	N(7)–C(39)–N(9)	115.57(2)

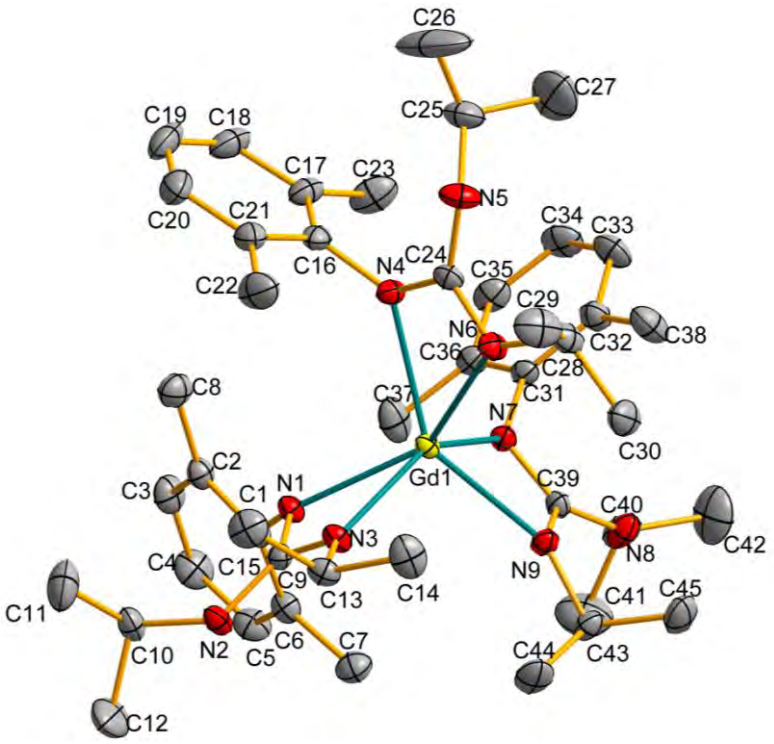

Figure 4–3. Molecular structure of $[Gd(L^1)_3]$ (**32**)

Table 4–4. Selected bond distances (Å) and angles (deg.) for compound **32**

$[Gd(L^1)_3]$ (**32**)			
Gd(1)–N(1)	2.401(3)	Gd(1)–N(3)	2.403(3)
Gd(1)–N(4)	2.428(3)	Gd(1)–N(6)	2.398(3)
Gd(1)–N(7)	2.413(2)	Gd(1)–N(9)	2.411(3)
N(1)–C(9)	1.341(4)	N(2)–C(9)	1.370(4)
N(3)–C(9)	1.330(4)	N(4)–C(24)	1.336(4)
N(5)–C(24)	1.373(4)	N(6)–C(24)	1.325(5)
N(7)–C(39)	1.346(4)	N(8)–C(39)	1.370(4)
N(9)–C(39)	1.332(4)		
N(1)–Gd(1)–N(3)	55.56(9)	N(4)–Gd(1)–N(6)	55.6(1)
N(7)–Gd(1)–N(9)	55.87(9)	N(1)–C(9)–N(3)	113.9(3)
N(4)–C(24)–N(6)	115.4(3)	N(7)–C(39)–N(9)	115.1(3)

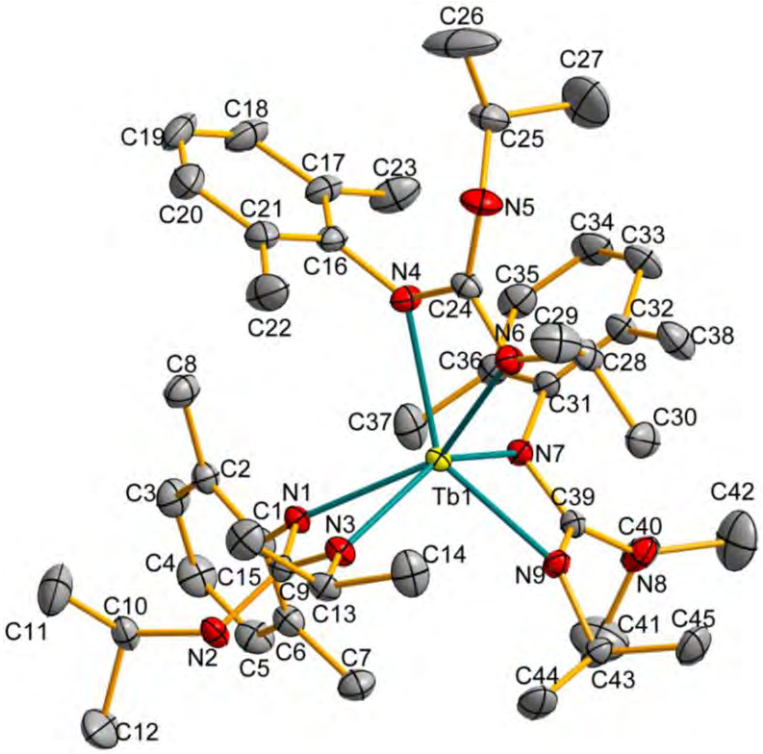

Figure 4–4. Molecular structure of $[Tb(L^1)_3]$ (**33**)

Table 4–5. Selected bond distances (Å) and angles (deg.) for compound **33**

$[Tb(L^1)_3]$ (**33**)			
Tb(1)–N(1)	2.386(3)	Tb(1)–N(3)	2.392(2)
Tb(1)–N(4)	2.417(2)	Tb(1)–N(6)	2.383(3)
Tb(1)–N(7)	2.394(2)	Tb(1)–N(9)	2.402(2)
N(1)–C(9)	1.341(4)	N(2)–C(9)	1.371(4)
N(3)–C(9)	1.333(4)	N(4)–C(24)	1.340(4)
N(5)–C(24)	1.378(4)	N(6)–C(24)	1.327(5)
N(7)–C(39)	1.338(4)	N(8)–C(39)	1.371(4)
N(9)–C(39)	1.335(4)		
N(1)–Tb(1)–N(3)	55.95(8)	N(4)–Tb(1)–N(6)	55.96(9)
N(7)–Tb(1)–N(9)	56.07(8)	N(1)–C(9)–N(3)	113.9(2)
N(4)–C(24)–N(6)	115.2(3)	N(7)–C(39)–N(9)	115.0(3)

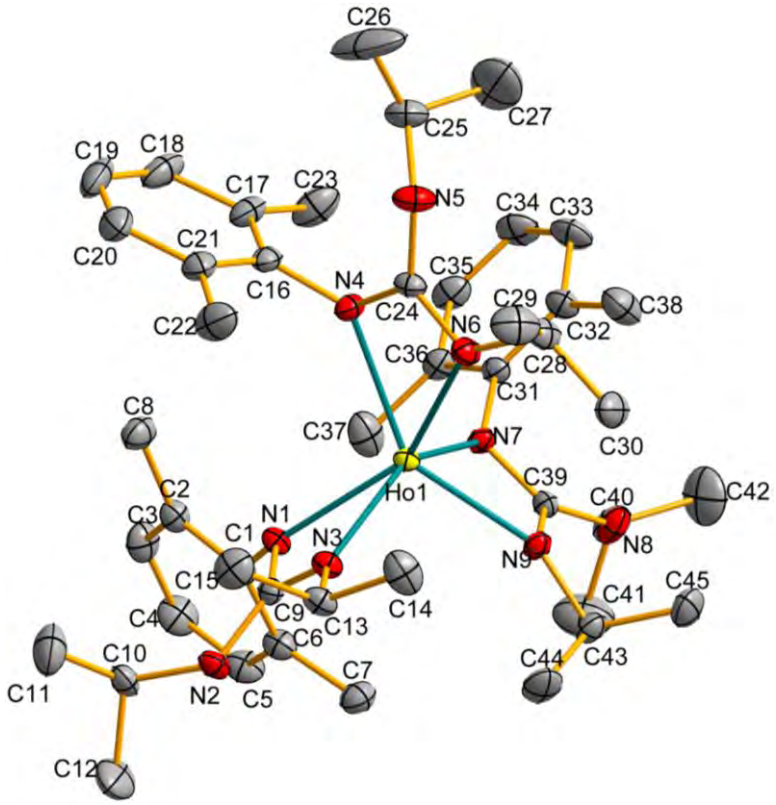

Figure 4–5. Molecular structure of $[Ho(L^1)_3]$ (**34**)

Table 4–6. Selected bond distances (Å) and angles (deg.) for compound **34**

$[Ho(L^1)_3]$ (**34**)			
Ho(1)–N(1)	2.362(3)	Ho(1)–N(3)	2.371(3)
Ho(1)–N(4)	2.392(3)	Ho(1)–N(6)	2.357(3)
Ho(1)–N(7)	2.371(2)	Ho(1)–N(9)	2.377(3)
N(1)–C(9)	1.350(4)	N(2)–C(9)	1.363(4)
N(3)–C(9)	1.331(4)	N(4)–C(24)	1.344(5)
N(5)–C(24)	1.377(5)	N(6)–C(24)	1.330(4)
N(7)–C(39)	1.342(4)	N(8)–C(39)	1.367(4)
N(9)–C(39)	1.338(4)		
N(1)–Ho(1)–N(3)	56.66(9)	N(4)–Ho(1)–N(6)	56.7(1)
N(7)–Ho(1)–N(9)	56.81(9)	N(1)–C(9)–N(3)	113.8(3)
N(4)–C(24)–N(6)	115.1(3)	N(7)–C(39)–N(9)	114.9(3)

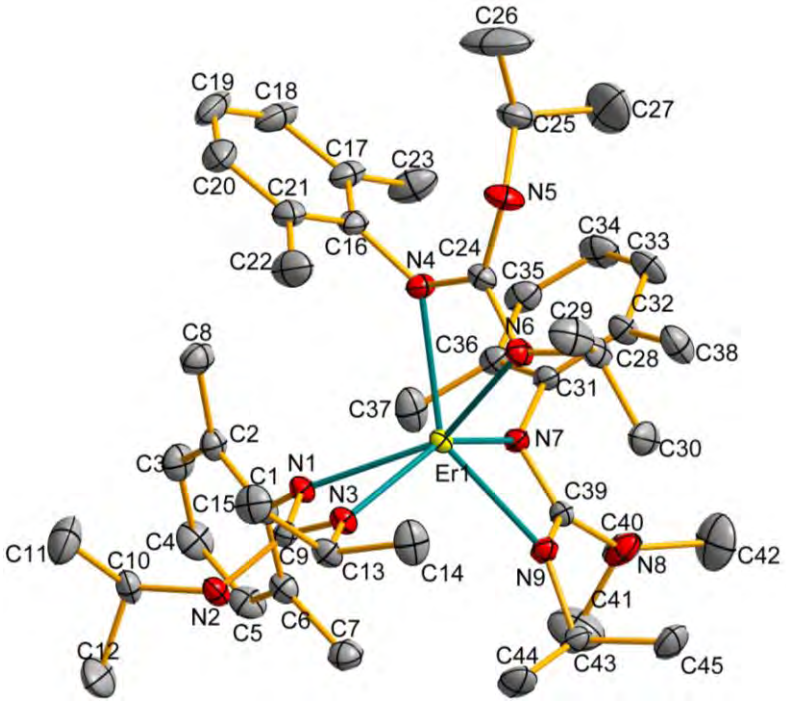

Figure 4–6. Molecular structure of $[Er(L^1)_3]$ (**35**)

Table 4–7. Selected bond distances (Å) and angles (deg.) for compound **35**

$[Er(L^1)_3]$ (**35**)			
Er(1)–N(1)	2.352(2)	Er(1)–N(3)	2.354(2)
Er(1)–N(4)	2.377(2)	Er(1)–N(6)	2.343(3)
Er(1)–N(7)	2.355(2)	Er(1)–N(9)	2.365(2)
N(1)–C(9)	1.343(3)	N(2)–C(9)	1.372(3)
N(3)–C(9)	1.337(3)	N(4)–C(24)	1.336(3)
N(5)–C(24)	1.375(3)	N(6)–C(24)	1.335(4)
N(7)–C(39)	1.335(3)	N(8)–C(39)	1.376(3)
N(9)–C(39)	1.332(3)		
N(1)–Er(1)–N(3)	57.06(7)	N(4)–Er(1)–N(6)	56.96(8)
N(7)–Er(1)–N(9)	56.98(7)	N(1)–C(9)–N(3)	114.0(2)
N(4)–C(24)–N(6)	114.9(2)	N(7)–C(39)–N(9)	115.1(2)

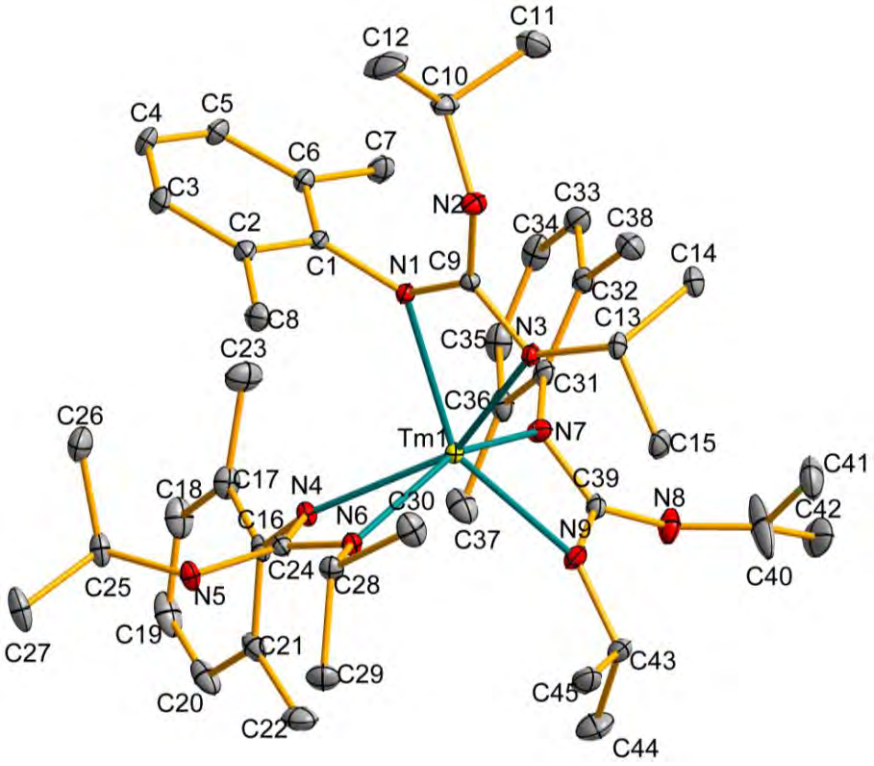

Figure 4–7. Molecular structure of $[Tm(L^1)_3]$ (**36**)

Table 4–8. Selected bond distances (Å) and angles (deg.) for compound **36**

$[Tm(L^1)_3]$ (**36**)			
Tm(1)–N(1)	2.368(2)	Tm(1)–N(3)	2.331(2)
Tm(1)–N(4)	2.344(2)	Tm(1)–N(6)	2.357(2)
Tm(1)–N(7)	2.332(2)	Tm(1)–N(9)	2.339(3)
N(1)–C(9)	1.345(4)	N(2)–C(9)	1.366(4)
N(3)–C(9)	1.338(4)	N(4)–C(24)	1.355(4)
N(5)–C(24)	1.372(4)	N(6)–C(24)	1.329(5)
N(7)–C(39)	1.331(4)	N(8)–C(39)	1.390(4)
N(9)–C(39)	1.324(4)		
N(1)–Tm(1)–N(3)	57.05(8)	N(4)–Tm(1)–N(6)	57.44(8)
N(7)–Tm(1)–N(9)	57.11(9)	N(1)–C(9)–N(3)	113.6(3)
N(4)–C(24)–N(6)	114.6(2)	N(7)–C(39)–N(9)	114.5(3)

2. $[\{Ln(L^1)_2(\mu\text{–}Cl)\}_2]$ [Ln = Ce (**37**), Lu (**38**)]

Complexes **37** and **38** crystallize in a dimeric form, in which each metal center is coordinated by two κ^2–bound L^1 ligands and two bridging chloride ligands. For complex **37**, the coordination geometry around Ce(1) {Ce(2)} can be best described as distorted octahedral. The two axial positions are occupied by N(6) and Cl(2) {N(9) and Cl(1)} [N(6)–Ce(1)–Cl(2) = 152.7(2)^o {N(9)–Ce(3)–Cl(1) = 147.3(1)^o}], whereas the equatorial plane consists of N(1), N(3), N(4) and Cl(1) {N(7), N(10), N(12) and Cl(2)} [sum of bond angles around Ce(1) = 369.8^o {Ce(2) = 371.9^o}]. The coordination geometry around the Lu(1) atom in **38** can also be described as distorted octahedral, with the two axial positions being occupied by N(1) and Cl(1)#1 [N(1)–Lu(1)–Cl(1)#1 = 152.6(1)^o], whereas the equatorial plane consists of N(3), N(4), N(6) and Cl(1) [sum of bond angles around Lu(1) = 363.5^o]. It is suggested that the difference in ionic radii of Ce^{3+} (1.01 Å) and Lu^{3+} (0.86 Å)[32] led to a different in the coordination geometry between complexes **37** and **38** (the axial position of the Ce(III) center is occupied by the nitrogen atom which is attached to an isopropyl substituent, whereas the axial position of the Lu(III) center is occupied by the nitrogen atom which is attached to an aryl substituent).

Complex **37** crystallizes in the triclinic space group $P\bar{1}$. The binuclear complex consists of a planar Ce_2Cl_2 core (angle sum of the Ce_2Cl_2 plane is 359.8^o).

The observed Ce–N distances of 2.421(5)–2.461(6) Å in **37** are shorter than those of 2.480(2)–2.514(2) Å in **30**. This may be due to a less steric congestion environment around the metal center exerted by the two chloride ligands as compared to one L^1 ligand. They are reasonably longer than those of 2.320(7) and 2.342(7) Å in the monodentate [{Ce(N(SiMe$_3$)$_2$)$_2$(μ–Cl)(THF)}$_2$],[33] but are similar to those of 2.423(6)–2.487(5) Å in the five–coordinate complex [Ce(Cl){(N(SiMe$_3$)C(Ph))$_2$CH}$_2$][34] and 2.438(4)–2.761(4) Å in the seven–coordinate complex [{Ce(N(SiMe$_3$)C(Ph)N(CH$_2$)$_3$NMe$_2$)$_2$(μ–Cl)}$_2$].[35]

The Ce–Cl distances of 2.847(2)–2.8712 Å in **37** are comparable to those of 2.843(2) and 2.859(2) Å in the dimeric [{Ce(N(SiMe$_3$)$_2$)$_2$(μ–Cl)(THF)}$_2$],[33] 2.866(2) and 2.884(2) Å in [{Ce(N(SiMe$_3$)C(Ph)N(CH$_2$)$_3$NMe$_2$)$_2$(μ–Cl)}$_2$],[35] but are longer than that of 2.697(2) Å in the monomeric [Ce(Cl){(N(SiMe$_3$)C(Ph))$_2$CH}$_2$].[34]

The observed $N^{(aryl)}$–Ce–$N^{(isopropyl)}$ bite angles of 54.7(2)–55.0(2)^o in **37** are comparable to those of 54.0(1) and 54.2(1)^o in the four–membered [{Ce(N(SiMe$_3$)C(Ph)N(CH$_2$)$_3$NMe$_2$)$_2$(μ–Cl)}$_2$],[35] but are smaller than those of 78.2(2) and 108.4(2)^o in the six–membered [Ce(Cl){(N(SiMe$_3$)C(Ph))$_2$CH}$_2$].[34] This suggests an increase in the metallocyclic ring size resulted in an increase in the N–M–N bite angle.

Complex **38** crystallizes in the tetragonal space group $P\bar{4}2_1c$. This complex

also has a planar Lu_2Cl_2 core (angle sum of the Lu_2Cl_2 plane is 358.7°) similar to that in complex **37**.

The observed Lu–N distances of 2.276(5)–2.290(5) Å in complex **38** is marginally longer than those of 2.184(3)–2.238(3) Å in the five–coordinated Lu(III) tris(amide) complex $[Lu\{N(SiMe_3)_2\}_3(THF)_2]$,[36] but are similar to those in the Lu(III) ate–complexs $[Lu\{(Me_3Si)_2NC(NPr^i)_2\}_2(\mu\text{–}Cl)_2Li(THF)_2]$ [2.285(1)–2.346(2) Å][14a] and $[Lu\{(Me_3Si)_2NC(NCy)_2\}_2(\mu\text{–}Cl)_2Li(THF)_2]$ [2.320(5) and 2.291(5) Å][10] and the Lu(III) bis(2–pyridylamide) complex $[LuAp'_2Cl(THF)]$ (Ap' = (2,6–diisopropyl)[6–(2,6–dimethylphenyl)pyridin–2–yl]amide) [$Lu\text{–}N^{(amide)}$ = 2.246(8) and 2.248(7) Å, $Lu\text{–}N^{(pyridyl)}$ = 2.422(8) and 2.46(1) Å].[37]

The Lu(1)–Cl(1) and Lu(1)–Cl(1)#1 distances of 2.651(1) and 2.677(2) Å in complex **38** are shorter than those of 2.7472 Å in $[Lu\{(Me_3Si)_2NC(NCy)_2\}_2(\mu\text{–}Cl)_2Li(THF)_2]$,[10] but are longer than those of 2.600(1) and 2.623(1) Å in $[Lu\{(Me_3Si)_2NC(NPr^i)_2\}_2(\mu\text{–}Cl)_2Li(THF)_2]$.[14a]

The N(4)–Lu(1)–N(6) and N(1)–Lu(1)–N(3) bite angles of 58.4(2) and 58.5(2)° are similar to those in other four–membered Lu(III) complexes, such as $[Lu\{(Me_3Si)_2NC(NPr^i)_2\}_2(\mu\text{–}Cl)_2Li(THF)_2]$ [57.86(6) and 57.87(6)°],[14a] $[Lu\{(Me_3Si)_2NC(NCy)_2\}_2(\mu\text{–}Cl)_2Li(THF)_2]$ [57.74(7)°][8] and $[LuAp'_2Cl(THF)]$ [56.7(3) and 58.7(2)°].[37]

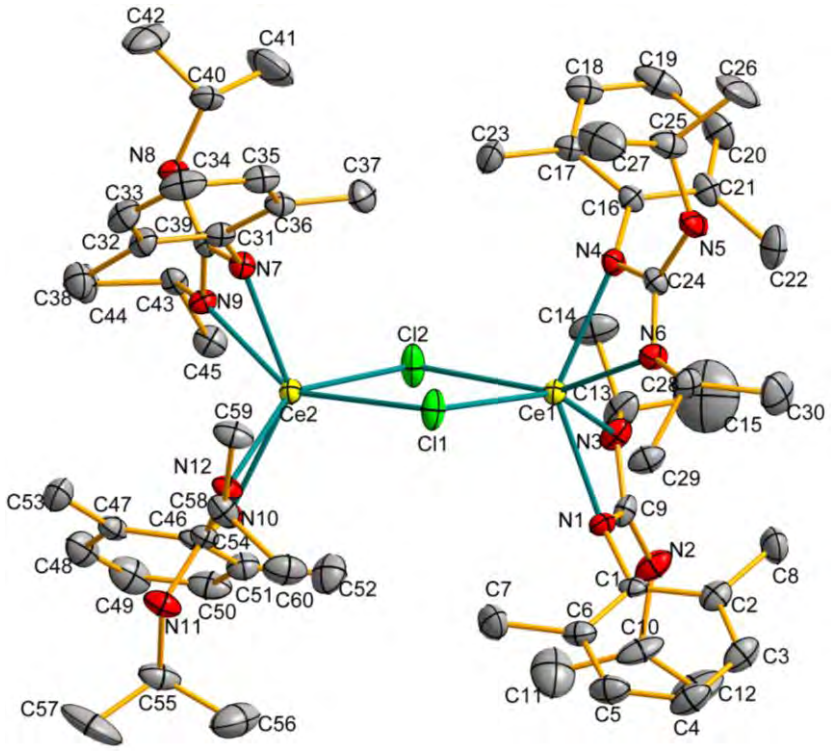

Figure 4–8. Molecular structure of [{Ce(L^1)$_2$(μ–Cl)}$_2$] (**37**)

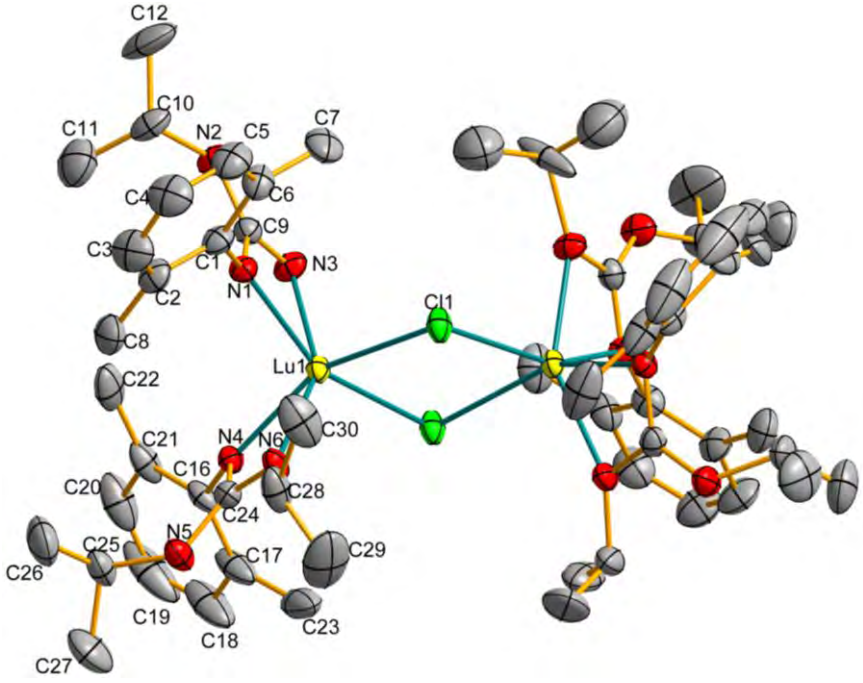

Figure 4–9. Molecular structure of [{Lu(L^1)$_2$(μ–Cl)}$_2$] (**38**)

Table 4–9. Selected bond distances (Å) and angles (deg.) for compound **37**

[{Ce(L^1)$_2$(μ–Cl)}$_2$] (**37**)			
Ce(1)–N(1)	2.421(5)	Ce(1)–N(3)	2.443(6)
Ce(1)–N(4)	2.435(5)	Ce(1)–N(6)	2.452(7)
Ce(2)–N(7)	2.438(5)	Ce(2)–N(9)	2.461(6)
Ce(2)–N(10)	2.459(4)	Ce(2)–N(12)	2.439(6)
Ce(1)–Cl(1)	2.860(2)	Ce(1)–Cl(2)	2.855(3)
Ce(2)–Cl(1)	2.871(2)	Ce(2)–Cl(2)	2.847(2)
N(1)–C(9)	1.346(8)	N(2)–C(9)	1.360(9)
N(3)–C(9)	1.356(9)	N(4)–C(24)	1.351(8)
N(5)–C(24)	1.375(8)	N(6)–C(24)	1.320(9)
N(7)–C(39)	1.360(8)	N(8)–C(39)	1.365(9)
N(9)–C(39)	1.340(8)	N(10)–C(54)	1.356(7)
N(11)–C(54)	1.365(8)	N(12)–C(54)	1.329(7)
N(1)–Ce(1)–N(3)	55.0(2)	N(4)–Ce(1)–N(6)	54.8(2)
N(7)–Ce(2)–N(9)	54.8(2)	N(10)–Ce(2)–N(12)	54.7(2)
Ce(1)–Cl(1)–Ce(2)	103.14(5)	Ce(1)–Cl(2)–Ce(2)	103.87(6)
Cl(1)–Ce(1)–Cl(2)	76.42(5)	Cl(1)–Ce(2)–Cl(2)	76.39(5)
N(6)–Ce(1)–Cl(2)	152.7(2)	N(9)–Ce(2)–Cl(1)	147.3(1)
N(1)–Ce(1)–Cl(1)	105.9(1)	N(4)–Ce(1)–Cl(1)	108.2(1)
N(3)–Ce(1)–N(4)	100.7(2)	N(7)–Ce(2)–Cl(2)	109.6(1)
N(10)–Ce(2)–Cl(2)	104.0(1)	N(7)–Ce(2)–N(12)	103.6(2)
N(1)–C(9)–N(3)	112.5(6)	N(4)–C(24)–N(6)	114.5(6)
N(7)–C(39)–N(9)	113.2(6)	N(10)–C(54)–N(12)	113.9(6)

Table 4–10. Selected bond distances (Å) and angles (deg.) for compound **38**

[{Lu(L^1)$_2$(μ–Cl)}$_2$] (**38**)			
Lu(1)–N(1)	2.284(5)	Lu(1)–N(3)	2.276(5)
Lu(1)–N(4)	2.276(5)	Lu(1)–N(6)	2.290(5)
Lu(1)–Cl(1)	2.651(1)	Lu(1)–Cl(1)#1	2.677(2)
N(1)–C(9)	1.333(8)	N(2)–C(9)	1.360(9)
N(3)–C(9)	1.332(8)	N(4)–C(24)	1.343(8)
N(5)–C(24)	1.376(8)	N(6)–C(24)	1.322(8)
N(1)–Lu(1)–N(3)	58.5(2)	N(4)–Lu(1)–N(6)	58.4(2)
Lu(1)–Cl(1)–Lu(1)#1	100.26(5)	Cl(1)–Lu(1)–Cl(1)#1	79.10(5)
N(1)–Lu(1)–Cl(1)#1	152.6(1)	N(3)–Lu(1)–Cl(1)	105.4(1)
N(3)–Lu(1)–N(4)	102.8(2)	N(6)–Lu(1)–Cl(1)	96.9(1)
N(1)–C(9)–N(3)	113.4(6)	N(4)–C(24)–N(6)	113.2(5)

Symmetry code: #1 –x, –y+1, z

4.3 Summary

A series of lanthanide(III) complexes supported by the guanidinate ligand $[(2,6\text{–}Me_2C_6H_3N)C(NHPr^i)(NPr^i)]^-$ (L^1) have been synthesized and structurally characterized. Metathetical reactions of $LnCl_3$ (Ln = Ce, Pr, Gd, Tb, Ho, Er, Tm) with three equivalents of $[KL^1 \cdot 0.5PhMe]_n$ (**1**) gave mononuclear, homoleptic complexes $[Ln(L^1)_3]$ [Ln = Ce (**30**), Pr (**31**), Gd (**32**), Tb (**33**), Ho (**34**), Er (**35**), Tm (**36**)]. Dimeric complexes $[\{Ln(L^1)_2(\mu\text{–}Cl)\}_2]$ [Ln = Ce (**37**), Lu (**38**)] were isolated by the reactions of $LnCl_3$ (Ln = Ce, Lu) with two equivalents of **1**.

4.4 Experimental Section for Chapter 4

Starting Materials:

Anhydrous $LnCl_3$ (Ln = Ce, Pr, Gd, Tb, Ho, Er, Tm, Lu) were purchased from Strem and used as received. The potassium reagent $[KL^1 \cdot 0.5PhMe]_n$ (**1**) was prepared according to the procedure as described in Chapter 2.

General procedure for the preparation of $[Ln(L^1)_3]$. To a slurry of $LnCl_3$ in THF(20 ml) at 0 ^oC was added dropwise a colorless solution of complex **1** (three equivalents) in the same solvent (20 ml). The reaction mixture was allowed to warm slowly to room temperature and stirred for 1 d. All the volatiles were removed in *vacuo* and the residue was extracted with pentane (30 ml). The solution was filtered and then concentrated to *ca*. 5 ml to give the desired complex $[Ln(L^1)_3]$.

Synthesis of $[Ce(L^1)_3]$ (30). $CeCl_3$: 0.57 g, 2.30 mmol; Complex **1**: 2.05 g, 6.20 mmol. Complex **30** was isolated as yellow crystals. Yield: 1.23 g, 1.4 mmol, 70%. M.p.: 174–176 ^oC. Anal. Found: C, 61.41; H, 8.51; N, 14.27%. Calc. for $C_{45}CeH_{72}N_9$: C, 61.47; H, 8.25; N, 14.33%.

Synthesis of $[Pr(L^1)_3]$ (31). $PrCl_3$: 0.68 g, 2.75 mmol; Complex **1**: 2.64 g, 7.96 mmol. Complex **31** was isolated as pale green crystals. Yield: 1.81 g, 2.05 mmol, 77%. M.p.: 189–192 ^oC. Anal. Found: C, 61.15; H, 8.88; N, 14.69%. Calc. for $C_{45}H_{72}N_9Pr$: C, 61.42; H, 8.25; N, 14.32%.

Synthesis of [Gd(L^1)$_3$] (32). $GdCl_3$: 0.74 g, 2.83 mmol; Complex **1**: 2.56 g, 7.73 mmol. Complex **32** was isolated as colorless crystals. Yield: 1.66 g, 1.85 mmol, 72%. M.p.: 176–178 ^oC. Anal. Found: C, 59.69; H, 8.38; N, 14.25%. Calc. for $C_{45}GdH_{72}N_9$: C, 60.30; H, 8.10; N, 14.06%.

Synthesis of [Tb(L^1)$_3$] (33). $TbCl_3$: 0.60 g, 2.26 mmol; Complex **1**: 2.11 g, 6.37 mmol. Complex **33** was isolated as colorless crystals. Yield: 1.43 g, 1.59 mmol, 75%. M.p.: 173–174 ^oC. Anal. Found: C, 59.94; H, 8.40; N, 14.34%. Calc. for $C_{45}H_{72}N_9Tb$: C, 60.19; H, 8.08; N, 14.03%.

Synthesis of [Ho(L^1)$_3$] (34). $HoCl_3$: 0.71 g, 2.61 mmol; Complex **1**: 2.37 g, 7.16 mmol. Complex **34** was isolated as pink crystals. Yield: 1.73 g, 1.91 mmol, 80%. M.p.: 173–174 ^oC. Anal. Found: C, 59.43; H, 8.26; N, 14.39%. Calc. for $C_{45}H_{72}HoN_9$: C, 59.79; H, 8.03; N, 13.94%.

Synthesis of [Er(L^1)$_3$] (35). $ErCl_3$: 0.65 g, 2.38 mmol; Complex **1**: 2.11 g, 6.37 mmol. Complex **35** was isolated as colorless crystals. Yield: 1.50 g, 1.66 mmol, 78%. M.p.: 162–164 ^oC. Anal. Found: C, 59.22; H, 8.59; N, 14.35%. Calc. for $C_{45}ErH_{72}N_9$: C, 59.63; H, 8.01; N, 13.90%.

Synthesis of [Tm(L^1)$_3$] (36). $TmCl_3$: 0.65 g, 2.37 mmol; Complex **1**: 2.33 g, 7.04 mmol. Complex **36** was isolated as colorless crystals. Yield: 1.75 g, 1.92 mmol, 82%. M.p.: 175–176 ^oC. Anal. Found: C, 59.27; H, 8.25; N, 14.14%. Calc. for

$C_{45}H_{72}N_9Tm$: C, 59.52; H, 7.99; N, 13.88%.

Synthesis of [{Ce(L^1)$_2$(μ–Cl)}$_2$] (37). To a slurry of $CeCl_3$ (0.79 g, 3.2 mmol) in THF (20 ml) at 0 ^oC was slowly added a colorless solution of complex **1** (2.12 g, 6.4 mmol) in the same solvent (20 ml). The reaction mixture was allowed to warm slowly to room temperature and stirred for 1 d. All the volatiles were removed in *vacuo* and the residue was extracted with hexane (30 ml). The solution was filtered and then concentrated to *ca*. 5 ml to give complex **37** as yellow crystals. Yield: 1.49 g, 1.12 mmol, 70%. M.p.: 180–181. ^oC. Anal. Found: C, 54.09; H, 7.73; N, 11.86%. Calc. for $C_{60}Ce_2Cl_2H_{96}N_{12}$: C, 53.92; H, 7.24; N, 12.57%.

Synthesis of [{Lu(L^1)$_2$(μ–Cl)}$_2$] (38). Complex **38** was prepared by a procedure similar to the synthesis of **37**, using 1.06 g (3.77 mmol) of $LuCl_3$ and 1.99 g (6.01 mmol) of complex **1**. Complex **38** was isolated as colorless crystals. Yield: 1.48 g, 2.10 mmol, 70%. M.p.: 189–190 ^oC. ^1H NMR (400.13 MHz, C_6D_6): δ 0.72 (br, 24H, CH(C*H*$_3$)$_2$), 0.78 (d, *J* = 6.8 Hz, 24H, CH(C*H*$_3$)$_2$), 2.17 (s, 24H, ArC*H*$_3$), 2.83 (d of septet, J_1 = 6.4 Hz, J_2 = 9.8 Hz, 4H, C*H*(CH$_3$)$_2$), 3.21 (septet, *J* = 6.3 Hz, 4H, C*H*(CH$_3$)$_2$), 3.71 (d, *J* = 9.9 Hz, 4H, N*H*), 6.66 (t, *J* = 7.4 Hz, 4H, *p*–Ar*H*), 6.81 (d, *J* = 7.4 Hz, 8H, *m*–Ar*H*). ^{13}C NMR (100.62 MHz, C_6D_6): δ 70.3, 74.7, 76.0, 95.1, 96.6, 172.7, 178.7, 184.1, 197.1, 214.3. Anal. Found: C, 51.80; H, 7.34; N, 12.48%. Calc. for $C_{60}Cl_2H_{96}Lu_2N_{12}$: C, 51.24; H, 6.88; N, 11.95%.

4.5 References for Chapter 4

1. a) Wilkinson, G.; Birmingham, J. M. *J. Am. Chem. Soc.* **1954**, *76*, 6210–6210.

   b) Birmingham, J. M.; Wilkinson, G. *J. Am. Chem. Soc.* **1956**, *78*, 42–44.

2. a) Schumann, H.; Meese-Marktscheffel, J. A.; Esser, L. *Chem. Rev.* **1995**, *95*, 865–986.

   b) Schaverien, C. J. *Adv. Organomet. Chem.* **1994**, *36*, 283–362.

   c) Evans, W. J. *Coord. Chem. Rev.* **2000**, *206*, 263–283.

   d) Evans, W. J.; Davis, B. L. *Chem. Rev.* **2002**, *102*, 2119–2136.

3. a) Edelmann, F. T. *Angew. Chem. Int. Ed.* **1995**, *34*, 2466–2488.

   b) Edelmann, F. T.; Freckmann, D. M. M.; Schumann, H. *Chem. Rev.* **2002**, *102*, 1851–1896.

   c) Roesky, P. W. *Z. Anorg. Allg. Chem.* **2003**, *629*, 1881–1894.

   d) Arndt, S.; Okuda, J. *Adv. Synth. Catal.* **2005**, *347*, 339–354.

4. a) Edelmann, F. T. *Chem. Soc. Rev.* **2009**, *38*, 2253–2268.

   b) Trifonov, A. A. *Coord. Chem. Rev.* **2010**, *254*, 1327–1347.

   c) Edelmann, F. T. *Struct. Bonding* **2010**, *137*, 109–164.

   d) Edelmann, F. T. *Chem. Soc. Rev.* **2012**, *41*, 7657–7672.

5. a) Milanov, A. P.; Fischer, R. A.; Devi, A. *Inorg. Chem.* **2008**, *47*, 11405–11416.

b) Milanov, A. P.; Thiede, T. B.; Devi, A.; Fischer, R. A. *J. Am. Chem. Soc.* **2009**, *131*, 17062–17063.

c) Thiede, T. B.; Krasnopolski, M.; Milanov, A. P.; de los Arcos, T.; Ney, A.; Becker, H. -W.; Rogalla, D.; Winter, J.; Devi, A.; Fischer, R. A. *Chem. Mater.* **2011**, *23*, 1430–1440.

6. a) Khazen, K.; von Bardeleben, H. J.; Cantin, J. L.; Bittar, A.; Granville, S.; Trodahl, H. J.; Ruck, B. *J. Phys. Rev. B* **2006**, *74*, 245330.

b) Leuenberger, F.; Parge, A.; Felsch, W.; Fauth, K. Hessler, M. *Phys. Rev. B* **2005**, *72*, 014427.

7. a) Chen, J. -L.; Yao, Y. -M.; Luo, Y. -J.; Zhou, L. -Y.; Zhang, Y.; Shen Q. *J. Organomet. Chem.* **2004**, *689*, 1019–1024.

b) Zhou, L.; Yao, Y.; Zhang, Y.; Xue, M.; Chen, J.; Shen, Q. *Eur. J. Inorg. Chem.* **2004**, 2167–2172.

c) Pang, X.; Sun, H.; Zhang, Y.; Shen, Q.; Zhang, H. *Eur. J. Inorg. Chem.* **2005**, 1487–1491.

d) Qian, C.; Zhang, X.; Li, J.; Xu, F.; Zhang, Y.; Shen, Q. *Organometallics* **2009**, *28*, 3856–3862.

e) Qian, C.; Zhang, X.; Zhang, Y.; Shen, Q. *J. Organomet. Chem.* **2010**, *695*, 747–752.

8. Zhou, Y.; Yap, G. P. A.; Richeson, D. S. *Organometallics*, **1998**, *17*, 4387–4391.

9. Yao, Y. -M.; Luo, Y. -J.; Shen, Q.; Yu, K. -B. *Chinese J. Struct. Chem.* **2004**, *23*, 391–394.

10. Trifonov, A. A.; Lyubov, D. M.; Fedorova, E. A.; Fukin, G. K.; Schumann, H.; Mühle, S.; Hummert, M.; Bochkarev, M. N. *Eur. J. Inorg. Chem.* **2006**, 747–756.

11. Lyubov, D. M.; Bubnov, A. M.; Fukin, G. K.; Dolgushin, F. M.; Yu. Antipin, M.; Pelcé, O.; Schappacher, M.; Guillaume, S. M.; Trifonov, A. A. *Eur. J. Inorg. Chem.* **2008**, 2090–2098.

12. Skvortsov, G. G.; Yakovenko, M. V.; Castro, P. M.; Fukin, G. K.; Cherkasov, A. V.; Carpentier, J. -F.; Trifonov, A. A. *Eur. J. Inorg. Chem.* **2007**, 3260–3267.

13. a) Luo, Y.; Yao, Y.; Shen, Q. *Macromolecules* **2002**, *35*, 8670–8671.

    b) Luo, Y.; Yao, Y.; Shen, Q.; Yu, K.; Weng, L. *Eur. J. Inorg. Chem.* **2003**, 318–323.

    c) Yao, Y.; Luo, Y.; Chen, J.; Zhang, Z.; Zhang, Y.; Shen, Q. *J. Organomet. Chem.* **2003**, *679*, 229–237.

14. a) Trifonov, A. A.; Fedorova, E. A.; Fukin, G. K.; Bochkarev, M. N. *Eur. J. Inorg. Chem.* **2004**, 4396–4401.

    b) Trifonov, A. A.; Skvortsov, G. G.; Lyubov, D. M.; Skorodumova, N. A.; Fukin, G. K.; Baranov, E. V.; Glushakova, V. N. *Chem. Eur. J.* **2006**, *12*,

5320–5327.

c) Ajellal, N.; Lyubov, D. M.; Sinenkov, M. A.; Fukin, G. K.; Cherkasov, A. V.; Thomas, C. M. Carpentier, J. -F.; Trifonov, A. A. *Chem*. *Eur*. *J*. **2008**, *14*, 5440–5448.

15. Giesbrecht, G. R.; Whitener, G. D.; Arnold, J. *J*. *Chem*. *Soc*., *Dalton Trans*. **2001**, 923–927.

16. Yuan, F.; Zhu, Y.; Xiong, L. *J*. *Organomet*. *Chem*. **2006**, *691*, 3377–3382.

17. Xu, X.; Zhang, Z.; Yao, Y.; Zhang Y.; Shen, Q. *Inorg*. *Chem*. **2007**, *46*, 9379–9388.

18. a) Zhang, J.; Cai, R.; Weng, L.; Zhou, X. *Organometallics* **2003**, *22*, 5385–5391.

b) Zhang, J.; Cai, R.; Weng, L.; Zhou, X. *J*. *Organomet*. *Chem*. **2003**, *672*, 94–99.

c) Zhang, J.; Cai, R.; Weng, L.; Zhou, X. *Organometallics* **2004**, *23*, 3303–3308.

d) Ma, L.; Zhang, J.; Cai, R.; Chen, Z.; Weng, L.; Zhou, X. *J*. *Organomet*. *Chem*. **2005**, *690*, 4926–4932.

e) Zhang, J.; Zhou, X.; Cai, R.; Weng, L. *Inorg*. *Chem*. **2005**, *44*, 716–722.

19. Päiväsaari, J.; Dezelah, IV, C. L.; Back, D.; EI-Kaderi, H. M., Heeg, M. J.;

Putkonen, M.; Niinistö, L.; Winter, C. H. *J. Mater. Chem.* **2005**, *15*, 4224–4233.

20. Dröse, P.; Hrib, C. G.; Edelmann, F. T. *J. Organomet. Chem.* **2010**, *695*, 1953–1956.

21. Dröse, P.; Hrib, C. G.; Blaurock, S.; Edelmann, F. T. *Acta Cryst.* **2010**, *E66*, m1474–m1474.

22. Richter, J.; Feiling, J.; Schmidt, H. -G.; Noltemeyer, M.; Brüser, W.; Edelmann, F. T. *Z. Anorg. Allg. Chem.* **2004**, *630*, 1269–1275.

23. Xue, M.; Jiao, R.; Zhang, Y.; Yao, Y.; Shen, Q. *Eur. J. Inorg. Chem.* **2009**, 4110–4118.

24. Evans, W. J.; Lee, D. S.; Rego, D. B.; Perotti, J. M.; Kozimor, S. A.; Moore, E. K.; Ziller, J. W. *J. Am. Chem. Soc.* **2004**, *126*, 14574–14582.

25. Baldamus, J.; Cole, M. L.; Helmstedt, U.; Hey-Hawkins, E. -M.; Jones, C.; Junk, P. C.; Lange, F.; Smithies, N. A. *J. Organomet. Chem.* **2003**, *665*, 33–42.

26. Müller-Buschbaum, K. *Z. Anorg. Allg. Chem.* **2003**, *629*, 2127–2132.

27. Hitchcock, P. B.; Hulkes, A. G.; Lappert, M. F.; Li, Z. *Dalton Trans.* **2004**, 129–136.

28. Rastätter, M.; Zulys, A.; Roesky, P. W. *Chem. Eur. J.* **2007**, *13*, 3606–3616.

29. Cole, M. L.; Deacon, G. B.; Forsyth, C. M.; Junk, P. C.; Konstas, K.; Wang, J. *Chem. Eur. J.* **2007**, *13*, 8092–8110.

30. Müller-Buschbaum, K.; Quitmann, C. C. *Inorg*. *Chem*. **2006**, *45*, 2678–2687.

31. Pfeiffer, D.; Guzei, I. A.; Liable-Sands, L. M.; Heeg, M. J.; Rheingold, A. L.; Winter, C. H. *J*. *Organomet*. *Chem*. **1999**, *588*, 167–175.

32. Shannon, R. D. *Acta Cryst*. **1976**, *A32*, 751–767.

33. Hitchcock, P. B.; Hulkes, A. G.; Lappert, M. F. *Inorg*. *Chem*. **2004**, *43*, 1031–1038.

34. Avent, A. G.; Caro, C. F.; Hitchcock, P. B.; Lappert, M. F.; Li, Z.; Wei, X. -H. *Dalton Trans*. **2004**, 1567–1577.

35. Doyle, D.; Gun'ko, Y. K.; Hitchcock, P. B.; Lappert, M. F. *J*. *Chem*. *Soc*., *Dalton Trans*. **2000**, 4093–4097.

36. Anwander, R.; Runte, O.; Eppinger, J.; Gerstberger, G.; Herdtweck, E.; Spiegler, M. *J*. *Chem*. *Soc*., *Dalton Trans*. **1998**, 847–858.

37. Qayyum, S.; Skvortsov, G. G.; Fukin, G. K.; Trifonov, A. A.; Kretschmer, W. P.; Döring, C.; Kempe, R. *Eur*. *J*. *Inorg*. *Chem*. **2010**, 248–257.

Chapter 5

Conclusion and Future Prospect

5.1 Summary of This Research Work

In the present research work, we have investigated the coordination chemistry of five related guanidinate ligands, namely $[(2,6\text{–}Me_2C_6H_3N)C(NHPr^i)(NPr^i)]^-$ (L^1), $[(2,6\text{–}Me_2C_6H_3N)C(NHCy)(NCy)]^-$ (L^2), $[(2,6\text{–}Me_2C_6H_3N)C\{N(SiMe_3)Cy\}(NCy)]^-$ (L^3), $[(2,6\text{–}Pr^i_2C_6H_3N)C\{N(SiMe_3)_2\}(NC_6H_3Pr^i_2\text{–}2,6)]^-$ (L^4) and $[(2,6\text{–}Pr^i_2C_6H_3N)C(NEt_2)(NC_6H_3Pr^i_2\text{–}2,6)]^-$ (L^5), towards chromium and the lanthanide metals. The reaction chemistry of divalent chromium and the lanthanide guanidinate complexes was also examined.

Utilizing the least bulky ligand L^1, we have successfully prepared homoleptic Cr(II) complex $[Cr(L^1)_2]$ (**3**). With the more bulky L^4 ligand, heteroleptic Cr(II) complexes $[Cr(L^4)(\mu\text{–}Cl)_2Li(THF)(Et_2O)]$ (**4**) and $[\{Cr(L^4)(\mu\text{–}Cl)\}_2]$ (**5**) were isolated. It is noted that the use of sterically more bulky guanidinate ligand does not favour the formation of Cr(II) bis(guanidinate) complexes. The reactivity of complex **3** as a reducing agent was also studied in this work. This led to the isolation of a few Cr(III) complexes, namely $[Cr(L^1)_2I]$ (**6**) and $[Cr(L^1)_2(EPh)]$ [E = S (**7**), Se (**8**), Te (**9**)], and a Cr(IV) complex $[Cr(L^1)_2\{N(1\text{–}Ad)\}]$ (**10**). Complex **4** underwent metathesis reaction with NaOMe, resulting in the formation of dimeric Cr(II) methoxide complex, $[\{Cr(L^4)(\mu\text{–}OMe)\}_2]$ (**11**).

The coordination chemistry of ligands L^1, L^2, L^3 and L^5 towards Ln(II) (Ln = Sm,

Eu, Yb) metal ions was studied. A series of divalent lanthanide complexes namely, $[\{Eu(L^1)(\mu\text{–}L^1)\}_2]$ (**15**), $[\{Eu(L^2)(\mu\text{–}L^2)\}_2 \cdot 2C_6H_{14}]$ (**16**), $[\{Yb(L^2)(\mu\text{–}L^2)\}_2]$ (**17**), $[Yb(L^2)_2(THF)_2]$ (**18**), $[Eu(L^3)_2(THF)_2 \cdot 0.25C_6H_{14}]$ (**19**), $[Yb(L^3)_2(THF)_2 \cdot 0.25C_6H_{14}]$ (**20**), $[\{Sm(L^3)(\mu\text{–}I)(THF)_2\}_2]$ (**21**) and $[Sm(L^5)_2]$ (**22**) were isolated. To our knowledge, complex **22** represents the second example of a square planar Sm(II) guanidinate, which has been structurally characterized.[1] Subsequent reactions of complexes **15**, **18**, **20** and **22** with various oxidizing reagents (I_2, PhSSPh, PhSeSePh, CuCl, PhNNPh and CS_2) gave the corresponding lanthanide(III) complexes: $[\{Eu(L^1)_2(\mu\text{–}I)\}_2]$ (**23**), $[\{Yb(L^2)_2(\mu\text{–}SPh)\}_2]$ (**24**), $[\{Yb(L^2)_2(\mu\text{–}SePh)\}_2]$ (**25**), $[\{Yb(L^2)_2(\mu\text{–}Cl)\}_2]$ (**26**), $[\{Yb(L^2)_2\}_2(\mu\text{–}\eta^2\text{:}\eta^2\text{–}PhNNPh)]$ (**27**), $Yb(L^3)_2(\eta^2\text{–}PhNNPh) \cdot PhMe]$ (**28**) and $[(L^5)_2Sm(\mu\text{–}\eta^3\text{:}\eta^2\text{–}S_2CSCS)Sm(L^5)_2]$ (**29**). The reaction chemistry of Sm(II) guanidinate complex $[Sm(Giso)_2]$ [Giso = $\{(2,6\text{–}Pr^i_2C_6H_3N)_2CNCy_2\}^-$] has been reported by Jones and co–workers.[2] However, a detailed investigation on the reaction chemistry of Eu(II) and Yb(II) guanidinate complexes remains rare. Our work represents the first systematic study on the reaction chemistry of Eu(II) and Yb(II) guanidinate complexes.

The synthesis and structure of trivalent lanthanide complexes supported by the L^1 ligand was examined. A series of mononuclear lanthanide(III) tris(guanidinate) complexes with the general formula $[Ln(L^1)_3]$ [Ln = Ce (**30**), Pr (**31**), Gd (**32**), Tb (**33**),

Ho (**34**), Er (**35**), Tm (**36**)] were isolated. The observed Ln–N bond distances of these complexes decrease across the row, which are consistent with the "lanthanide contraction". In addition, two binuclear lanthanide(III) bis(guanidinate) complexes [{Ce(L^1)$_2$(μ–Cl)}$_2$] (**37**) and [{Lu(L^1)$_2$(μ–Cl)}$_2$] (**38**)] were also synthesized in this work.

5.2 Future Prospect

After an exhaustive study on the coordination chemistry of L^1–L^5 with chromium and the lanthanide metal ions, it is our intention to extend our work to the applications of these complexes in polymer chemistry and material science in the future work.

Nitrogen–based chromium complexes have been proven to be excellent non–metallocene catalysts for olefin polymerizations.[3] This provide insights on the catalytic study of our chromium guanidinate complexes **3**–**11** towards olefin polymerization chemistry.

Lanthanide complexes are good initiators for the ring–opening polymerization of lactones, probably because of their oxophilic behavior. Recently, Shen and co–workers have demonstrated the polymerization of ε–caprolactone by using lanthanide guanidinate complexes as active initiators.[4] Therefore, a detailed study on the catalytic propertied of the lanthanide(III) guanidinate complexes **30**–**38**

towards the ring opening polymerization of ε–caprolactone will be carried out in the future work. Besides, the reaction conditions will be studied carefully to find out an optimal reaction condition for the achievement of specific molecular weights and polydispersity indexes for polylactone.

Lanthanide guanidinate complexes can also be applied to material chemistry. Devi and co–workers have reported on the deposition of lanthanide oxides and lanthanide nitrides thin films on semiconductors by MOCVD or ALD methods,[5] using lanthanide(III) tris(guanidinate) complexes as precursors due to their high volatility and high thermal stability. Based on the above results, a study of using lanthanide tris(guanidinate) complexes **30**–**36** as precursors for the deposition of the corresponding lanthanide oxide and lanthanide nitride thin films can be carried out in the future. Lanthanide oxide thin films being coated on a metal surface can act as corrosion–resistant coatings,[6] whereas lanthanide nitride thin films can be used as materials for semi–conductor.[7]

5.3 References for Chapter 5

1. Heitmann, D.; Jones, C.; Junk, P. C.; Lippert, K. -A.; Stasch, A. *Dalton Trans*. **2007**, 187–189.

2. Heitmann, D.; Jones, C.; Mills, D. P.; Stasch, A. *Dalton Trans*. **2010**, *39*, 1877–1882.

3. a) Gibson, V. C.; Spitzmesser, S. K. *Chem*. *Rev*. **2003**, *103*, 283–315.

   b) Ballem, K. H. D.; Shetty, V.; Etkin, N.; Patrick, B. O.; Smith, K. M. *Dalton Trans*. **2004**, 3431–3433.

   c) MacAdams, L. A.; Buffone, G. P.; Incarvito, C. D.; Rheingold, A. L.; Theopold, K. H. *J*. *Am*. *Chem*. *Soc*. **2005**, *127*, 1082–1083.

4. (a) Luo, Y.; Yao, Y.; Shen Q.; Y, K.; Weng, L. *Eur*. *J*. *Inorg*. *Chem*. **2003**, 318–323.

   (b) Chen, J. -L.; Yao, Y. -M.; Luo, Y. -J.; Zhou, L. -Y.; Zhang, Y.; Shen, Q. *J*. *Organomet*. *Chem*. **2004**, *689*, 1019–1024.

5. a) Milanov, A. P.; Fischer, R. A.; Devi, A. *Inorg*. *Chem*. **2008**, *47*, 11405–11416.

   b) Milanov, A. P.; Thiede, T. B.; Devi, A.; Fischer, R. A. *J*. *Am*. *Chem*. *Soc*. **2009**, *131*, 17062–17063.

   c) Thiede, T. B.; Krasnopolski, M.; Milanov, A. P.; de los Arcos, T.; Ney, A.;

Becker, H. -W.; Rogalla, D.; Winter, J.; Devi, A.; Fischer, R. A. *Chem*. *Mater*. **2011**, *23*, 1430–1440.

6. Bonnet, G.; Lachkar, M.; Colson, J. C.; Larpin, J. P. *Thin Solid Films* **1995**, *261*, 31–36.

7. Duan, C. -G.; Sabirianov, R. F.; Mei, W. N.; Dowben, P. A.; Jaswal, S. S.; Tsymbal, E. Y. *J*. *Phys*.: *Condens*. *Matter* **2007**, *19*, 315220.

Appendix 1

General Procedures, Physical Measurements and X–Ray Diffraction Analysis

All manipulations were carried out using standard Schlenk techniques or in a MBRAUN MB 150–M drybox under an atmosphere of purified nitrogen. Solvents were dried over sodium wire and distilled under nitrogen from sodium benzophenone (diethyl ether and THF) or Na/K alloy (hexane, pentane and toluene), and degassed twice by freeze–thaw cycles before use.

^{1}H and ^{13}C NMR spectra were recorded on a Bruker Avance III 400 NMR Spectrometer at 400.13 and 100.61 MHz, respectively. Chemical shifts were referenced to residue protons of C_6D_6 (7.16 ppm for ^{1}H and 128.06 ppm for ^{13}C), toluene–d_8 (7.09 ppm for ^{1}H and 20.43 ppm for ^{13}C) and THF–d_8 (3.58 ppm for ^{1}H and 67.21 ppm for ^{13}C). Magnetic moments were measured in C_6D_6 solutions at 298 K by the Evans NMR method using a Bruker Avance III 400 NMR Spectrometer (Equation A1–1. to Equation A1–3.).[†] Melting–points were recorded on an Electrothermal melting point apparatus and were uncorrected. IR spectra were recorded on a PerkinElmer Spectrum I FTIR Spectrometer or a PerkinElmer RXI FTIR Spectrometer. UV–Vis spectra were recorded by a CARY 5G UV–Vis–NIR

[†] Schubert, E. M. *J. Chem. Educ.* **1992**, *69*, 62.

Spectrophotometer. Elemental analysis (C, H, N) was performed by MEDAC Ltd., U.K.

Single–crystals of compounds **1**–**12** and **14**–**38** suitable for X–ray diffraction studies were mounted in glass capillaries and sealed under nitrogen. Data were collected on a Bruker SMART CCD diffractometer or a Bruker KAPPA APEX II diffractometer with graphite–monochromatized Mo–K_α radiation (λ = 0.71073 Å) using φ and ω scan. The structures were solved by direct phase determination using the computer program SHELX–97 and refined by full–matrix least squares with anisotropic thermal parameters for the non–hydrogen atoms.[†] Hydrogen atoms were introduced in their idealized positions and included in structure factor calculations with assigned isotropic temperature factors.

Equation A1–1. :

$$\chi_g = \frac{3\Delta f}{4\pi f m} + \chi_s$$

χ_g = mass susceptibility of the solute (cm^3/g)

Δf = observed frequency shift of reference resonance (Hz)

f = spectrometer frequency (Hz)

χ_s = mass susceptibility of solvent (7×10^{-7} cm^3/g for C_6D_6)

m = mass of substance per cm^3 of solvent (g/cm^3)

[†] Scheldrick, G. M. *SHELX–97; Package for Crystal Structure Solution and Refinement*; University of Göttingen: Göttingen, Germany, **1997**.

Equation A1–2. :

$$\chi_m = MW \cdot \chi_g$$

χ_m = molar susceptibility of the solute (cm^3/mol)

MW = molar mass of the solute (g/mol)

Equation A1–3. :

$$\mu_{eff} = 2.84\sqrt{\chi_m \cdot T}$$

μ_{eff} = effective magnetic moment (μ_B)

T = Temperature (K)

Appendix 2

NMR Spectra of Compounds

Figure A2–1. ^{1}H NMR Spectrum of $[KL^{1} \cdot 0.5PhMe]_n$ (**1**).

Figure A2–2. ^{13}C NMR Spectrum of $[KL^{1} \cdot 0.5PhMe]_n$ (**1**).

Figure A2–3. Variable Temperature ^{1}H NMR Spectra of $[KL^{1} \cdot 0.5PhMe]_n$ (**1**) in THF–d_8 from –80^{o}C to 30^{o}C.

Figure A2–4. ^{1}H NMR Spectrum of $[LiL^{4}(Et_2O)]$ (**2**).

Figure A2–5. ^{13}C NMR Spectrum of $[LiL^{4}(Et_2O)]$ (**2**).

Figure A2–6. ^{13}C NMR(Dept 135) Spectrum of $[LiL^{4}(Et_2O)]$ (**2**).

Figure A2–7. Variable Temperature ^{1}H NMR Spectra of $[LiL^{4}(Et_2O)]$ (**2**) in toluene-d_8 from 20^{o}C to 65^{o}C.

Figure A2–8. ^{1}H NMR Spectrum of $[KL^{2}(THF)_{0.5}]_n$ (**12**).

Figure A2–9. ^{13}C NMR Spectrum of $[KL^{2}(THF)_{0.5}]_n$ (**12**).

Figure A2–10. ^{1}H NMR Spectrum of KL^{3} (**13**).

Figure A2–11. ^{13}C NMR Spectrum of KL^{3} (**13**).

Figure A2–12. ^{1}H NMR Spectrum of $[KL^{4}(THF)_2]$ (**14**).

Figure A2–13. ^{13}C NMR Spectrum of $[KL^{4}(THF)_2]$ (**14**).

Figure A2–14. ^{1}H NMR Spectrum of $[\{Yb(L^{2})(\mu–L^{2})\}_2]$ (**17**).

Figure A2–15. ^{13}C NMR Spectrum of $[\{Yb(L^{2})(\mu–L^{2})\}_2]$ (**17**).

Figure A2–16. Variable Temperature ^{1}H NMR Spectra of [{Yb(L^{2})(μ–L^{2})}$_2$] (**17**) in toluene–d_8 from 25°C to 90°C.

Figure A2–17. ^{1}H NMR Spectrum of [{Yb(L^{2})$_2$(THF)$_2$] (**18**).

Figure A2–18. ^{13}C NMR Spectrum of [{Yb(L^{2})$_2$(THF)$_2$] (**18**).

Figure A2–19. ^{1}H NMR Spectrum of [Yb(L^{3})$_2$(THF)$_2$·0.25C_6H_{14}] (**20**).

Figure A2–20. ^{13}C NMR Spectrum of [Yb(L^{3})$_2$(THF)$_2$·0.25C_6H_{14}] (**20**).

Figure A2–21. ^{1}H NMR Spectrum of [{Lu(L^{1})$_2$(μ–Cl)}$_2$] (**38**).

Figure A2–22. ^{13}C NMR Spectrum of [{Lu(L^{1})$_2$(μ–Cl)}$_2$] (**38**).

Figure A2–1. ^{1}H NMR Spectrum of $[KL^{1} \cdot 0.5PhMe]_n$ (**1**).

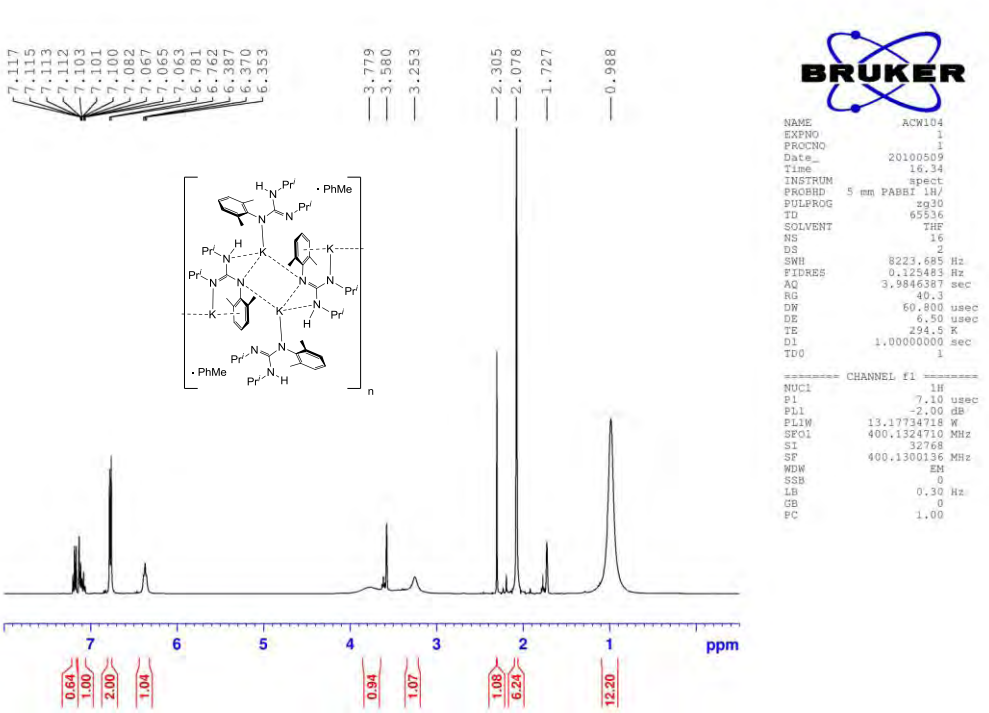

Figure A2–2. ^{13}C NMR Spectrum of $[KL^{1} \cdot 0.5PhMe]_n$ (**1**).

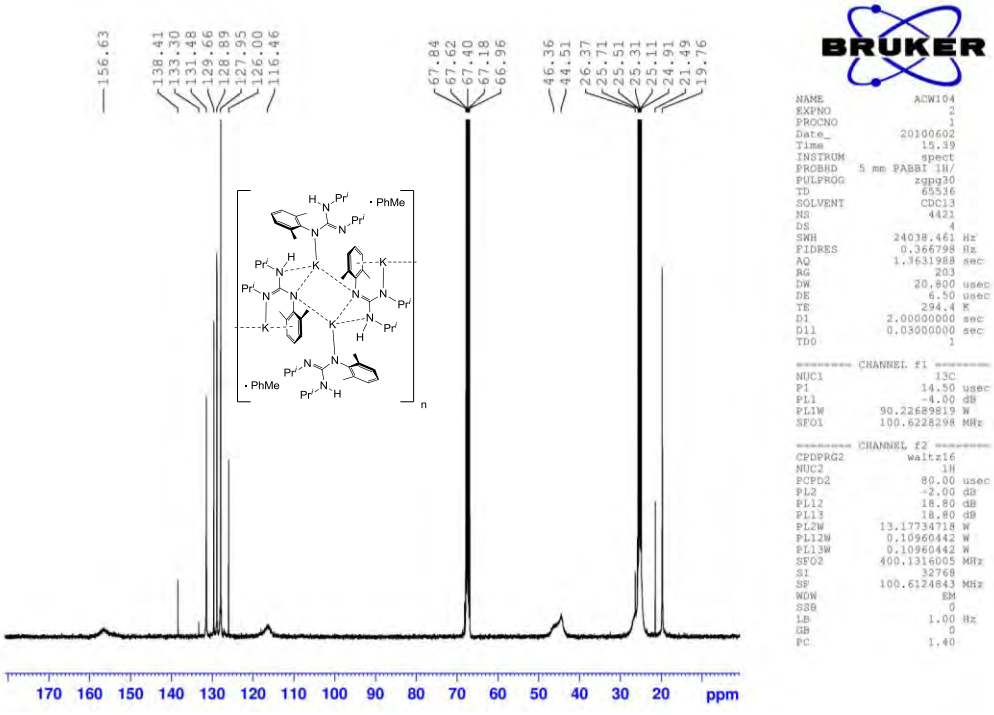

Figure A2–3. Variable Temperature ^{1}H NMR Spectra of $[KL^{1}\cdot 0.5PhMe]_n$ (**1**) in THF–d_8 from –80°C to 30°C.

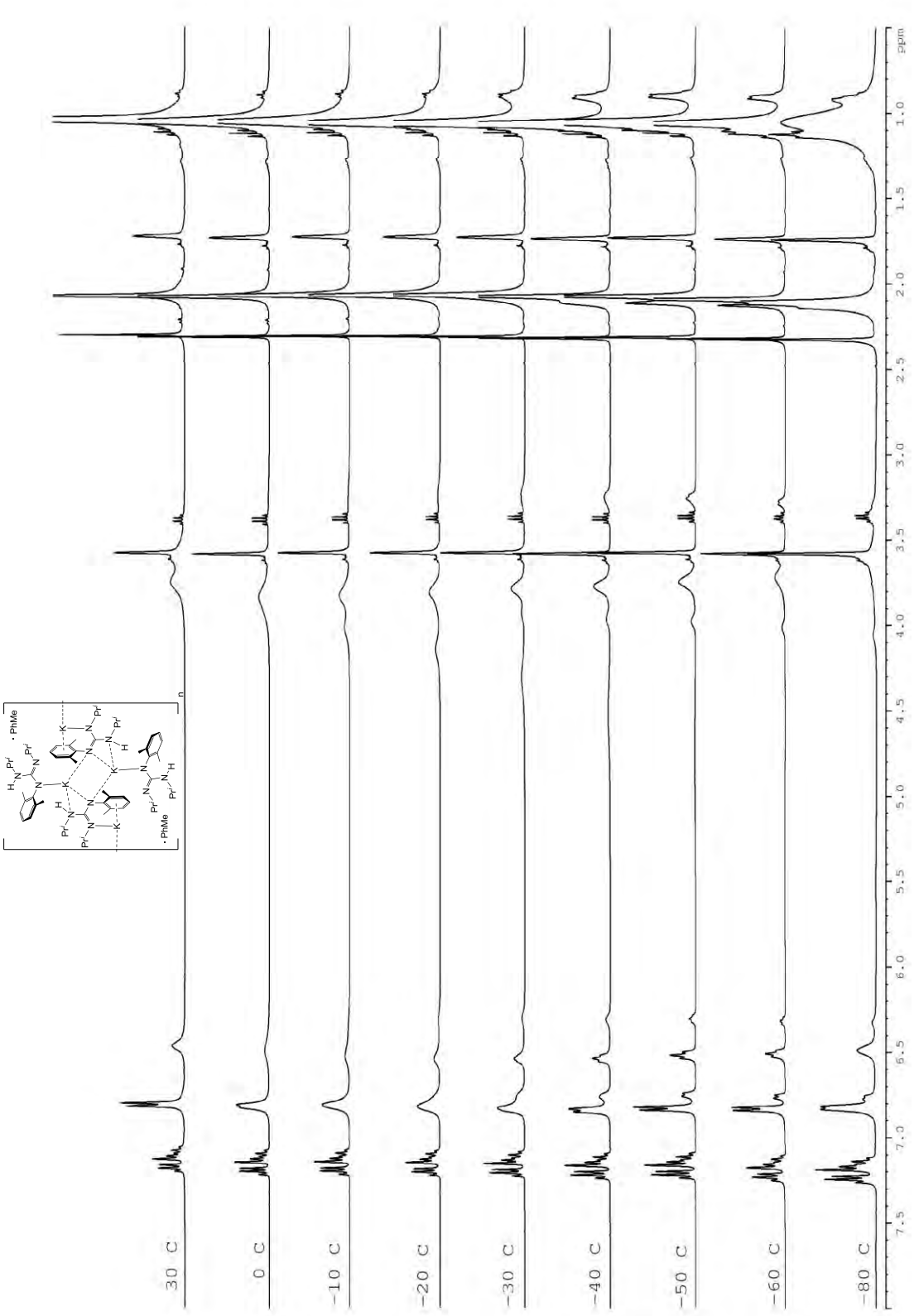

Figure A2–4. ^{1}H NMR Spectrum of [LiL^{4}(Et$_2$O)] (**2**).

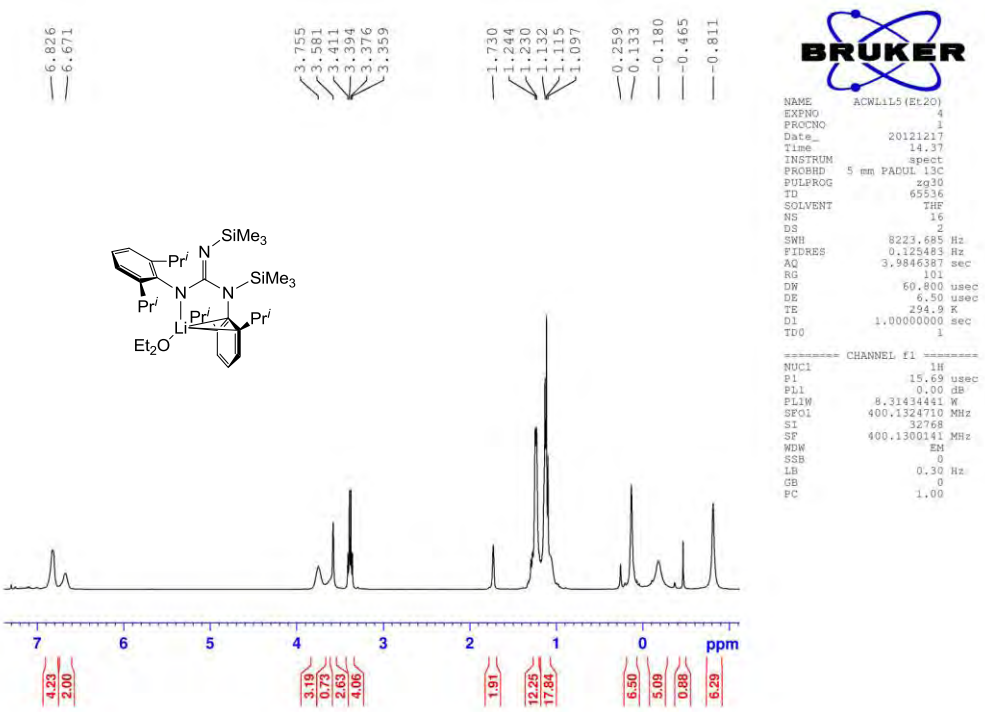

Figure A2–5. ^{13}C NMR Spectrum of [LiL^{4}(Et$_2$O)] (**2**).

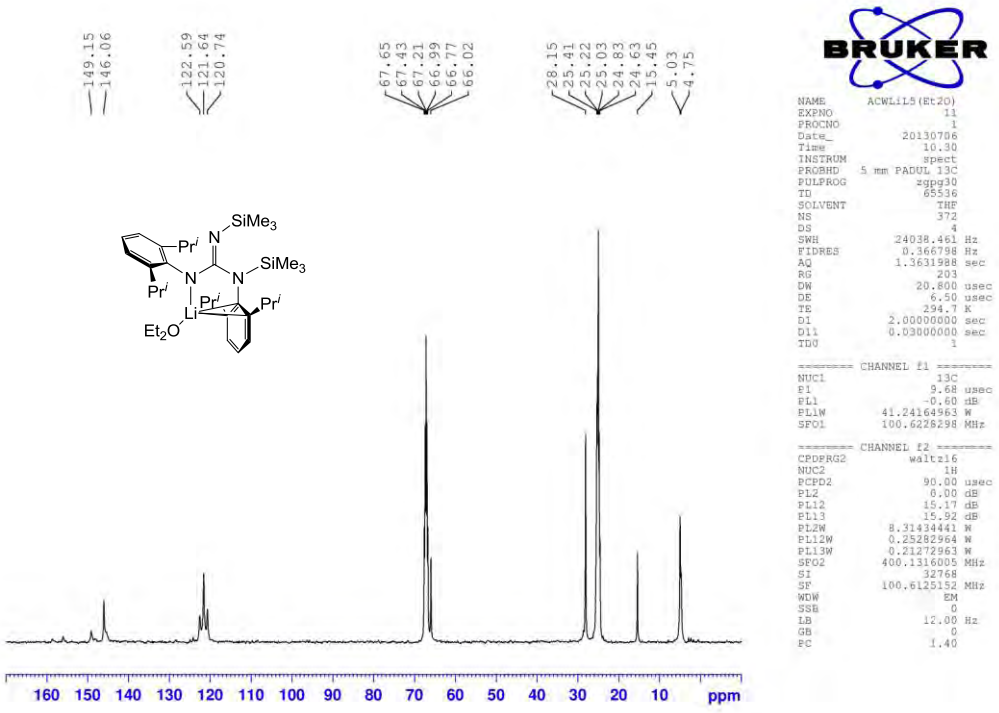

Figure A2–6. ^{13}C NMR(Dept 135) Spectrum of [LiL^4(Et_2O)] (**2**).

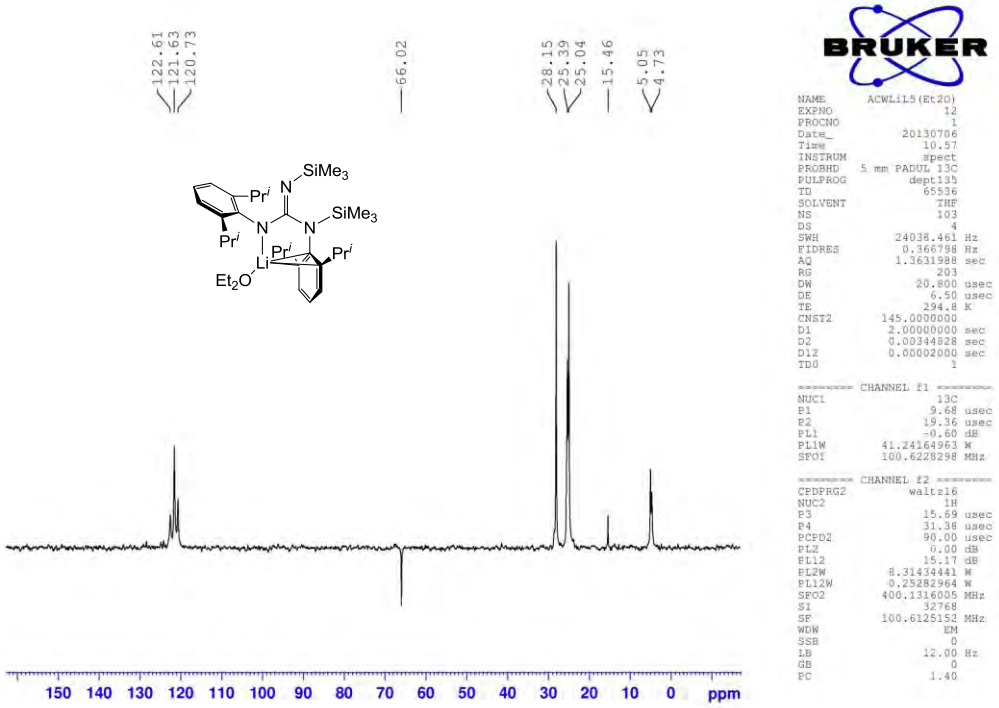

Figure A2–7. Variable Temperature ^{1}H NMR Spectra of $[LiL^{4}(Et_2O)]$ (**2**) in toluene-d_8 from 20°C to 65°C.

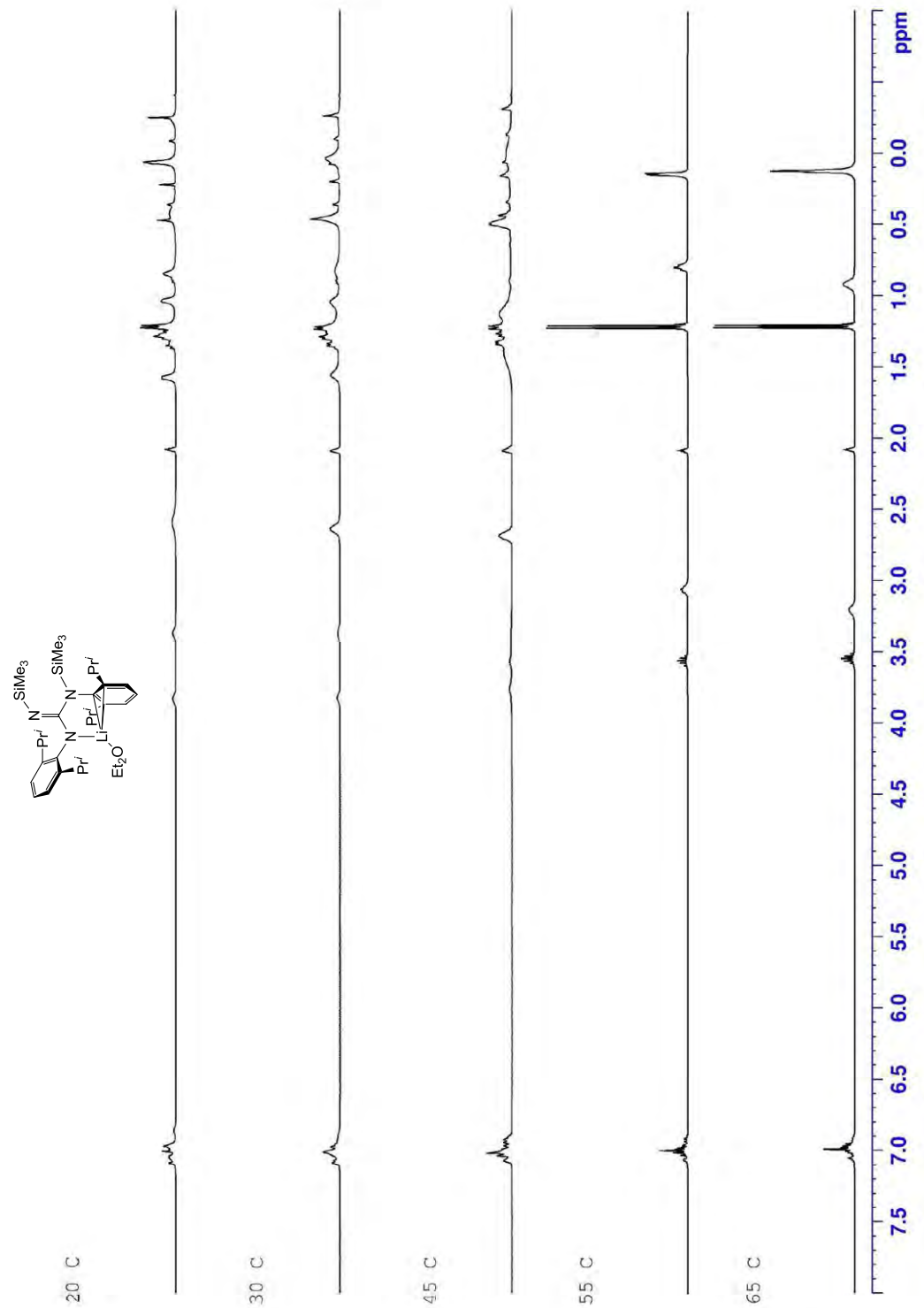

Figure A2–8. ^{1}H NMR Spectrum of $[KL^{2}(THF)_{0.5}]_n$ (**12**).

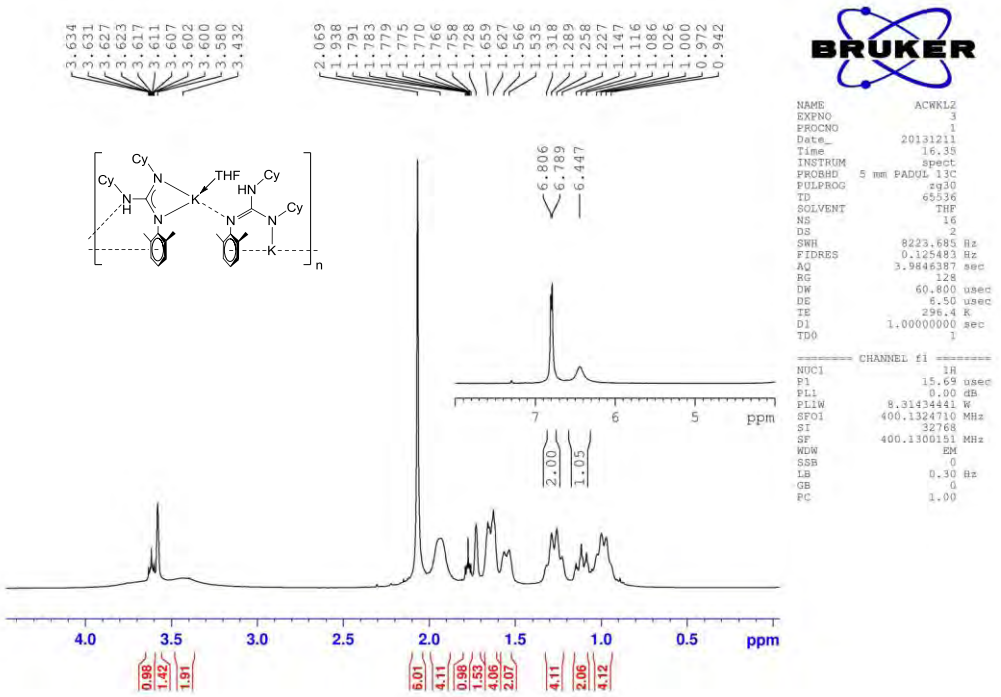

Figure A2–9. ^{13}C NMR Spectrum of $[KL^{2}(THF)_{0.5}]_n$ (**12**).

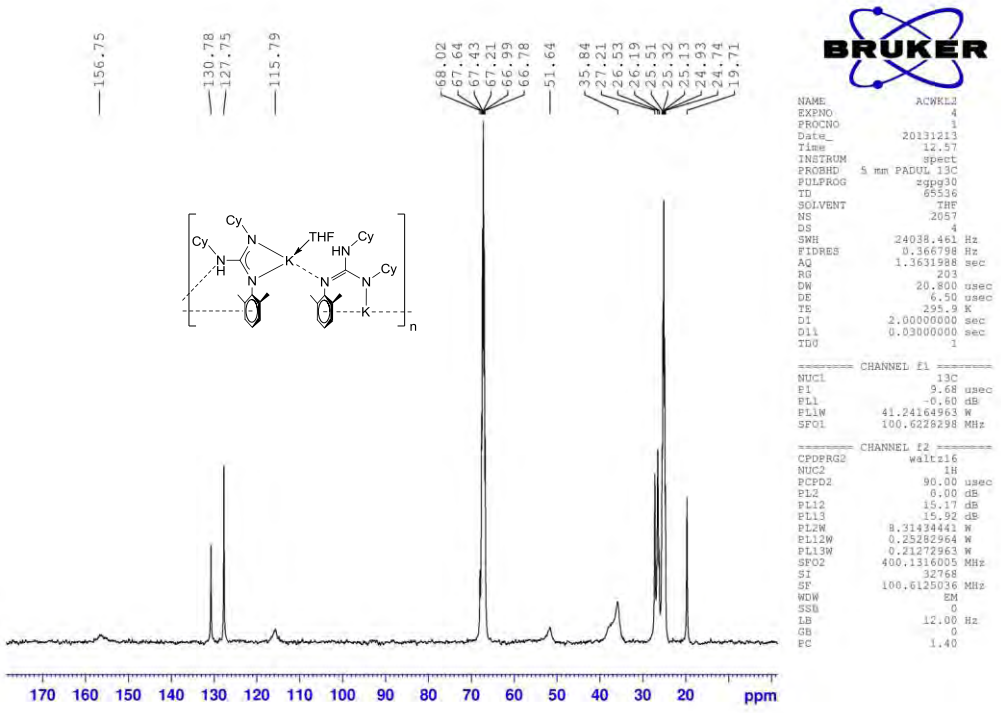

Figure A2–10. ^{1}H NMR Spectrum of KL^{3} (**13**).

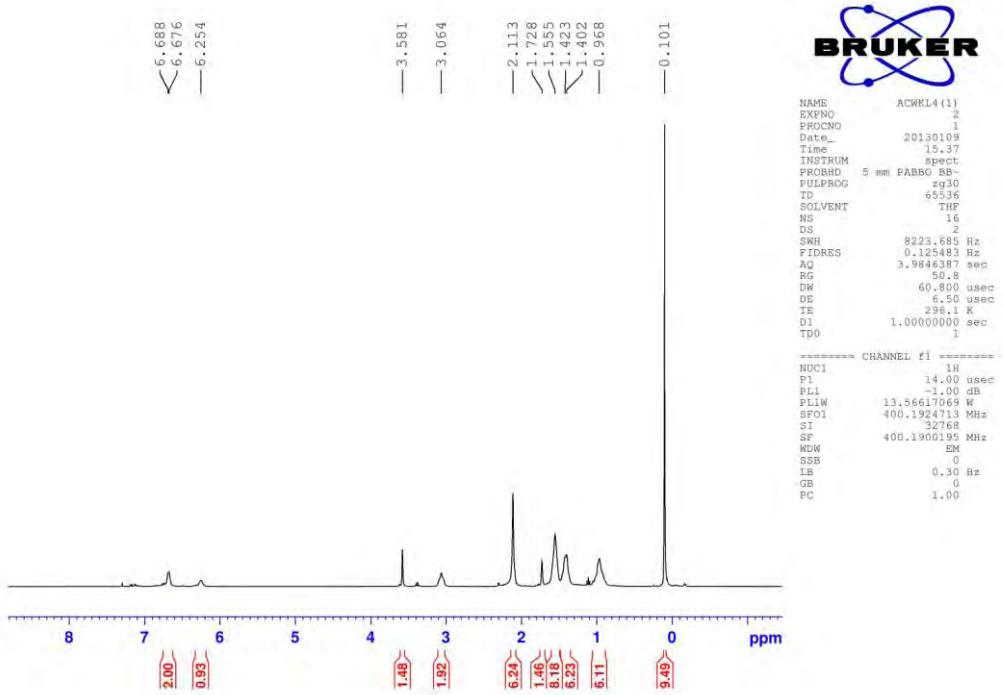

Figure A2–11. ^{13}C NMR Spectrum of KL^{3} (**13**).

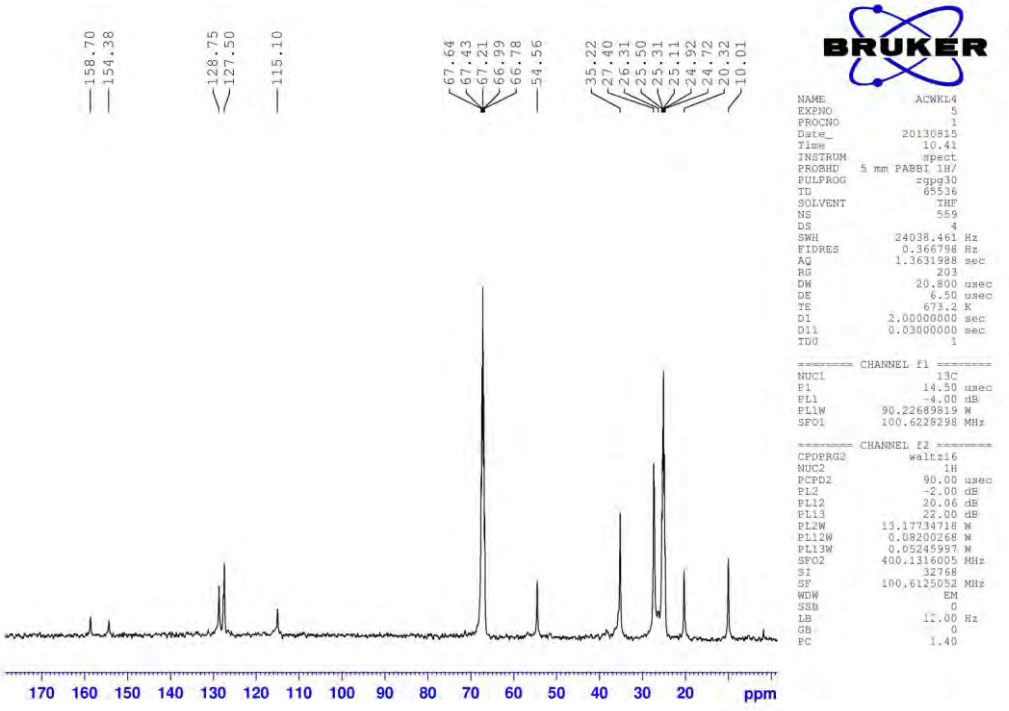

Figure A2–12. ^{1}H NMR Spectrum of [KL^{4}(THF)$_2$] (**14**).

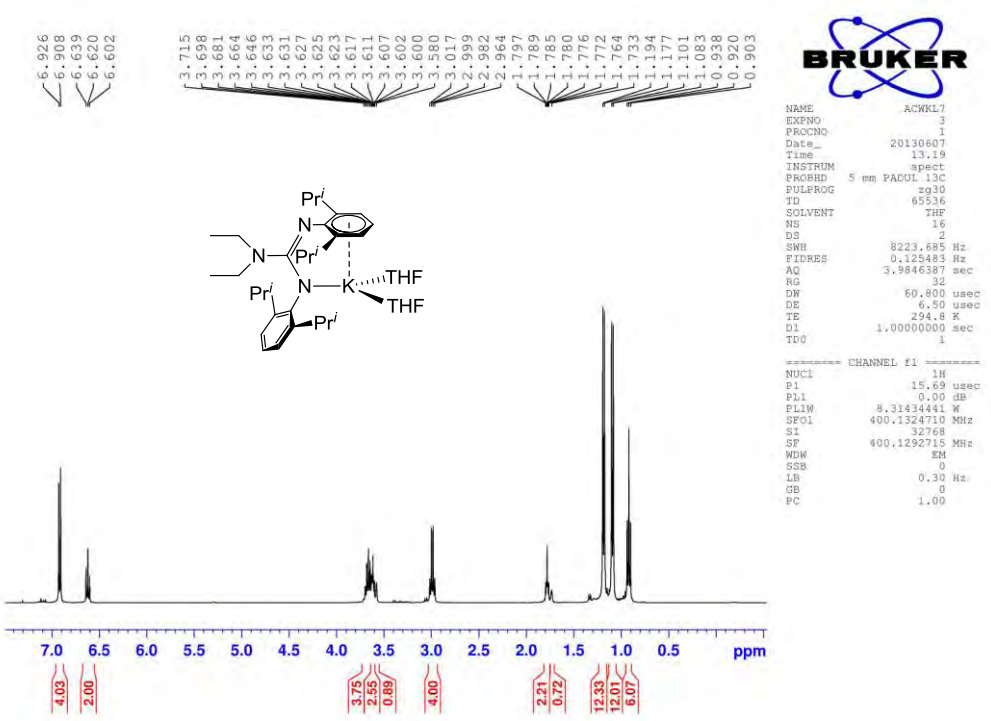

Figure A2–13. ^{13}C NMR Spectrum of [KL^{4}(THF)$_2$] (**14**).

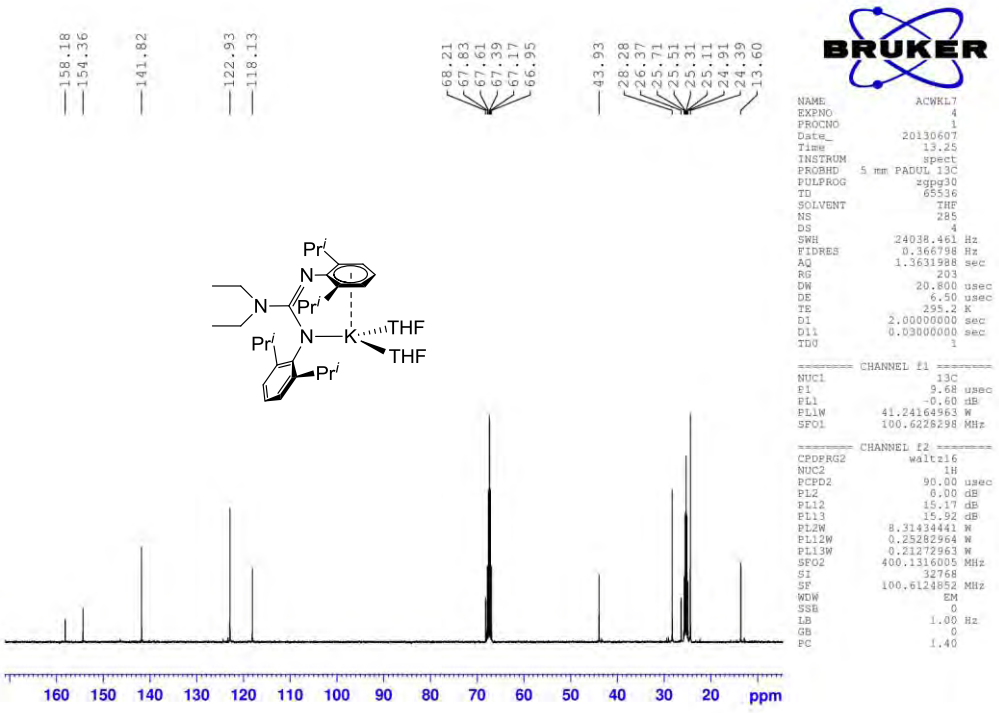

Figure A2–14. ^{1}H NMR Spectrum of [{Yb(L^2)(μ–L^2)}$_2$] (**17**).

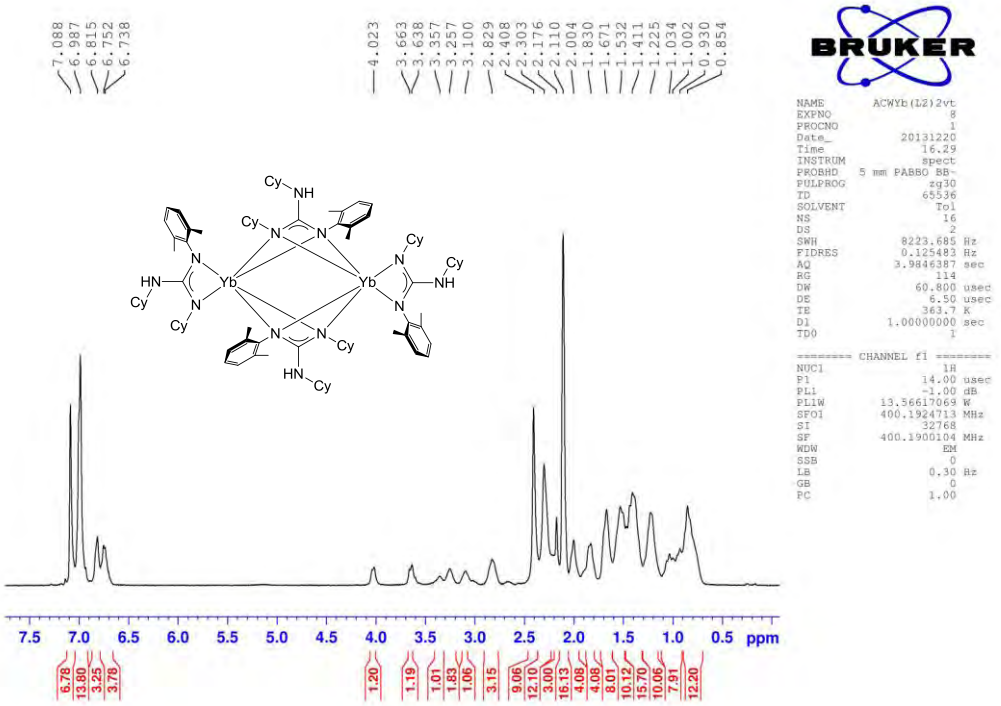

Figure A2–15. ^{13}C NMR Spectrum of [{Yb(L^2)(μ–L^2)}$_2$] (**17**).

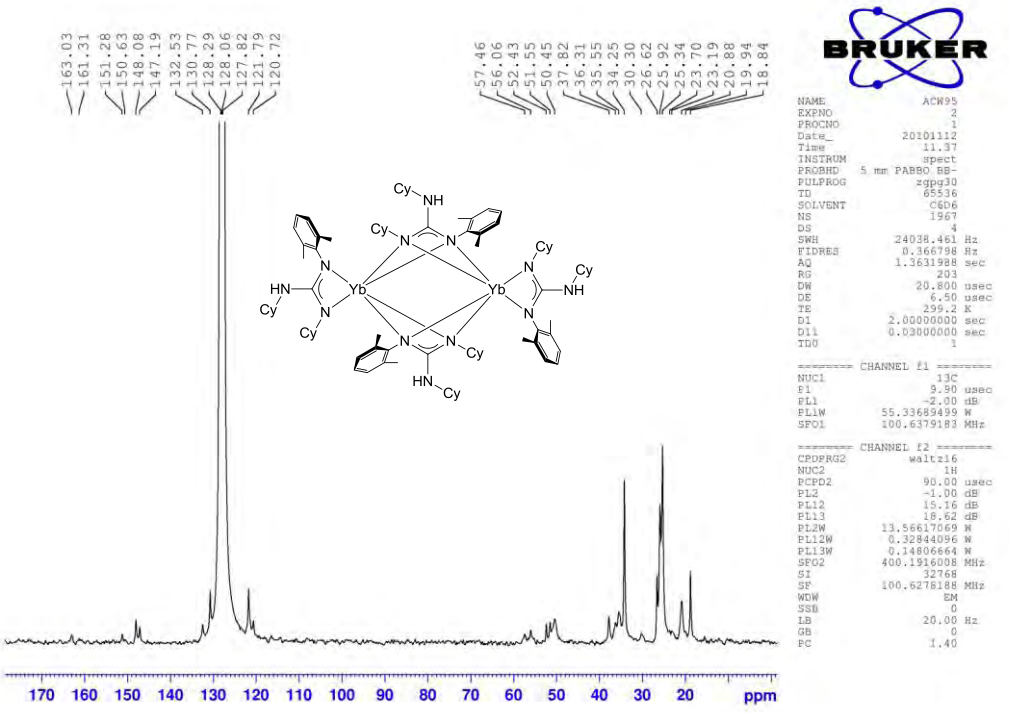

Figure A2–16. Variable Temperature ^{1}H NMR Spectra of [{Yb(L^2)(μ–L^2)}$_2$] (**17**) in toluene–d_8 from 25°C to 90°C.

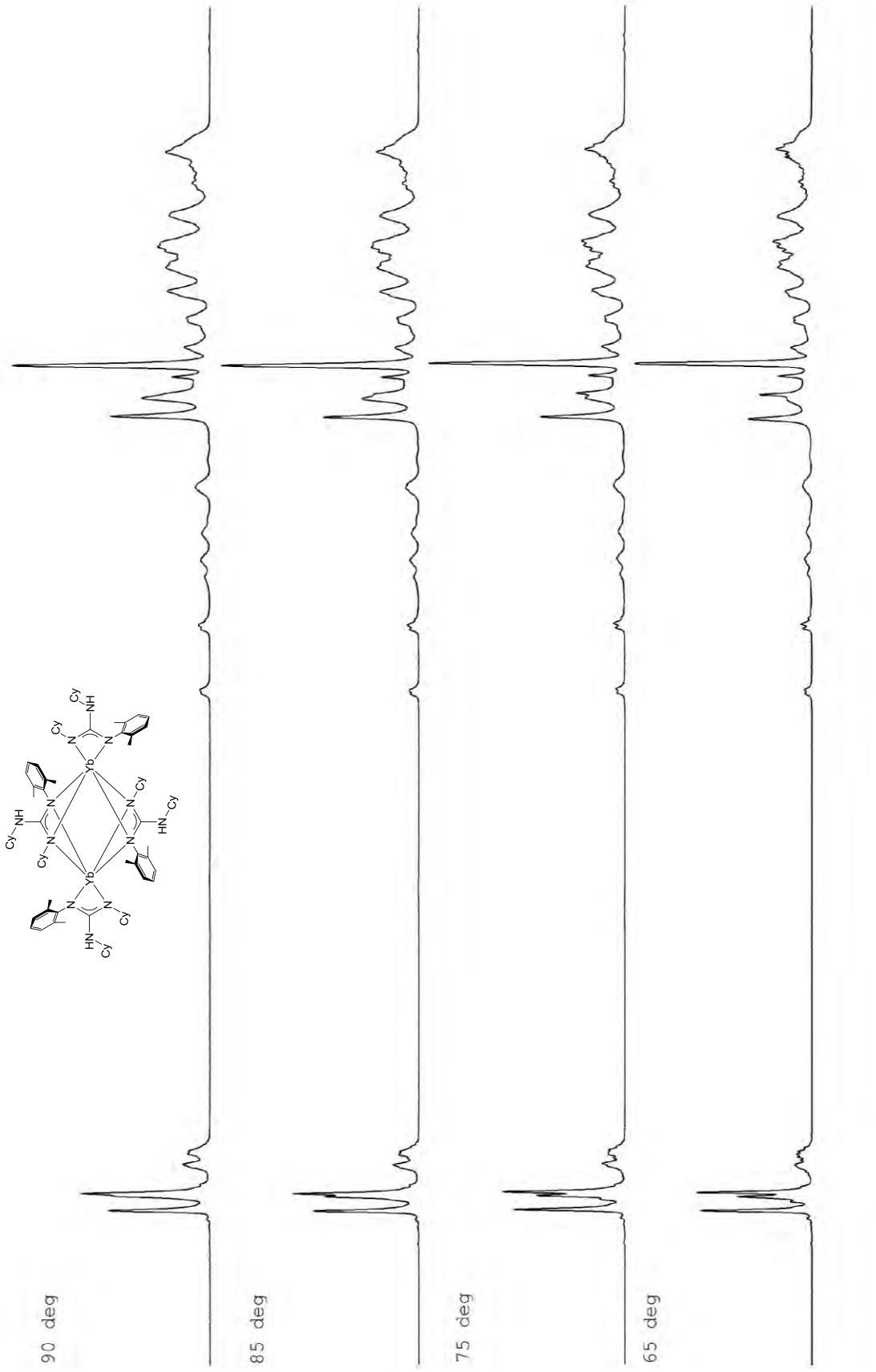

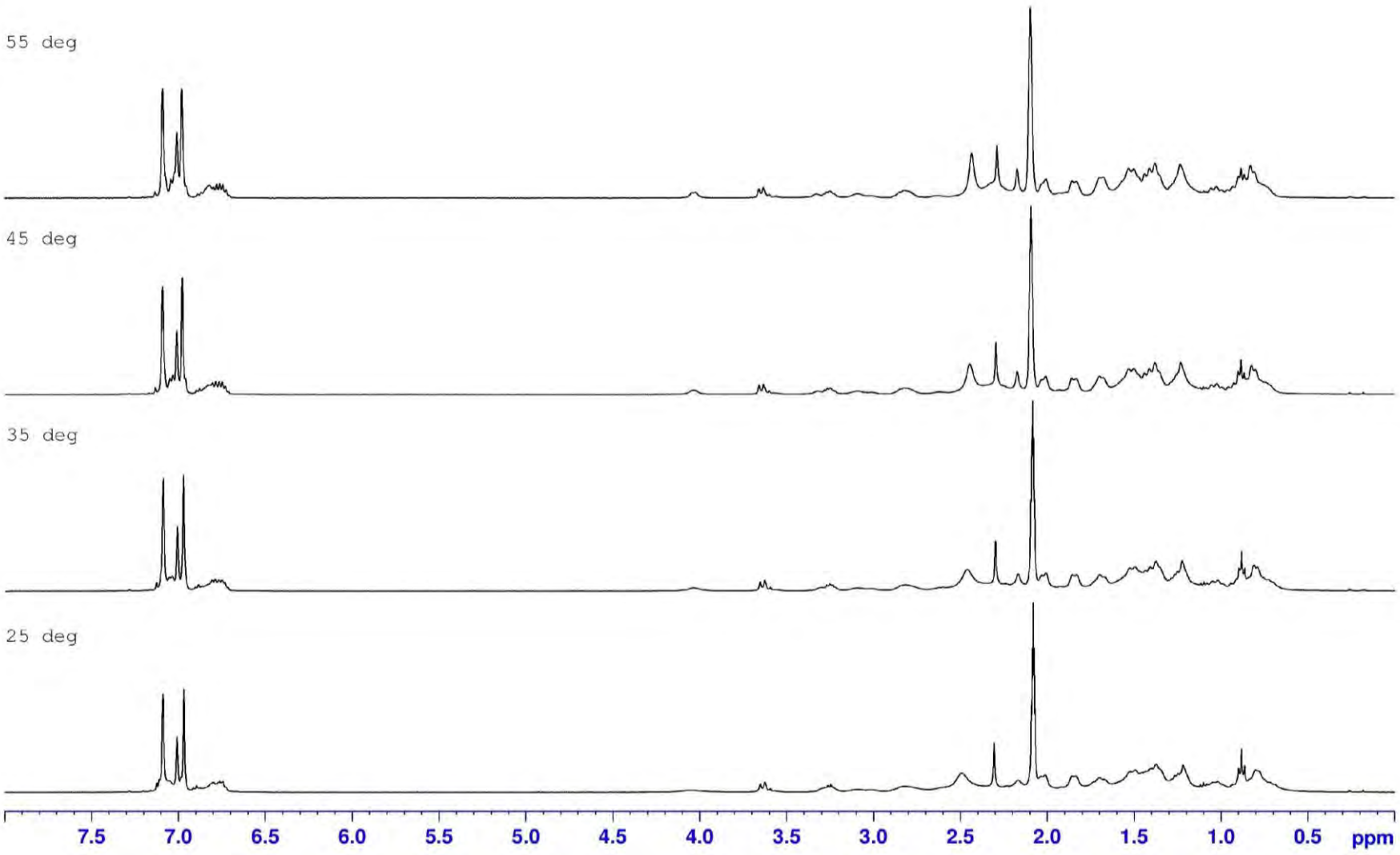
55 deg
45 deg
35 deg
25 deg
7.5
7.0
6.5
6.0
5.5
5.0
4.5
4.0
3.5
3.0
2.5
2.0
1.5
1.0
0.5
ppm

Figure A2–17. ^{1}H NMR Spectrum of [{Yb(L^{2})$_2$(THF)$_2$] (**18**).

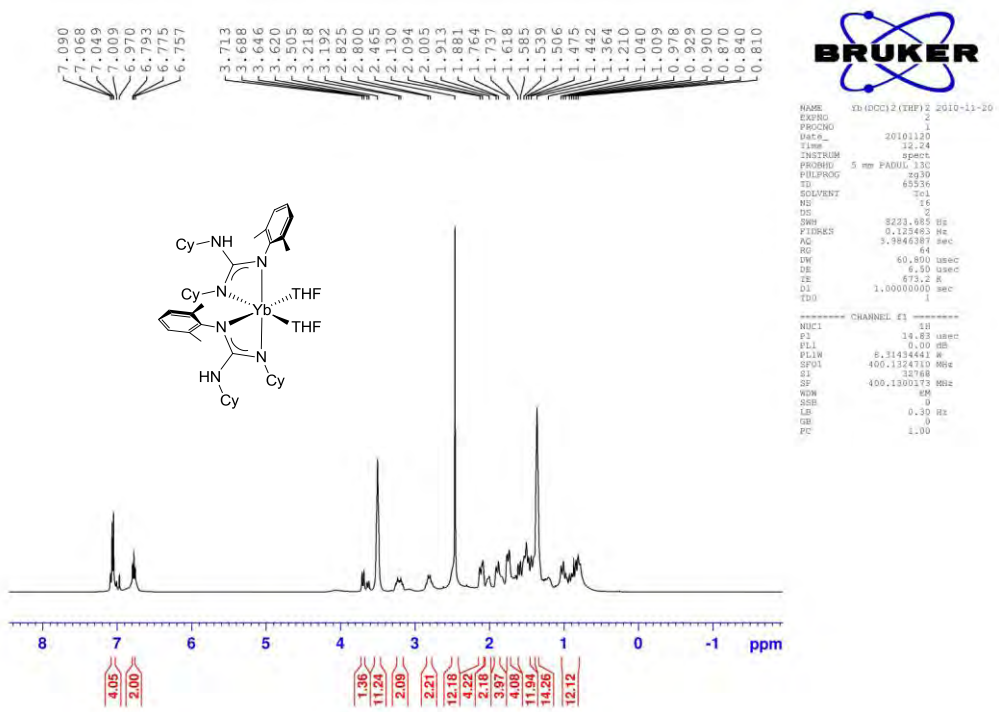

Figure A2–18. ^{13}C NMR Spectrum of [{Yb(L^{2})$_2$(THF)$_2$] (**18**).

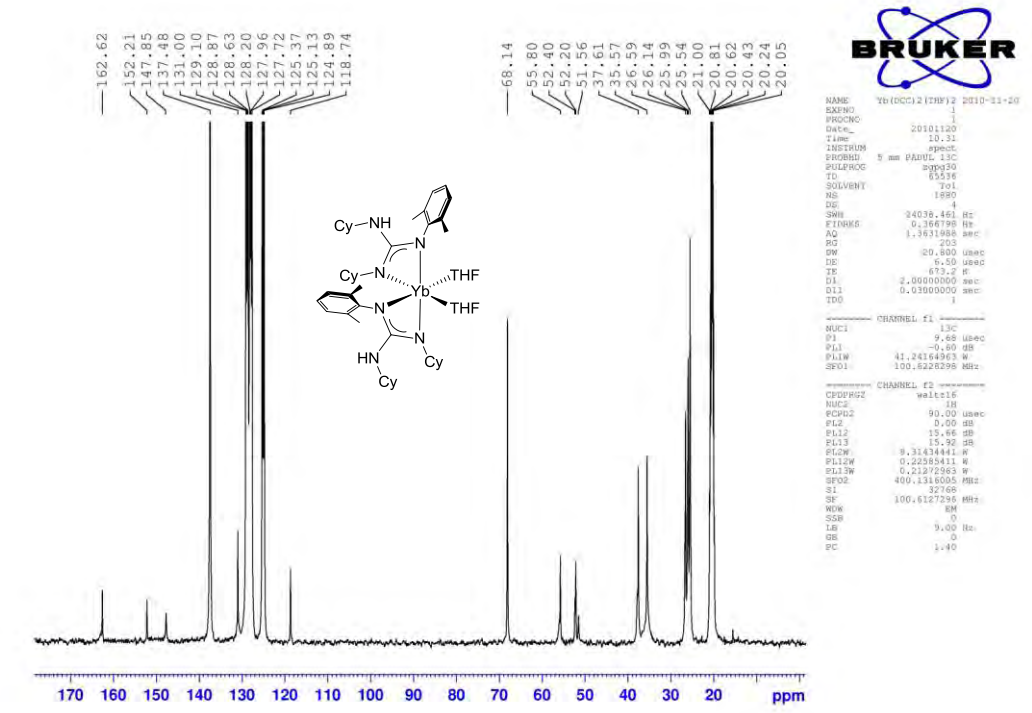

Figure A2–19. ^{1}H NMR Spectrum of $[Yb(L^{3})_2(THF)_2 \cdot 0.25C_6H_{14}]$ (**20**).

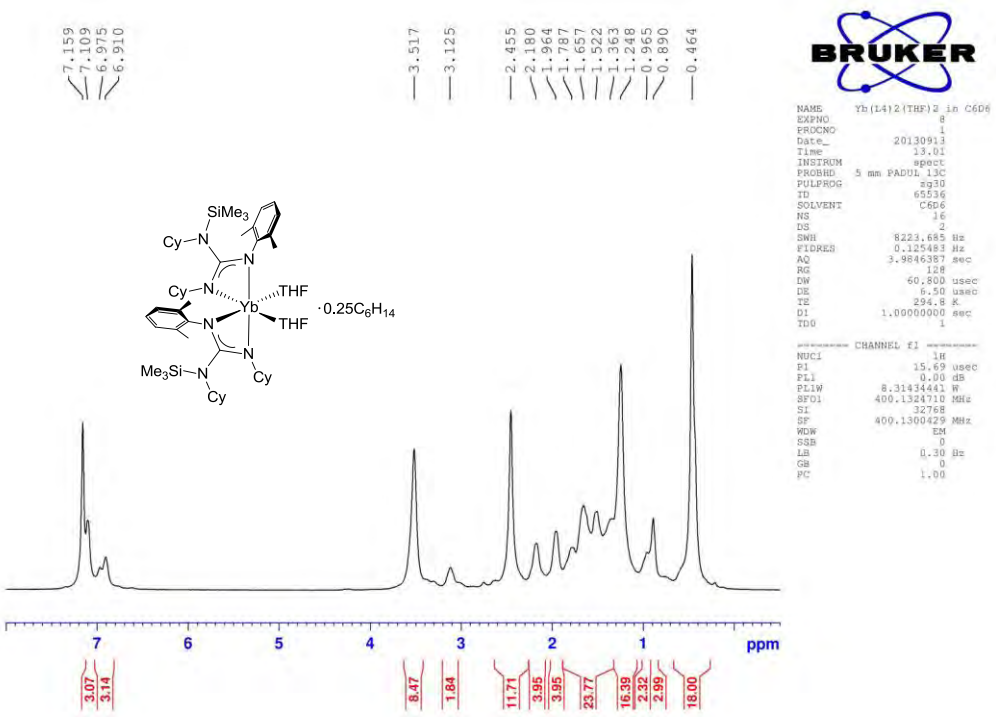

Figure A2–20. ^{13}C NMR Spectrum of $[Yb(L^{3})_2(THF)_2 \cdot 0.25C_6H_{14}]$ (**20**).

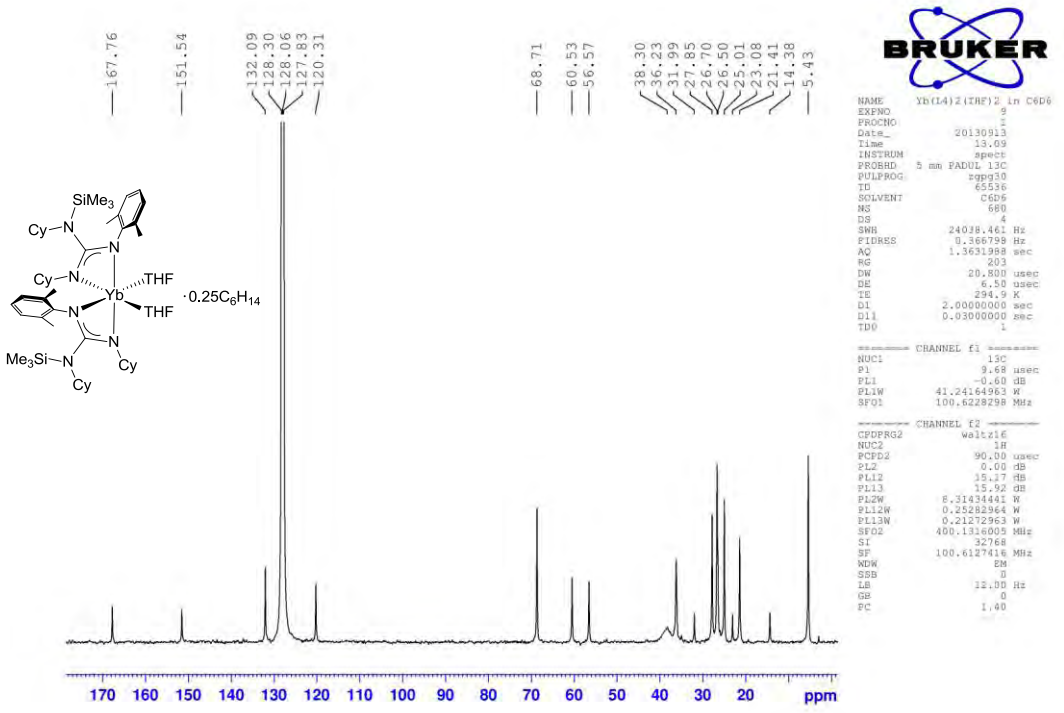

Figure A2–21. ^{1}H NMR Spectrum of [{Lu(L^{1})$_2$(μ–Cl)}$_2$] (**38**).

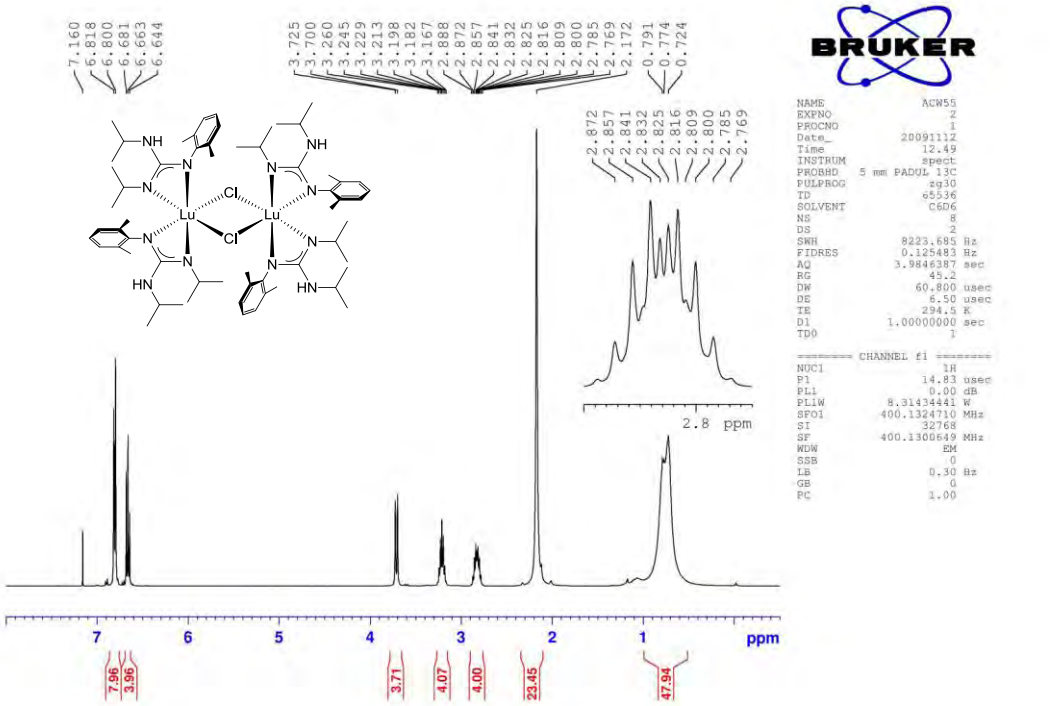

Figure A2–22. ^{13}C NMR Spectrum of [{Lu(L^{1})$_2$(μ–Cl)}$_2$] (**38**).

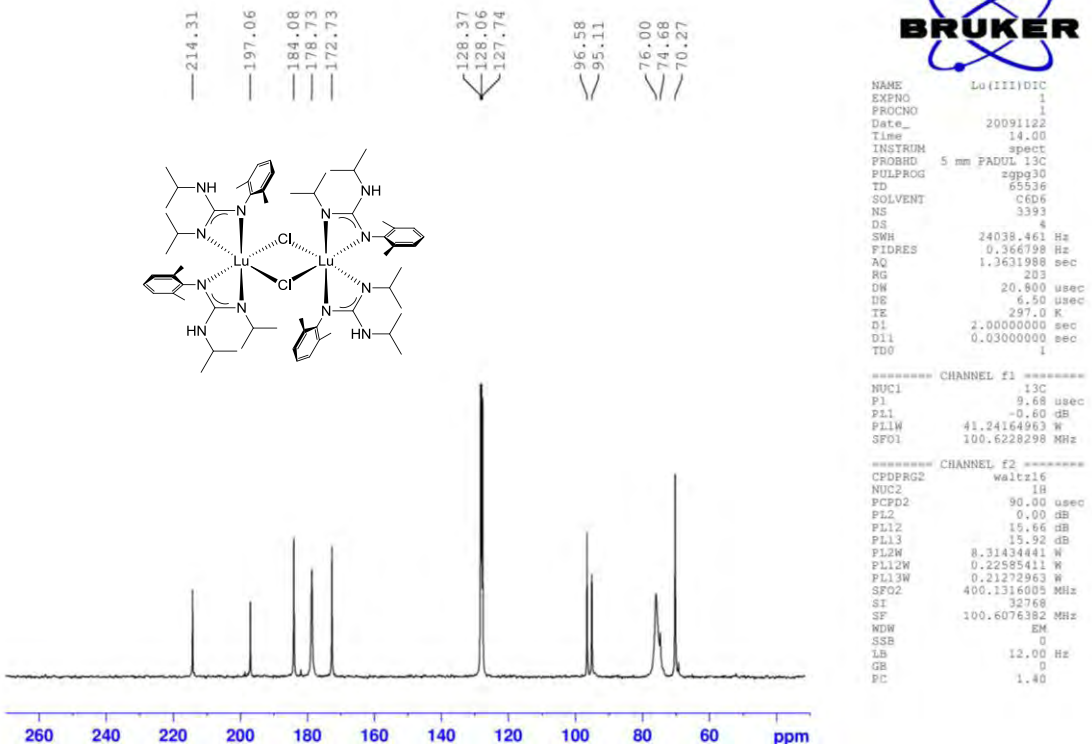

Appendix 3

Selected Crystallographic Data

Table A3–1. Selected Crystallographic Data for Compounds **1** and **2**.

	1	**2**
Molecular formula	$C_{18.5}H_{28}KN_3$	$C_{35}H_{62}LiN_3OSi_2$
Formula weight	331.54	604.00
Crystal size, mm3	0.40×0.30×0.20	0.50×0.40×0.30
Crystal system	Orthorhombic	Monoclinic
Space group	*Pbca*	$P2_1/c$
a, Å	18.6048(7)	11.908(1)
b, Å	20.1569(8)	10.3673(9)
c, Å	21.3578(8)	31.194(3)
α, deg	90	90
β, deg	90	92.766(2)
γ, deg	90	90
Z	16	4
V, $Å^3$	8009.5(5)	3846.7(6)
Density, gcm^{-3}	1.100	1.043
Abs coeff., mm^{-1}	0.267	0.120
Temperature, K	296(2)	173(2)
Reflections collected	65777	28633
Independent reflections	7246	6965
Obs. Data with I≥2σ(I)	3384	4462
Final R indices [I≥2σ(I)]*	$R1 = 0.0697$	$R1 = 0.0837$
	$wR2 = 0.1802$	$wR2 = 0.2181$
R indices (all data)*	$R1 = 0.1631$	$R1 = 0.1277$
	$wR2 = 0.2505$	$wR2 = 0.2528$

*$R1 = \Sigma||Fo| - |Fc||/ \Sigma|Fo|$; $wR2 = \{\mathrm{Pw}(Fo^2 - Fc^2)^2/\Sigma w(Fo^2)^2\}^{1/2}$

Table A3–2. Selected Crystallographic Data for Compounds **3**–**5**.

	3	**4**	**5**
Molecular formula	$C_{30}H_{48}CrN_6$	$C_{39}H_{70}Cl_2LiN_3O_2Si_2$	$C_{62}H_{104}Cl_2Cr_2N_6Si_4$
Formula weight	544.74	799.00	1220.77
Crystal size, mm3	0.50×0.40×0.30	0.50×0.40×0.30	0.50×0.40×0.20
Crystal system	Monoclinic	Monoclinic	Triclinic
Space group	*Pc*	$P2_1/c$	$P\bar{1}$
a, Å	7.8571(7)	15.585(1)	10.8072(8)
b, Å	11.3359(9)	12.459(1)	17.407(1)
c, Å	17.827(2)	23.918(2)	20.433(2)
α, deg	90	90	107.964(2)
β, deg	99.110(2)	97.999(2)	98.249(2)
γ, deg	90	90	95.354(2)
Z	2	4	2
V, $Å^3$	1567.8(2)	4599.0(7)	3579.9(5)
Density, g cm^{-3}	1.154	1.154	1.132
Abs coeff., mm^{-1}	0.392	0.450	0.483
Temperature, K	173(2)	173(2)	293(2)
Reflections collected	13019	44419	20010
Independent reflections	6650	8381	12909
Obs. Data with I≥2σ(I)	5944	6278	5907
Final R indices [I≥2σ(I)]*	*R*1 = 0.0783	*R*1 = 0.0846	*R*1 = 0.0728
	*wR*2 = 0.1936	*wR*2 = 0.2234	*wR*2 = 0.1681
R indices (all data)*	*R*1 = 0.0860	*R*1 = 0.1075	*R*1 = 0.1485
	*wR*2 = 0.2025	*wR*2 = 0.2383	*wR*2 = 0.2168

*$R1 = \Sigma||Fo| - |Fc||/\Sigma|Fo|$; $wR2 = \{Pw(Fo^2 - Fc^2)^2/\Sigma w(Fo^2)^2\}^{1/2}$

Table A3–3. Selected Crystallographic Data for Compounds **6**–**8**.

	6	**7**	**8**
Molecular formula	$C_{30}H_{48}CrIN_6$	$C_{36}H_{53}CrN_6S$	$C_{36}H_{53}CrN_6Se$
Formula weight	671.64	653.90	700.80
Crystal size, mm3	0.50×0.40×0.30	0.50×0.40×0.30	0.50×0.40×0.30
Crystal system	Orthorhombic	Monoclinic	Monoclinic
Space group	$Pca2_1$	$P2_1$	$P2_1$
a, Å	15.845(2)	8.4456(7)	8.553(2)
b, Å	11.633(1)	19.250(2)	18.958(4)
c, Å	18.244(2)	11.551(1)	11.519(3)
α, deg	90	90	90
β, deg	90	104.298(2)	104.480(4)
γ, deg	90	90	90
Z	4	2	2
V, $Å^3$	3362.8(7)	1819.8(3)	1808.4(7)
Density, g cm^{-3}	1.327	1.193	1.287
Abs coeff., mm^{-1}	1.285	0.404	1.355
Temperature, K	173(2)	296(2)	296(2)
Reflections collected	26039	17445	18564
Independent reflections	4775	6483	6424
Obs. Data with I≥2σ(I)	4388	5606	4478
Final R indices [I≥2σ(I)]*	$R1 = 0.0677$	$R1 = 0.0888$	$R1 = 0.0858$
	$wR2 = 0.1752$	$wR2 = 0.2048$	$wR2 = 0.1990$
R indices (all data)*	$R1 = 0.0729$	$R1 = 0.0973$	$R1 = 0.1184$
	$wR2 = 0.1815$	$wR2 = 0.2127$	$wR2 = 0.2208$

*$R1 = \Sigma||Fo| - |Fc||/ \Sigma|Fo|$; $wR2 = \{Pw(Fo^2 - Fc^2)^2/\Sigma w(Fo^2)^2\}^{1/2}$

Table A3–4. Selected Crystallographic Data for Compounds **9–11**.

	9	**10**	**11**
Molecular formula	$C_{36}H_{53}CrN_6Te$	$C_{40}H_{63}CrN_7$	$C_{64}H_{110}Cr_2N_6O_2Si_4$
Formula weight	749.44	693.97	1211.94
Crystal size, mm3	0.50×0.40×0.30	0.40×0.30×0.20	0.50×0.40×0.30
Crystal system	Monoclinic	Monoclinic	Monoclinic
Space group	$P2_1$	$P2_1/c$	$P2_1/c$
a, Å	8.8222(6)	13.083(7)	14.815(2)
b, Å	19.024(1)	21.22(1)	21.685(3)
c, Å	22.851(2)	19.51(1)	23.423(3)
α, deg	90	90	90
β, deg	96.643(2)	132.038(9)	95.354(2)
γ, deg	90	90	90
Z	4	4	4
V, $Å^3$	3809.4(5)	4023(4)	7492(2)
Density, g cm^{-3}	1.307	1.146	1.074
Abs coeff., mm^{-1}	1.082	0.320	0.394
Temperature, K	296(2)	173(2)	296(2)
Reflections collected	32967	27213	58884
Independent reflections	13637	7277	13563
Obs. Data with I≥2σ(I)	10812	3191	7010
Final R indices [I≥2σ(I)]*	$R1 = 0.0876$	$R1 = 0.1462$	$R1 = 0.0651$
	$wR2 = 0.2070$	$wR2 = 0.3446$	$wR2 = 0.1430$
R indices (all data)*	$R1 = 0.1041$	$R1 = 0.2610$	$R1 = 0.1300$
	$wR2 = 0.2187$	$wR2 = 0.4006$	$wR2 = 0.1649$

*$R1 = \Sigma||Fo| - |Fc||/ \Sigma|Fo|$; $wR2 = \{Pw(Fo^2 - Fc^2)^2/\Sigma w(Fo^2)^2\}^{1/2}$

Table A3–5. Selected Crystallographic Data for Compounds **12** and **14**.

	12	**14**
Molecular formula	$C_{46}H_{72}K_2N_6O$	$C_{37}H_{60}KN_3O_2$
Formula weight	803.30	617.98
Crystal size, mm3	0.50×0.40×0.30	0.50×0.40×0.30
Crystal system	Monoclinic	Orthorhombic
Space group	$P2_1/c$	*Pbcn*
a, Å	12.6390(9)	30.825(4)
b, Å	31.967(3)	12.904(2)
c, Å	12.3032(9)	18.639(2)
α, deg	90	90
β, deg	106.698(2)	90
γ, deg	90	90
Z	4	8
V, $Å^3$	4761.3(6)	7413(2)
Density, g cm^{-3}	1.121	1.107
Abs coeff., mm^{-1}	0.237	0.177
Temperature, K	293(2)	173(2)
Reflections collected	33225	59676
Independent reflections	8626	6718
Obs. Data with I≥2σ(I)	4026	3078
Final R indices [I≥2σ(I)]*	$R1 = 0.0796$	$R1 = 0.0879$
	$wR2 = 0.1937$	$wR2 = 0.1925$
R indices (all data)*	$R1 = 0.1664$	$R1 = 0.2029$
	$wR2 = 0.2447$	$wR2 = 0.2573$

*$R1 = \Sigma||Fo| - |Fc||/ \Sigma|Fo|$; $wR2 = \{Pw(Fo^2 - Fc^2)^2/\Sigma w(Fo^2)^2\}^{1/2}$

Table A3–6. Selected Crystallographic Data for Compounds **15**–**17**.

	15	**16**	**17**
Molecular formula	$C_{60}H_{96}Eu_2N_{12}$	$C_{96}H_{156}Eu_2N_{12}$	$C_{84}H_{128}N_{12}Yb_2$
Formula weight	1289.41	1782.25	1652.06
Crystal size, mm3	0.40×0.30×0.20	0.40×0.30×0.20	0.40×0.30×0.20
Crystal system	Monoclinic	Monoclinic	Monoclinic
Space group	$P\bar{1}$	$C2/c$	$C2/c$
a, Å	12.5913(5)	30.248(2)	19.835(1)
b, Å	12.6419(5)	12.8148(8)	17.083(1)
c, Å	22.0619(9)	25.013(2)	26.262(2)
α, deg	87.151(1)	90	90
β, deg	87.699(1)	105.971(2)	91.071(1)
γ, deg	67.551(1)	90	90
Z	2	4	4
V, $Å^3$	3240.8(2)	9321(1)	8897.0(9)
Density, g cm^{-3}	1.321	1.270	1.233
Abs coeff., mm^{-1}	1.962	1.383	2.135
Temperature, K	296(2)	173(2)	296(2)
Reflections collected	41719	63666	36680
Independent reflections	11596	8451	8028
Obs. Data with I≥2σ(I)	9736	6776	5630
Final R indices [I≥2σ(I)]*	$R1 = 0.0235$	$R1 = 0.0426$	$R1 = 0.0399$
	$wR2 = 0.0607$	$wR2 = 0.0982$	$wR2 = 0.0896$
R indices (all data)*	$R1 = 0.0331$	$R1 = 0.0605$	$R1 = 0.0666$
	$wR2 = 0.0699$	$wR2 = 0.1083$	$wR2 = 0.0967$

*$R1 = \Sigma||Fo| - |Fc||/ \Sigma|Fo|$; $wR2 = \{Pw(Fo^2 - Fc^2)^2/\Sigma w(Fo^2)^2\}^{1/2}$

Table A3–7. Selected Crystallographic Data for Compounds **18**–**20**.

	18	**19**	**20**
Molecular formula	$C_{50}H_{80}YbN_6O_2$	$C_{57.5}H_{99.5}EuN_6O_2Si_2$	$C_{57.5}H_{99.5}YbN_6O_2Si_2$
Formula weight	970.24	1115.07	1136.15
Crystal size, mm3	0.50×0.40×0.30	0.50×0.40×0.30	0.50×0.40×0.30
Crystal system	Monoclinic	Monoclinic	Monoclinic
Space group	$P2_1/c$	$P2_1/c$	$P2_1/c$
a, Å	19.9680(8)	22.394(2)	22.205(1)
b, Å	11.5152(4)	15.539(1)	15.3818(7)
c, Å	23.8955(9)	19.528(1)	19.4972(8)
α, deg	90	90	90
β, deg	109.047(1)	109.203(1)	108.275(1)
γ, deg	90	90	90
Z	4	4	4
V, $Å^3$	5193.6(3)	6417.4(8)	6323.4(5)
Density, g cm^{-3}	1.241	1.154	1.193
Abs coeff., mm^{-1}	1.841	1.055	1.558
Temperature, K	296(2)	296(2)	296(2)
Reflections collected	46863	48824	47423
Independent reflections	12461	11573	11453
Obs. Data with I≥2σ(I)	8338	8452	8864
Final R indices [I≥2σ(I)]*	$R1 = 0.0566$	$R1 = 0.0455$	$R1 = 0.0455$
	$wR2 = 0.1172$	$wR2 = 0.1168$	$wR2 = 0.1208$
R indices (all data)*	$R1 = 0.0951$	$R1 = 0.0706$	$R1 = 0.0638$
	$wR2 = 0.1308$	$wR2 = 0.1373$	$wR2 = 0.1374$

*$R1 = \Sigma||Fo| - |Fc||/\Sigma|Fo|$; $wR2 = \{Pw(Fo^2 - Fc^2)^2/\Sigma w(Fo^2)^2\}^{1/2}$

Table A3–8. Selected Crystallographic Data for Compounds **21**–**23**.

	21	**22**	**23**
Molecular formula	$C_{64}H_{112}I_2N_6O_4Si_2Sm_2$	$C_{58}H_{88}N_6Sm$	$C_{60}H_{96}Eu_2N_{12}I_2$
Formula weight	1640.28	1019.69	771.60
Crystal size, mm3	0.50×0.40×0.30	0.50×0.40×0.30	0.50×0.40×0.30
Crystal system	Triclinic	Orthorhombic	Monoclinic
Space group	$P\bar{1}$	$Pna2_1$	$P2_1$
a, Å	10.1716(6)	26.589(2)	11.7137(6)
b, Å	11.9918(7)	12.6447(8)	27.338(1)
c, Å	16.800(1)	16.905(1)	11.7288(6)
α, deg	83.039(1)	90	90
β, deg	73.060(1)	90	110.400(1)
γ, deg	71.636(1)	90	90
Z	1	4	4
V, $Å^3$	1859.5(2)	5683.7(6)	3520.4(3)
Density, g cm^{-3}	1.465	1.192	1.456
Abs coeff., mm^{-1}	2.470	1.072	2.684
Temperature, K	296(2)	173(2)	296(2)
Reflections collected	26788	45464	23148
Independent reflections	6700	10182	12377
Obs. Data with I≥2σ(I)	5181	8094	11396
Final R indices [I≥2σ(I)]*	$R1 = 0.0452$	$R1 = 0.0701$	$R1 = 0.0588$
	$wR2 = 0.1143$	$wR2 = 0.1695$	$wR2 = 0.1454$
R indices (all data)*	$R1 = 0.0647$	$R1 = 0.0892$	$R1 = 0.0638$
	$wR2 = 0.1324$	$wR2 = 0.1829$	$wR2 = 0.1476$

*$R1 = \Sigma||Fo| - |Fc||/\Sigma|Fo|$; $wR2 = \{Pw(Fo^2 - Fc^2)^2/\Sigma w(Fo^2)^2\}^{1/2}$

Table A3–9. Selected Crystallographic Data for Compounds **24**–**26**.

	24	**25**	**26**
Molecular formula	$C_{96}H_{138}Yb_2N_{12}S_2$	$C_{96}H_{138}Yb_2N_{12}Se_2$	$C_{84}H_{128}Yb_2N_{12}Cl_2$
Formula weight	1870.38	1964.18	1722.96
Crystal size, mm3	0.50×0.40×0.30	0.40×0.30×0.20	0.50×0.40×0.30
Crystal system	Triclinic	Orthorhombic	Triclinic
Space group	$P\bar{1}$	*Pnma*	$P\bar{1}$
a, Å	12.5820(7)	14.748(7)	15.363(2)
b, Å	13.3965(8)	28.46(2)	18.375(2)
c, Å	15.2189(9)	23.05(1)	19.499(2)
α, deg	103.845(1)	90	62.761(2)
β, deg	103.087(1)	90	76.820(2)
γ, deg	100.546(1)	90	67.830(2)
Z	1	4	2
V, $Å^3$	2348.4(2)	9675(9)	4522.3(9)
Density, g cm^{-3}	1.323	1.348	1.265
Abs coeff., mm^{-1}	2.073	2.722	2.160
Temperature, K	173(2)	296(2)	173(2)
Reflections collected	57836	51930	62394
Independent reflections	8484	11751	16231
Obs. Data with I≥2σ(I)	7897	2551	12270
Final R indices [I≥2σ(I)]*	*R*1 = 0.0231	*R*1 = 0.0689	*R*1 = 0.0715
	*wR*2 = 0.0589	*wR*2 = 0.1119	*wR*2 = 0.1913
R indices (all data)*	*R*1 = 0.0267	*R*1 = 0.3091	*R*1 = 0.0921
	*wR*2 = 0.0628	*wR*2 = 0.1907	*wR*2 = 0.2116

*$R1 = \Sigma||Fo| - |Fc||/\Sigma|Fo|$; $wR2 = \{Pw(Fo^2 - Fc^2)^2/\Sigma w(Fo^2)^2\}^{1/2}$

Table A3–10. Selected Crystallographic Data for Compounds **27**–**29**.

	27	**28**	**29**
Molecular formula	$C_{96}H_{138}Yb_2N_{14}$	$C_{67}H_{98}YbN_8Si_2$	$C_{118}H_{178}Sm_2N_{12}S_4$
Formula weight	1834.28	1244.75	2193.66
Crystal size, mm3	0.40×0.30×0.20	0.50×0.40×0.30	0.40×0.30×0.30
Crystal system	Triclinic	Monoclinic	Monoclinic
Space group	$P\bar{1}$	$P2_1/c$	$P2_1/n$
a, Å	13.6166(4)	25.352(2)	26.803(2)
b, Å	17.0139(6)	12.899(1)	14.455(1)
c, Å	22.5322(8)	21.329(2)	32.322(3)
α, deg	97.562(1)	90	90
β, deg	95.937(1)	101.424(2)	93.384(2)
γ, deg	108.687(1)	90	90
Z	2	4	4
V, $Å^3$	4842.6(3)	6837(1)	12501(2)
Density, g cm^{-3}	1.258	1.209	1.166
Abs coeff., mm^{-1}	1.969	1.446	1.044
Temperature, K	296(2)	173(2)	173(2)
Reflections collected	70445	60251	144699
Independent reflections	17453	12347	22648
Obs. Data with I≥2σ(I)	12020	8686	15081
Final R indices [I≥2σ(I)]*	*R*1 = 0.0409	*R*1 = 0.0795	*R*1 = 0.0635
	*wR*2 = 0.0948	*wR*2 = 0.1924	*wR*2 = 0.1432
R indices (all data)*	*R*1 = 0.0691	*R*1 = 0.1094	*R*1 = 0.1010
	*wR*2 = 0.1033	*wR*2 = 0.2052	*wR*2 = 0.1568

*$R1 = \Sigma||Fo| - |Fc||/\Sigma|Fo|$; $wR2 = \{Pw(Fo^2 - Fc^2)^2/\Sigma w(Fo^2)^2\}^{1/2}$

Table A3–11. Selected Crystallographic Data for Compounds **30**–**32**.

	30	**31**	**32**
Molecular formula	$C_{45}H_{72}CeN_9$	$C_{45}H_{72}PrN_9$	$C_{45}H_{72}GdN_9$
Formula weight	879.24	880.03	896.37
Crystal size, mm3	0.50×0.40×0.30	0.50×0.40×0.30	0.40×0.30×0.30
Crystal system	Triclinic	Triclinic	Triclinic
Space group	$P\bar{1}$	$P\bar{1}$	$P\bar{1}$
a, Å	11.5658(8)	11.5725(5)	11.5581(5)
b, Å	13.290(1)	13.2914(6)	13.1891(6)
c, Å	17.547(1)	17.5415(8)	17.4853(7)
α, deg	85.731(1)	85.734(1)	85.649(1)
β, deg	88.732(1)	88.762(1)	88.670(1)
γ, deg	65.707(1)	65.646(1)	65.466(1)
Z	2	2	2
V, $Å^3$	2451.4(3)	2451.1(2)	2417.7(2)
Density, g cm^{-3}	1.191	1.192	1.231
Abs coeff., mm^{-1}	0.966	1.031	1.409
Temperature, K	296(2)	296(2)	296(2)
Reflections collected	33124	28584	39829
Independent reflections	8746	8726	8692
Obs. Data with I≥2σ(I)	8198	7897	7190
Final R indices [I≥2σ(I)]*	$R1 = 0.0246$	$R1 = 0.0307$	$R1 = 0.0309$
	$wR2 = 0.0772$	$wR2 = 0.0787$	$wR2 = 0.0695$
R indices (all data)*	$R1 = 0.0272$	$R1 = 0.0355$	$R1 = 0.0465$
	$wR2 = 0.0811$	$wR2 = 0.0826$	$wR2 = 0.0778$

*$R1 = \Sigma||Fo| - |Fc||/ \Sigma|Fo|$; $wR2 = \{Pw(Fo^2 - Fc^2)^2/\Sigma w(Fo^2)^2\}^{1/2}$

Table A3–12. Selected Crystallographic Data for Compounds **33**–**35**.

	33	**34**	**35**
Molecular formula	$C_{45}H_{72}TbN_9$	$C_{45}H_{72}HoN_9$	$C_{45}H_{72}ErN_9$
Formula weight	898.04	904.05	906.38
Crystal size, mm3	0.50×0.40×0.30	0.40×0.30×0.20	0.50×0.40×0.30
Crystal system	Triclinic	Triclinic	Triclinic
Space group	$P\bar{1}$	$P\bar{1}$	$P\bar{1}$
a, Å	11.5873(6)	11.5930(5)	11.5898(5)
b, Å	13.1778(7)	13.1483(6)	13.1235(5)
c, Å	17.5017(9)	17.4971(8)	17.4851(7)
α, deg	85.556(1)	85.534(1)	85.490(1)
β, deg	88.587(1)	88.551(1)	88.496(1)
γ, deg	65.385(1)	65.301(1)	65.270(1)
Z	2	2	2
V, $Å^3$	2422.2(2)	2415.6(2)	2408.0(2)
Density, g cm^{-3}	1.231	1.243	1.250
Abs coeff., mm^{-1}	1.498	1.676	1.781
Temperature, K	296(2)	296(2)	296(2)
Reflections collected	28017	27211	35045
Independent reflections	8630	8570	8686
Obs. Data with I≥2σ(I)	7901	7782	8135
Final R indices [I≥2σ(I)]*	$R1 = 0.0275$	$R1 = 0.0303$	$R1 = 0.0237$
	$wR2 = 0.0709$	$wR2 = 0.0769$	$wR2 = 0.0623$
R indices (all data)*	$R1 = 0.0322$	$R1 = 0.0351$	$R1 = 0.0264$
	$wR2 = 0.0771$	$wR2 = 0.0810$	$wR2 = 0.0649$

*$R1 = \Sigma||Fo| - |Fc||/ \Sigma|Fo|$; $wR2 = \{Pw(Fo^2 - Fc^2)^2/\Sigma w(Fo^2)^2\}^{1/2}$

Table A3–13. Selected Crystallographic Data for Compounds **36–38**.

	36	**37**	**38**
Molecular formula	$C_{45}H_{72}TmN_9$	$C_{60}H_{96}Ce_2Cl_2N_{12}$	$C_{60}H_{96}Lu_2Cl_2N_{12}$
Formula weight	908.05	1336.63	1406.33
Crystal size, mm3	0.50×0.40×0.30	0.50×0.40×0.30	0.50×0.40×0.30
Crystal system	Triclinic	Triclinic	Tetragonal
Space group	$P\bar{1}$	$P\bar{1}$	$P\bar{4}2_1c$
a, Å	11.8912(6)	11.6785(7)	16.9100(6)
b, Å	12.5865(6)	27.000(2)	16.9100(6)
c, Å	16.3279(8)	11.7304(7)	23.9556(8)
α, deg	88.072(1)	90	90
β, deg	85.358(1)	110.550(1)	90
γ, deg	78.573(1)	90	90
Z	2	2	4
V, $Å^3$	2387.1(2)	3463.5(4)	6850.1(4)
Density, g cm^{-3}	1.263	1.282	1.364
Abs coeff., mm^{-1}	1.897	1.417	2.986
Temperature, K	296(2)	296(2)	296(2)
Reflections collected	29138	38997	52941
Independent reflections	8627	12031	6232
Obs. Data with I≥2σ(I)	8120	7782	5509
Final R indices [I≥2σ(I)]*	$R1 = 0.0277$	$R1 = 0.0303$	$R1 = 0.0287$
	$wR2 = 0.0742$	$wR2 = 0.0769$	$wR2 = 0.0708$
R indices (all data)*	$R1 = 0.0299$	$R1 = 0.0351$	$R1 = 0.0385$
	$wR2 = 0.0764$	$wR2 = 0.0810$	$wR2 = 0.0809$

*$R1 = \Sigma||Fo| - |Fc||/\Sigma|Fo|$; $wR2 = \{\mathrm{Pw}(Fo^2 - Fc^2)^2/\Sigma w(Fo^2)^2\}^{1/2}$

Appendix 4

IR Spectra of Compounds

Figure A4–1. IR Spectrum of [{Yb(L^2)$_2$}$_2$(μ–η^2:η^2–PhNNPh)] (**27**).

Figure A4–2. IR Spectrum of [Yb(L^3)$_2$(η^2–PhNNPh)·PhMe] (**28**).

Figure A4–1. IR Spectrum of [{Yb(L^2)$_2$}$_2$(μ–η^2:η^2–PhNNPh)] (**27**).

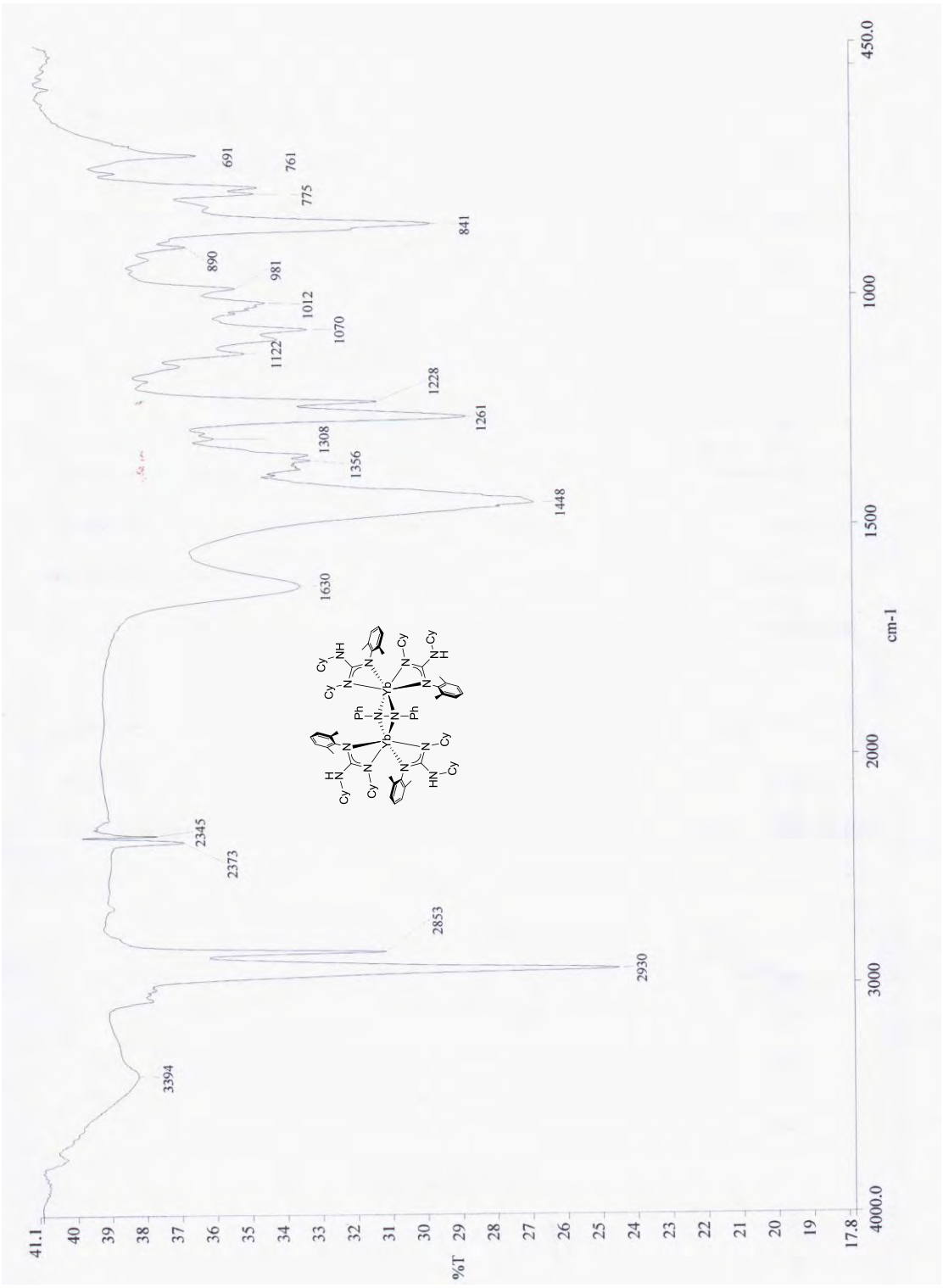

Figure A4–2. IR Spectrum of $[Yb(L^3)_2(\eta^2\text{–PhNNPh})\cdot PhMe]$ (**28**).

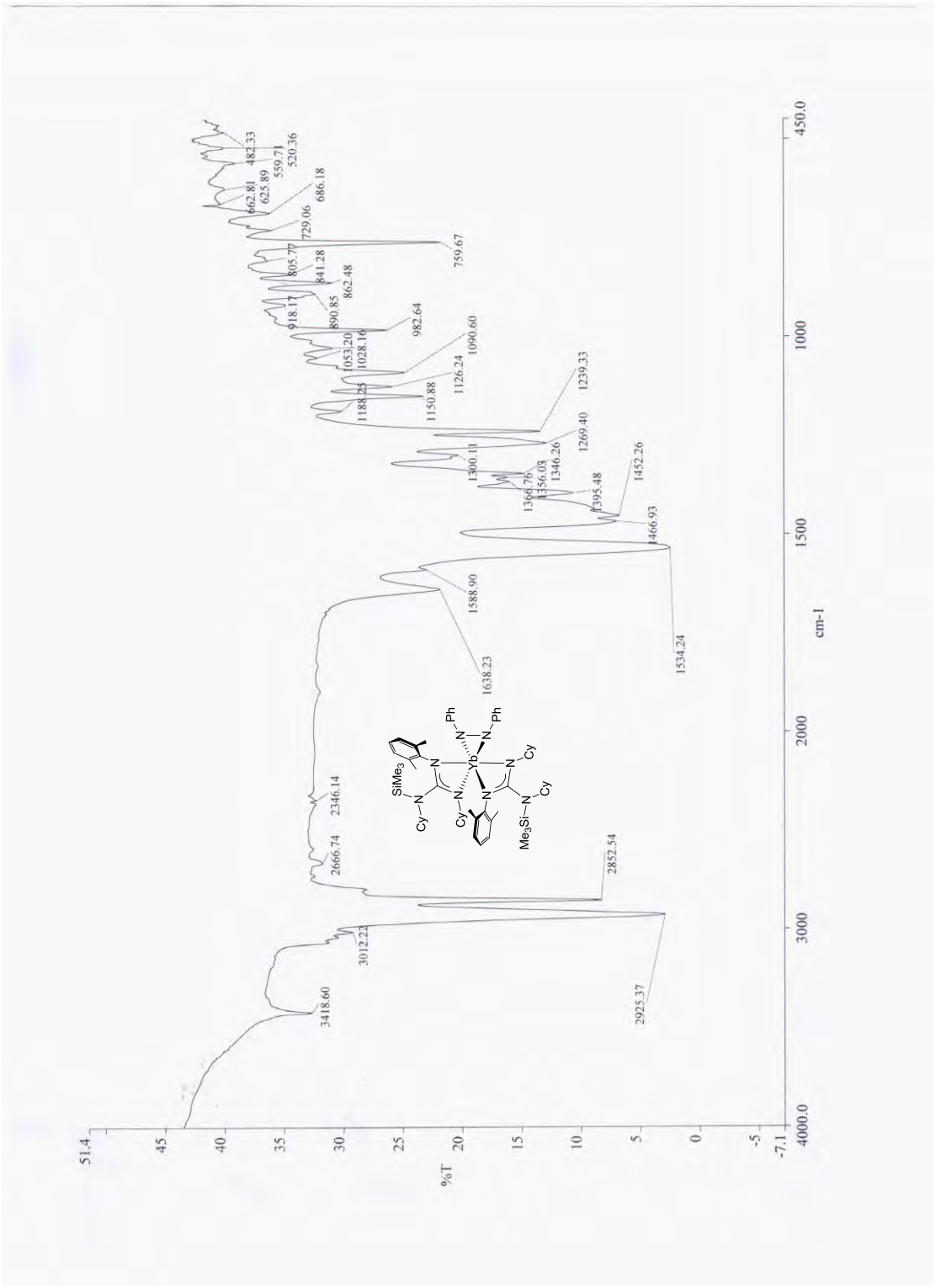

Appendix 5

UV–Vis Spectra of Compounds

Figure A5–1. UV–Vis Spectrum of $[Cr(L^1)_2]$ (**3**).

Figure A5–2. UV–Vis Spectrum of $[Cr(L^1)_2(SPh)]$ (**7**).

Figure A5–3. UV–Vis Spectrum of $[Cr(L^1)_2(SePh)]$ (**8**).

Figure A5–4. UV–Vis Spectrum of $[Cr(L^1)_2(TePh)]$ (**9**).

Figure A5–5. UV–Vis Spectrum of $[\{Yb(L^2)_2\}_2(\mu\text{–}\eta^2\text{:}\eta^2\text{–PhNNPh})]$ (**27**).

Figure A5–6. UV–Vis Spectrum of $[Yb(L^3)_2(\eta^2\text{–PhNNPh})\cdot PhMe]$ (**28**).

Figure A5–1. UV–Vis Spectrum of $[Cr(L^1)_2]$ (**3**).

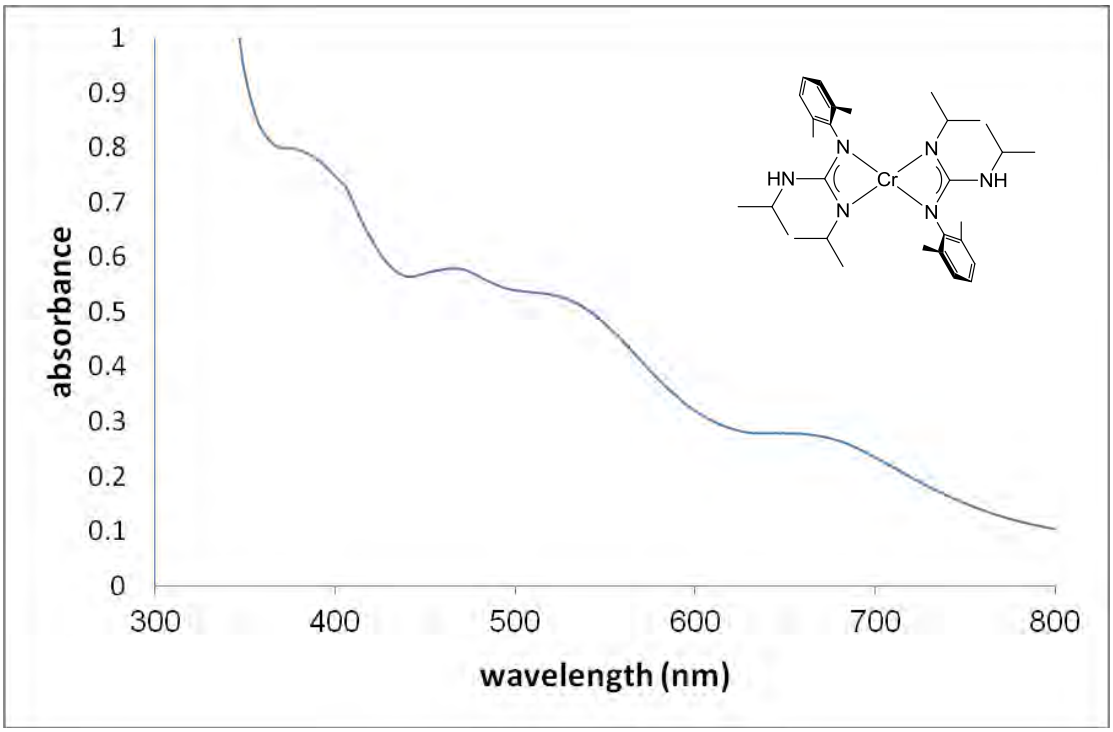

Figure A5–2. UV–Vis Spectrum of $[Cr(L^1)_2(SPh)]$ (**7**).

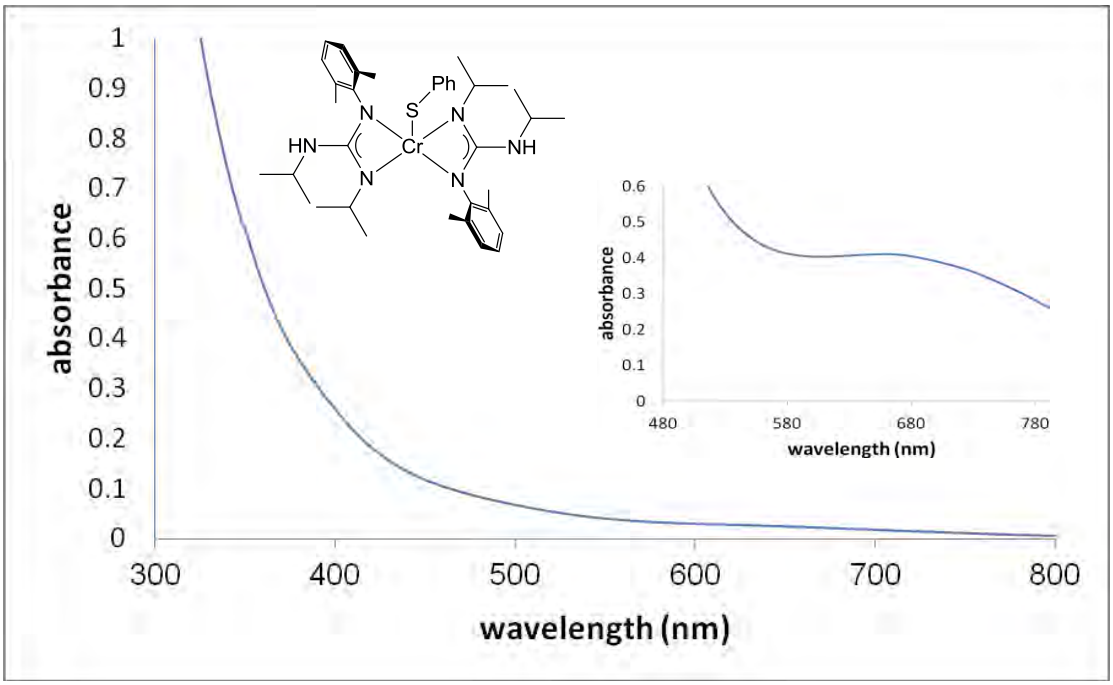

Figure A5–3. UV–Vis Spectrum of $[Cr(L^1)_2(SePh)]$ (**8**).

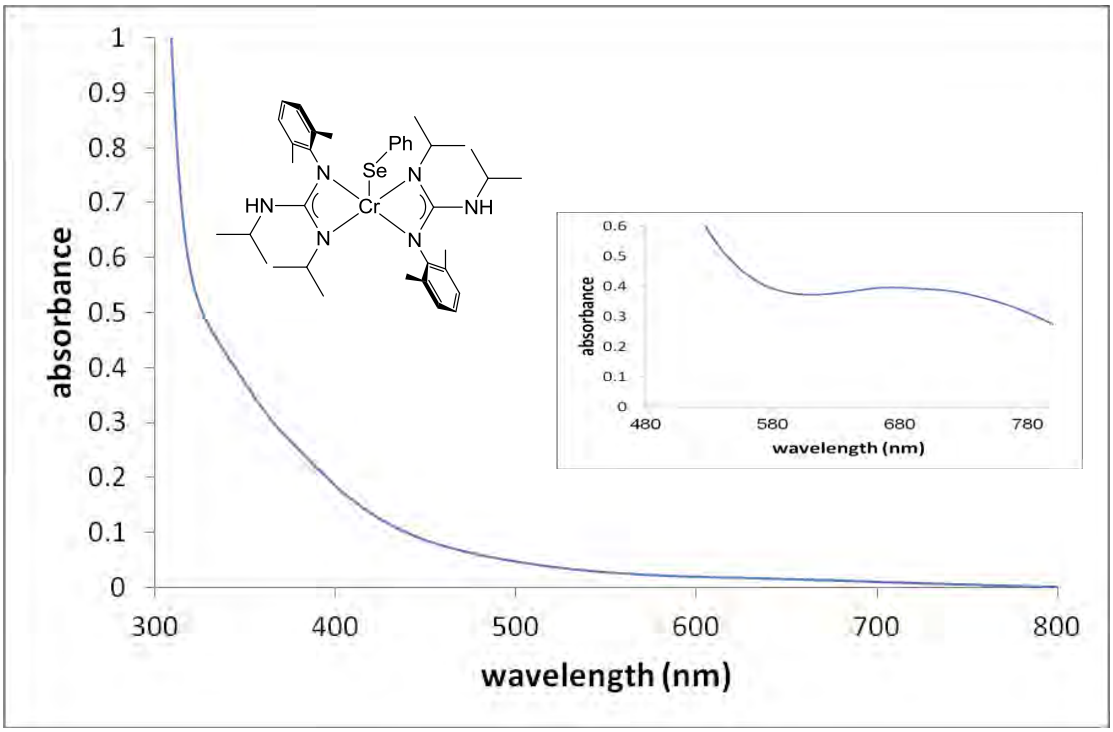

Figure A5–4. UV–Vis Spectrum of $[Cr(L^1)_2(TePh)]$ (**9**).

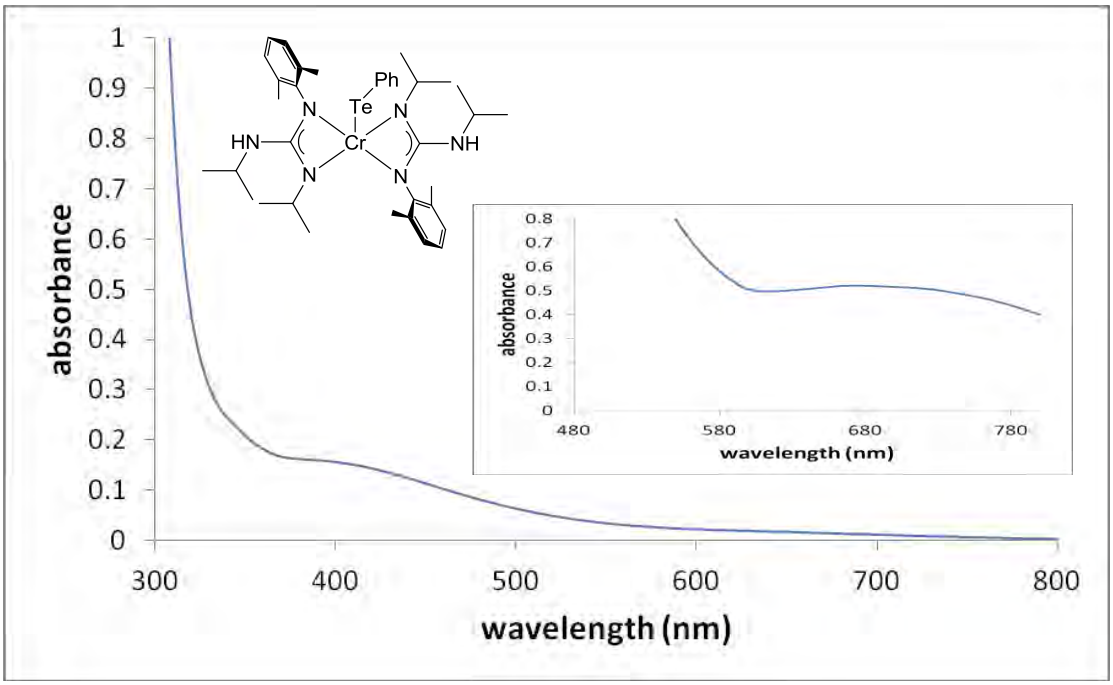

Figure A5–5. UV–Vis Spectrum of [{Yb(L^2)$_2$}$_2$(μ–η^2:η^2–PhNNPh)] (**27**).

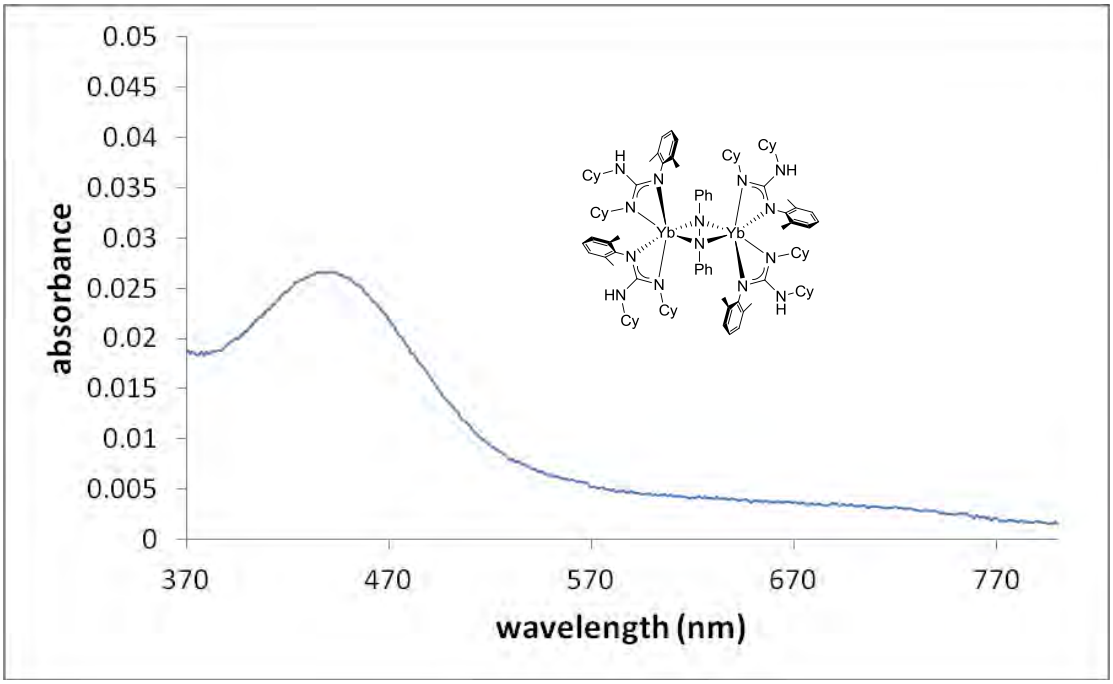

Figure A5–6. UV–Vis Spectrum of [Yb(L^3)$_2$(η^2–PhNNPh)·PhMe] (**28**).